Clemson University
TigerPrints

All Dissertations | Dissertations

August 2020

A pH Sensor for Non-Invasive Detection and Monitoring of pH Changes During Implant-Associated Infection Using X-ray Excited Luminescence Chemical Imaging

Unaiza Uzair
Clemson University, unaizauzair@gmail.com

Follow this and additional works at: https://tigerprints.clemson.edu/all_dissertations

Recommended Citation

Uzair, Unaiza, "A pH Sensor for Non-Invasive Detection and Monitoring of pH Changes During Implant-Associated Infection Using X-ray Excited Luminescence Chemical Imaging" (2020). *All Dissertations*. 2655.
https://tigerprints.clemson.edu/all_dissertations/2655

This Dissertation is brought to you for free and open access by the Dissertations at TigerPrints. It has been accepted for inclusion in All Dissertations by an authorized administrator of TigerPrints. For more information, please contact kokeefe@clemson.edu.

A pH SENSOR FOR NON-INVASIVE DETECTION AND MONITORING OF pH CHANGES DURING IMPLANT-ASSOCIATED INFECTION USING X-RAY EXCITED LUMINESCENCE CHEMICAL IMAGING

A Dissertation
Presented to
the Graduate School of
Clemson University

In Partial Fulfillment
of the Requirements for the Degree
Doctor of Philosophy
Chemistry

---

by
Unaiza Uzair
August 2020

Accepted by:
Dr. Jeffrey N. Anker, Committee Chair
Dr. Tzuen-Rong Jeremy Tzeng
Dr. Stephen Creager
Dr. Carlos D. Garcia
Dr. Jason D. McNeill

ABSTRACT

Implant-associated infection is a leading cause of fixation failures and these infections are resistant to antibiotics especially after mature biofilms have been established on the implant surface. These infections can also be challenging to detect, especially at early stages or during antibiotic treatment, due to lack of symptoms and specific tests to detect localized infection. Low pH is believed to be associated with infection as bacteria and inflammatory responses can cause a pH drop in the affected area. Detecting changes in pH on the implant surface can provide a better understanding and help to detect, treat and monitor such infections more effectively thereby reducing the need for revision surgeries. We developed a novel X-ray Excited Luminescence Chemical Imaging (XELCI) technique to measure surface specific chemical concentrations with sub-millimeter spatial resolution. A focused X-ray beam (~0.3 mm) passes through tissue and irradiates scintillators coated on an orthopedic implant; these scintillators generate visible and near infrared light which is partially absorbed by a pH indicator film (e.g., bromocresol green or bromothymol blue pH dye encapsulated in a PEG hydrogel) altering the luminescence spectrum in a pH-dependent manner. Images are acquired by scanning the beam point-by-point and measuring the spectrum at each point. We developed, synthesized and tested pH indicator films and measured the signal intensity, noise level, and knife-edge spatial resolution through varying thicknesses of chicken breast tissue and through 11 mm of human cadaveric tissue in a tibial fixation specimen. For example, we observed a knife-edge (80/20) spatial resolution of ~0.5 mm

through up to 1 cm of tissue and an average pH noise level of 0.25 ±0.05 pH units. We also implanted the pH sensor in rabbits to image pH during infection. The in vivo studies found that the sensors continued to function well for the 11-day experiments. During infection, the pH did not significantly drop compared to uninfected implants on opposite legs (<0.5 pH unit change). For sensors that were initially acidic and infected, the pH neutralized in time, and this neutralization could be delayed by enclosing the implant in cavity with a 1 mm aperture to slow perfusion and diffusion. These studies show applicability provide useful insight into the pH changes that occur on implant surface during infection and can have important implications for antibiotic treatments. Future directions include improving the collection efficiency, adding an X-ray chopper to measure background signal and luminescence lifetime, scanning scintillator nanoparticles in three dimensions for tomography, detecting additional analytes, and studying pH changes on the device surface during infection followed by antibiotic treatment in animal models and to develop a model for pH changes during osteomyelitis.

DEDICATION

I dedicate this work, the fruit of my PhD journey, to my parents,

Uzair Ahmad and **Mumtaz Uzair**; my sister, **Zunaira Uzair**; my brother, **Muhammad Hassan Uzair** and my husband, **Michael Akins**, for their unconditional love and support.

ACKNOWLEDGMENTS

I would like to acknowledge the guidance, support and patience of my PhD advisor, Dr. Jeffrey Anker throughout my PhD journey. He has always been there to answer my questions, listen to my concerns and help me learn and articulate scientific thoughts. I wish to thank all the people whose assistance was a milestone in the completion of this project especially my PhD committee, Drs. Stephen Creager, Carlos D. Garcia, Jason D. McNeill and Tzuen-Rong (Jeremy) Tzeng.

This research would not have been possible without the collaborative support of Dr. Tzeng's lab and other group members of Anker lab, and the insightful conversations that we had during the weekly project meetings over all these years. Specifically, the microbiology experiments were performed by Shayesteh Beladi-Behbahani, Md. Arifuzzaman helped in the synthesis of the optimized hydrogels, Donald Benza built the initial XELCI setup, and Paul Millhouse machined the acrylic light guide and helped with optimization of the XELCI system. The implants were machined by the Clemson University Machining and Technical Services, and the implant lids were cut at the Clemson University Student Makerspace. This work is based on the initial proof of concept work done by Fenglin Wang.

I wish to show my gratitude to the wonderful staff at the Godley-Snell Research Center, Dr. John Parish for performing the animal surgeries, Travis Pruitt, Tina Parker, Cindy Smoak and Jessica Privett for handling and caring for the rabbits. I would also like to thank the faculty and staff in the Chemistry Department, especially Heather Shelton for being responsive to all my inquiries.

A good support system is important for surviving a PhD journey where one is climbing the hills, falling and tumbling, and climbing back up especially in a foreign land. I am indebted to the Fulbright program for this life changing experience that enabled me to come out of my comfort zone and try my best. I am grateful for all the friends I've made during this time at Clemson especially my host family, roommates, Anker Lab members and fellow Fulbrighters who are now scattered all around the world; I'll never forget the many wonderful brunches, tea times and fun activities we've had together. I am also grateful for the co-curricular engagements and leadership opportunities that I've had at Clemson University.

I wish to acknowledge the support and great love of my family; my hard-working parents who strived to provide me, my sister and brother with the best educational opportunities; my sister and brother who have been my best friends and secret-keepers; my extended family, grandparents, uncles and aunts; and my husband whom I met during this journey and who trained me on the mechanical aspects needed for this project such as using a drill, tapping a hole, explaining the quarter twenty system of screw thread specifications (since I was familiar with the metric system only), etc. and he also helped me in putting together the enclosure for the XELCI system. They kept me going forward and this work would not have been possible without their non-judgmental emotional support and encouragement, especially when I was irritable and depressed; they instilled the confidence in me, and I love them all dearly.

This research was funded by the National Institutes of Health (NIH) under grant 5R01AR070305, NSF CAREER Award CHE1255535 and SCBioCRAFT COBRE grant

(5P20GM10344407). Human cadaveric specimens were obtained via the Hawkins Foundation (Greenville SC) from Restore Life USA (Elizabethton, TN), a nonprofit donation program, and donors had consented their body to be used for medical education and research in accordance with the Uniform Anatomical Gift Act (UAGA).

TABLE OF CONTENTS

Page

LIST OF FIGURES

Figure Page

LIST OF TABLES

Table Page

1. INTRODUCTION

We have developed a pH sensor and a novel imaging technique, X-ray excited luminescence chemical imaging (XELCI), to non-invasively monitor chemical changes associated with infection on the surface of modified implanted devices. This is an important topic because about half of hospital-acquired infections are associated with implanted medical devices and bacteria which colonize on the device surfaces are resistant to the host's immune system and antibiotics. Once the infection is established, the device usually needs to be surgically removed in order to treat the infection. Research on elucidating the pH near implants is important for developing methods to detect, monitor, and treat implant associated infections. The treatment of implant associated infections usually depends on infection duration, implant stability, condition of the surrounding soft tissue and pathogen susceptibility to antibiotics.[1] Common treatment options for patients with orthopedic implant associated infection include (1) Irrigation and debridement with retention of implant and long-term (usually 3 months) treatment with antimicrobial agents, (2) One-stage replacement with or without the use of antimicrobial cement and long-term treatment with antimicrobial agents (3-6 months), (3) Two-stage replacement with or without use of antimicrobial cement and long-term treatment with antimicrobial agents, (4) Suppressive antimicrobial therapy (in patients who cannot undergo surgical procedures).[2] Among antibiotic treatments, Rifampin has proven efficacy against slow growing and adherent staphylococci, and it must always be combined with quinolones to prevent emergence of resistant strains but increasing antimicrobial resistance requires evaluation of alternative combination agents.[3] There is

ongoing research to develop intelligent implant surfaces with chemically modified micro/nano-topology of outer layer to reduce bacterial adhesion and produce self-sterilizing surfaces.[4–7] These include antibiotic-eluting implants and bioactive coatings with sustained drug release,[8,9] silver-impregnated surfaces,[10,11] and tethered-antibiotic implants (antimicrobial peptides covalently attached to implant surface).[12]

Our approach was focused on studying the pH changes occurring on and around the implant surface during implant-associated infection and to harness these pH changes for early diagnosis and monitoring of the infection. We have fabricated pH sensing films and have shown that the pH decreases during metabolic activity from biofilms such as those present in implant-associated infections. We wanted to develop a tool to investigate how pH would change during normal healing versus infection, how uniform the pH was in these conditions, and what parameters influenced the pH. Our expectations were: (1) the pH would decrease in the case of infection both in vitro and in vivo; (2) Our novel XELCI system would be able to observe this pH change non-invasively in vivo; (3) the pH change would depend upon the environment tested and time, especially whether the infection is well perfused or in a cavity or adjacent to the bone; (4) We would be able to distinguish infection from inflammation associated from injury and surgery by the time course of the pH change and its response to vancomycin.

Our group has previously shown that the luminescent signal from scintillator particles can be detected at one wavelength but this was done by irradiating only a single location in living mice and a 2D image or scan was not performed. Even though the proof of principle was shown in vitro, infection was not imaged in vivo. This dissertation

demonstrates that the pH changes can be measured non-invasively through ex vivo chicken breast, human cadaveric tissue and in live animals. We collected live animal data to show that the principle works for detecting in vivo surface specific pH on implanted devices and studied how the presence of cavities or proximity of bone affect the local microenvironment of the infection.

1.1. DESCRIPTION OF THESIS

Chapter 1 introduces the hypotheses for the research presented in this dissertation and explains the significance of research followed by a brief description of the research explained in each chapter.

Chapter 2 describes the development of the X-ray excited luminescence chemical imaging (XELCI) technique, provides a comparison with other techniques available and discusses the improvements made to optimize the XELCI system to increase signal collection. It also characterizes the system in terms of spatial resolution, point spread function of light through tissue and the size of the focused X-ray beam width.

Chapter 3 describes the pH sensor that attaches to implants to noninvasively image local pH with high spatial resolution. The sensor was covered with varying thickness slices of chicken breast tissue (0-19 mm) to evaluate how tissue affects signal intensity and ratio. The sensor was attached to an orthopedic plate affixed to a human cadaveric tibia and imaged through tissue.

Chapter 4 describes a method to conformally coat scintillator particles onto the surface of a titanium plate followed by a pH sensitive hydrogel coating using a roughed epoxy coating. The pH sensor coated orthopedic plate was imaged with XELCI through

tissue with different pH to acquire a calibration curve. The plates were also imaged through tissue with acidic pH region from a Staphylococcus aureus biofilm grown on one section. These studies demonstrate the use of pH sensor coated orthopedic plates for mapping the surface pH through tissue during biofilm formation using XELCI.

Chapter 5 discusses the preliminary in vivo studies conducted to test sensor performance. We conducted 15 rabbit studies that are classified into single plate region (Part I) and partitioned plate regions (Part II). These are further divided into Phase A, B, C and D for clarification with Phase A comprising of all the single plate region studies discussed in Part I (Chapter 5). The single plate region implant is coated with two types of preliminary sensors to evaluate the sensor performance in vivo, develop the imaging technique and ensure practice in placing the implant and performing the imaging. Even though we did not observe a pH change during infection, we were able to successfully image the implanted sensors through in the live animal and gained useful insights to optimize the sensor and the imaging system.

Chapter 6 discusses the in vivo studies conducted in Phase B and C with a partitioned plate region orthopedic implant. Based on the results of the preliminary studies in Phase A, the sensor was optimized to be able to better monitor small changes in physiological pH with a working pH range of pH 6 – 8. The X-ray excited luminescence chemical imaging (XELCI) system was also modified to capture more light and increase the signal to noise ratio as described in Chapter 2. The optimized sensor and the modified XELCI system were tested to make sure the system works properly in live rabbits. We

studied different case scenarios of infection on the implant surface, in a cavity and the rate of neutralization of pH with and without a biofilm.

Chapter 7 provides an overall summary of the research, discusses the research hypotheses and the conclusions to the hypotheses, with the implications of the research. The chapter is concluded with potential directions for future studies including development of a model for pH changes during osteomyelitis.

Appendices provide the MATLAB scripts used to generate the XELCI images and a Phase D study to evaluate bone pH.

1.2. REFERENCES

(1) Trampuz, A.; Widmer, A. F. Infections Associated with Orthopedic Implants. *Curr. Opin. Infect. Dis.* **2006**, *19* (4), 349–356. https://doi.org/10.1097/01.qco.0000235161.85925.e8.

(2) Widmer, A. F. New Developments in Diagnosis and Treatment of Infection in Orthopedic Implants. *Clin. Infect. Dis. Off. Publ. Infect. Dis. Soc. Am.* **2001**, *33 Suppl 2*, S94-106. https://doi.org/10.1086/321863.

(3) Zimmerli, W.; Widmer, A. F.; Blatter, M.; Frei, R.; Ochsner, P. E. Role of Rifampin for Treatment of Orthopedic Implant-Related Staphylococcal Infections: A Randomized Controlled Trial. Foreign-Body Infection (FBI) Study Group. *JAMA* **1998**, *279* (19), 1537–1541. https://doi.org/10.1001/jama.279.19.1537.

(4) Del Curto, B.; Brunella, M. F.; Giordano, C.; Pedeferri, M. P.; Valtulina, V.; Visai, L.; Cigada, A. Decreased Bacterial Adhesion to Surface-Treated Titanium. *Int. J. Artif. Organs* **2005**, *28* (7), 718–730. https://doi.org/10.1177/039139880502800711.

(5) Campoccia, D.; Montanaro, L.; Arciola, C. R. The Significance of Infection Related to Orthopedic Devices and Issues of Antibiotic Resistance. *Biomaterials* **2006**, *27* (11), 2331–2339. https://doi.org/10.1016/j.biomaterials.2005.11.044.

(6) Tiller, J. C.; Liao, C. J.; Lewis, K.; Klibanov, A. M. Designing Surfaces That Kill Bacteria on Contact. *Proc. Natl. Acad. Sci. U. S. A.* **2001**, *98* (11), 5981–5985. https://doi.org/10.1073/pnas.111143098.

(7) *Handbook of Bacterial Adhesion: Principles, Methods, and Applications*; An, Y. H., Friedman, R. J., Eds.; Humana Press, 2000. https://doi.org/10.1007/978-1-59259-224-1.

(8) Stigter, M.; Bezemer, J.; de Groot, K.; Layrolle, P. Incorporation of Different Antibiotics into Carbonated Hydroxyapatite Coatings on Titanium Implants, Release and Antibiotic Efficacy. *J. Control. Release Off. J. Control. Release Soc.* **2004**, *99* (1), 127–137. https://doi.org/10.1016/j.jconrel.2004.06.011.

(9) Milović, N. M.; Wang, J.; Lewis, K.; Klibanov, A. M. Immobilized N-Alkylated Polyethylenimine Avidly Kills Bacteria by Rupturing Cell Membranes with No Resistance Developed. *Biotechnol. Bioeng.* **2005**, *90* (6), 715–722. https://doi.org/10.1002/bit.20454.

(10) Furkert, F. H.; Sörensen, J. H.; Arnoldi, J.; Robioneck, B.; Steckel, H. Antimicrobial Efficacy of Surface-Coated External Fixation Pins. *Curr. Microbiol.* **2011**, *62* (6), 1743–1751. https://doi.org/10.1007/s00284-011-9923-3.

(11) Juan, L.; Zhimin, Z.; Anchun, M.; Lei, L.; Jingchao, Z. Deposition of Silver Nanoparticles on Titanium Surface for Antibacterial Effect. *Int. J. Nanomedicine* **2010**, *5*, 261–267.

(12) Hickok, N. J.; Shapiro, I. M. Immobilized Antibiotics to Prevent Orthopaedic Implant Infections. *Adv. Drug Deliv. Rev.* **2012**, *64* (12), 1165–1176. https://doi.org/10.1016/j.addr.2012.03.015.

2. X-RAY EXCITED CHEMICAL LUMINESCENCE IMAGING (XELCI)

2.1. ABSTRACT

We developed a novel X-ray excited luminescent chemical imaging (XELCI) technique to map chemical concentrations on the surface of medical devices embedded in tissue and applied it to image pH changes during implant-associated infection using a pH sensor coated on orthopedic implants. X-ray resolution, implant surface specificity and chemical sensitivity are the three key features of XELCI and it is comparable to other imaging techniques such as photoacoustic tomography (PAT), single photon emission computed tomography (SPECT), positron emission tomography (PET) and magnetic resonance imaging (MRI) in terms of image resolution and depth of imaging. Initially, the XELCI system was limited by the acceptance angle of the liquid light guide to collect signal from the sample since the light spreads at different angles when passing through tissue. It was later optimized to improve the signal collection with the use of solid light guide. XELCI provides high spatial resolution images mainly limited by X-ray beam width with minimum increase from X-ray scattering in the tissue. It allows point by point mapping of the surface with minimum background.

2.2. INTRODUCTION

X-ray excited luminescent chemical imaging uses the penetration depth of the X-rays to reach deep into the soft tissue without much scattering and produce a luminescent signal from the embedded sensor. This luminescent signal is detected using a

photodetector and resolved into the constituent wavelengths of interest using a spectrometer or a combination of photomultiplier tubes coupled with optical filters. A schematic of the XELCI system is shown in figure 2.1A. The technique works in conjunction with a sensor that is coated on the surface of the implanted device, the design of which is given in figure 2.1B. The pH sensor consists of two layers: the bottom layer contains scintillator particles which when irradiated by the x-rays emits red light, 620 nm and 700 nm emission for europium doped gadolinium oxysulfide phosphors. The scintillator layer is covered by a pH indicating hydrogel layer that changes color with pH. The absorbance of the pH layer overlaps with the emission of the scintillator layer such that when the pH is high, the pH layer absorbs more of the 620 nm light compared to when the pH is acidic, thus modulating the luminescent signal from the scintillator layer and allowing for the mapping of surface pH. The 700 nm emission remains unaltered as it is not absorbed by the pH layer and serves as an in situ spectral reference to account for pH-independent attenuation of the luminescent signal such as due to absorbance by tissue. Low pH is associated with the formation of biofilms due to the acidic products from bacterial metabolism. Bacteria and inflammatory responses from the body cause a pH drop in affected area and pH shifts to acidic from physiological pH that can indicate infection. By coating the surface of the medical implants with the pH sensor layers, we can use XELCI to image the pH changes associated with implant-associated infections such as those commonly observed with orthopedic implants. Figure 2.1B shows an orthopedic plate coated with the sensor layers and the pH layer is changing color (turning yellow) in areas of biofilm growth indicating infection. This color change otherwise

impossible to see with the naked eye or even with plain X-ray images can be visualized using XELCI.

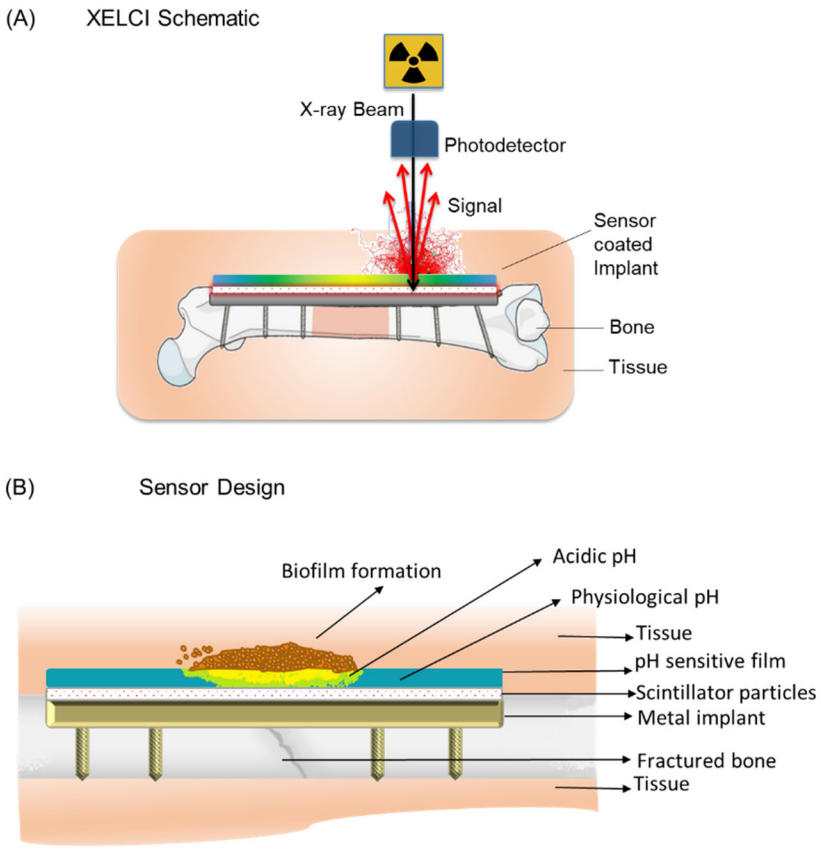

Figure 2.1: X-ray excited chemical luminescence imaging (XELCI). A) Schematic of XELCI imaging. The sample is irradiated with a focused X-ray beam and the resulting luminescent signal collecting with a photodetector. B) Schematic of sensor design. An orthopedic plate is coated with a scintillator layer that luminescence when excited by the X-ray. The scintillator layer is covered with a pH sensitive layer that changes color depending on the surface pH and modulates the luminescence of the underlying layer indicating pH.

2.3. INNOVATION

Low pH is usually associated with infections related to medical implants as demonstrated by the presence of brushite and uncarbonated apatite materials in cavities and infected bone indicating the effect of acid generated changes in bone mineral composition indicative of lower pH. X-ray and MRI images of bones show erosion and

formation of sinus tract both of which reflects low pH.[1] Local acidosis has been observed which is consistent with studies of collagen degradation, implant pitting, and metal ion release in patients with septic loosening.[2] pH microelectrodes were used to measure pH adjacent to a prosthetic hip implant intraoperatively and pH was found to be particularly acidic 'near the implant' in patients with septic loosening.[3] But no pH images of the 'implant surface' were generated. These observations are a direct evidence of low pH in the surrounding tissue of the infected medical implants and contribute to the indirect evidence that pH on the 'surface' of infected implants is acidic than in situ pH but no quantitative pH imaging of the implant surface has been acquired yet. Moreover, the degree of pH drop varies based on the situation such as type of implant and fracture, type of infection, patient immune response, etc. For example, there are reports of pH measurements ranging from pH 5 to 7.8 even for apparently aseptic implant loosening and as low as pH 4.5 measured intraoperatively in the femoral cavity in the case of septic implant loosening.[3] The average pH of synovial fluid was measured to be at pH 7.78 ± 0.38 in natural joints with osteoarthritis and was found to be slightly lower (pH 7.55 ± 0.25) at revision surgeries for septic loosening of prosthetic joints.[4] Another study, compared the synovial fluid pH measurements for osteoarthritis patients undergoing revision surgeries for the uninfected revision group (mean pH 7.23 ± 0.09) and the infected revision group (mean pH 7.06 ± 0.12).[5] Both studies show variable mean pH for the infected and uninfected groups, but the pH was significantly lower for the infected cases compared to the non-infected groups in both studies. Similarly, Thomas T.Ward and Roy T.Steigbigel demonstrated a correlation between an increasing white blood cell

count and a decreasing pH in the synovial fluid of patients with septic arthritis.[6] In contrast to evidence of low pH in implant-associated infections, the urinary pH usually increases (> pH 8) in case of urinary tract infections indicating the presence of urea splitting organisms and is used as a diagnostic indicator of infection.[7] Compared to the intraoperative pH measurements and the aspiration of synovial fluid (generally performed under a local anesthetic), our approach is non-invasive and provides potential for long term monitoring of pH changes on the implant surface not only during the infection but also after antibiotic treatments to indicate resurfacing of the biofilm.

There are several ways of pH sensing from conventional glass electrodes to functionalized nanoparticles. Yuqing et al., provides a review of different technologies being developed for pH sensing including pH sensors based on optical fibers, mass-sensitive hydrogels, metal-oxides, conducting polymers, nano-constructed cantilevers and magnetoelastic effect.[8] Implantable pH sensors are promising but active sensors need to overcome issues of power, telemetry, drift and biofouling. Wireless pH sensors, for example, the one based on carbon nanotube chemiresistor coupled with an RFID tag can provide remote wireless chemical sensing but a major limitation would be continuous coating of the implant surface with the chemiresistor and RFID tags.[9] Electrochemical sensors are notorious for biofouling when implanted in vivo due to adsorption of the proteins on the sensor surface hence causing a drift in the measurements of electric current, a non-equilibrium process.[10] Optical sensors, on the other hand, measures the equilibrium response of a pH dye that does not suffer from drift. Passive sensors such as those based on XELCI, radiographic sensors and optical sensors perform better in vivo as

their sensing mechanisms are less susceptible to be affected by biofouling and does not require complex circuitry and can be easily adapted to different types of implants. Nuclear imaging techniques (bone scintigraphy) have limited accuracy and are expensive. Computed Tomography (CT) and Magnetic Resonance Imaging (MRI) provide information on extent of bone necrosis and soft tissue abnormalities respectively but have the disadvantage of imaging interferences in vicinity of metal implants. PET (Positron Emission Tomography) can provide important information for diagnosis of implant associated osteomyelitis.[11] None of these methods provide sufficient means for early detection of implant associated infection which can be helpful for successful treatment of infection without the need to remove the implant and avoid extra medical and surgical expenses. It is also important to monitor the course of infection during treatment to evaluate the success of treatment. After an antibiotic therapy, there is a good chance for the surviving bacteria to slowly re-establish a biofilm[12] which necessitates a need for continuous monitoring of implant-infection during and after the treatment. These methods can be used in parallel with our approach to confirm clinical findings.

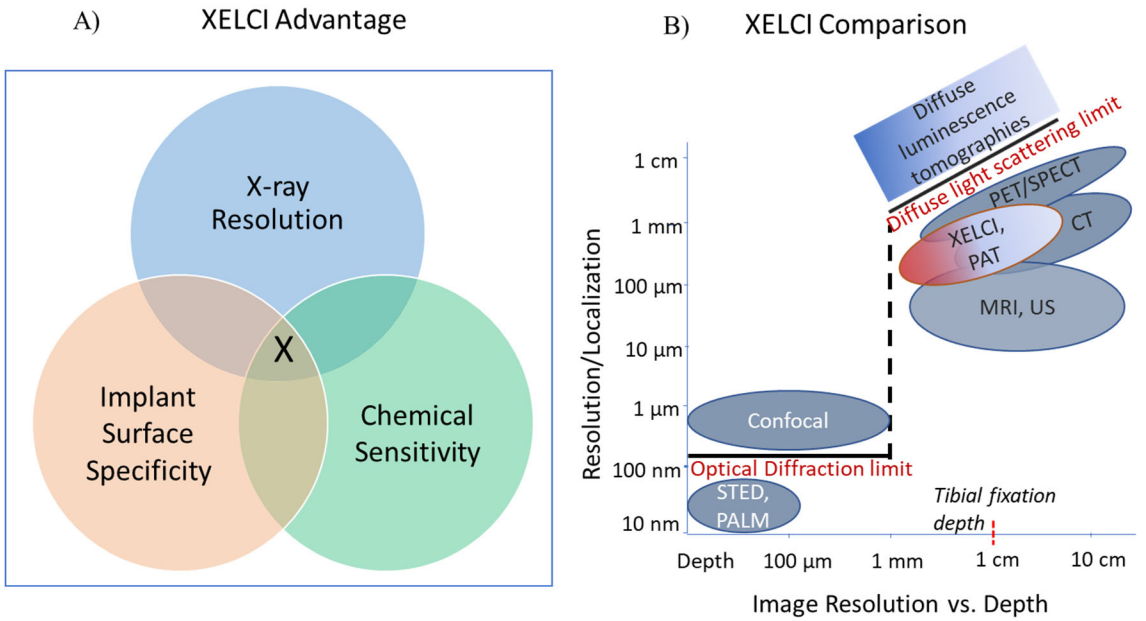

Figure 2.2: XELCI advantage and comparison. A) Venn diagram summarizing the three key features of X-ray excited luminescent chemical imaging (XELCI): X-ray resolution, Implant surface specificity and chemical sensitivity. X represents XELCI. B) Placement of XELCI in comparison to different imaging techniques in terms of image resolution and depth of imaging. Typical tissue thickness for a tibial fixation is indicated for reference.

Figure 2.2 outlines the three key features of XELCI in a Venn diagram and compares it with other imaging techniques in terms of imaging resolution and tissue depth. XELCI sits right next to Photoacoustic Tomography (PAT), Single Photon Emission Computed Tomography (SPECT), Positron Emission Tomography (PET), X-ray Computed Tomography (CT) and Magnetic Resonance Imaging (MRI), and can image through deep tissue at least up to 2 cm thick with high resolution (about 500 µm) unlike fluorescence imaging techniques such as confocal microscopy that provide a higher spatial resolution close to the optical diffraction limit but cannot image through deep tissue (limited to 1 mm thick sample depths). In addition to deep tissue imaging, XELCI provides chemical sensitivity and surface specific information such as localized

pH changes that are specific to the surface of medical implants. Our approach is innovative because no other medical imaging technique measures surface-specific chemical concentrations at high-resolution through thick tissue. Other techniques (e.g., MRI, CT, ultrasound and PET) lack surface-specific pH contrast agents, and optical tomography techniques have poor lateral resolution through tissue (>1 mm thick because tissue scatters and prevents the incident optical beam from focusing).

XELCI can be categorized as functional radiography providing chemical sensitivity coupled with the penetration depth of plain radiography. Figure 2.3 shows a side by side comparison of XELCI with plain radiography. There are three targets in the figure: (1) Different line widths cut out in a black paper that blocks visible light, (2) A radio-opaque metal target (Luck charm) and (3) a 3D printed holder with seven pH sensor discs consisting of scintillator layer and pH sensitive gel at different pHs (Left to right: pH 8, 7, 6, 5, 4 , 3 and a scintillator only reference disc without the pH gel). The pH dye used in these sensor gels had an active range between pH 3-6 and the gels were not pre-leached resulting in different amount of leaching in different buffers, for example, the sensor disc in pH 8 buffer (left most disc) appears lighter in color than the pH 7 and pH 6 discs. The first two target are placed on a glass slide covered with a scintillator layer. Images of these targets were acquired using a digital camera, X-ray radiograph and XELCI first without any tissue and later covered with a piece of 1 cm thick chicken tissue. None of the targets can be seen in the photograph taken with a digital camera when covered with tissue. The X-ray radiography shows 2 out of the 3 targets as it can distinguish the radio-opaque metal target and the x-ray absorbing scintillator film but the

paper target cannot be seen in the radiographs even without tissue. We can see the piece of tissue in the radiograph due to slight attenuation of the X-ray by soft tissue. All the discs in the third target also appears the same and the color and pH of the individual discs cannot be differentiated because we can only visualize the bottom scintillator layer in the pH discs but cannot see the effect of pH on the gel layer of the discs. The XELCI images with and without tissue clearly shows the three targets and provides chemical sensitivity with regards to the pH of the discs. The XELCI images provide high spatial resolution as we can see the lines in the paper target and clearly read the letters of the metal target. The width of the lines in the paper target were 0.2, 0.5, 1 and 2 mm (left to right).

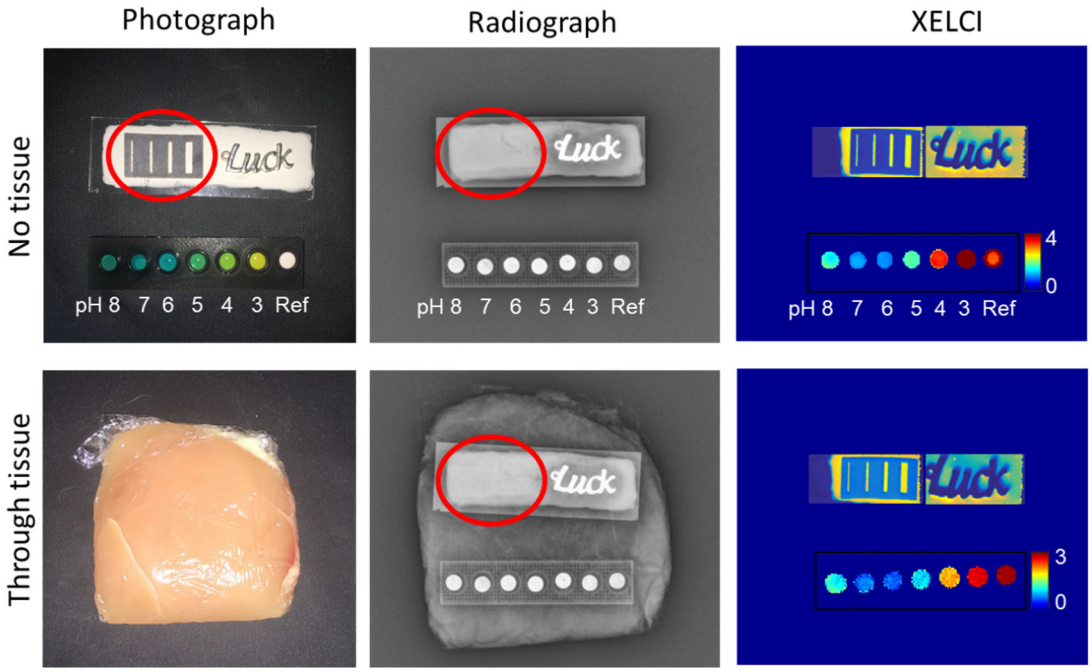

Figure 2.3: Plain radiography vs. functional radiography. Images of three targets acquired using a digital camera, X-ray radiograph and XELCI. Targets were: (1) Different size lines cut out in a black paper (Line widths, left to right: 0.2, 0.5, 1 and 2 mm), (2) A radio-opaque metal target, (3) pH sensor discs consisting of scintillator and pH sensitive gel at different pHs (Left to right: pH 8, 7, 6, 5, 4 , 3 and a scintillator only reference disc without the pH gel). The first two target are placed on a glass slide covered with a scintillator layer.

XELCI can also spectrally distinguish between different types of scintillators with the right optical filters. For example, figure 2.4 shows the photograph and XELCI image intensities of two types of scintillators, Gadolinium oxysulfide terbium doped (Gd_2O_2S:Tb) and Gadolinium oxysulfide europium doped (Gd_2O_2S:Eu). Letters of Tb and Eu were formed using a piece of insulated wire (black) for letters T and E, and pH sensitive gel (green at pH 7) for letters b and u. The scintillator films were made with 1:1 ratio of scintillator particles in Polydimethylsiloxane (PDMS). The Tb doped phosphors have a predominantly green emission (540 nm main peak and smaller peaks at 490, 590 620 and 680 nm) while the Eu doped phosphors have red to near IR emission (620 and 700 nm) as shown in the emission spectrum of both in figure 2.4. The XELCI system is currently set up to detect 620 and 700 nm light intensities. We can see the Tb film appearing much brighter in the ratio XELCI image compared to the Eu film since the Tb film does not have much of the 700 nm intensity. In fact, we expected the 700 nm intensity image to be much darker for the Tb film but we do see some emission. This can be due to the minor peaks around 680 nm in the Tb spectrum and in part due to some cross talk between the PMTs as determined by the efficiency of the filter used to transmit the 700 nm wavelength while blocking the 620 nm intensity for PMT2. Nevertheless, we can differentiate the Tb film from the Eu film while being able to see the radio-opaque wire targets and the pH sensitive gels. This demonstrates both spectral and spatial resolution in the same XELCI image in addition to pH sensitivity with the use of different scintillators in the sensor.

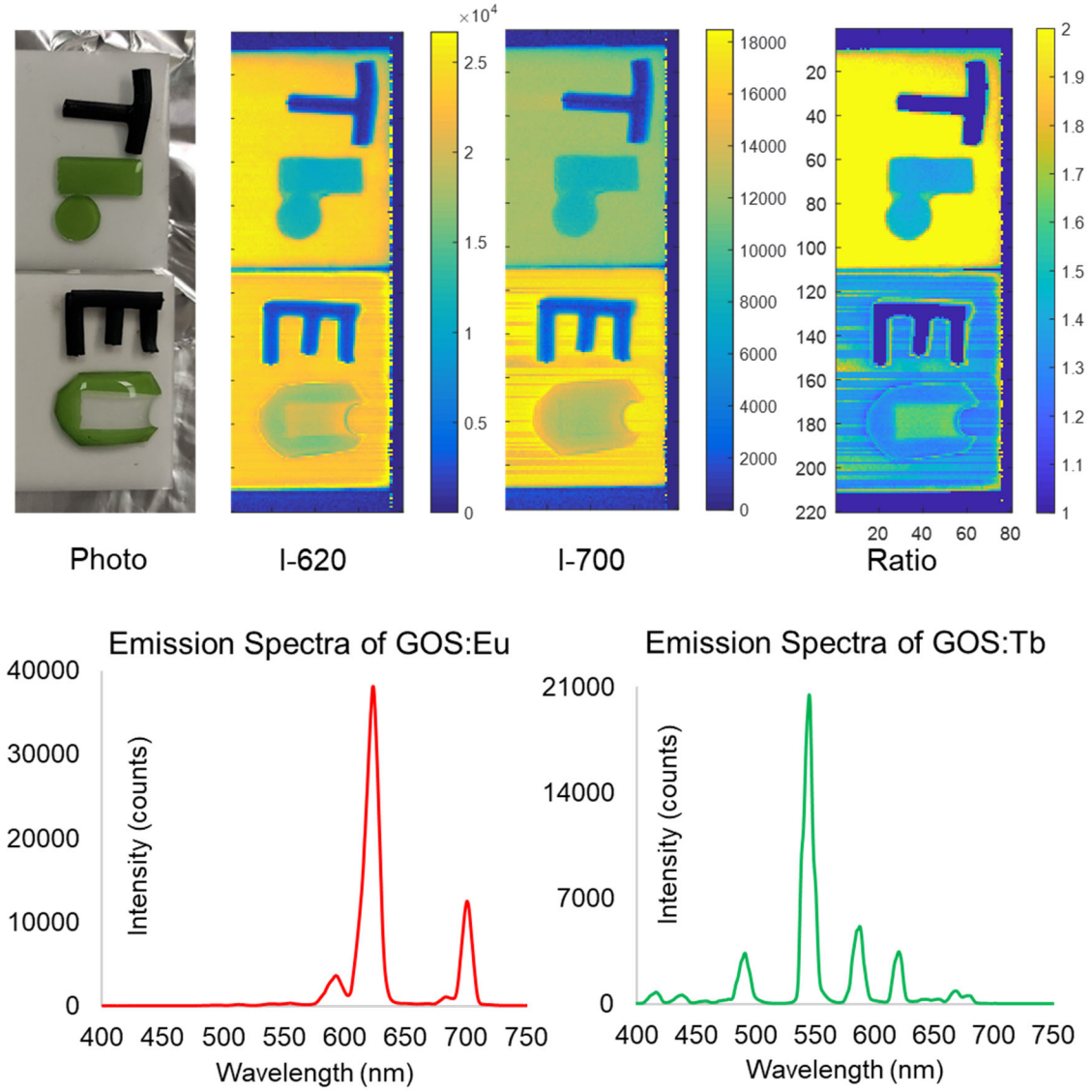

Figure 2.4: Spectral resolution. Two different scintillator films, Gadolinium oxysulfide terbium doped (Tb) and Gadolinium oxysulfide europium doped (Eu) with letters formed using a piece of insulated wire (black) and pH sensitive gel (green at pH 7) were imaged using XELCI. Photograph, 620 nm intensity, 700 nm intensity and ratiometric XELCI images of the films. Emission spectra of scintillators, red line: Eu doped Gadolinium oxysulfide (GOS:Eu), green line: Tb doped Gadolinium oxysulfide (GOS:Tb).

2.4. METHODS

2.4.1. XELCI Imaging

The sample is placed on an x-y-z motorized stage with 30 x 15 x 6 cm travel (Models: LTS300 and LTS150, Thorlabs Inc., Newton, NJ, USA for x and y axis and Motorized Linear Vertical Stage Model AT10-60, Motion Control, Smithtown, NY, USA for the z-stage) and positioned under the focused x-ray beam (iMOXS, Institute for Scientific Instruments GmbH, Berlin, Germany) and detecting optics.

An X-ray beam of 50 keV and 600 μA is focused using a polycapillary lens (5 cm focal distance from capillary tip) and excites the scintillator particles generating luminescence. This luminescence passes through the pH-indicating film which modulates the spectrum according to pH, and some of the light diffuses through the tissue where it is collected using either a liquid light guide (Model 77638, Newport Corporation, Irvine, CA, United States) or an in-house machined acrylic light guide and directed to a splitter. The splitter sends the light to two photomultiplier tubes (PMTs) (Model P25PC-16, SensTech, Surrey, UK) with a band pass filter in front of each (one passing 620 nm light, the other passing 700 nm). The whole setup is enclosed in a light-tight box. Pulses from each PMT are counted using a Data Acquisition (DAQ) board (NI cDAQ™-9171, National Instruments, Austin, TX). The stage position is controlled with a program written in LabVIEW (National Instruments, Austin, TX), which also records PMT counts and stage position versus time, and displayed an image on the computer screen during acquisition.

2.4.2. Data Analysis

A custom LabVIEW program controls the motorized stage and collects both stage position versus time and photon counts versus time for the 620 nm and 700 nm PMTs. From this raw data, custom MATLAB scripts allocate the photon counts per second to specific pixels based on the motor position at the time acquired. The 620 nm and 700 nm signal intensities were displayed as pseudo-colored images after background subtraction for each data set. Ratiometric images were displayed in a similar manner; a threshold intensity at 620 nm and 700 nm used to avoid showing highly noisy pixels. To plot the calibration curves, the average signal intensity for each pH-sensor disc in its particular pH buffer, the 620 nm, 700 nm intensity and ratio was calculated for each chicken slice thickness (0 – 19 mm) and through the human cadaveric tissue. The ratios were then normalized to the reference disc signal for each data set and plotted as a calibration curve on a single graph. Normalization is done by dividing the average ratio values for each pH disc by the average ratio value of the reference disc for the respective tissue thicknesses.

2.4.3. Point Spread Function through Tissue

LED setup: A red LED was set up on a circuit and photographs taken with a Nikon D5500 Digital SLR camera (Nikon Corporation, Japan) with the room light on for the setup photo and in the dark with the LED turned on. The LED was covered with a piece of 1 cm tissue and photographed again in the dark.

X-ray setup: A scintillator film was made with 1:1 ratio of gadolinium oxysulfide europium doped (Gd_2O_2S:Eu) scintillator particles in polydimethylsiloxane (PDMS) on a glass slide. The slide was placed under the focused X-ray beam (iMOXS, Institute for

Scientific Instruments GmbH, Berlin, Germany) at a distance of 5 cm from the tip of the focusing optics. A Nikon digital camera was set up on a stand to remotely take photographs of the scintillator film from above when irradiated by the X-ray beam. The scintillator film was covered with a piece of chicken tissue either 5 mm or 10 mm thick and photographs taken with the camera under X-ray exposure.

Chicken breast tissue was cut into slices of desired thickness using an electric food slicer (Model 630, Chef's Choice, Avondale, PA, USA). Due to the spongy nature of the material, the thickness varied between ±1 mm based on the measurements of the slices tissue.

2.4.4. X-ray Beam Width

A radiochromic film (Gafchromic EBT3-1417, Lot # 09241801, Ashland Global Specialty Chemicals Inc., DE, USA) was roughly cut into small rectangular pieces and places at 5 mm intervals in a 3D printed holder that had 15 slots 5 mm apart. The holder with the pieces of radiochromic film was placed vertically under the X-ray beam with the radiochromic piece in the 0 mm slot directly in contact with the focusing optics (polycapillary) of the X-ray and exposed to the X-ray beam (at 50 kV and 600 μA) for 30 seconds. The spot size was measured in ImageJ.

2.5. SYSTEM OPTIMIZATION

We demonstrated pH imaging through up to 2 cm of chicken tissue and 11 mm of human cadaveric tissue using XELCI as explained in Chapter 3. This tissue thickness range tested for XELCI imaging provides a reasonable range for human tibial

implantation and was greater than the typical tissue thickness measured in most of the in vivo studies (the tissue covering the implant on the rabbit femur was about 1 cm thick). The anatomical thickness of the cadaveric human tissue covering the implant was measured to be 11 mm. A major limitation of the XELCI system was the amount of signal being collected with the liquid light guide especially as observed in the preliminary in vivo experiments (Chapter 5) due to orientation of the embedded sensor in the animal and the time limitation on imaging due to administration of anesthesia to the animal. Since light spreads after passing through tissue, we visualized the point spread function to figure out the area we need to be collecting the light from.

2.5.1. Point Spread Function through Tissue

To visualize the transmittance of light from a point source through tissue, we used a red-light LED and photographed it with a digital camera in the dark and then covered with a piece of 1 cm chicken tissue. The images were analyzed with MATLAB to plot the red-light intensity. The red light from the LED generated a 0.7 mm spot compared to a 20.9 mm spot after passing through 1 cm tissue indicating a spread of about 30x.Figure 2.5 shows the photographs of the LED setup and the images obtained in the dark. The red point is the red LED turned on in the dark when photographed without any tissue and it spreads to about a 2 cm blurred spot when covered with tissue.

Since we are using a focused X-ray beam to generate light in vivo using the red-emitting scintillator layer, the experiment was repeated to get a more realistic idea of the point spread function for XELCI imaging. The scintillator film was set up at 5 cm (optimum focusing distance for the X-ray focusing optics) from the focused x-ray beam

and photographed in the dark with X-ray on. We see the red luminescence spot generated by the X-ray beam as a result of irradiation of the scintillator film in figure 4.6. It appears as the bright cyan color spot in the pseudo color MATLAB image and is plotted to determine the full width half max of the red-light intensity. The spot size was measured to be 0.38 mm. The scintillator film was then covered with a 5 mm and 10 mm (±1 mm) thick piece of chicken tissue and photographed again. We can see the spot size increased from 0.38 mm without any tissue to about 6.5 mm and 8.6 mm after passing through 5 mm and 1 cm thick chicken tissue respectively indicating a point spread of 17 – 22 x.

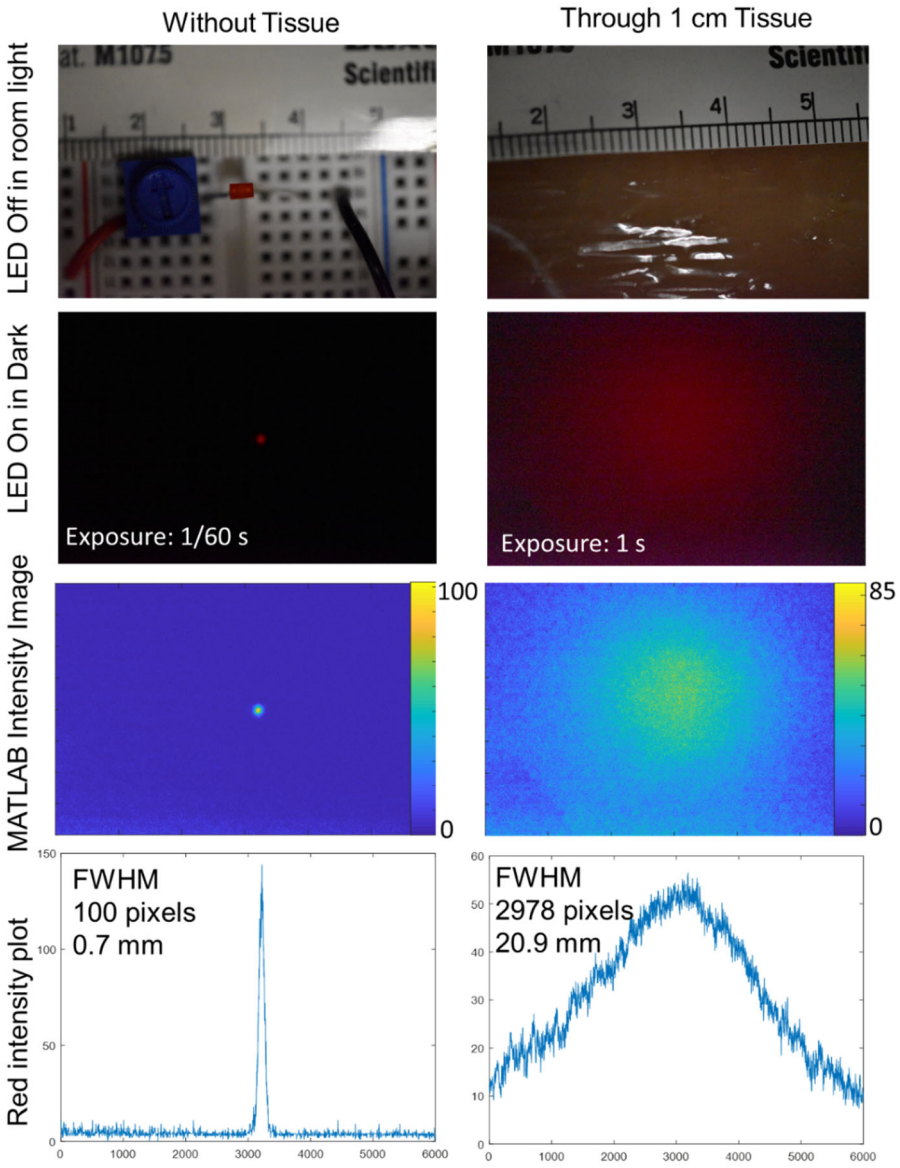

Figure 2.5: Point spread function (LED). Photograph of a red-light LED point source without any covering and covered with a piece of 1 cm thick tissue. LED was turned on and imaged with a digital camera in the dark with and without the tissue covering. Images were analyzed using MATLAB and red-light intensity plotted to calculate the point spread function of the LED point source without and through tissue.

The spot is not uniform after passing through tissue especially through 5 mm thick tissue indicating the inhomogeneity and variation in the chicken tissue thickness.

The increase in the point spread after passing through tissue is evident by the width of the peaks in the intensity plots given in figure 2.6. However, the absolute intensity (counts/pixel) is almost constant due to different exposure times to obtain enough signal for proper analysis but decreases significantly (1000 - 10,000x) when normalized to exposure time (counts/pixel/sec).

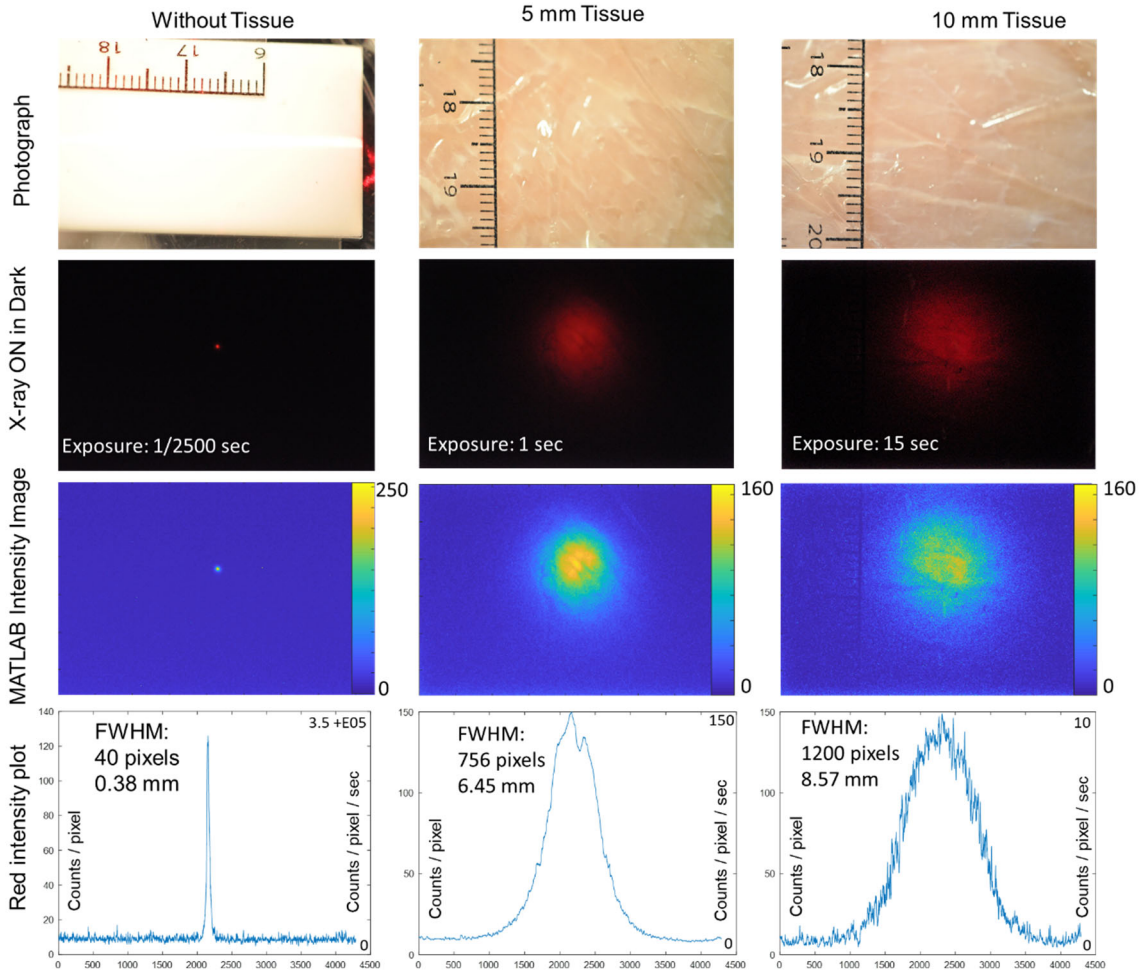

Figure 2.6: Point spread function (scintillator film irradiated with a focused x-ray beam). Photograph of scintillator film without any covering and covered with 5 mm and 1 cm thick pieces of tissue. The scintillator film was irradiated with a focused x-ray beam to generate red light and imaged with a digital camera in the dark with and without the tissue coverings. Images were analyzed using MATLAB and red-light intensity (counts/pixel) plotted to calculate the point spread function of the irradiated spot without and through tissue. FWHM: Full width at half maximum.

2.5.2. Acrylic Light Guide

In the XELCI setup, the X-ray is positioned to come straight from the top directly perpendicular to the sample stage but the liquid light guide collecting the signal was at a slight angle (not completely perpendicular to the sample stage) as it would obstruct the X-ray beam if placed directly under the X-ray beam and the placement of the liquid light guide varied between experiments. For light to propagate through an optical fiber or a light guide, it must enter at an angle less than the maximum acceptance angle to the axis of the light guide. Any light entering the light guide at an angle greater than the acceptance angle will not be able to propagate through and will be lost. With the liquid light guide having a core diameter of 7.6 mm, numerical aperture of 0.52 and acceptance cone of 62°, we were collecting only 19% of the incident light. Another loss comes from refraction between the liquid and the cladding of the liquid light guide. By using a light guide with a large acceptance angle, we can dramatically increase the signal collection by collecting light from more angles after it is being scattered through the tissue. Acrylic (Polymethyl methacrylate) in air essentially accepts everything with a maximum acceptance angle of 90° and we can theoretically collect about 5x more signal using the same diameter acrylic rod as with the liquid light guide. We can also collect light from a larger area by increasing the core diameter. As indicated by the point spread function experiment, the light can diffuse to a spot size of up to 2 cm after passing through tissue and with a 7.6 mm core diameter light guide, we were not able to collect all the signal. Figure 2.7 shows a schematic and a 3D rendering of the XELCI system with a horizontal acrylic rod as the light guide. In addition to offering the advantage of collecting more

light with a greater acceptance angle, the acrylic light guide can be placed almost in close contact with tissue and increasing the core diameter of the acrylic rod to collect light from a larger area. It can also be aligned with the X-ray beam in a straight line by having an alignment hole in the elbow shaped mirror attachment that collects and reflects the signal into the acrylic rod.

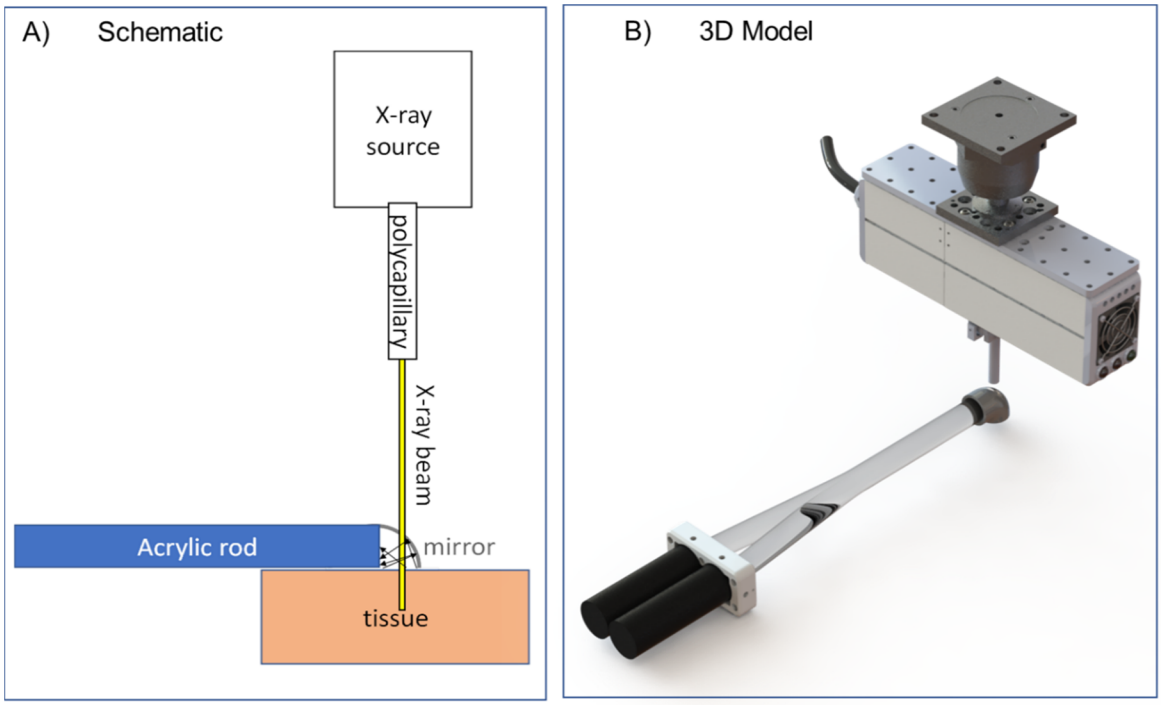

Figure 2.7: Optimized XELCI setup. A) Schematic of the optimized XELCI system with a horizontal acrylic light guide for signal collection. B) SOLIDWORKS 3D rendering of (A).

Figure 2.8 shows the experimental setup of the XELCI system with both the liquid light guide and the acrylic light guide. We can see the better and more consistent alignment of the acrylic light guide with the X-ray polycapillary (focusing optics) compared to that of the liquid light guide that has to be placed at an angle. The acrylic

light guide has a core diameter of 2 cm compared to 7.6 mm for the liquid light guide. The acrylic light guide consists of an encased acrylic rod that is coupled to 2 PMTs using an acrylic splitter. The collection end of the acrylic light guide has a 3D printed elbow with a mirror finish on the inside and a hole in the top to line up with the X-ray. PMT1 collected all wavelengths while PMT2 had an optical filter to pass the 700 nm light and filter out 580 – 660 nm wavelengths. XELCI with the liquid light guide set up had both PMTs equipped a filter with PMT1 collecting the 620 nm and PMT2 collecting the 700 nm light. The MATLAB code to plot the data as images representative of the 620 nm, 700 nm and the ratio intensities was modified to reflect this change of light collection filters. The in vivo studies imaged with this optimized system showed considerable improvement in the signal to noise ratio that is obvious in the images as discussed in Chapter 6. Briefly, the XELCI images taken with the optimized system were clear, sharp with a clean background (no speckles) and high signal to noise ratio as the signal intensities for 620 and 700 nm were much higher for the data collected using the acrylic light guide compared to the data collected with the liquid light guide. The scanning time was also reduced as the implant could be located during one low resolution scan and imaged at a higher resolution for the final scan eliminating the need for multiple scans over a larger area to locate the implant through the tissue.

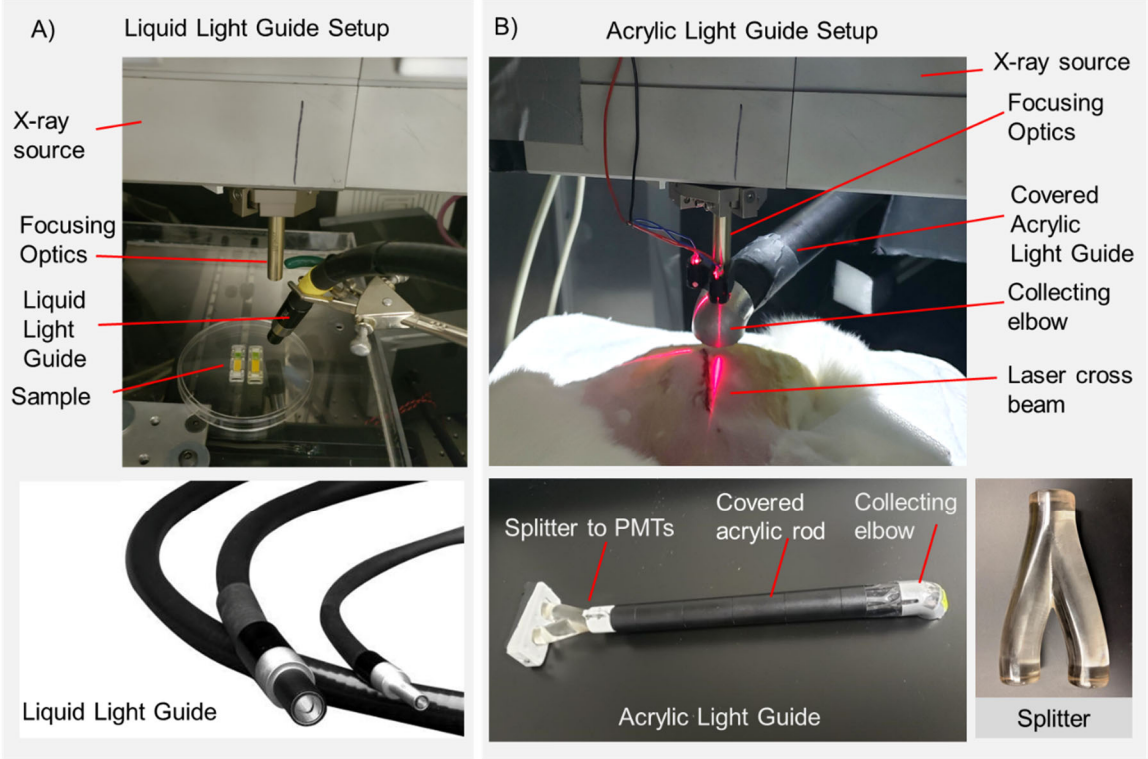

Figure 2.8: Comparison of initial and optimized XELCI system. A) XELCI setup with the liquid light guide to collect signal. B) XELCI setup with the acrylic light guide to collect signal with a light splitter to couple the acrylic light guide to the PMTs.

2.6. SYSTEM CHARACTERIZATION

2.6.1. X-ray Beam Width and Intensity

The X-ray source is fitted with a polycapillary that focus the X-ray beam to a fine spot. We characterized the spot size of the X-ray beam as a function of height to find the optimum distance where the X-ray beam is best focused. A radiochromic film (Gafchromic) was used to visualize the X-ray beam spot. Radiochromic films are self-developing films containing a dye that changes color when exposed to ionising radiation,

thus allowing the level of exposure and beam profile to be characterized. Figure 2.9A shows the experimental setup where the radiochromic films are lined up under the X-ray beam at 5 mm intervals starting at a height of 0 mm from the polycapillary to 7 cm below it. The radiochromic films were exposed simultaneously for 30 seconds to an X-ray beam of 50 kV and 600 μA (same as used for XELCI imaging). The spot size is plotted as a function of height in figure 2.9B and a photograph of the radiochromic films after exposure visualizing the X-ray beam spot is shown in figure 2.9C. The X-ray beam has a width of 4.16 mm when it exits the polycapillary at 0 mm that gradually decreases and is focused to a fine spot of 0.36 mm at a vertical distance of 5 cm from the polycapillary. The beam width starts increasing again after 5 cm. Therefore, 5 cm is the optimum imaging distance between the sample and the X-ray polycapillary to make sure the X-ray beam is properly focused. This is in agreement with the spot size (0.38 mm) calculated using the FWHM of the red-light intensity spot generated on the scintillator film when irradiated by a focused X-ray beam at a distance of 5 cm (figure 2.6). However, we expect the actual X-ray beam width to be slightly smaller than the spot size generated on the scintillator film as the thickness of the scintillator film can also diffuse the light generated by the X-ray beam. XELCI collects the signal generated from point by point excitation of the scintillator film with the X-ray beam and the width of the X-ray beam is the key factor in determining the spatial resolution.

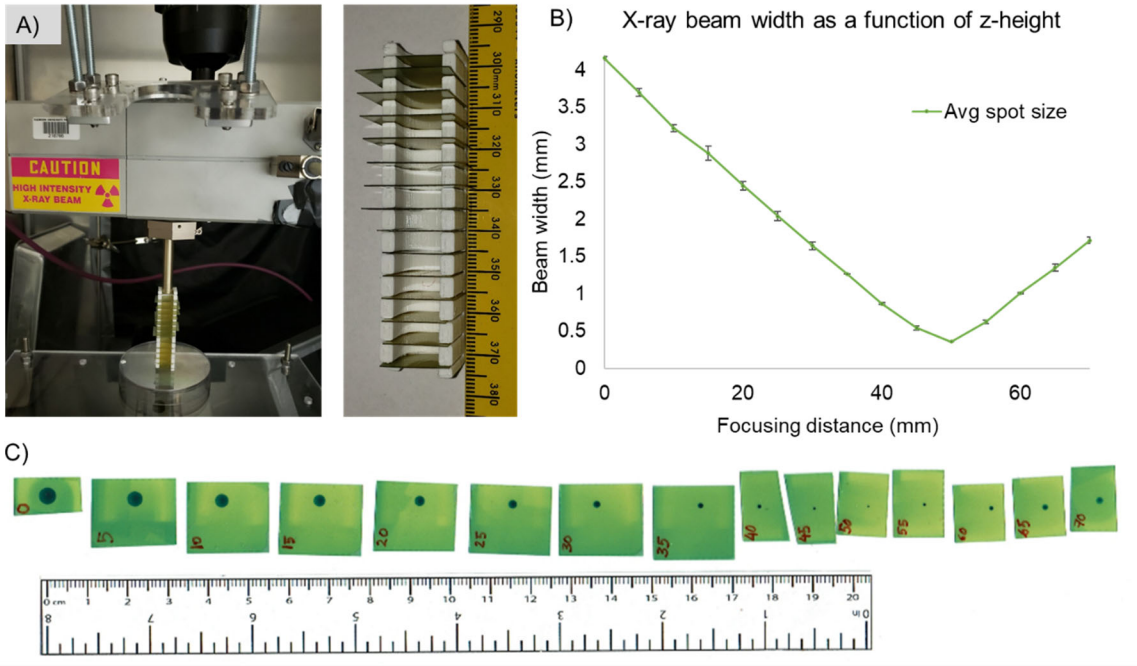

Figure 2.9: Determination of X-ray beam width at different heights. A) Photograph of the experimental setup. Pieces of radiochromic film were lined up at different heights in a 3D printed holder and placed under the X-ray focusing optics. B) Plot of the spot size generated by the X-ray beam at different heights. C) Photograph of the spot sizes generated by the focused X-ray beam at different heights.

The intensity of the X-ray beam at the focusing height (5 cm) was also determined by comparing the radiochromic film with the exposure calibration reference of the same film provided by the manufacturer. At a scan speed of 5 mm/sec with a stepsize of 250 µm, the local absorbed dose was found to be 50 rad or 0.5 Gy and it depends on the scanning speed, stepsize and duration of the scan. This is below the limit for causing cutaneous radiation injury also known as radiation burns that can occur from a radiation dose as low as 2 Gy.[13] The 0.5 Gy dose represents the localized dose absorbed at the skin and will be much lower within the muscle tissue underneath the skin as we are using a relatively lower energy X-ray beam (50keV). However, to compare the X-ray dose from

XELCI, we need to convert this localized absorbed dose to an average full body effective dose. Since, we are using the imaging for rabbits that weighed an average of 5 Kg and assuming the imaging area to be 1 cm^2, we get a mass of about 1g of tissue within which all the X-ray energy will be deposited giving us a full body average dose of 0.1 mSv. This is typical of a chest X-ray exam that is about 70x less than that of a chest CT scan (7 mSv). Standard radiographic exams range from 0.01 – 10 mSv while CT scans can have an effective radiation dose of 2 – 20 mSv.[14]

2.6.2. Spatial Resolution

Spatial resolution is a measure of the smallest feature that can be resolved or distinguished in space. In microscopy, it is defined as the shortest distance between two points on a specimen that can still be distinguished by the observer or camera system as separate. Due to high penetration depth of the X-ray beam with minimum increase from X-ray scattering in the tissue, we expect XELCI to have high spatial resolution mainly limited by the width of the X-ray beam. A line target was prepared by cutting out lines of defined width in a black (optically absorbing) paper and imaged with XELCI though tissue and without any tissue covering. The lines had a width of 2.3 mm, 1.3 mm, 0.9 mm and 0.5 mm. A photograph of the line target placed on the scintillator film and the 620 nm intensity XELCI images of the target scanned with and without tissue are shown in figure 2.10 along with the intensity plots. We can clearly see all the lines in the XELCI images for both with and without tissue. The signal is plotted as an intensity plot for the area shown by the red rectangle in the XELCI images in 2.10 B and E. The areas

containing the cut out lines in the paper allowed transmittance of optical signal as indicated by the peaks and the area that was covered with black paper did not allow the signal to pass (valleys in the intensity plot). To determine the knife edge resolution for 20–80% intensity transition, the falling edge of the 2.3 mm line peak was selected (zoomed in, figure 2.10 D and G). The 20–80% intensity transition occurred over a distance of 400 μm for without tissue and 550 μm with tissue. The spatial resolution should not vary with or without tissue as it is determined by the X-ray beam width and the observed slight difference could be due to positioning of the target as it appears to be the case in the XELCI image (figure 2.10 E) where the target might not be completely flat on the scintillator film. Analysis of the rising edge for the 1 mm line gives the 20–80% knife edge resolution to be 450 μm for tissue. Same experiment was performed with liquid light guide before optimizing the XELCI system with the acrylic light guide and the 20–80% knife edge resolution was calculated to be 475 μm ± 50 μm that is almost the same as the 20–80% knife edge resolution (400-450 μm) with the acrylic light guide as it does not depend on the collection optics but only on x-ray beam width.

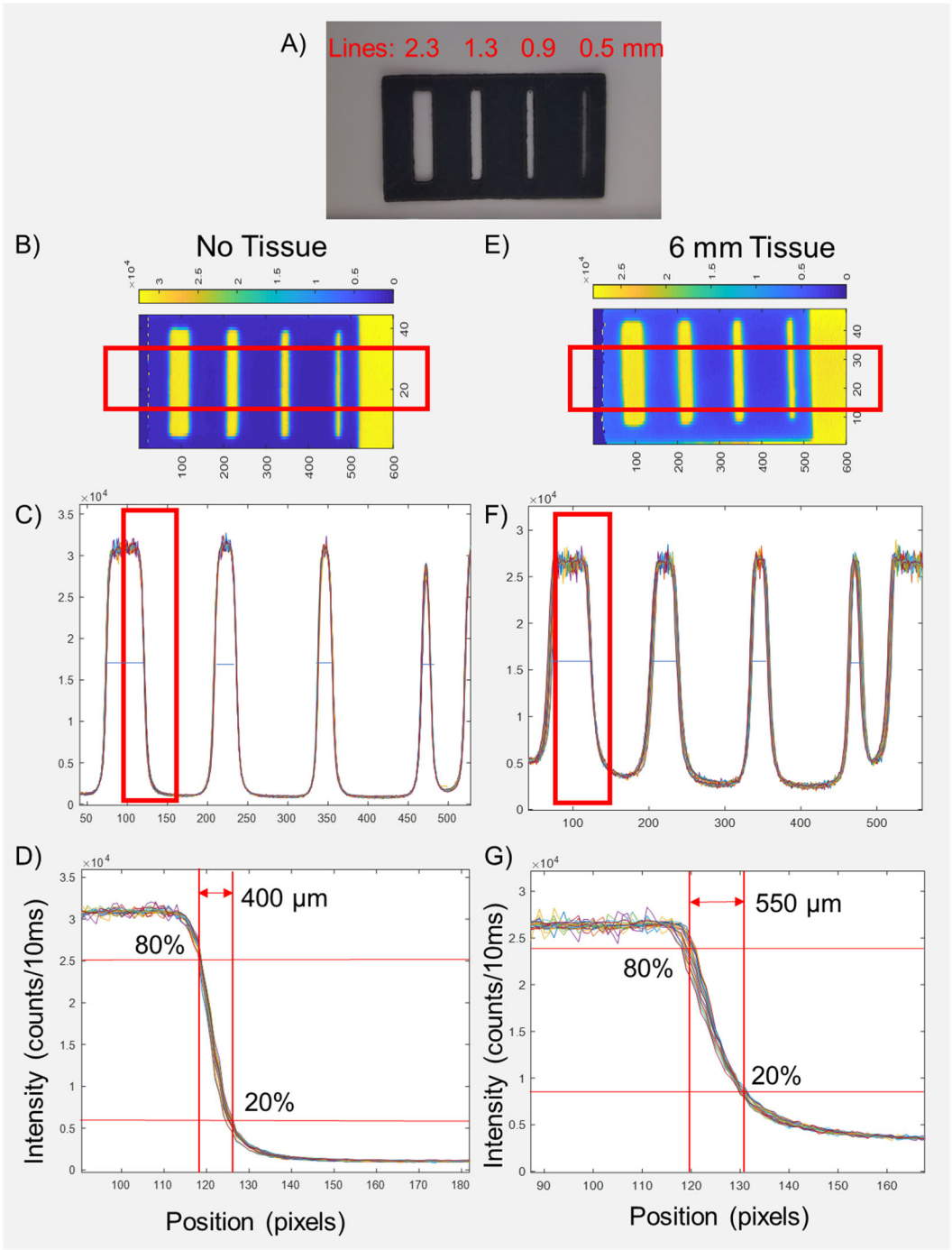

Figure 2.10: Spatial resolution. A) Black paper with lines of different width cut using a laser cutter. B) 620 nm intensity images of the line target imaged using XELCI covered with 6 mm of tissue and without any covering. C) Intensity plots of the images in (B). D) Close up view of intensity plots in (C) showing the intensity change for the 2 mm wide line to calculate 80-20 knife edge resolution.

2.7. CONCLUSION

X-ray excited luminescent chemical imaging (XELCI) is a novel technique to map chemical concentrations on the surface of medical devices embedded in tissue. It combines the spatial resolution of X-ray with surface specific chemical sensitivity for deep tissue imaging. The system was characterized in terms of X-ray beam width and spatial resolution. The X-ray beam can be focused to a 0.36 mm fine spot for point by point excitation of the sample. The spatial resolution of the XELCI images is limited exclusively by the width of the X-ray beam and was determined to be about 400 μm. The point spread function of light from a point source passing through tissue was characterized and the XELCI system optimized to collect more signal by increasing the core diameter and the acceptance angle of the signal collecting light guide. We applied XELCI to non-invasively image surface pH to monitor pH changes during implant associated infection.

2.8. REFERENCES

(1) Esmonde-White, K. A.; Esmonde-White, F. W. L.; Holmes, C. M.; Morris, M. D.; Roessler, B. J. Alterations to Bone Mineral Composition as an Early Indication of Osteomyelitis in the Diabetic Foot. *Diabetes Care* **2013**, *36* (11), 3652–3654. https://doi.org/10.2337/dc13-0510.

(2) Abu-Amer, Y.; Darwech, I.; Clohisy, J. C. Aseptic Loosening of Total Joint Replacements: Mechanisms Underlying Osteolysis and Potential Therapies. *Arthritis Res. Ther.* **2007**, *9* (Suppl 1), S6. https://doi.org/10.1186/ar2170.

(3) Konttinen, Y. T.; Takagi, M.; Mandelin, J.; Lassus, J.; Salo, J.; Ainola, M.; Li, T.-F.; Virtanen, I.; Liljeström, M.; Sakai, H.; Kobayashi, Y.; Sorsa, T.; Lappalainen, R.; Demulder, A.; Santavirta, S. Acid Attack and Cathepsin K in Bone Resorption Around Total Hip Replacement Prosthesis. *J. Bone Miner. Res.* **2001**, *16* (10), 1780–1786. https://doi.org/10.1359/jbmr.2001.16.10.1780.

(4) Milošev, I.; Levašič, V.; Vidmar, J.; Kovač, S.; Trebše, R. PH and Metal Concentration of Synovial Fluid of Osteoarthritic Joints and Joints with Metal Replacements. *J. Biomed. Mater. Res. B Appl. Biomater.* **2017**, *105* (8), 2507–2515. https://doi.org/10.1002/jbm.b.33793.

(5) Synovial Fluid pH as an Indicator of Infected Joint Arthroplasty http://www.orthoteers.org/(S(i0lr3tzi44ui4vqos04fxuch))/owls.aspx?section=37&article=196 (accessed Apr 23, 2020).

(6) Ward, T. T.; Steigbigel, R. T. Acidosis of Synovial Fluid Correlates with Synovial Fluid Leukocytosis. *Am. J. Med.* **1978**, *64* (6), 933–936. https://doi.org/10.1016/0002-9343(78)90446-1.

(7) Bono, M. J.; Reygaert, W. C. Urinary Tract Infection. In *StatPearls*; StatPearls Publishing: Treasure Island (FL), 2020.

(8) Yuqing, M.; Jianrong, C.; Keming, F. New Technology for the Detection of PH. *J. Biochem. Biophys. Methods* **2005**, *63* (1), 1–9. https://doi.org/10.1016/j.jbbm.2005.02.001.

(9) Gou, P.; Kraut, N. D.; Feigel, I. M.; Bai, H.; Morgan, G. J.; Chen, Y.; Tang, Y.; Bocan, K.; Stachel, J.; Berger, L.; Mickle, M.; Sejdić, E.; Star, A. Carbon Nanotube Chemiresistor for Wireless PH Sensing. *Sci. Rep.* **2015**, *4* (1), 4468. https://doi.org/10.1038/srep04468.

(10) Frost, M. C.; Meyerhoff, M. E. Implantable Chemical Sensors for Real-Time Clinical Monitoring: Progress and Challenges. *Curr. Opin. Chem. Biol.* **2002**, *6* (5), 633–641. https://doi.org/10.1016/S1367-5931(02)00371-X.

(11) Trampuz, A.; Zimmerli, W. Diagnosis and Treatment of Infections Associated with Fracture-Fixation Devices. *Injury* **2006**, *37 Suppl 2*, S59-66. https://doi.org/10.1016/j.injury.2006.04.010.

(12) Broekhuizen, C. a. N.; Sta, M.; Vandenbroucke-Grauls, C. M. J. E.; Zaat, S. a. J. Microscopic Detection of Viable Staphylococcus Epidermidis in Peri-Implant Tissue in Experimental Biomaterial-Associated Infection, Identified by Bromodeoxyuridine Incorporation. *Infect. Immun.* **2010**, *78* (3), 954–962. https://doi.org/10.1128/IAI.00849-09.

(13) Wagner, L. Radiation Injury Is a Potentially Serious Complication to Fluoroscopically-Guided Complex Interventions. *Biomed. Imaging Interv. J.* **2007**, *3* (2). https://doi.org/10.2349/biij.3.2.e22.

(14) Mettler, F. A.; Huda, W.; Yoshizumi, T. T.; Mahesh, M. Effective Doses in Radiology and Diagnostic Nuclear Medicine: A Catalog. *Radiology* **2008**, *248* (1), 254–263. https://doi.org/10.1148/radiol.2481071451.

3. NONINVASIVELY IMAGING pH AT THE SURFACE OF IMPLANTED ORTHOPEDIC DEVICES WITH X-RAY EXCITED LUMINESCENCE CHEMICAL IMAGING (XELCI).

The material in this chapter was published as a journal article: U Uzair, D Benza, CJ Behrend, JN Anker, ACS Sensors 2019 4(9), 2367–2374 doi:10.1021/acssensors.9b00962

3.1. ABSTRACT

Implanted medical device-associated infections are a leading cause of fixation failure and early diagnosis is key to successful treatment. During infection, acidosis near the implant plays a role in antibiotic resistance and low pH is a potential infection indicator. Herein, we describe a pH sensor which attaches to implants to noninvasively image local pH with high spatial resolution. The sensor has two layers: a scintillator layer which emits 620 and 700 nm light upon X-ray irradiation, and a pH Indicator layer containing bromocresol green dye that absorbs 620 nm luminescence in neutral/basic pH and passes 700 nm light at all pH. We also developed a dedicated imaging system capable of scanning relatively large specimens through thick tissue. A focused X-ray beam irradiates one spot on the sensor, and the 620 to 700 nm peak ratio is measured to determine local pH; images are acquired by scanning the X-ray beam across the surface and measuring pH point-by-point. The sensor was covered with varying thickness slices of chicken breast tissue (0-19 mm) to evaluate how tissue affects peak intensity and ratio. Thick tissue attenuated both 620 nm and 700 nm light, with more attenuation at 620 nm than 700 nm. Although this spectral distortion shifted the pH calibration curve, the effect could be corrected for using a scintillator film region with no pH-indicator layer as a

spectral reference. The sensor was attached to an orthopedic plate affixed to a human cadaveric tibia and imaged through tissue. The approach provides both high spatial resolution from focused X-ray excitation, and surface chemical specificity from the indicator dye providing a tool for imaging local pH through tissue.

3.2. INTRODUCTION

As the population ages, orthopedic devices are increasingly used to treat fractures and replace joints. While the devices improve mobility and quality of life, infection is a significant risk despite improvements in surgical procedures (e.g., short operating times, clean room environment and administration of perioperative local antibiotic prophylaxis). In the US, about 2 million fracture-fixation devices are inserted annually, and nearly 5% of these become infected with an average estimated cost of $15,000 for medical and surgical treatment together.[1,2] Open fractures have higher chances of infection after fixation (>30%) as compared to closed fractures (1-2%);[3,4,5] other risk factors include diabetes, smoking, and immunodeficiency states. Implants increase both the risk and severity of infections as pathogens can form biofilms on implants which are resistant to antibiotics and the host's immune system. If the infection can be diagnosed near its onset, treatment through surgical debridement and antibiotics without implant removal is often successful;[6] however, mature biofilms usually require implant removal followed by reinsertion of the medical device after the infection is eradicated.[7,8] Sensors are needed at nidus of infection on the implant surface for early detection monitoring treatment, and for elucidating the local biochemical milieu to rationally develop therapeutics.

Common signs of infection include fever, pain, redness, swelling, as well as elevated blood levels of C-reactive protein (CRP) and erythrocyte sedimentation rates (ESR), but these are not specific for implant infection and can also occur for systemic infection.[9] Another challenge is to differentiate between septic and aseptic loosening of implant and in the case of chronic infection, clinical signs and symptoms of infection may be entirely absent.[10] Histopathological testing of intraoperative tissue, radiology and bone scans are all used in conjunction to diagnose implant associated infection but lack high sensitivity and specificity.[11] In many cases, infections are obvious based on sinus tracts, discharge, radiolucence near implants, and other signs and symptoms, but there are also cases where physicians are uncertain, even intraoperatively.

We are developing a pH sensor to non-invasively detect, monitor, and study implant associated infection in situ using X-ray excited luminescence chemical imaging (XELCI). pH is selected as target analyte because local acidosis (from the acidic products from bacterial metabolism and immune cells) cause a drop in pH, especially in dormant and poorly perfused regions, and is indicative of infection.[12,13] Local acidosis plays a role in immune response and antibiotic effectiveness, and is a potential therapeutic target based on drug release in infected acidic regions, or pH restoration.[14] It is also a potential indicator for implant infection diagnosis and monitoring. pH in infection has been reported to depend on the environment, for example, in well mixed synovial joint fluid, it correlates with white blood cell count and threshold for infection is decrease from pH 7.5 to 7.[15] In osteomyelitis or implant loosening, it can drop to as low as pH 4 and cause formation of brushite and bone erosion [16, 17, 18] while within the biofilm it maybe

heterogeneous with local acidosis at base of biofilm even if surroundings are neutral.[19] Since the behavior depends on the context, sensors are needed at nidus of persistent infection at the surface of the implant under the biofilm to detect, understand and treat the infection.

XELCI uses a combination of focused X-ray excitation and optical emission to image chemical concentrations on the surface of implanted sensors which can be coated or attached to implanted medical devices. When the sensors are irradiated with an X-ray beam, the sensor's scintillator layer generates luminescence and its pH-indicator film absorbs some of this light which modulates the spectrum according to pH. The approach combines the chemical sensitivity and surface specificity of an optical pH indicator film with the low background and high spatial resolution of scanning X-ray excited optical luminescence imaging. A variety of luminescence studies have been performed with optical sensor films based on fluorescence,[20–23] surface enhanced Raman spectroscopy (SERS),[24] upconversion,[25–27] and other techniques that can respond to various physical and chemical stimuli such as pH, temperature, pressure, ions, light and humidity.[28] While these can provide average chemical measurements, optical scattering of the excitation and emission light in thick tissue limits the spatial resolution and is approximately the depth of the tissue or worse.[29] This low resolution prevents observation of small and localized acidic regions during infection and treatment or spatially distinct sensor and reference regions to account for spectral distortion and detect multiple analytes with multiple sensors.

In previous studies, we have shown proof of principle for XELCI measurement of pH concentrations in silica-coated glass slides imaged in vitro through 6 mm of chicken breast tissue using a microscope-coupled spectrograph.30 We were able to observe a spatially separate sensor region and observed a pH drop during in vitro bacterial culture followed by pH neutralization after antibiotic treatment.[30] Herein we developed a clip that can be added to an orthopedic tibial plate with a more robust hydrogel-based sensor, developed a dedicated scanning X-ray system measuring optical transmittance at two wavelengths, studied effect of chicken breast tissue thickness up to 19 mm thick, and demonstrated imaging on a human cadaveric tibia (which is larger, has more attenuating tissue, and more medically relevant). By more efficiently collecting light and scanning, the system could acquire 40 x 40 mm^2 images in 15 minutes with a pixel size of 300 μm at a higher resolution and through thicker samples compared to a 7.5 x 7.5 mm^2 image in the same time with a microscope (over 20-fold faster). The hydrogel was far more robust than the fragile glass coverslip previously used. Unlike the microscope system, the sample was imaged from the same side as the incident X-ray, and sample size could be increased to allow imaging of cadaveric samples and future rabbit studies.

3.3. METHODS

All experiments were performed at room temperature and atmospheric pressure unless noted otherwise. All chemical reagents were purchased from Sigma-Aldrich (St. Louis, MO) and standard buffer solutions from VWR (Radnor, PA) unless otherwise indicated. Following buffers were used: BDH5014 (pH 3.00 ± 0.01 at 25°C, containing potassium hydrogen phthalate, hydrochloric acid), BDH5024 (pH 4.00 ± 0.01 at 25°C,

containing potassium hydrogen phthalate), BDH5034 (pH 5.00 ± 0.01 at 25°C, containing potassium hydrogen phthalate, sodium hydroxide), BDH5038 (pH 6.00 ± 0.01 at 25°C, containing potassium phosphate monobasic, sodium phosphate dibasic), BDH5052 (pH 7.00 ± 0.01 at 25°C, containing potassium phosphate monobasic, sodium phosphate dibasic), BDH5060 (pH 8.00 ± 0.01 at 25°C, containing potassium phosphate monobasic, sodium phosphate dibasic) and PBS 10X Solution (J373) diluted to 1X (pH 7.2 – 7.4 at 25°, containing 137 mM NaCl, 2.7 mM KCl, 9.8 mM Phosphate buffer).

3.3.1. Sensor Fabrication

The sensor consists of two layers. A bottom layer of scintillator particles (Gd_2O_2S:Eu) encapsulated in polydimethylsiloxane (PDMS), and a pH-sensitive top layer synthesized from biocompatible polyethylene glycol (PEG) hydrogel incorporating the pH-indicator dye bromocresol green (BCG). Both the pH-sensing film and scintillating particles are placed in a 3D printed holder made from polylactic acid (PLA) that can be attached to the orthopedic plate.

3.3.2. Sensor Fabrication

The sensor consists of two layers. A bottom layer of scintillator particles (Gd_2O_2S:Eu) encapsulated in polydimethylsiloxane (PDMS), and a pH-sensitive top layer synthesized from biocompatible polyethylene glycol (PEG) hydrogel incorporating the pH-indicator dye bromocresol green (BCG). Both the pH-sensing film and scintillating particles are placed in a 3D printed holder made from polylactic acid (PLA) that can be attached to the orthopedic plate.

3.3.3. Scintillator layer

Silicone elastomer and curing agent (SYLGARD™ 184 Silicone Elastomer base and curing agent, Dow Corning, Midland, Michigan, United States) were mixed in 10:1 (w/w) ratio and ~8.0 µm diameter Gd_2O_2S:Eu scintillator particles (UKL63/N-R1, Phosphor Technologies Inc., Stevenage, England) were added in 5:1 (w/w) ratio to form a final mixture of 5 g scintillator particles per 1 g of PDMS. This mixture was spread on a glass slide and cured in the oven at 100 °C to form about 1 mm thick scintillator-PDMS layer. It was cut into either 5 mm or 7 mm discs using a hole puncher.

3.3.4. pH sensitive layer

To synthesize the hydrogel films, a solution was prepared containing 79% (w/w of sol.) 700 MW polyethylene glycol diacrylate (PEGDA), 9.9% (w/w of sol.) glycerol, 9.9% (w/w of sol.) water, 0.8% (w/w of sol.) photoinitiator (2,2-dimethoxy-2-phenylacetophenone) and 0.4% (w/w of sol.) bromocresol green (pH-indicating dye). This mixture was stirred on a magnetic plate for 30 minutes and the resulting solution was drop coated and sandwiched between two clean cover slips and cured under UV for 2 minutes. The films were immersed in water to swell and delaminate from the coverslips and washed several times before cutting into discs of desired size using hole punchers.

3.3.5. Characterization of pH-indicating film

Spectra were obtained for the pH dye free in solution and encapsulated in the hydrogel at different pH. For the free dye, a solution of the dye was prepared in ethanol (1 mg/ml) and 20 µl of this dye solution was added to 2 ml of standard buffers of pH 3 - 8

and spectra obtained. A 96 well plate was prepared with the pH film samples kept in 100 µl of each pH buffer solution from pH 3 to 8 for at least two hours to reach maximum response and spectra obtained for each pH with a spectrometer (DNS 300, DeltaNu, Laramie, WY, United States). For reversibility study, a 5 mm pH film was fixed to a sample holder and cycled between pH 4 and phosphate saline (~pH 7.2) buffers. Spectra was acquired on the same spectrometer every 1 second for a total of 30 minutes in each buffer and repeated for 5 cycles. To measure the attenuation of the scintillator emission signal by the pH dye, the sensor (a piece of pH film covered by scintillator film) immersed in standard buffer solution was placed on the stage of an inverted microscope (DMI 5000, Leica Microsystems, Germany) and irradiated with a focused x-ray beam. The pH modulated emission of the scintillator film was collected by a 5X objective lens and focused to a spectrometer (DNS 300, DeltaNu, Laramie, WY, USA), equipped with a cooled CCD camera (iDUS-420BV, Andor, South Windsor, CT, United States). Spectra were collected for each pH after immersing the pH film in the respective buffers.

3.3.6. XELCI Setup

Figure 3.1 shows the setup schematic. The sample is placed on an x-y-z motorized stage with 30 x 15 x 6 cm travel (Models: LTS300 and LTS150, Thorlabs Inc., Newton, NJ, USA for x and y axis and Motorized Linear Vertical Stage Model AT10-60, Motion Control, Smithtown, NY, USA for the z-stage) and positioned under the focused x-ray beam (iMOXS, Institute for Scientific Instruments GmbH, Berlin, Germany) and detecting optics.

An X-ray beam is focused using a polycapillary lens (5 cm focal distance from capillary tip) and excites the scintillator particles generating luminescence. This luminescence passes through the pH-indicating film which modulates the spectrum according to pH, and some of the light diffuses through the tissue where it is collected using a liquid light guide (Model 77638, Newport Corporation, Irvine, CA, United States), collimated with a lens, and directed to a beam splitter. The beam splitter sends the light to two photomultiplier tubes (PMTs) (Model P25PC-16, SensTech, Surrey, UK) with a band pass filter in front of each (one passing 620 nm light, the other passing 700 nm). The whole setup is enclosed in a light-tight box. Pulses from each PMT are counted using a Data Acquisition (DAQ) board (NI cDAQ™-9171, National Instruments, Austin, TX). The stage position is controlled with a program written in LabVIEW (National Instruments, Austin, TX), which also records PMT counts and stage position versus time, and displayed an image on the computer screen during acquisition. The scanning process and signal processing is explained in our previous work.[31]

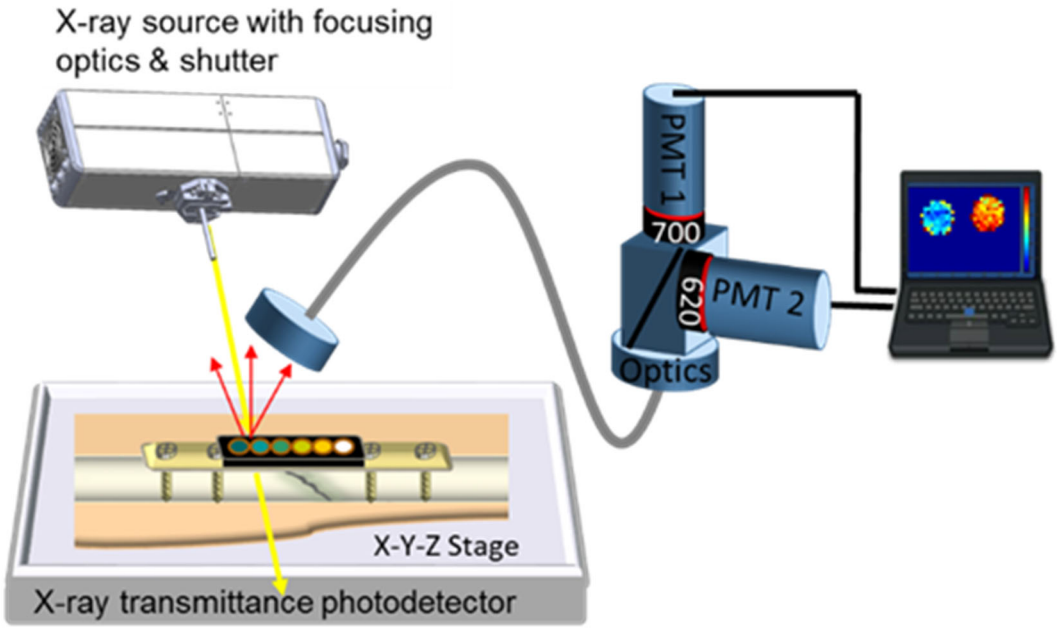

Figure 3.1: Schematic drawing of the XELCI experimental setup. The sample is placed on an x-y-z motorized stage and irradiated with a focused X-ray beam. The luminescence signal is transmitted via liquid light guide to two photomultiplier tubes (PMTs), measuring light intensity at 620 nm and 700 nm respectively. The intensities and ratios are monitored as the stage scans, with real time image shown on the computer screen.

3.3.7. Imaging through Tissue

Chicken breast tissue was cut into slices of desired thickness using an electric food slicer (Model 630, Chef's Choice, Avondale, PA, USA). A 5 mm thick slice of chicken breast tissue was wrapped in clear plastic and placed on the stage. The 3D printed holder containing 5 pH sensor discs (in pH buffers 4, 5, 6, 7 and 8) and a reference disc as well as a reference strip was placed on top of the tissue and scanned from the top using XELCI. The XELCI imaging was repeated after adding another slice of chicken breast tissue (either 1, 3, 5, 7, 9, 11, 13, 15, 17 or 19 mm thick) over top of the

sensor. From this data, calibration curves could be plotted showing peak ratio and intensity vs. pH and depth.

3.3.8. Imaging through Human Cadaveric Tissue

The pH sensor discs were placed in a 3D printed holder and incubated with pH 4, 5, 6, 7, and 8 using respective pH buffers. The holder was attached on a tibial orthopedic plate affixed to a cadaveric human tibia with an induced fracture. The cadaveric tissue covering the top of the orthopedic plate was cut off to allow for imaging of the sensor discs without tissue. This tissue flap (about 11 mm thick) was then placed back over the sensor discs and imaged again using XELCI to obtain the signal intensity at each pH through the human cadaveric tissue.

3.3.9. pH Reversibility

To observe reversible pH changes through the tissue, two adjacent wells on the 3D printed holder were selected. One well contained the reference disc (with no pH film) and the second well contained a pH sensor disc. The pH of the second well containing the pH sensor disc was cycled between pH 4 and pH 7 using the respective pH buffers to show reversibility imaged through the human cadaveric tissue using XELCI for each case.

3.3.10. Data Analysis

A custom LabVIEW program controls the motorized stage and collects both stage position versus time and photon counts versus time for the 620 nm and 700 nm PMTs. From this raw data, custom MATLAB scripts allocate the photon counts per second to

specific pixels based on the motor position at the time acquired. The 620 nm and 700 nm signal intensities were displayed as pseudo-colored images after background subtraction for each data set. Ratiometric images were displayed in a similar manner; a threshold intensity at 620 nm and 700 nm used to avoid showing highly noisy pixels. To plot the calibration curves, the average signal intensity for each pH-sensor disc in its particular pH buffer, the 620 nm, 700 nm intensity and ratio was calculated for each chicken slice thickness (0 – 19 mm) and through the human cadaveric tissue. The ratios were then normalized to the reference disc signal for each data set and plotted as a calibration curve on a single graph. Normalization is done by dividing the average ratio values for each pH disc by the average ratio value of the reference disc for the respective tissue thicknesses.

3.4. RESULTS AND DISCUSSION

3.4.1. Sensor Characterization

The sensor attaches to an implant surface and has two components: an X-ray scintillator layer (Gd_2O_2S:Eu microphosphors in a PDMS film) covering a metal implant surface (or clip which can attach to an implant), and a pH-sensitive film (bromocresol green in a PEG hydrogel) covering the scintillator film (Figure 3.2a). Under irradiation, the X-ray excited optical luminescent signal has very low background from tissue unlike most fluorescence-based measurements through tissue.[32] The luminescence spectrum is modulated by the pH indicator film: In neutral and basic conditions, the bromocresol green film appears blue and strongly absorb 620 nm light from the scintillators, while in acidic media, the film appears yellow and transmits most 620 nm light (Figure 3.2b); absorption at 700 nm is minimal regardless of pH. Figure 3.2c shows how this pH-

dependent absorption modulates the X-ray excited luminescence spectrum acquired through the indicator layer. Taking a ratio between 620 nm and 700 nm peaks normalizes the data to account for pH-independent variation in X-ray intensity and optical collection efficiency. Figure 3.2c inset shows peak ratio versus pH.

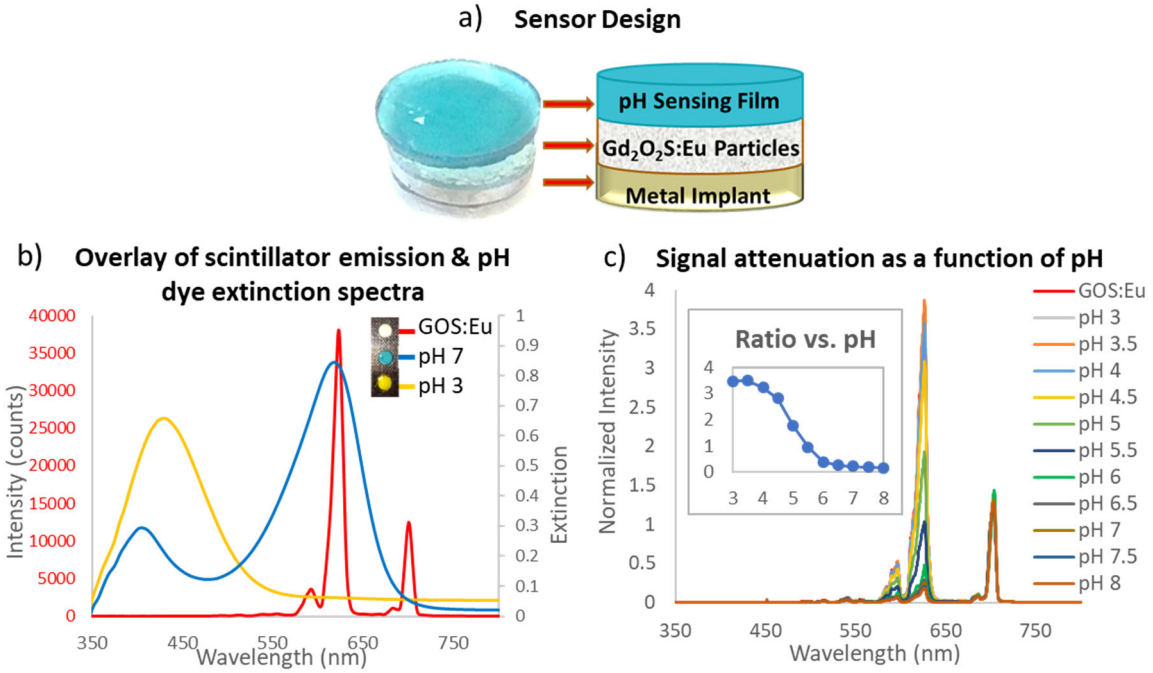

Figure 3.2: Sensor design. (a) The sensor consists of two layers: A top pH-indicating film made of PEG hydrogel with encapsulated BCG dye. A bottom layer of scintillating particles (Gd_2O_2S:Eu) encapsulated in PDMS and covered by the pH sensing film. (b) Luminescence spectrum of scintillators (Gd_2O_2S:Eu) (red line, right y-axis) and the extinction spectra of BCG-doped PEG films in pH 3.0 buffer (yellow line, left y-axis) and pH 7.0 buffer (blue line, left y-axis). Inset: Sensor discs (scintillator + pH film) showing color change at acidic pH (yellow), physiological pH (blue-green) and reference disc (white) containing only scintillators with no pH film covering it. (c) Attenuation of the scintillator emission signal by the BCG pH dye in PEG hydrogel at different pH. Inset: Ratio of 620 and 700 nm intensities plotted for each pH (ratio vs. pH on log scale available in ESI, S2).

The sensor has is able to distinguish from pH 4-6. The curve is shifted by about 1 pH unit compared to free dye because the hydrogel alters the local microenvironment and effective pKa[24,33] Interestingly, after encapsulation we observe a small spectral blue-shift to the protonated absorption peak and a red-shift to the deprotonated peak. This indicates that the dye in the gel experience a different local environment which affects the absorption photophysics, although we do not know the specific mechanism. Full absorption spectra of the film and dye as a function of pH and the inset of ratio vs. pH (log scale) are shown in Figures 3.3 and 3.4. The sensor is reversible and has a τ90% time constant of approximate 25 minutes going from pH5 to pH 7.4 and 5 minutes going from pH 7.4 to pH 5 (Figure 3.5), which is adequate for most in vivo applications where pH shifts over hours.

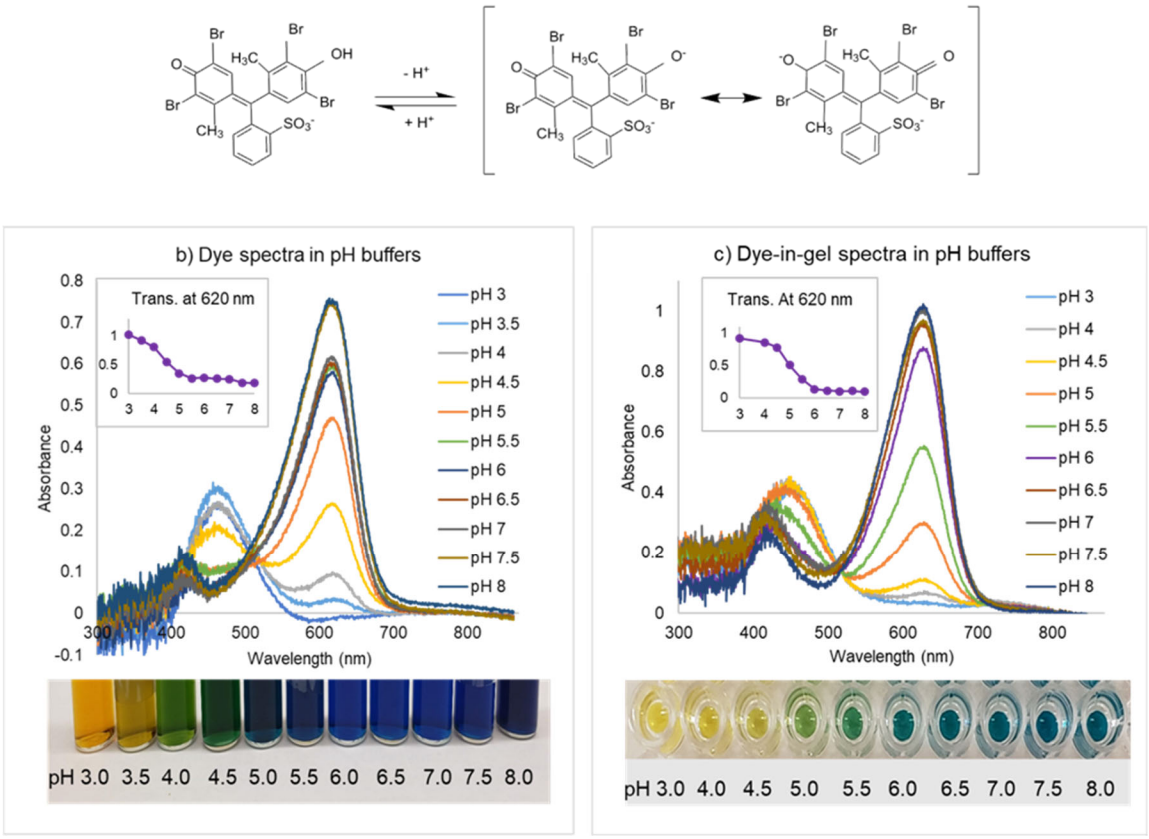

Figure 3.3: Absorption spectra of bromocresol green (BCG) pH dye as a function of pH. (a) Molecular structure of BCG. (b) Absorption spectra of the pH dye in free form (aqueous solution) taken at different pH (3-8) and photographs showing color change at the respective pH. Inset: Transmittance of BCG dye at 620 nm in different pH. (b) Absorption spectra of the pH dye encapsulated in the hydrogel taken at different pH (3-8) and photographs showing color change at the respective pH. Spectra shown is the average from 3 sample films per pH. Inset: Transmittance of BCG dye-in-gel at 620 nm in different pH.

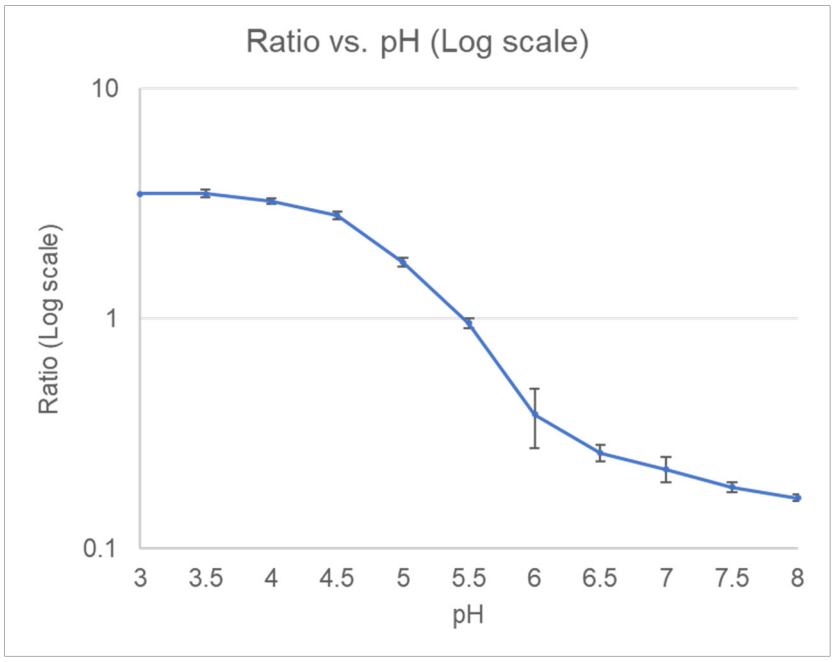

Figure 3.4: Ratio vs. pH. Attenuation of the scintillator emission signal by the pH dye (bromocresol green) in PEG hydrogel at different pHs. Ratio of 620 and 700 nm intensities plotted on a log scale for each pH with 0.5 pH unit intervals. Error bars represent standard deviation of 3 samples at each pH.

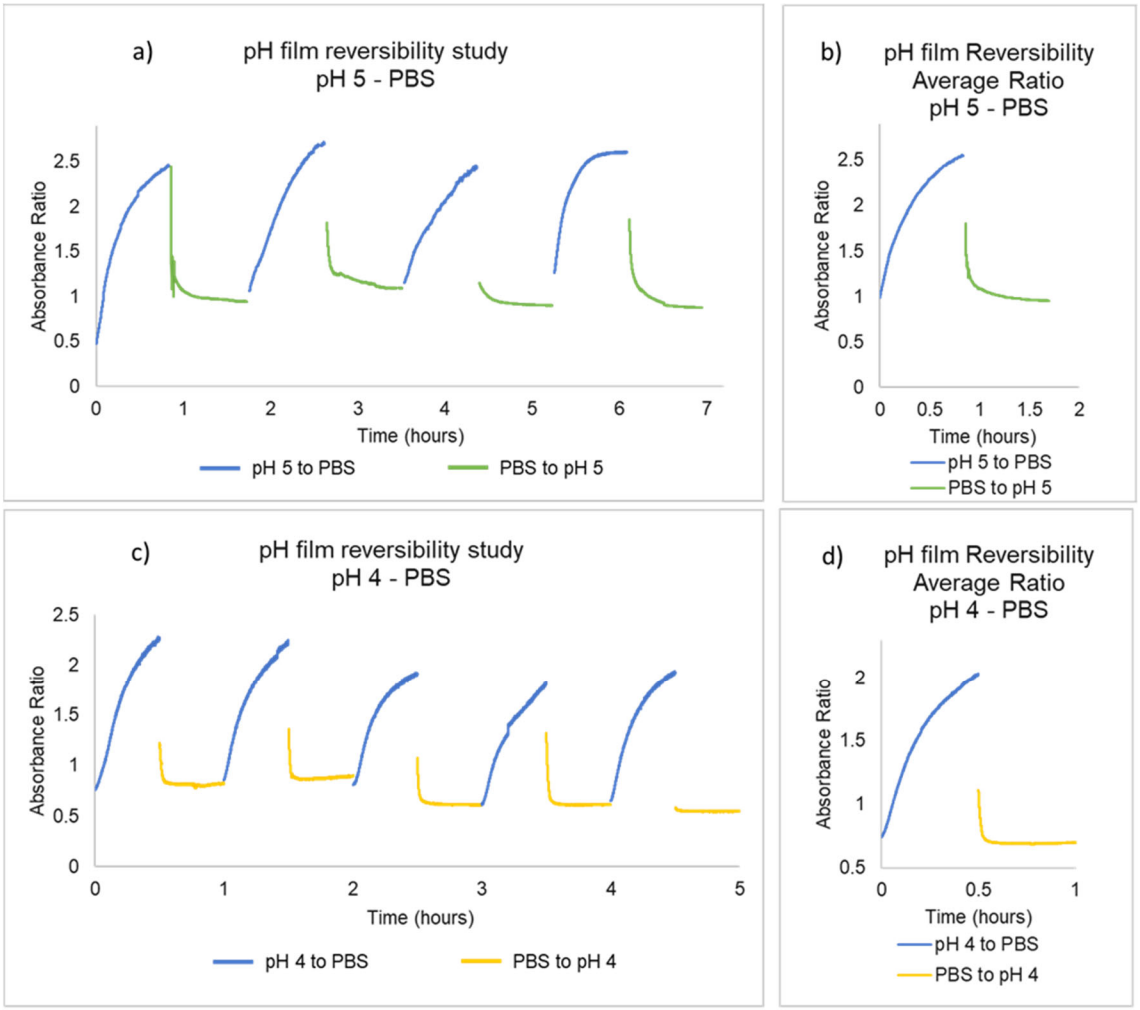

Figure 3.5: Reversibility study of the pH sensor film (PEG hydrogel with bromocresol green pH dye). (a) Phosphate buffered saline solution (PBS, pH 7.4) was added to the pH film that was initially kept in water and spectra recorded every 1 second for a total of 50 minutes. The film was cycled between PBS and pH 5 buffer and spectra recorded for 50 minutes in each buffer. The film did not reach the initial absorbance as it started in a more acidic medium (leaching of free acid from gel into the unbuffered water) but cycles between green (in pH 5 buffer) and blue (in PBS). (b) Average absorbance ratio of the 4 cycles in (a). (c) pH film was cycled between PBS and pH 4 buffer and spectra recorded every 1 second for 30 minutes in each buffer. (d) Average absorbance ratio of the 5 cycles in (c). Gaps correspond to times when the pH buffers were being changed and spectra acquisition was paused to prevent artefacts during pipetting of buffer solutions.

We designed the sensor using biocompatible materials minimizing the toxicity associated with potential leaching of the pH indicator dye, and photoinitiator by an initial pre-leaching treatment (Figure 3.6). PEG is widely used in tissue engineering applications because of its hydrophilicity, resistance to protein adsorption and customizability by modification of the chain length and addition of functional groups.[34,35] The gadolinium particles enclosed in PDMS do not leach out or dissolve even in 1 M sulfuric acid. Gadolinium (Gd) compounds are used as contrast agents in MRI and the amount of Gd used in the sensor (18 mg of Gd_2O_2S:Eu per 1 cm^2 of area) is less than the recommended dose for MRI (0.1 mM of Gd-chelate per kg of body weight).[36]

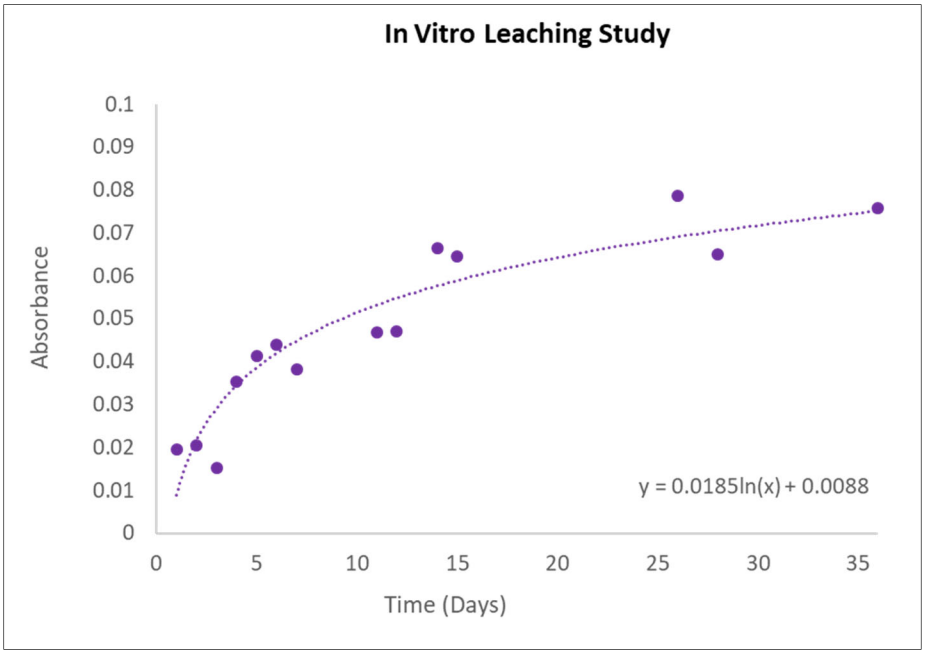

Figure 3.6: In vitro leaching study: Plot showing accumulative absorbance (at 610 nm) of the bromocresol green dye leaching from a18x18 mm piece of sensor gel kept in 10 ml of phosphate saline buffer (pH 7.4) over a period of 36 days with less than 10% of the total dye leached. Data was fitted to a logarithmic trendline.

3.4.2. Effect of Tissue Thickness on Signal Intensity

pH calibration curves were collected through a series of chicken breast tissue thicknesses (0-19 mm). Six 5 mm sensor discs were placed together on a clip and imaged using XELCI: one disc was a spectral reference with no pH-indicator film; the other five discs were pH-sensors in standard pH buffers at pH 4.0, 5.0, 6.0, 7.0, and 8.0 (Figure 3.7). The discs changed color from yellow at low pH to blue at high pH, with a white reference disc with no pH film (Figure 3.7a). Similarly, the XELCI 620/700 nm ratio images show decreasing ratio going from acid to base (increasingly blue in pseudo-colored ratio images, Figure 3.7c). When the clip was covered with tissue, the tissue obscured the clip from view in the photo, but the clips were readily apparent in the XELCI ratio image. With increasing tissue thickness, the 620 nm/700 nm ratio decreased at all pH (due to stronger tissue absorption at 620 nm), evident as a "blue shift" in the pseudo colored ratio images. The underlying 620 nm and 700 nm images are shown in Figure 3.8, and the average values are shown in Figure 3.9. Absolute intensity depends on several factors including alignment of optics, PMT sensitivity, scintillator film thickness and tissue thickness/properties. However, the spectral peak ratio accounts for these variations. For example, Figure 3.9a-b shows that both 620 and 700 nm light was above the trendline intensity through 9 mm of tissue, (about 1.4 times higher than expected at pH 4); however, the ratio of 620 nm to 700 nm light was consistent with other curves (Figure 3.9c-d). At any given thickness, the sensors in basic media consistently absorbed more 620 nm than 700 nm light and the 5 mm discs were clear through even 19 mm of tissue.

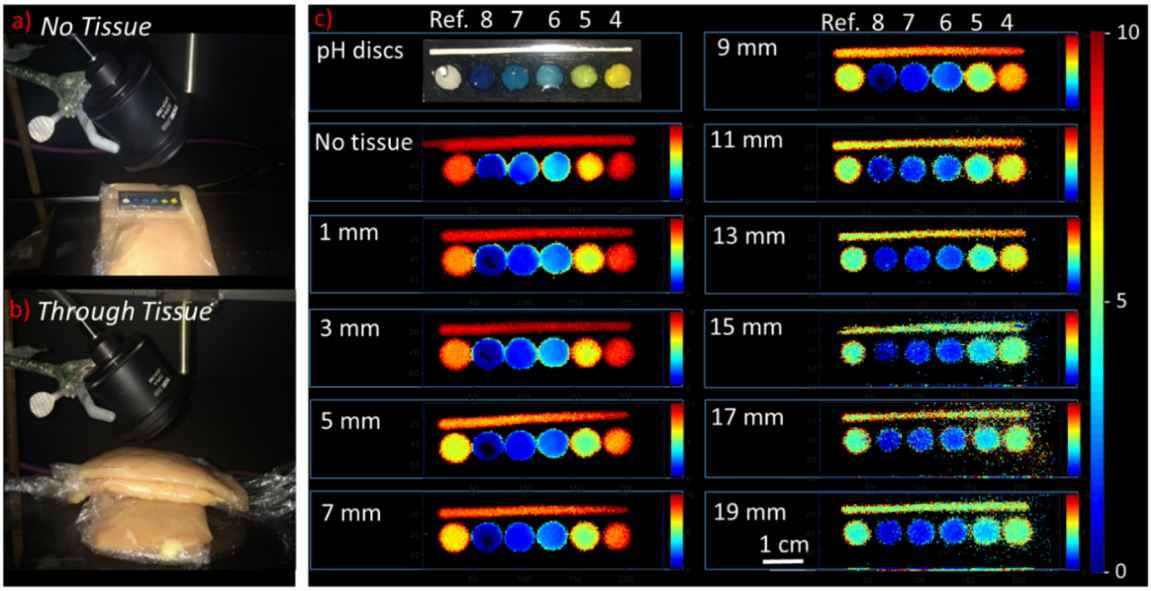

Figure 3.7: Imaging pH through varying tissue thickness. (a) Photo of pH sensor discs placed on a piece of tissue. (b) Photo of pH sensor discs sandwiched between two slices of chicken breast tissue. Thickness of the top slice was increased from 1 – 19 mm with 2 mm intervals. (c) Photograph of pH sensor discs (7 mm in diameter) placed in a 3-D printed holder in pH buffers 8, 7, 6, 5 and 4 and a reference disc without any pH coating. A reference strip is placed along the length of the holder to account for variation in signal intensity caused by variation in tissue thickness. Ratiometric XELCI images (ratio of 620 nm and 700 nm intensities) of the pH sensor discs at respective pH obtained without tissue and through 1 – 19 mm of chicken tissue.

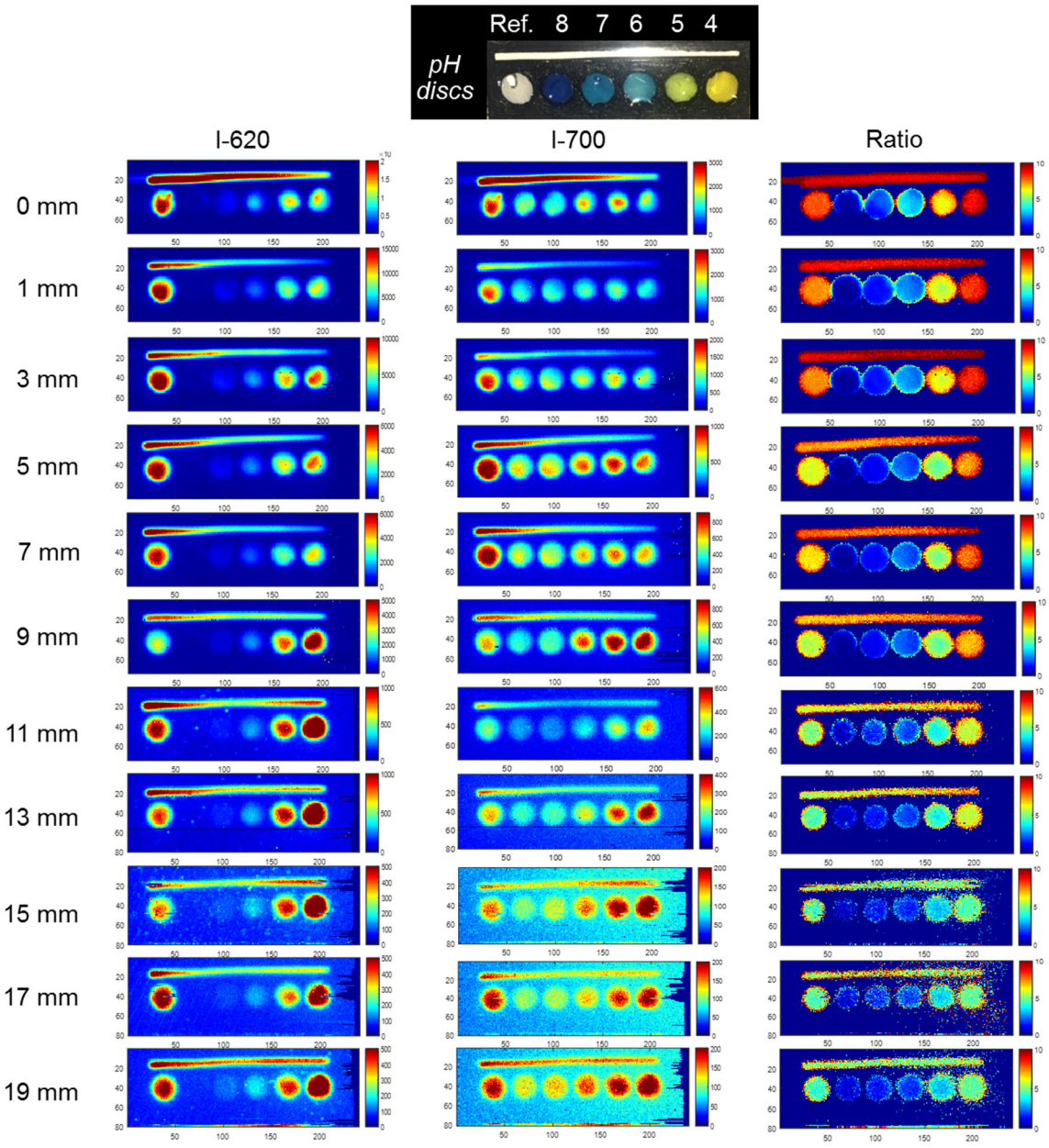

Figure 3.8: Sensor images of signal intensities through chicken tissue. Photograph showing the pH sensor discs placed in a 3-D printed holder in pH buffers 8, 7, 6, 5 and 4 and a reference disc without any pH coating. The holder was sandwiched between two pieces of chicken tissue and thickness of the top piece was increased from 1 – 19 mm with 2 mm intervals. XELCI images showing the 620 nm, 700 nm and ratio of 620 to 700 nm signal intensities of the pH sensor discs at respective pH obtained without tissue and through 1 – 19 mm of chicken tissue.

To quantify how the 620 nm, 700 nm and ratio signal changed with tissue thickness, we calculated the average intensity for each pH disc (Figure 3.9). Luminescence intensity at both wavelengths decreased exponentially with tissue thickness due to a combination of X-ray attenuation and optical absorption in the tissue (with a long path length due to multiple optical scattering events). The 620 nm light was more rapidly attenuated: After passing through 19 mm of tissue, the reference disc's average luminescence intensity decreased to 2.6% of its intensity without tissue at 620 nm, and to 6.1% at 700 nm. Similar attenuation was observed for all the pH-indicating discs (Figure 3.9c). This spectral distortion implies that tissue has a higher effective attenuation coefficient, μeff, at 620 nm than 700 nm, which is expected from its higher underlying absorption coefficient, μa, and slightly higher reduced scattering coefficient, μs. For example, Marquez and co-workers found that μeff in chicken breast tissue depended on the sample and muscle fiber orientation but ranged between 0.56 – 1.28 cm^{-1} at 620 nm with an average of 0.99 cm^{-1} and 0.35 – 0.85 cm^{-1} at 700 nm with an average of 0.57 cm^{-1}.[37] These average values suggest a loss of 1.74 times more at 620 vs 700 nm per cm and is consistent with the chicken data reference intensity values observed in our experiments corresponding to a loss of 1.58 – 1.95 times in going from 0 to 9 mm and from 0 to 11 mm of chicken tissue, respectively.

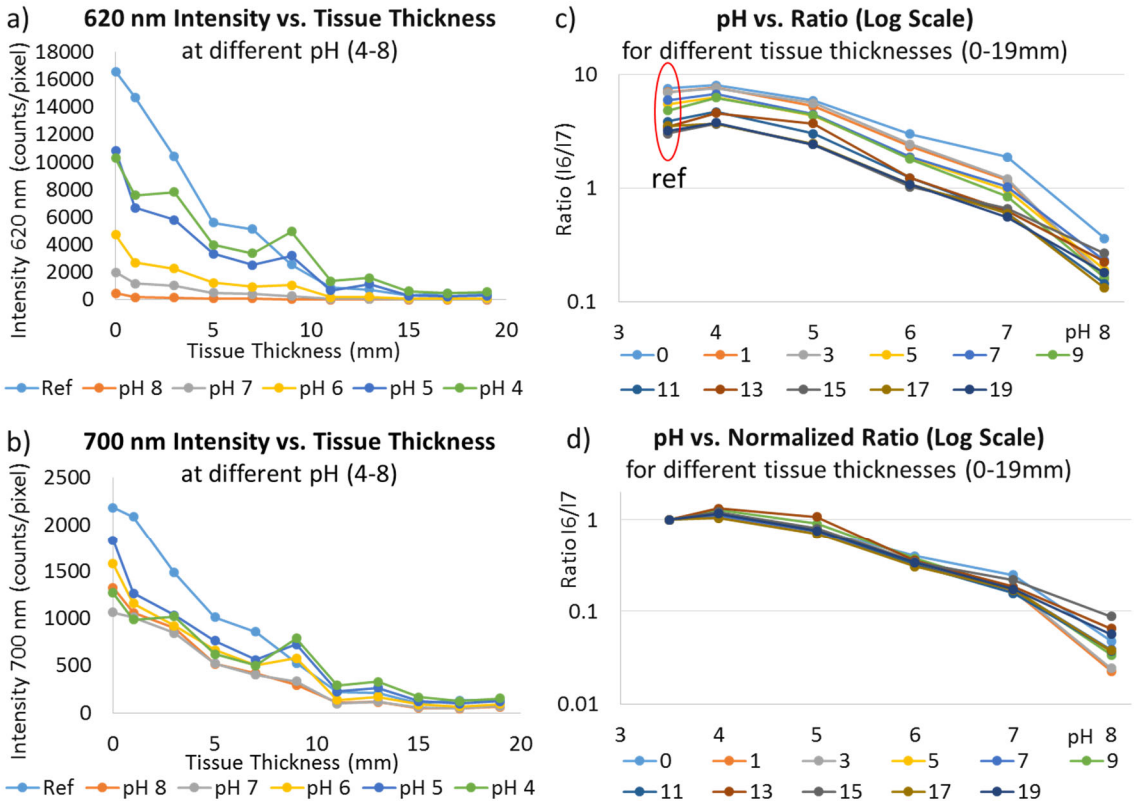

Figure 3.9: Effect of tissue thickness on signal intensity. (a) 620 nm light intensity vs. tissue thickness (0 – 19 mm) at pH 4, 5, 6, 7, 8 and uncoated reference. (b) 700 nm light intensity vs. tissue thickness (0 – 19 mm) at pH 4, 5, 6, 7, 8, and uncoated reference. (c) Ratio of 620 and 700 nm intensities for each tissue thickness (0 – 19 mm) at pH 4, 5, 6, 7 and 8. Note y-axis log scale. Reference is pH-independent and represents maximum signal intensity in absence of pH dependent absorption and was plotted at an arbitrary pH of 3.5. (d) Plot (c) normalized to reference value. All tissue intensities (0 – 19 mm) show good overlap at different pH except for pH 8 due to relatively weak signal intensity and higher signal to noise ratio at pH 8. Note y-axis log scale.

Since the spectral distortion at any given tissue thickness was consistent for all pH, the reference disc spectrum could be used to measure and account for this distortion. The reference disc consists of only scintillator layer without a pH sensitive gel layer and is not affected by pH changes. It represents the maximum signal intensity in absence of any pH dependent absorption and can be used to account for signal attenuation caused by

the tissue. This pH independent attenuation is same for sensor discs and reference disc as long the tissue is uniform. The ratio at each tissue thickness was normalized to the ratio measured for the reference disc ratio (Figure 3.9d). These normalized calibration curves overlap well with each other allowing a tissue depth-independent calibration. This normalization is effective provided the tissue is homogeneous over the distance between the sample and the reference. The standard deviation in normalized ratio at different tissue thicknesses corresponded to about 0.2 pH units between pH 4-8.

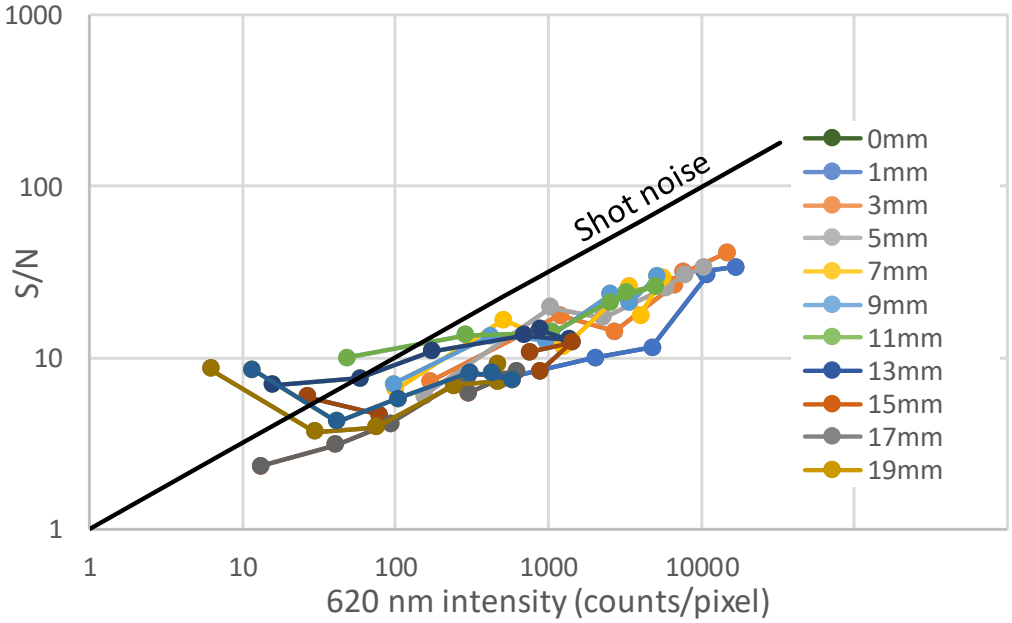

Figure 3.10: Signal/Noise ratio (Ratio/standard deviation of ratio) as a function of average 620 nm intensity for discs imaged through 0-19 mm of chicken breast tissue.

The pixel-to-pixel noise level within any disc could be found by dividing the ratio standard deviation by the calibration curve slope. This noise depended strongly on the light intensity at 620 nm and increased with both pH and tissue depth: At 1 mm tissue the noise ranged from 0.015 pH units at pH 4 to 0.17 at pH 7; at 11 mm, it ranged from

0.067 at pH 4 to 0.54 at pH 7; and at 19 mm it ranged from 0.12 pH units at pH 4 to 1.4 pH units at pH 7. The signal to noise ratio (S/N) appeared to be limited by shot noise at low 620 nm signal intensity (10-100 counts per pixel at 620 nm) implying increasing signal intensity/pixel would increase the S/N (Figure 3.10). This could be achieved by slowing acquisition, averaging over several of the 250 μm pixels, optimizing the pH film for a given pH (e.g., less dye would give better resolution at higher pH), or improving the optical collection and detection efficiency of the setup. Nevertheless, the results showed reasonably good pH resolution even through 19 mm of tissue at low pH or averaged across a disc.

3.4.3. Cadaver Study

The pH sensors were next imaged with XELCI on a human cadaveric lower leg. A series of pH sensor discs were prepared in a similar manner except that the pH indicating film was pre-leached in the buffer for several days resulting in slightly shifted pH spectra as the excess dye leached out. Figure 3.11a shows a photograph of the pH discs that were placed on an orthopedic plate fixed on the cadaveric human tibia and imaged through the tissue and skin. The reconstructed XELCI images for both 620 nm and 700 nm intensities as well their ratio (I6/I7) through the cadaveric tissue are shown in Figure 3.11b. The image has high spatial resolution (like Figure 3.7 through chicken breast) due to the sharp focus of the incident X-ray beam. Analysis of the XELCI images reveal a spatial resolution (80%-20% knife edge resolution) of about 500 μm for both the 620 and 700 nm signal intensities through tissue. XELCI has sub-millimeter spatial resolution that is comparable to most of the radiation based imaging techniques such as

X-ray projection computed tomography (typical spatial resolution of about 0.5 mm for medical CT systems and higher for μCT), single photon emission computed tomography (spatial resolution of 15–20 mm for a SPECT of human brain) and positron emission tomography (spatial resolution of 1–3 mm for μ-PET and 5–10 mm for clinical PET). Usually, there is a tradeoff between high spatial resolution, sensitivity, energy of the x-rays used and radiation dose.[38] Reference and acidic pH discs appear brighter and the higher pH discs are less intense except for pH 8 that was on the edge with light leaking out as the tissue could have been thinner or a good possibility that it was not properly covered all the way on that end. The pH discs closer to the reference are also normalized better than those away from the reference and again this effect is especially pronounced for pH 8. This is because the cadaveric tissue was not uniform over the whole length of the sensor discs as can be seen in the 700 nm intensity image and changes in tissue thickness affects signal normalization. The 700 nm intensity can be used to address tissue discrepancies.

A plain radiograph of the cadaveric lower leg with the pH sensors affixed to the tibial orthopedic plate was also obtained and super-imposed with a ratiometric XELCI image of the same (figure 3.11c). This combination of structural (radiograph) and functional (XELCI) X-ray imaging can provide useful information about bone healing and implant associated infection.

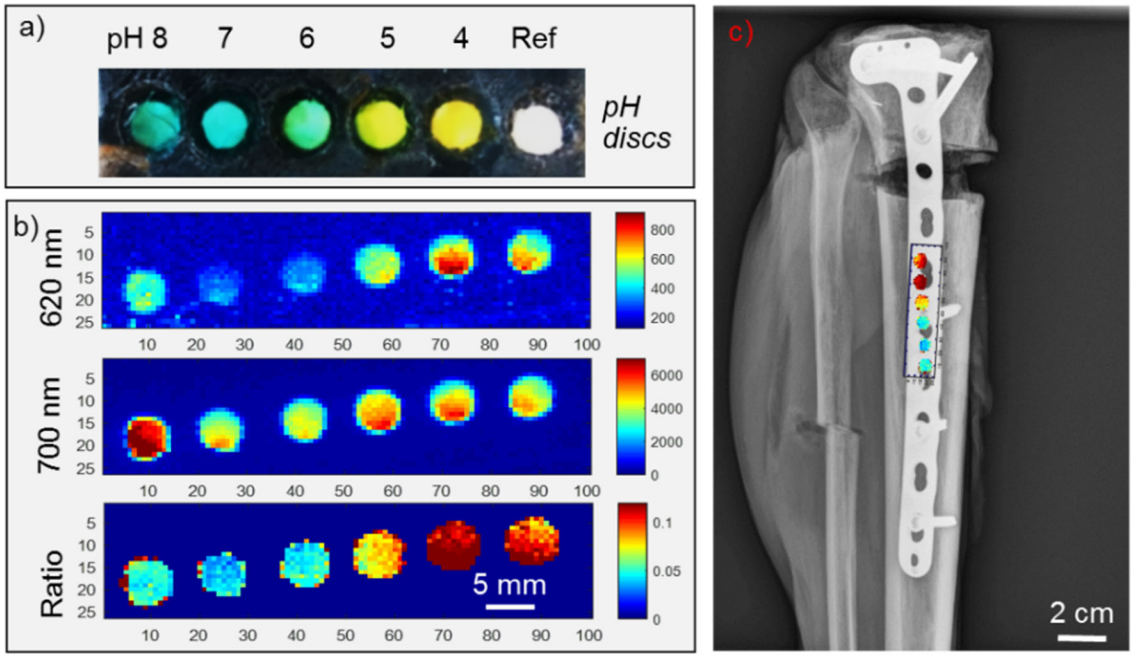

Figure 3.11: Imaging pH sensor discs fixed on a tibial plate on a cadaveric specimen. (a) Photograph of pH sensor discs (5 mm in diameter) placed in a 3-D printed clip in pH buffers (left to right) 8, 7, 6, 5, 4, and a reference disc without any pH coating. (b) XELCI images of the pH sensor clip fixed on the tibial plate: Top image: 620 nm light intensity; middle image: 700 nm light intensity; bottom image: Ratio of 620/700 nm intensities. (c) X-ray radiograph of the human cadaveric tibia superimposed with XELCI image of the pH sensor discs.

The calibration curve through the human cadaveric tissue is shown in figure 3.12. The error bars represent the pixel to pixel standard deviation within each disc. The standard deviation for the ratio was calculated separately from the ratio image and is smaller than the standard deviation for the underlying intensities in some cases. This is because the intensities are correlated and not independent variables. For example, the total intensity affects the individual 620 and 700 nm intensities in tandem; when 620 is higher, 700 nm intensity is also higher and vice versa. Consequently, the ratio will be constant that can result in a lower standard deviation for the ratio when compared to the

individual intensities. The standard deviation depends on the distribution and emission of the scintillator particles, collection efficiency, x-ray intensity and pH absorption.

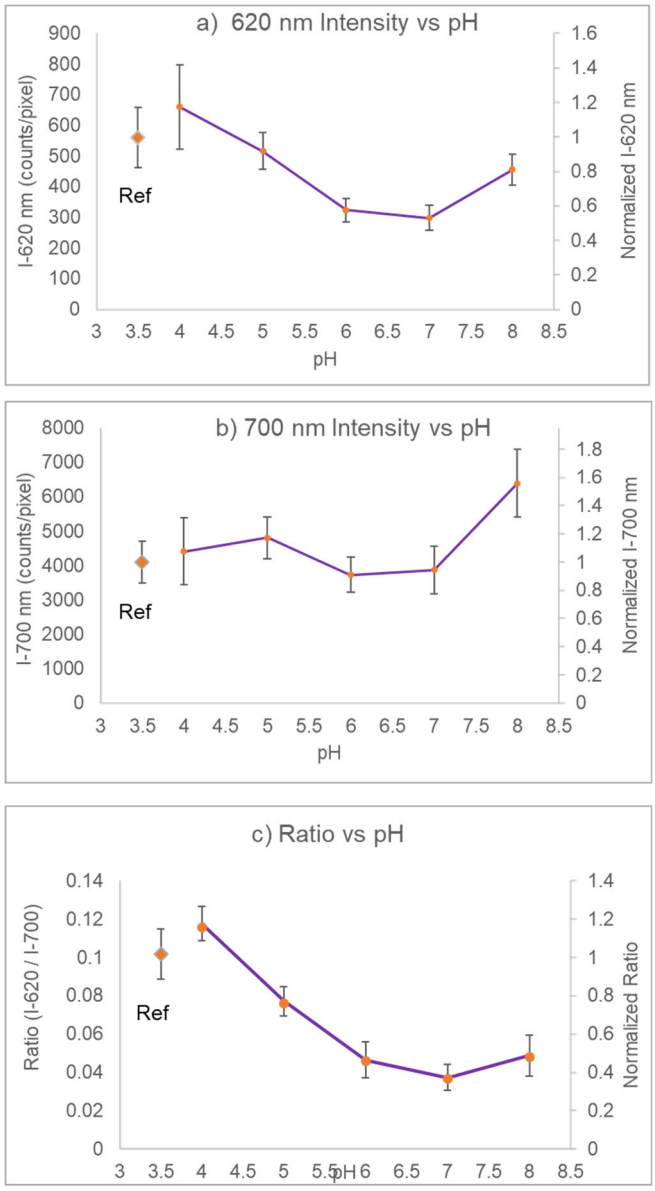

Figure 3.12: Plot of signal intensities as a function of pH through human cadaveric tissue. (a) 620 nm light intensity at pH 4, 5, 6, 7 and 8 after passing through 1 cm of human cadaveric tissue. (b) 700 nm light intensity at pH 4, 5, 6, 7 and 8 after passing through 1 cm of human cadaveric tissue. (c) Ratio of 620 and 700 nm intensities at pH 4, 5, 6, 7 and 8 after passing through 1 cm of human cadaveric tissue. Note: Right axis scale in each plot is normalized with respective to reference disc. Error bars represent the pixel-to-pixel standard deviation within a disc and depends on the scintillator particles, collection efficiency, x-ray intensity and pH absorption.

Although the calibration curve in the cadaveric specimen was similar to the chicken breast tissue, the signal intensity ratio was 5 times weaker for the same tissue depth (a distortion factor of 5x for chicken tissue as compared to 25x for cadaveric tissue) and the overall signal intensity was much lower too. This is qualitatively consistent with reported absorption values in literature for human muscle tissue (for example, μa value of 11.2 cm^{-1} at 633 nm) compared to the white chicken tissue (μa value of 0.12 – 0.17 cm^{-1} at 633 nm) mainly because of absorption by blood and also depends on the measurement and modelling techniques used.[39] Covering the sensors with 11 mm of cadaveric tissue decreases the signal by 1600x at 620 nm and 140x at 700 nm, more than expected based solely on in vivo extinction coefficient of human extremities: Taroni et al reported that the 1/e penetration depth of light through a live human forearm (probably similar to lower leg) was 0.26 cm at 620 nm and 0.42 cm at 700 nm, corresponding to an expected plane wave attenuation through 11 mm of tissue of 69x at 620 nm and 15x at 700 nm.[40] The comparatively weaker signal we observed is likely a combination of incident X-ray attenuation, lateral diffusion of the light to a spot size larger than the 7.6 mm core liquid light guide, and differences in the skin and tissue after freeze thaw cycles. Even with a large attenuation, however, high spatial resolution pH maps were acquired through the tissue in a plated lower leg specimen. Also, the principle of luminescence imaging and referencing through tissue worked for both cadaveric and chicken breast tissue and would apply to any homogeneous tissue sample whether it absorbs and scatters more or less than in a cadaveric specimen. The tray is large enough to accommodate animals as large as rabbits. For such studies, additional considerations would need to be given for shaving

the fur, anesthetizing the animal to keep it still during the scan, and using multiple reference regions to account for possible variation in tissue thickness and optical properties; these will be discussed in forthcoming chapters.

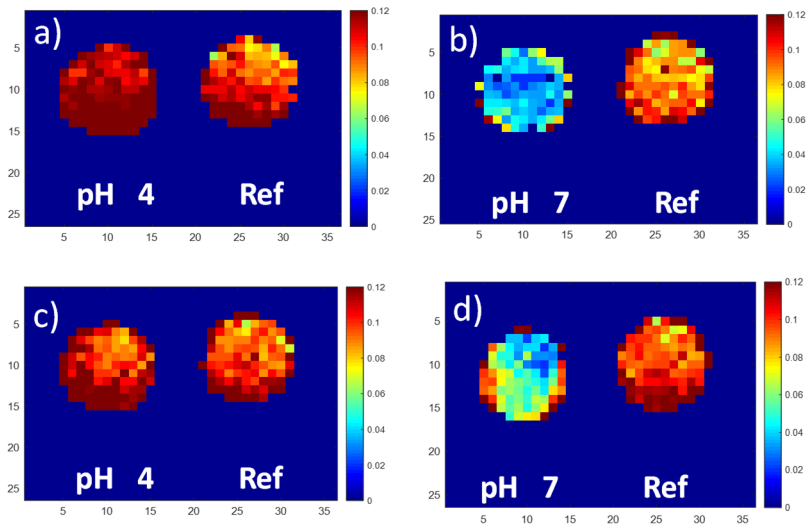

Figure 3.13: pH reversibility through cadaveric tissue. XELCI ratiometric images (I700/I620 nm) of the pH sensor clip with two wells fixed on a tibial plate through human cadaveric tissue. Right well contained only the reference scintillator film and the left well had the pH sensing gel film on top of the scintillator layer. The pH of the left well was cycled between 4 and 7 by rinsing with pH 4 and pH 7 buffers alternatively followed by imaging with XELCI through tissue. (a) and (c), set to pH 4. (b) and (d), set to pH 7.

To show the changes in pH on the same pH sensor can be imaged through tissue using XELCI, a sensor disc was cycled through pH 4 and pH 7 and scanned through the human cadaveric tissue. pH 4 and 7 were chosen as these represent the two extremes of the pH spectrum with one being neutral/physiological and the other acidic.[30] We also observed a pH drop from pH 7.4 to 5 during the in vitro biofilm study reported in our previous work. Figure 3.13 shows the XELCI ratiometric images of a reference disc

(right) and the cycled pH sensor disc (left). The change in signal intensity indicating the change in pH and reversible response can be clearly seen (consistent with the in vitro reversibility study on the pH sensor film, Figure 3.5). The intensity ratio for each pH agree with the respective values of the pH calibration curve obtained through the human cadaveric tissue. Placement of flap of the human cadaveric tissue varied each time as the pH discs were cycled between the two pH. This resulted in minor differences in the signal intensities for pH 7 in Figure 3.13a and 3.13c, and for pH 4 in Figure 3.13b and 3.13d because of differences in thickness of the cadaveric tissue, the same is also true for the reference disc. This can be accounted for by calculating the difference in intensity values for the reference disc between each measurement.

3.5. CONCLUSIONS

We imaged and resolved different pH through human cadaveric tissue and evaluated the effect of increasing tissue (chicken) thickness on the signal from our sensors. Although the tissue attenuates the signal intensity, we were able to resolve different pH through as much as 19 mm thick tissue. The data obtained through the human cadaveric tissue agree with the chicken tissue measurements demonstrating the consistency of sensor response and the imaging technique (XELCI). Sensor design can be modified to develop a method to uniformly coat the whole implant with the pH sensor layers. In addition, the imaging system is far from optimized and optical collection can improved using red-efficient photodetectors (the PMTs were 5% efficient at 620 nm and 2% at 700 nm), and replacing the 7.6 mm core liquid light guide with a larger air/acrylic light guide to increase collection area and acceptance angle. Further studies will be

conducted to measure pH changes on the surface of implanted medical devices in a rabbit model to help diagnose and gain insight into implant associated infection.

3.6. REFERENCES

(1) Darouiche, R. O. Treatment of Infections Associated with Surgical Implants. New England Journal of Medicine 2004, 350 (14), 1422–1429. https://doi.org/10.1056/NEJMra035415.

(2) Isiklar, Z. U.; Darouiche, R. O.; Landon, G. C.; Beck, T. Efficacy of Antibiotics Alone for Orthopaedic Device Related Infections. Clin. Orthop. Relat. Res. 1996, No. 332, 184–189.

(3) McGraw, J. M.; Lim, E. V. Treatment of Open Tibial Shaft Fractures. External Fixation and Secondary Intramedullary Nailing. J Bone Joint Surg Am 1988, 70 (6), 900–911.

(4) Mody, R. M.; Zapor, M.; Hartzell, J. D.; Robben, P. M.; Waterman, P.; Wood-Morris, R.; Trotta, R.; Andersen, R. C.; Wortmann, G. Infectious Complications of Damage Control Orthopedics in War Trauma. J Trauma 2009, 67 (4), 758–761. https://doi.org/10.1097/TA.0b013e3181af6aa6.

(5) Raahave, D. Postoperative Wound Infection After Implant and Removal of Osteosynthetic Material. Acta Orthopaedica Scandinavica 1976, 47 (1), 28–35. https://doi.org/10.3109/17453677608998968.

(6) Trampuz, A.; Widmer, A. F. Infections Associated with Orthopedic Implants. Curr. Opin. Infect. Dis. 2006, 19 (4), 349–356. https://doi.org/10.1097/01.qco.0000235161.85925.e8.

(7) Widmer, A. F. New Developments in Diagnosis and Treatment of Infection in Orthopedic Implants. Clin. Infect. Dis. 2001, 33 Suppl 2, S94-106. https://doi.org/10.1086/321863.

(8) Broekhuizen, C. a. N.; Sta, M.; Vandenbroucke-Grauls, C. M. J. E.; Zaat, S. a. J. Microscopic Detection of Viable Staphylococcus Epidermidis in Peri-Implant Tissue in Experimental Biomaterial-Associated Infection, Identified by Bromodeoxyuridine Incorporation. Infect. Immun. 2010, 78 (3), 954–962. https://doi.org/10.1128/IAI.00849-09.

(9) Piper, K. E.; Fernandez-Sampedro, M.; Steckelberg, K. E.; Mandrekar, J. N.; Karau, M. J.; Steckelberg, J. M.; Berbari, E. F.; Osmon, D. R.; Hanssen, A. D.; Lewallen, D. G.; et al. C-Reactive Protein, Erythrocyte Sedimentation Rate and Orthopedic Implant Infection. PLoS ONE 2010, 5 (2), e9358. https://doi.org/10.1371/journal.pone.0009358.

(10) Konttinen, Y. T.; Takagi, M.; Mandelin, J.; Lassus, J.; Salo, J.; Ainola, M.; Li, T. F.; Virtanen, I.; Liljeström, M.; Sakai, H.; et al. Acid Attack and Cathepsin K in Bone Resorption Around Total Hip Replacement Prosthesis. Journal of Bone and Mineral Research 2001, 16 (10), 1780–1786. https://doi.org/10.1359/jbmr.2001.16.10.1780.

(11) Trampuz, A.; Zimmerli, W. Diagnosis and Treatment of Infections Associated with Fracture-Fixation Devices. Injury 2006, 37 Suppl 2, S59-66. https://doi.org/10.1016/j.injury.2006.04.010.

(12) Stewart, P. S.; Costerton, J. W. Antibiotic Resistance of Bacteria in Biofilms. The Lancet 2001, 358 (9276), 135–138. https://doi.org/10.1016/S0140-6736(01)05321-1.

(13) Grinstein, S.; Swallow, C. J.; Rotstein, O. D. Regulation of Cytoplasmic PH in Phagocytic Cell Function and Dysfunction. Clin. Biochem. 1991, 24 (3), 241–247.

(14) Erra Díaz, F.; Dantas, E.; Geffner, J. Unravelling the Interplay between Extracellular Acidosis and Immune Cells. Mediators Inflamm 2018, 2018. https://doi.org/10.1155/2018/1218297.

(15) Ward, T. T.; Steigbigel, R. T. Acidosis of Synovial Fluid Correlates with Synovial Fluid Leukocytosis. The American Journal of Medicine 1978, 64 (6), 933–936. https://doi.org/10.1016/0002-9343(78)90446-1.

(16) Esmonde-White, K. A.; Esmonde-White, F. W. L.; Holmes, C. M.; Morris, M. D.; Roessler, B. J. Alterations to Bone Mineral Composition as an Early Indication of Osteomyelitis in the Diabetic Foot. Diabetes Care 2013, 36 (11), 3652–3654. https://doi.org/10.2337/dc13-0510.

(17) Abu-Amer, Y.; Darwech, I.; Clohisy, J. C. Aseptic Loosening of Total Joint Replacements: Mechanisms Underlying Osteolysis and Potential Therapies. Arthritis Res Ther 2007, 9 (Suppl 1), S6. https://doi.org/10.1186/ar2170.

(18) Konttinen, Y. T.; Takagi, M.; Mandelin, J.; Lassus, J.; Salo, J.; Ainola, M.; Li, T. F.; Virtanen, I.; Liljeström, M.; Sakai, H.; et al. Acid Attack and Cathepsin K in Bone Resorption Around Total Hip Replacement Prosthesis. Journal of Bone and Mineral Research 2001, 16 (10), 1780–1786. https://doi.org/10.1359/jbmr.2001.16.10.1780.

(19) Hidalgo, G.; Burns, A.; Herz, E.; Hay, A. G.; Houston, P. L.; Wiesner, U.; Lion, L. W. Functional Tomographic Fluorescence Imaging of PH Microenvironments in Microbial Biofilms by Use of Silica Nanoparticle Sensors. Appl. Environ. Microbiol. 2009, 75 (23), 7426–7435. https://doi.org/10.1128/AEM.01220-09.

(20) Dansby-Sparks, R. N.; Jin, J.; Mechery, S. J.; Sampathkumaran, U.; Owen, T. W.; Yu, B. D.; Goswami, K.; Hong, K.; Grant, J.; Xue, Z. L. Fluorescent-Dye-Doped Sol−Gel Sensor for Highly Sensitive Carbon Dioxide Gas Detection below Atmospheric Concentrations. Anal. Chem. 2010, 82 (2), 593–600. https://doi.org/10.1021/ac901890r.

(21) Li, Z.; Liang, R.; Liu, W.; Yan, D.; Wei, M. A Dual-Stimuli-Responsive Fluorescent Switch Ultrathin Film. Nanoscale 2015, 7 (40), 16737–16743. https://doi.org/10.1039/C5NR05376E.

(22) Yang, Y.; Wang, K. Z.; Yan, D. Ultralong Persistent Room Temperature Phosphorescence of Metal Coordination Polymers Exhibiting Reversible PH-Responsive Emission. ACS Appl. Mater. Interfaces 2016, 8 (24), 15489–15496. https://doi.org/10.1021/acsami.6b03956.

(23) Zhang, Y.; Li, S.; Pan, G.; Yang, H.; Qile, M.; Chen, J.; Song, Q.; Yan, D. Stretchable Nanofibrous Membranes for Colorimetric/Fluorometric HCl Sensing: Highly Sensitive Charge Transfer Excited State. Sensors and Actuators B: Chemical 2018, 254, 785–794. https://doi.org/10.1016/j.snb.2017.07.040.

(24) Wang, F.; Widejko, R. G.; Yang, Z.; Nguyen, K. T.; Chen, H.; Fernando, L. P.; Christensen, K. A.; Anker, J. N. Surface-Enhanced Raman Scattering Detection of PH with Silica-Encapsulated 4-Mercaptobenzoic Acid-Functionalized Silver Nanoparticles. Anal. Chem. 2012, 84 (18), 8013–8019. https://doi.org/10.1021/ac3018179.

(25) Chen, H.; Qi, B.; Moore, T.; Wang, F.; Colvin, D. C.; Sanjeewa, L. D.; Gore, J. C.; Hwu, S.-J.; Mefford, O. T.; Alexis, F.; et al. Multifunctional Yolk-in-Shell Nanoparticles for PH-Triggered Drug Release and Imaging. Small 2014, 10 (16), 3364–3370. https://doi.org/10.1002/smll.201303769.

(26) Wang, F.; Raval, Y.; Chen, H.; Tzeng, T. R. J.; DesJardins, J. D.; Anker, J. N. Development of Luminescent PH Sensor Films for Monitoring Bacterial Growth Through Tissue. Advanced Healthcare Materials 2014, 3 (2), 197–204. https://doi.org/10.1002/adhm.201300101.

(27) Mahata, M. K.; Bae, H.; Lee, K. T. Upconversion Luminescence Sensitized PH-Nanoprobes. Molecules 2017, 22 (12), 2064. https://doi.org/10.3390/molecules22122064.

(28) Gao, R.; Fang, X.; Yan, D. Recent Developments in Stimuli-Responsive Luminescent Films. Journal of Materials Chemistry C 2019, 7 (12), 3399–3412. https://doi.org/10.1039/C9TC00348G.

(29) Shimizu, K.; Tochio, K.; Kato, Y. Improvement of Transcutaneous Fluorescent Images with a Depth-Dependent Point-Spread Function. Appl. Opt., AO 2005, 44 (11), 2154–2161. https://doi.org/10.1364/AO.44.002154.

(30) Wang, F.; Raval, Y.; Tzeng, T. R. J.; Anker, J. N. X-Ray Excited Luminescence Chemical Imaging of Bacterial Growth on Surfaces Implanted in Tissue. Advanced Healthcare Materials 2015, 4 (6), 903–910. https://doi.org/10.1002/adhm.201400685.

(31) Benza, D.; Uzair, U.; Raval, Y.; Tzeng, T. R. J.; Behrend, C. J.; Anker, J. N. X-Ray Excited Luminescent Chemical Imaging (XELCI) for Non-Invasive Imaging of Implant Infections. In Frontiers in Biological Detection: From Nanosensors to Systems IX; International Society for Optics and Photonics, 2017; Vol. 10081, p 100810K. https://doi.org/10.1117/12.2256049.

(32) Troy, T.; Jekic-McMullen, D.; Sambucetti, L.; Rice, B. Quantitative Comparison of the Sensitivity of Detection of Fluorescent and Bioluminescent Reporters in Animal Models. 2004, 3 (1), 15.

(33) Yamaguchi, A.; Namekawa, M.; Kamijo, T.; Itoh, T.; Teramae, N. Acid−Base Equilibria inside Amine-Functionalized Mesoporous Silica. Analytical Chemistry 2011, 83 (8), 2939–2946. https://doi.org/10.1021/ac102935q.

(34) Qiu, Y.; Park, K. Environment-Sensitive Hydrogels for Drug Delivery. Advanced Drug Delivery Reviews 2012, 64, 49–60. https://doi.org/10.1016/j.addr.2012.09.024.

(35) Wu, Y.; Joseph, S.; Aluru, N. R. Effect of Cross-Linking on the Diffusion of Water, Ions, and Small Molecules in Hydrogels. J. Phys. Chem. B 2009, 113 (11), 3512–3520. https://doi.org/10.1021/jp808145x.

(36) Penfield, J. G.; Reilly, R. F. What Nephrologists Need to Know about Gadolinium. Nat Clin Pract Nephrol 2007, 3 (12), 654–668. https://doi.org/10.1038/ncpneph0660.

(37) Marquez, G.; Wang, L. V.; Lin, S. P.; Schwartz, J. A.; Thomsen, S. L. Anisotropy in the Absorption and Scattering Spectra of Chicken Breast Tissue. Appl. Opt., AO 1998, 37 (4), 798–804. https://doi.org/10.1364/AO.37.000798.

(38) Chen, H.; Rogalski, M. M.; Anker, J. N. Advances in Functional X-Ray Imaging Techniques and Contrast Agents. Phys. Chem. Chem. Phys. 2012, 14 (39), 13469–13486. https://doi.org/10.1039/C2CP41858D.

(39) Cheong, W. F.; Prahl, S. A.; Welch, A. J. A Review of the Optical Properties of Biological Tissues. IEEE Journal of Quantum Electronics 1990, 26 (12), 2166–2185. https://doi.org/10.1109/3.64354.

(40) Taroni, P.; Pifferi, A.; Torricelli, A.; Comelli, D.; Cubeddu, R. In Vivo Absorption and Scattering Spectroscopy of Biological Tissues. Photochem. Photobiol. Sci. 2003, 2 (2), 124–129. https://doi.org/10.1039/B209651J.

4. CONFORMAL COATING OF ORTHOPEDIC PLATES WITH X-RAY SCINTILLATORS AND pH INDICATORS FOR X-RAY EXCITED LUMINESCENCE CHEMICAL IMAGING THROUGH TISSUE

4.1. ABSTRACT

X-ray excited luminescence chemical imaging (XELCI) is a technique to noninvasively measure chemical concentrations at the surface of modified implanted medical devices. This is useful for detecting implant associated infection and elucidating how the local biochemical environment changes during infection and treatment. XELCI uses a focused X-ray beam to irradiate scintillators coated on the implant and the X-ray excited optical luminescence spectrum is modulated by indicator dyes to provide a chemically sensitive measurement with low background; scanning the X-ray beam across the implant surface generates high spatial resolution chemical measurements. A challenge is how to conformally coat the implant with scintillators and pH indicator dyes in order to make measurements over a large area; in the past, we have physically pressed or glued a pH-sensitive hydrogel sensor to the surface of an implant, but this is impractical for imaging over large device areas such as an orthopedic plate with holes and edges. Herein we describe a method to conformally coat scintillator particles (Gd_2O_2S:Eu) onto the surface of a titanium plate followed by a pH sensitive hydrogel coating using a roughed epoxy coating. A two-part commercial grade epoxy film was tested and found to make the coating of pH sensitive layer adhere better to the titanium surface. Sugar and salt particles were added to the surface of the epoxy as it cured to create a roughened surface and increase surface area. On this roughened surface, a secondary layer of diacrylated

polyethylene glycol (PEG) hydrogel, containing a pH sensitive dye, was polymerized. This layer was found to adhere well to the epoxy-coated implant unlike other previously tested polymer surfaces which delaminated when exposed to water or humidity. The pH sensor coated orthopedic plate was imaged with XELCI through tissue with different pH to acquire a calibration curve. The plates were also imaged through tissue with low pH region from a *Staphylococcus aureus* biofilm grown on one section. These studies demonstrate the use of pH sensor coated orthopedic plates for mapping the surface pH through tissue during biofilm formation using XELCI.

4.2. INTRODUCTION

Orthopedic surgeons routinely use orthopedic plates and screws to hold fractured bones in place and allow them to heal. While these surgeries restore ability and improve quality of life, introducing implants increases the risk of infection, and more importantly bacteria can form biofilms on the implant surface which are resistant to antibiotics and the host's immune system. Roughly 5% of 2 million fracture fixation devices installed annually in the US become infected, with higher rates for immune compromised patients and traumatic injuries including about 40% of internally fixated battlefield injuries which often have debris in the wounds.[1,2] If the infections are caught early, they can often be treated with retention of the hardware using surgical irrigation and debridement, and antibiotics. After about 3 weeks, however, the device usually needs to be removed to treat the infection, followed by replacement after eradicating the infection.[3,4] Imaging techniques to catch these infections within the first 3 weeks of growth could help prevent risks associated with the infection, additional surgeries, and hospitalization. While some

imaging methods such as plain radiography, computed tomography (CT), ultrasound, positron emission tomography (PET) and single photon emission computed tomography (SPECT) have been used in diagnosis, they either have a low resolution to accurately image the surface of the implant, or are only effective at later infection stages.[5,6] They also do not provide chemical sensitivity and specificity to the implant surface to study the local environment at the nidus of resistant infections.

To noninvasively detect and monitor infection localized on the surface of an implanted medical device, and to study the local chemical environment, sensors must be placed on that surface and interrogated remotely. XELCI uses indicator dyes encapsulated in polymer films to determine the local chemical concentration. An implant (usually titanium alloy or stainless-steel plate) is coated with X-ray scintillator in a polymer matrix and this scintillator film is further coated with a film containing pH indicator dyes. After implantation, the scintillator layer is excited by a focused beam of X-rays and the resulting light emission diffuses through the tissue and is collected by a spectrometer or two bandpass-filtered photodetectors to find the spectral peak ratio. To generate an image, the beam is scanned over the sample, while the ratio is measured point by-point. This provides a chemically specific measurement with high spatial resolution (because of the small X-ray beam spot size) and low background signal (because of minimal X-ray luminescence from the tissue).

We are particularly interested in monitoring pH as a method to detect and track infections on implanted medical devices. Previously, we have shown pH changes occurring during bacterial culture in vitro for silica based pH sensors deposited on glass

slides.[5,7] We also improved our pH sensor to be more robust and biocompatible by shifting to a hydrogel based sensor and evaluated the performance by imaging it at various pH through different thicknesses of chicken tissue and human cadaveric tissue.[8] The goal in this study was to develop the pH sensor into a conformal coating which could be applied to titanium orthopedic implants eventually for studies in small animals.

In order to image these implants, they must be coated with scintillator particles. While these particles can be effectively added into a biocompatible polydimethylsiloxane (PDMS) coating, this hydrophobic coating does not stick well to the surface of the implant and the subsequent hydrophilic polyethylene glycol (PEG) film containing the dye. Scintillator particles can also be sintered, however the temperatures needed are too high for the implants themselves to withstand (sintering temperature of ~1700 ºC versus the melting point of titanium at ~1650 ºC).[9,10] Even once the temperature is lowered with the use of sintering agents, such as sodium fluoride, the scintillator particles can diffuse together without adhering to the titanium implant. Therefore, we tested a roughed epoxy polymer coating to serve both as a scintillator layer and an anchor layer for PEG hydrogel that contain the pH dye. We used sugar and coarse sea salt to create a roughed surface that allows for better adhesion of the hydrogel coating. With this method, our group achieved results that could lead to an applicable whole implant coating for imaging through tissue.

4.3. METHODS

4.3.1. Epoxy and Hydrogel Coating

The epoxy film was prepared by mixing Gd_2O_2S:Eu scintillator particles (UKL63/N-R1, Phosphor Technologies Inc., Stevenage, England) with two-part epoxy (Loctite Epoxy Quick Set, Loctite® Brand, Henkel Corporation, Westlake, OH, USA) in 1:4 ratio. These were stirred together on Aluminum foil using a disposable pipette. The epoxy was then spread on aluminum foil to make 12 small samples (roughly 1 cm x 2 cm). To create a rough surface, six of the samples were then coated with granular sugar and six coated with coarse sea salt. The samples were covered and left to cure 24 hours. Once cured, the samples were put in a beaker of water to dissolve the sugar and salt off the surface. These were then dried and dip coated in PEG hydrogel solution described earlier [8] at concentrations of 10%, 50%, and 80% (w/w) PEG in a water/glycerol solution containing a pH dye (either bromocresol green or bromothymol blue). A sugar (sucrose) and salt (sodium chloride) roughened epoxy sample was used for each concentration, the sample being dip coated in polymer solution under nitrogen atmosphere and cured under UV for one minute. A second coating was then applied, and the sample left to cure under UV for 5 minutes. The final cured samples were left in an inert atmosphere for at least two hours and then taken out and put in water to test adherence of the polymer layer to epoxy-scintillator layer. One half of the sugar-roughened epoxy sample coated with the 10% PEG hydrogel was dipped in a pH 4 buffer and the other half in a pH 7 buffer until half of the sample was green and half blue (pH 4 and pH 7 respectively). This sample was then imaged using XELCI.

4.3.2. Spectra

The spectra of the uncoated epoxy-scintillator film and the pH dye containing hydrogel coated epoxy-scintillator layer were taken using an inverted Leica DMI-5000 microscope (Leica Microsystems, Germany) with no emission filter in the beam path. An Amptek Mini-X (Amptek, Inc., Bedford, MA) X-ray source was used to excite the sample with the x-rays (source placed at about 6.7 cm from the sample and no collimator in place). Radioluminescence was directed to a spectrometer (DNS 300, DeltaNu, Laramie, WY, United States), equipped with a cooled CCD camera (iDUS-420BV, Andor, South Windsor, CT, United States). The CCD exposure time was 0.1 seconds in full vertical binning mode.

4.3.3. XELCI Imaging

The sample of interest (epoxy-hydrogel coating or the pH sensor coated orthopedic plate) was placed on a piece of porcine tissue and imaged using XELCI with no tissue covering and with a second piece of 6 mm or 1 cm thick porcine tissue on top of the sample. The XELCI imaging set up consists of a focused x-ray beam (iMOXS, Institute for Scientific Instruments GmbH, Berlin, Germany) focused on a sample on an x-y movable stage (Models: LTS300 and LTS150, Thorlabs Inc., Newton, NJ, United States for x and y axis and Motorized Linear Vertical Stage Model AT10-60, Motion Control, Smithtown, NY, United States for the z-stage) and employs the use of photomultiplier tube as photo detectors to detect the light of different wavelengths of interest using optical filters. This sample was imaged at 5 mm/s with a 250 μm step size.

The scintillator particles used (Gd_2O_2S:Eu) emit 620 and 700 nm wavelengths of light. The pH dyes used absorb the 620 nm light at basic pH but the absorbance blue-shift at acidic pH resulting in higher intensity of the 620 nm light under acidic conditions. The 700 nm light however remains unaffected at all pHs and is not absorbed by the dye. Images were taken at wavelengths of 620 nm and 700 nm, the 620 nm showing changes in light intensity, due to absorption by the pH dye containing hydrogel layer, and the 700 nm showing a constant light intensity. The 700 nm light intensity is used to normalize the image (calculating the ratio of 600 nm to 700 nm light at each pixel) to account for variation in optical collection efficiency and X-ray intensity from sample to sample.

4.3.4. Toxicity Study

Three sets of studies were conducted to evaluate the potential toxicity of the epoxy film, these include: Study 1: Toxicity study of different adhesives with bacterial cells. Study 2: Toxicity comparison of pre-leached and non-leached regular (quick set) epoxy samples with bacterial cells. Study 3: Toxicity comparison of pre-leached and non-leached regular (quick set) epoxy samples with mammalian cells.

4.3.4.1. Toxicity Study 1

Samples of different types of adhesives were prepared according to manufacturer instructions for toxicity study with bacterial and mammalian cells. The different types of adhesives tested were: (i) Marine Epoxy (Loctite Epoxy Marine, Loctite® Brand, Henkel Corporation, OH, USA); (ii) Regular Epoxy (Loctite Epoxy Quick Set, Loctite® Brand, Henkel Corporation, OH, USA) ; (iii) Vinyl Adhesive (Vinyl, Fabric and Plastic Clear

Fabric Repair Adhesive, Loctite® Brand, Henkel Corporation, OH, USA); (iv) Gorilla Glue (White Gorilla Glue Pen, The Gorilla Glue Company, OH, USA). These samples were cut into discs 9 mm in diameter and 1 mm thick (unless otherwise stated). The samples were placed in a 24 well plates. 2 ml of fresh TSB (tryptic soy broth) medium was added to each well containing 5000 of *S. aureus* cells as inoculum. The plate was incubated at 37 °C for 24 hours. Then the media was diluted in to 10^{-1}, 10^{-2}, 10^{-3} and 10^{-4} and cultured on TSA plates. After 24 hour of incubation the colonies were counted and based on the formula below, the concentration of bacteria given as colony forming units per mL (CFU/mL)in each well was calculated. If the number of colonies on all the plates are more than 300 more dilutions are needed. CFU/ml = (No. of colonies/ Volume plated) x (1/dil. Factor).

4.3.4.2. Toxicity Study 2 (Bacterial Culture)

Toxicity comparison of pre-leached and non-leached regular (quick set) epoxy samples. This study was done to compare the effect of pre-leaching the cured epoxy resin with different surface roughness to non-leached cured epoxy resin with different surface roughness. The different samples tested are as follows. (1) Pre-leached smooth surface epoxy; (2) pre-leached roughed surface epoxy with small pore size (sugar roughened); (3) pre-leached roughed surface epoxy with large pore size (salt roughened); (4) non-leached smooth surface epoxy; (5) non-leached roughed surface epoxy with small pore size (sugar roughened); (6) non-leached roughed surface epoxy with small pore size (salt roughened). These were cut into discs 5 mm in diameter and 1 mm thick and were placed in a 24 well plates. 2 ml of fresh TSB (tryptic soy broth) medium was added to each well

containing 5000 of *S. aureus* cells as inoculum. The plate was incubated at 37 °C for 24 hours. Then the media was diluted in to 10^{-1}, 10^{-2}, 10^{-3} and 10^{-4} and cultured on TSA plates. After 24 hour of incubation the colonies were counted and based on the formula below, the concentration of bacteria given as colony forming units per mL (CFU/mL)in each well was calculated. If the number of colonies on all the plates are more than 300 more dilutions are needed.

4.3.4.3. Toxicity Study *3 (Mammalian Cells)*

Fibroblasts L929 Cells (T192755Z) were used with an initial cell concentration of 2.5 x 10^4 cells and exposed to the different types of epoxy discs for 24 hours in 37°C. The cells were then imaged using a fluorescent microscope.

4.3.5. Conformal coating of orthopedic plate

The epoxy film containing the scintillator particles was prepared in the same manner as described above except that the film was coated on to the surface of a titanium animal orthopedic plate (2.7mm 4 Hole Limited Contact Ti Compression Plate, 38mm, part no. 308-04LC , Animal Orthopaedics, Inc., Bremen, IN, USA) and allowed to cure (with sugar roughened surface) followed by dip coating the epoxy coated plate in 10% (w/w) PEG hydrogel solution containing a pH dye to create a pH sensitive smart orthopedic plate.

4.3.5.1. Coating Evaluation

Autoclave: The sensor coated plate was autoclaved under the following condition:121°C, 1 atm, 15 min.

Load Test: The sensor coated plate was fixed on a movable stage positioned under a rolling pin attached to a mechanical loading device (Mark-10, Mark-10 Corporation, Copiague, NY, USA). The stage was moved at a velocity of 1.5 mm/sec causing the rolling pin in contact with the sensor coated plate to roll over the plate while applying a variable load of up to 22 N.

Friction Test: The sensor coated plate was fixed on a wooden block with two screws and rubbed with a piece of 2.5 cm thick chicken tissue. Both the plate and tissue were moistened with PBS and manually rubbed together 10 times. Pictures were taken before and after rubbing to look for any coating residue on the tissue.

Irrigation and Debridement: The sensor coated plate was tested in conditions simulating high pressure irrigation during irrigation and debridement by placing under a high flow of pressurized water with a flow rate of 300 mL/s and photographed before, during, and after treatment to look for potential delamination or wear.

4.3.6. Calibration

pH calibration curves were constructed first for a bromocresol green (BCG) indicator dye, and then for bromothymol blue (BTB). A sample of epoxy-PEG film containing the pH dye, was prepared as described in the epoxy and hydrogel coating section and cut into either 5 or 7 mm discs using a hole punch. These discs were equilibrated overnight in pH 3, 4, 5, 6, 7, and 8 buffers to achieve the color change

response associated with the respective pH. A reference disc was also prepared that consisted of just the scintillator particles in the epoxy matrix without any hydrogel and pH dye coating. These discs were then placed in 3D printed holder containing the different pH buffers. Reference disc was placed in PBS. This was then imaged using XELCI through 6 mm and 11 mm of porcine tissue and the 620 nm and 700 nm intensity images were obtained. The raw data (620 nm PMT counts, 700 nm PMT counts, and stage position vs. time) was processed using a MATLAB script to form the 620 nm, 700 nm, and ratio images vs. stage position. The signal was averaged over each disc and normalized to the reference signal.

4.3.7. Biofilm formation

The sensor coated plate was sterilized and initial pH of the whole plate was set to physiological pH by immersing in sterile PBS. *Staphylococcus aureus* biofilm was grown on one half of the sensor coated plate in TSA (tryptic soy agar) medium and incubate at 37 °C for 24 hours. The other half of the plate was kept moist by covering in agar containing PBS so that it maintained the physiological pH. The part of the plate covered in biofilm dropped in pH within 24 hours and was evident by the color change of the pH coating. The pH sensor coated plate covered with biofilm was imaged using XELCI.

4.4. RESULTS AND DISCUSSION

4.4.1. Epoxy and Hydrogel Coating

We developed a pH sensor read with XELCI to map the surface pH of the orthopedic devices in order to help detect and monitor implant associated infection.[5,8] In

order to show the proof of concept and to characterize the sensor's luminescent signal through tissue, we previously used a 3D printed clip to attach the the sensor to the orthopedic plate. However, our ultimate goal is to develop the pH sensor into a conformal coating that can be used to cover the full surface of the orthopedic implant in order to map the surface pH of the whole implant. The sensor consists of two layers: a luminscent layer and a pH modulated absorbance / pH indicating layer. Figure 4.1 shows how the sensor and XELCI works: An implant (usually titanium alloy or stainless steel plate) coated with X-ray scintillator in a polymer matrix (luminescent layer) and this scintillator film is further coated with a film containing pH indicator dyes (pH indicating layer). The pH dye is selected such that the absorption of the pH dye overlaps the emission of the scintillator particles at a certain pH range so that the hydrogel coating containing the pH dye modulates the scintillator emission. For example, figure 4.2 shows the absorption spectra of the two pH dyes used in this study, Bromocresol green and Bromothymol blue. After implantation, the scintillator layer is excited point by point by a focused beam of X-rays and the resulting light emission diffuses through the tissue and is collected by a spectrometer or photodetector with filters to collect and analyze specific frequencies. The principle has been explained in detail in our previous publication.[8]

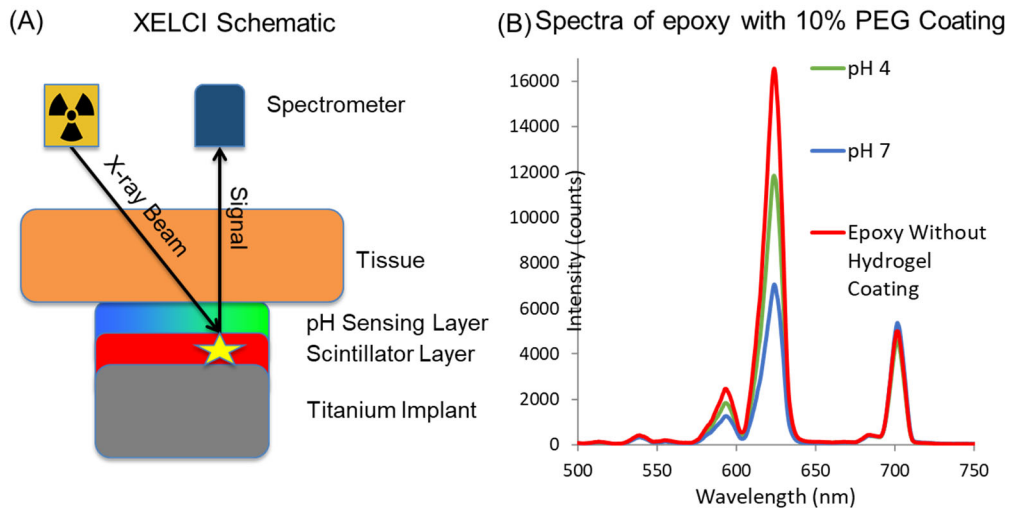

Figure 4.1: (A) Schematic of XELCI set up. (B) Spectra of 10% PEG Hydrogel coating with BCG pH dye on top of epoxy film containing Gd_2O_2S:Eu scintillator particles at pH 7 (blue), pH 4 (green), and without pH-indicator PEG hydrogel (red).

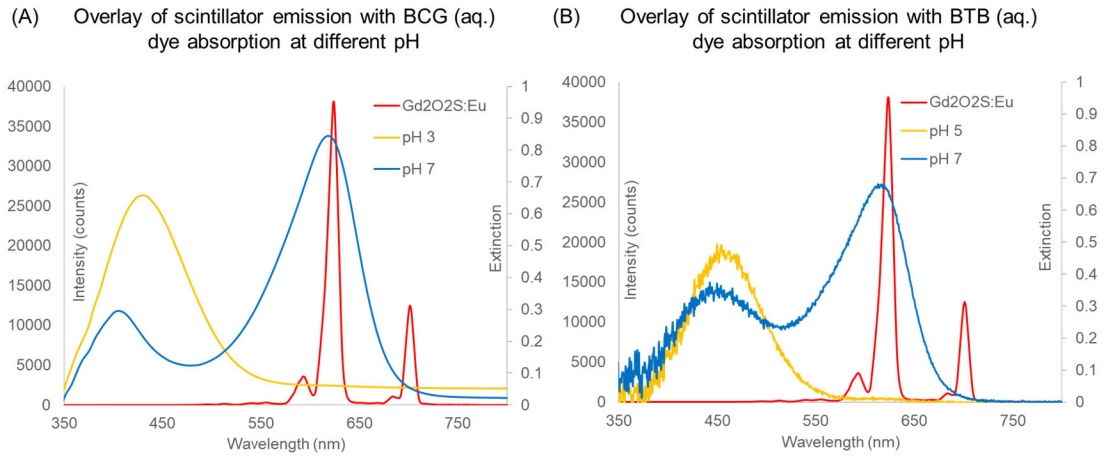

Figure 4.2: Overlay of scintillator emission & pH dye extinction spectra. (A) Luminescence spectrum of scintillator particles (Gd_2O_2S:Eu) (red line, intensity y -axis) and the extinction spectra of Bromocresol green (BCG) pH dye in pH buffer 3.0 (yellow line, extinction y-axis) and pH buffer 7.0 (blue line, extinction y-axis). (B) Luminescence spectrum of scintillator particles (Gd_2O_2S:Eu) embedded in epoxy matrix (red line, intensity y -axis) and the extinction spectra of Bromothymol blue (BTB) pH dye in pH buffer 3.0 (yellow line, extinction y-axis) and pH buffer 7.0 (blue line, extinction y-axis).

Previously, the luminescent layer was comprised of hydrophobic inert polymer (PDMS) enclosing the scintilllator partilcles while the pH indicating layer was made from a hydrophilic biocompatible PEG hydrogel containing a pH indicating dye. The pH indicating layer needs to be H+ permeable or hydrophilic to allow for the exchange of H^+ ions to indicate pH. Due to the contradictory nature of both layers, it is hard to polymerize the hydrophilic hydrogel on the hydrophobic PDMS. We tried various approaches to hold both layers together such as the use of silanes for surface functionalization of PDMS, trying various hydrogel compositions, different types of glues and 3D printed clips to physically press them together but to no avail. Bailey et al., reported an interesting preparation of a hybrid hydrogel from methacrylated star polydimethylsiloxane and diacrylated polyethylene glycol macromers using a solvent-induced phase separation (SIPS) that could be used as continuous gradient scaffolds for tissue engineering applcations but would yield non-uniform films if applied to our sensor bilayer structure due to macroporous nature of the hybrid hydrogel.[11,12] We also tried to incorporate the scintillaor particles in a PEG hydrogel matrix instead of PDMS to avoid the issues caused by the hydrophobic nature of PDMS used in the luminescent layer. This approach, however, is not feasible for the conformal coating of the orthopedic plates due to the swelling nature of hydrogel when exposed to humidity causing the hydrogel coating to peel off of the surface of the plate (Figure 4.3A). The use of an epoxy based polymer for the luminescent layer combined with a roughed surface allows good adhesion of the pH indicating PEG hydrogel layer. The benefit of this approach is two folds; it not only serves as an anchor layer for the hydrogel but also adheres to the metal

surface of orthopedic plates. To test if this approach would work for imaging, we obtained spectra of the epoxy based luminescent layer covered with the pH sensitive hydrogel layer. Figure 4.1B shows the emission of Gd_2O_2S:Eu microphosphor scintillators embedded in an epoxy matrix (red line) and the modulated scintillator emission when the epoxy layer is further coated with hydrogel containing bromocresol green dye at pH 4 (green line) and pH 7 (blue line).

We prepared small samples of the luminescent epoxy film and coated them with different concentrations of the PEG hydrogel containing the pH indicator. We tried coatings with different hydrogel compositions containing 10%, 50% and 80% (w/w) PEG. The original sensor consisted of 80% PEG hydrogel but this concentration yielded thick non-uniform coatings that chips-off the surface of the epoxy layer. 10% PEG hydrogel formed the best coating when polymerized onto the epoxy layer. The epoxy layer was also roughed to create more surface area and to allow for better adhesion of the polymerized PEG hydrogel. Photographs of the different formulations tested including the surface roughening treatments and the concentrations of the PEG gels used are shown in Figure 4.3.

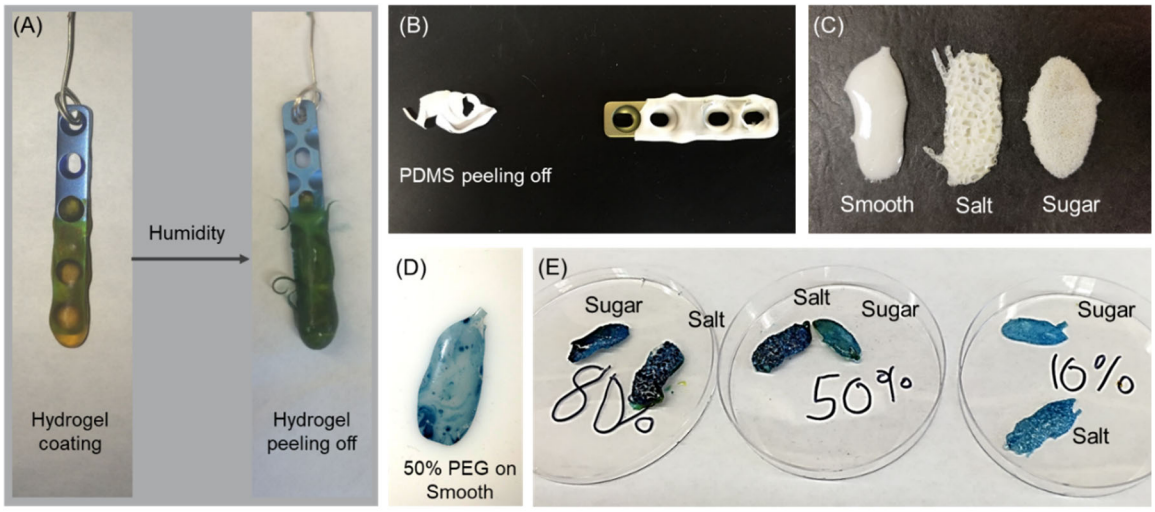

Figure 4.3: Different formulations tested for coating a plate. (A) Problem of hydrogel pH coating peeling off the plate. Left: Animal orthopedic plate dip-coated in pH sensing hydrogel. Right: The pH sensing coating peels off after it is immersed in pH 7 buffer or when exposed to liquid/humidity. (B) Photograph a small veterinary orthopedic plate coated with a layer of polydimethylsiloxane (PDMS) containing scintillator particles and a piece of this PDMS-scintillator coating that broke and came off the plate. (C) Epoxy samples with 3 different surface treatments: smooth, salt roughed with big pores and sugar roughed with small pores. (C) A piece of smooth epoxy coated with 50% PEG hydrogel that is coming off at some points and uneven coating. (D) Pieces of epoxy roughed with either salt or sugar and coated with 80%, 50% and 10% PEG hydrogel layers. 80% and 50% PEG yields a thick coating that comes off easily. 10% PEG hydrogel gives a more uniform coating without any peeling issues.

Granular sugar and coarse sea salt were used as the roughening agents since these can be easily dissolved away after the epoxy layer has cured producing a rough surface based on the imprints left by the sugar and salt crystals on the curing epoxy layer. Similar approach using salt leaching has been reported in literature to create a porous surface.[13] When exposed to humidity or even immersed in water, the PEG hydrogel coating remain stuck to the roughed areas of the epoxy for both the salt and sugar roughened surfaces. The pore size of the roughed surface depends on the size of the sugar or salt particle. Granular sugar produces a more uniformly roughed surface with smaller pore sizes. Due to the larger size of the coarse sea salt crystals, surface roughening was also dependant on

the orientation of the salt crystals and produced an overall less uniformly roughed surface with larger non-uniform pore sizes. Based on these results, we proceeded with the 10% PEG hydrogel composition and sugar as the roughening agent to prepare the epoxy-PEG coatings for further testing.

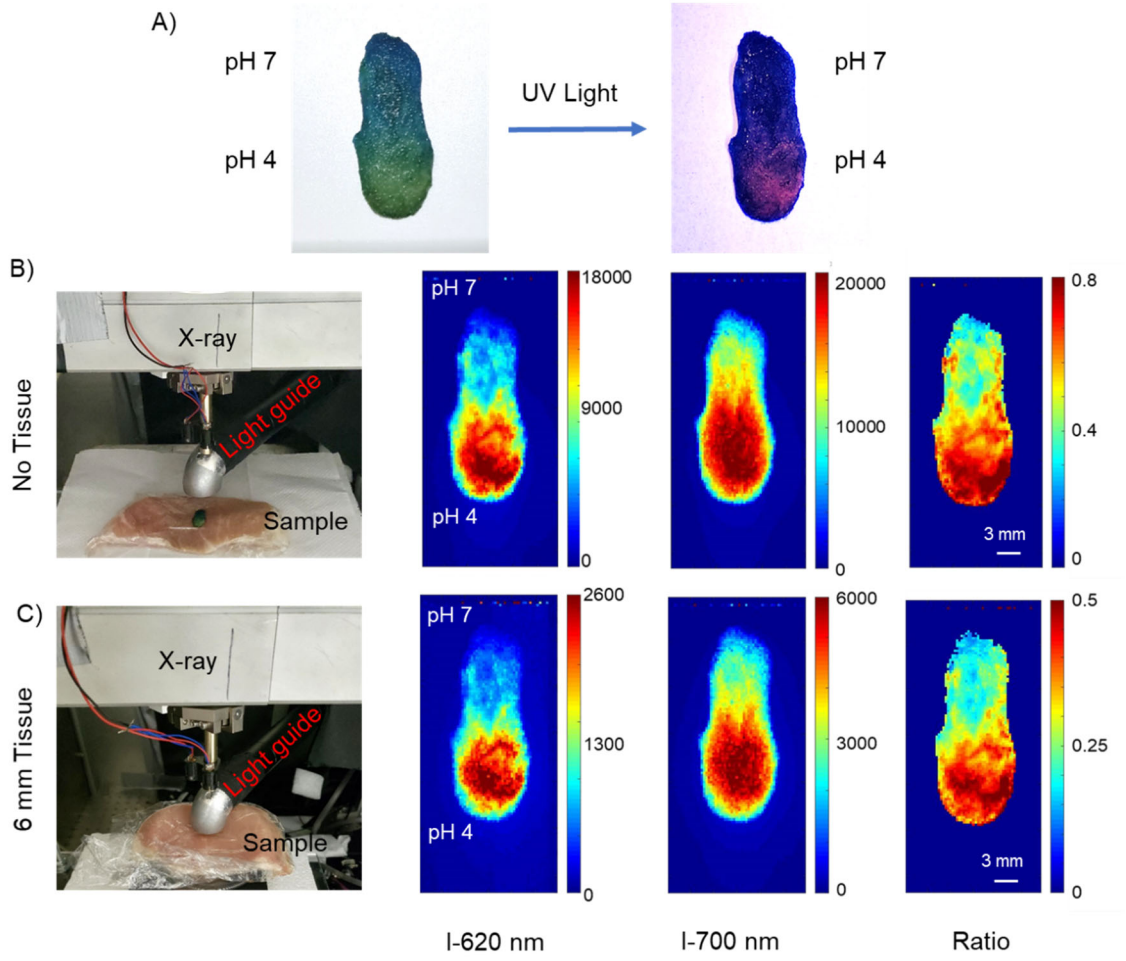

Figure 4.4: A) Epoxy coated with PEG hydrogel containing BCG pH dye and immersed in two different pH buffer solutions (green is pH 4, blue is pH 7) shown under room light and UV light. B) Setup photograph of (A) placed on top of tissue and XELCI images of sample at 600 nm and 700 nm intensities and ratio. C) Setup photograph of (A) sandwiched between two slices of tissue and XELCI images of sample at 600 nm and 700 nm intensities and ratio through 6 mm of porcine tissue.

These epoxy-PEG films retain the pH sensing properties as evident by the change in color of the film with a change in pH of the surrounding medium. Figure 4.4A shows a photograph of a sugar-roughed epoxy coated with 10% PEG hydrogel containing bromocresol dye. One half of this epoxy-PEG film was dipped in pH 7 buffer (blue in color) and the other half in pH 4 buffer (green color). The luminescence of the scintillator particles can be seen under the UV light, since at acidic pH, the pH dye does not absorb the red emission from the scintillator particles, the acidic half of the film dipped in pH 4 buffer appears bright red in color while the basic half dipped in pH 7 buffer shows a weak red luminescnce due to absorption of the red emission by the pH dye at higher pH. The epoxy-PEG film was plaaced on a piece of porcine tissue and imaged uncovered and then covered with another 6 mm piece of porcine tissue on the top using X-ray excited luminscent chemical imaging. We are measuring the pH modulated 620 nm emission and the pH-independent 700 nm light from the X-ray excited scintillator particles in the epoxy-PEG film. A ratio of these intensties is plotted to correct for any background and tissue attenuation.The sample showed a clear difference in light intensity where the hydrogel showed a change in pH for both with and without tissue as shown by the respective images in Figure 4.4B-C. The 600 nm emission showed a change in intensity with change in the surface pH of the sample, as expected. The image measured at 620 nm wavelength gives good indication of pH changes, and all images show good resolution to differentiate the two pH regions of the film with and without tissue. Since the 700 nm intensity is not absorbed by the pH dye at any pH, it is used to normalize the 620 intensity for changes caused by variations in the coating surface and attenuation by the

tissue. This is done by taking a ratio of both intensities and the resulting ratiometric images are shown that look very similar for both with and without tissue.

4.4.2. Conformal coating of orthopedic plate

Finding the new epoxy-PEG coating generated decent XELCI images, a sample was made with the same coating on a titanium orthopedic implant. Figure 4.5 shows the different stages of the coating process. The pH sensitive coated plate was then tested in two buffers of pH 4 and pH 7 to show a pH response. Figure 4.3A shows a titanium orthopedic plate that was coated with the PEG hydrogel alone without the epoxy layer. The hydrogel coating peels off the implant plate as soon as it is exposed to humidity or fluids due to swelling of the hydrogel. The use of epoxy as an anchor layer for the hydrogel overcomes this issue and make the coating more robust and easier to handle.

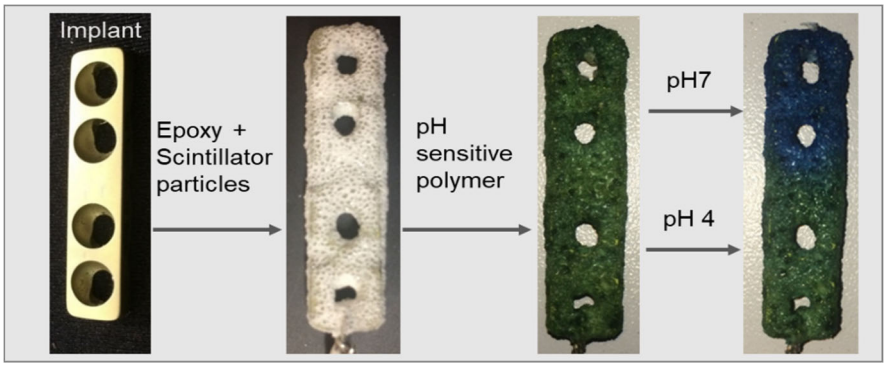

Figure 4.5: Preparation schematic for conformal coating of the whole implant plate with pH sensitive coating.

4.4.2.1. Coating Evaluation

To check the robustness of the epoxy-hydrogel coating, the coated plate was subject to several tests. These include autoclaving the coated plate, testing it under a mechanical load, friction test and simulation of high-pressure irrigation during irrigation and debridement. The epoxy-based pH sensor coated plate was found to be able to withstand the temperature and pressure required to autoclave and does not peel off under high flow of water (flow rate of 300 mL/s) or crack under the tested mechanical load. The friction test was performed to simulate the rubbing of the plate against the soft tissue when implanted in the body. For the friction test, the plate and tissue were moistened with PBS before rubbing and we did not see any residue or debris from the coating on the tissue after rubbing as shown in the photographs in Figure 4.6. Similarly, we did not observe any delamination of the coating under a high flow of water simulating irrigation and debridement as shown in the before and after photographs of the plate in Figure 4.7.

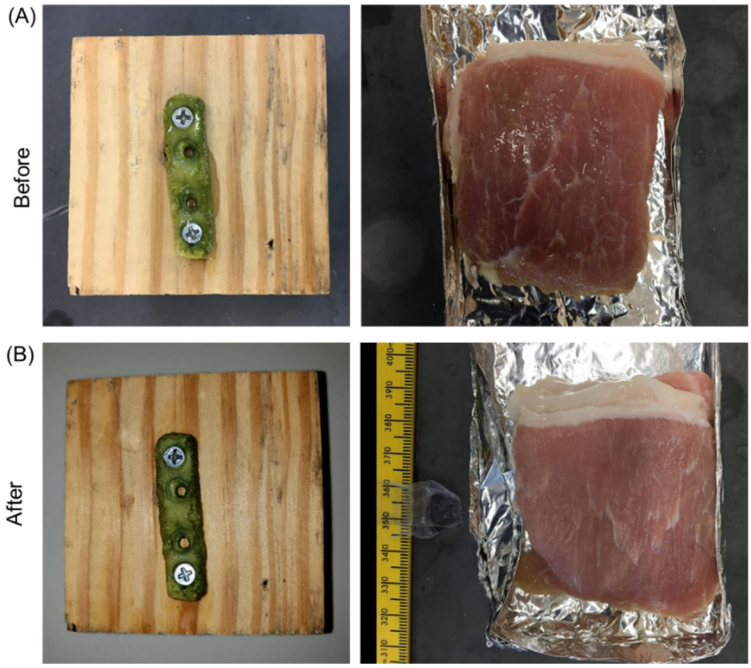

Figure 4.6: Friction testing of the epoxy-PEG coated plate. (A) Photographs of the epoxy-PEG coated orthopedic plate fixed to a wooden block with screws and a piece of tissue before the test. (B) Photographs of the epoxy-PEG coated orthopedic and piece of tissue after the test.

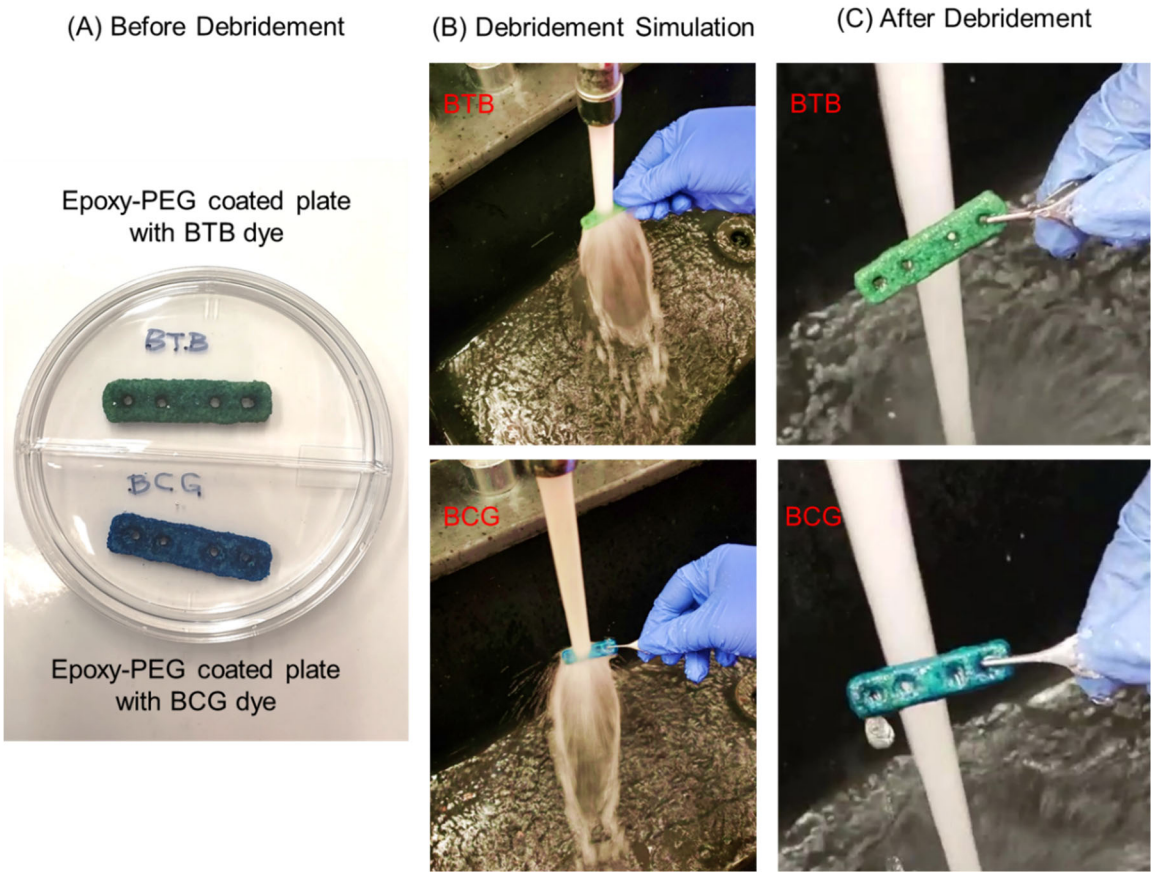

Figure 4.7: Debridement testing of the epoxy-PEG coated plates. (A) Two orthopedic plates coated with epoxy-PEG coating containing bromothymol blue (BTB) and bromocresol green (BCG) pH dyes before testing for debridement. (B) Epoxy-PEG coated plates in (A) subject to debridement simulation under high flow of water (300mL/s). (C) Photos of the coated plates immediately after debridement testing.

4.4.3. Toxicity Study

In order to determine the effect of toxic leachates from epoxy, we conducted toxicity studies with both bacterial and mammalian cells. We did a preliminary study with different adhesives, bacteria grew on all of them and we selected the regular epoxy for further evaluation due to similar cell growth to control, was readily available and worked well due to quick setting time. The different sets of studies conducted were: (1)

Toxicity study of different adhesives with bacterial cells, (2) Toxicity comparison of pre-leached and non-leached regular (quick set) epoxy samples with bacterial cells, (3) Toxicity comparison of pre-leached and non-leached regular (quick set) epoxy samples with mammalian cells, Results are shown as bar charts in Figures 4.8, 4.9 and 4.10.

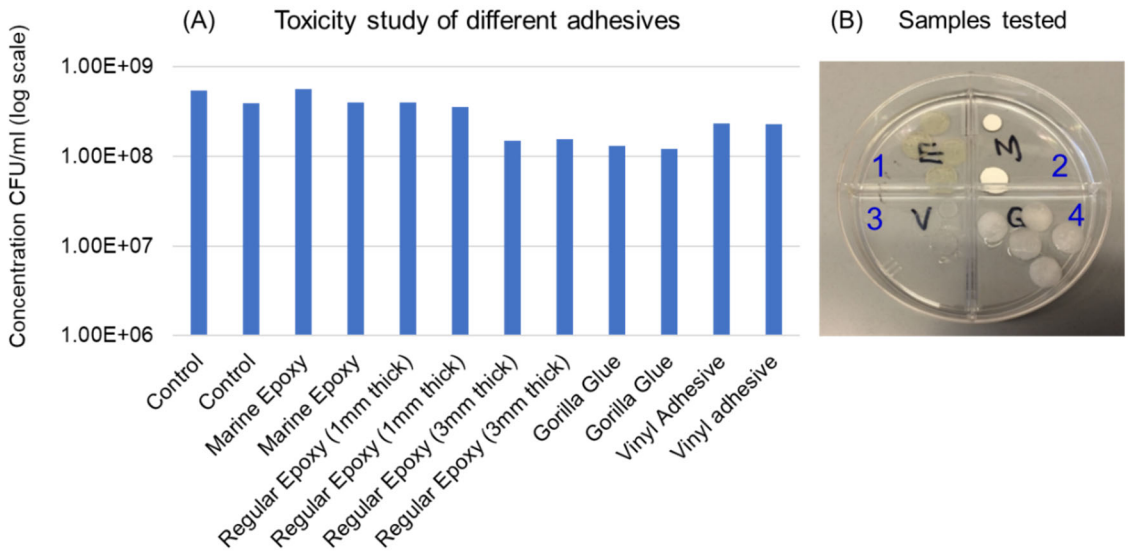

Figure 4.8: Toxicity study of different adhesives (run in duplicates) to bacterial cells (*S. aureus*). (A) Bacterial count in CFU/ml represented on log scale for the bacterial culture exposed to different types of adhesives (non-leached) for 24 hours. (B) Photograph of different adhesives tested for toxicity to bacteria (cured and cut into discs). (1) Regular quick set 5-minute epoxy, (2) Marine epoxy, (3) Vinyl adhesive, (4) Gorilla glue.

The bacterial cells (*S. aureus*) did not show significant toxicity to any of the types tested as shown in Figure 4.8. Moreover, we did not observe a significant difference between the toxicity results of leached and non-leached epoxy resins on bacterial cells (Figure 4.9). The mammalian cells (fibroblasts L929) were proliferating in all wells despite morphological changes observed in some cells (Figure 4.10). Final cell concentration after 24 hours in all wells ranged between 2.7 – 3.0 x 10^4. This is contrast

to the results of the cytotoxicity study done by Ejserholm et al. where they developed a flexible polymer based on epoxy and Off-Stoichiometry Thiol-Enes for neural implants. They observed that the polymer leached in water for a week did not show cytotoxicity to mouse L929 fibroblasts as tested by the Methyl Tetrazolium (MTT) assays whereas the non-leached polymer showed cytotoxicity.[14] However, we did not observe a significant difference in cytotoxicity results of leached and non-leached epoxy resins but this could be due to the type of resin used.

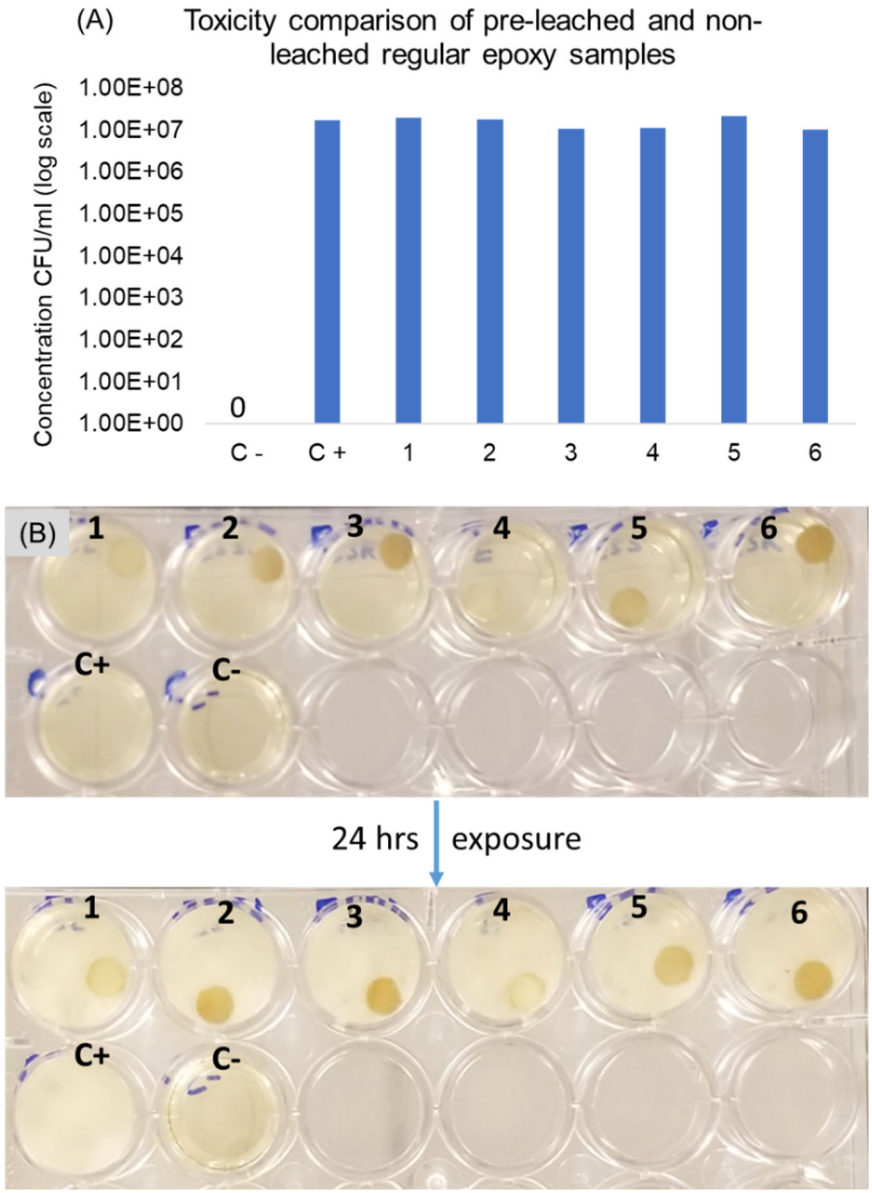

Figure 4.9: Toxicity evaluation of pre-leached and non-leached regular epoxy samples containing scintillator particles to bacteria cells (*S. aureus*). (A) Bacterial count in CFU/ml on log scale for the bacterial culture exposed to pre-leached and non-leached epoxy samples for 24 hours. (B) Photograph of the samples tested. Well numbers 1-6 contain bacterial inoculum (*S. aureus*) exposed to epoxy samples with different surface roughness and leaching treatment. After 24 hours exposure to the epoxy samples, turbidity of the media in the wells indicate bacterial growth. The different samples tested in (A) and (B) were: (1) Pre-leached smooth surface epoxy, (2) Pre-leached roughed surface epoxy with small pore size (sugar roughened), (3) Pre-leached roughed surface epoxy with large pore size (salt roughened), (4) Non-leached smooth surface epoxy, (5) Non- leached roughed surface epoxy with small pore size (sugar roughened), (6) Non-leached roughed surface epoxy with small pore size (salt roughened), (C+) positive control, (C-) Negative control.

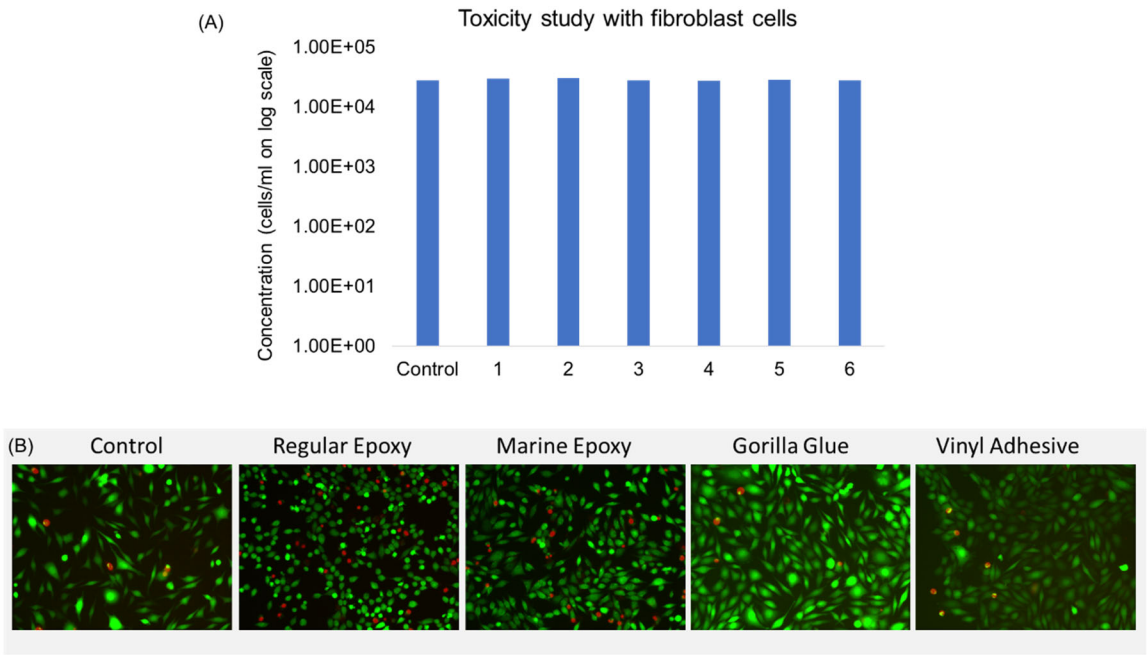

Figure 4.10: Toxicity evaluation of pre-leached and non-leached regular epoxy samples containing scintillator particles to fibroblasts L929 Cells (T192755Z). (A) Fibroblast cell count plotted on log scale for the fibroblast cells exposed to pre-leached and non-leached epoxy samples for 24 hours at 37°C. The different samples tested were: (1) Pre-leached smooth surface epoxy, (2) Pre-leached roughed surface epoxy with small pore size (sugar roughened), (3) Pre-leached roughed surface epoxy with large pore size (salt roughened), (4) Non-leached smooth surface epoxy, (5) Non-leached roughed surface epoxy with small pore size (sugar roughened), (6) Non-leached roughed surface epoxy with small pore size (salt roughened), (Control) positive control. Initial cell conc. 2.5 E+04 cells. (B) Fluorescent microscopy images of the fibroblasts exposed to different types of adhesives. The different adhesives tested were regular (5-minute quick set) epoxy, marine epoxy, gorilla glue and vinyl adhesive. Green and red cells represent live and dead cells respectively.

The results of these three toxicity studies performed by our group indicate a lack of toxicity and are consistent with the toxicity studies done on other epoxy-based resins that are widely used in the medical applications such as endodontic sealers.[15] Bagheri et al., report a Carbon Fiber-Flax-Epoxy composite as a potential candidate for orthopedic implants to replace the metal plates used for bone fractures and confirmed the biocompatibility of the material in vitro. They also found the material to not affect the

osteogenesis process negatively.[16] Eventually, we plan to move on to a medical grade epoxy to conformally coat the orthopedic plates but this lack of toxicity even for the non-medical grade epoxy is an important and necessary step for establishing biocompatibility of the coating.

4.4.4. Calibration Curve

pH calibration curves for epoxy-PEG coatings containing bromocresol green (BCG), and bromothymol blue (BTB) were acquired through tissue using XELCI imaging of the sensor discs in pH buffer solutions (Figure 4.11). A reference disc with just epoxy layer and no pH-indicator coating was used to account for the pH-independent attenuation caused by tissue or variation in the film thickness. The sample and reference discs are shown in the photo (Figure 4.11A&E) with the respective ratiometric images through two thicknesses of tissue (Figure 4.11B-C and 4.5F-G). Reconstructed images of the 620 nm and 700 nm raw signal intensities through porcine tissue are shown in Figure 4.12.

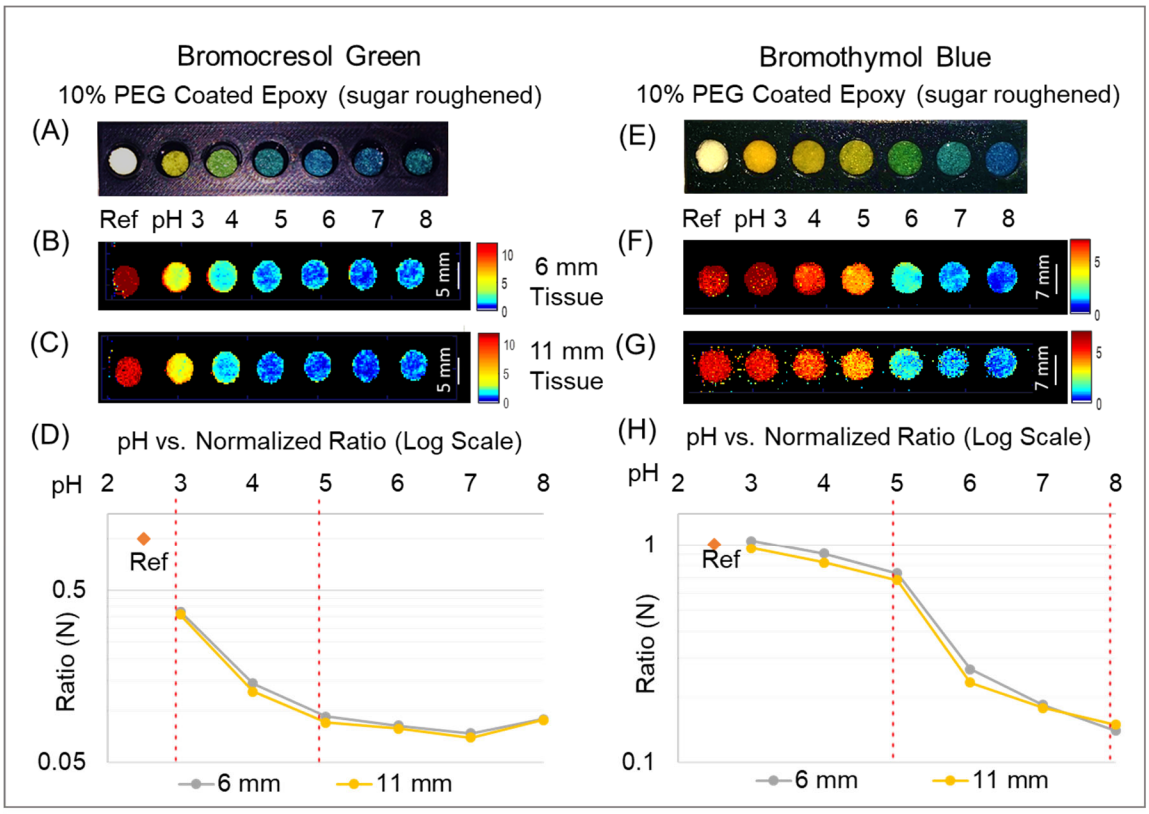

Figure 4.11: pH calibration curve using two dyes: Bromocresol green (range pH 3-5) and Bromothymol blue (range pH 5-8). Left (Bromocresol green): (A) Photograph of sugar roughened epoxy discs coated with 10% PEG hydrogel containing bromocresol green dye. (B) XELCI ratiometric images of (A) through 6 mm and (C) through 11 mm of porcine tissue. pH sensor coated epoxy discs were placed in pH 3 – 8 buffers and a non-coated epoxy reference was also imaged for each case. (D) Plots of ratio normalized to reference at pH 3 – 8 for 6 mm and 11 mm tissue. Reference is plotted arbitrarily as pH 2.5. Right (Bromothymol blue): (E) Photograph of sugar roughened epoxy discs coated with 10% PEG hydrogel containing bromothymol blue dye. (F) XELCI ratiometric images of (A) through 6 mm and (G) 11 mm of porcine tissue. pH sensor coated epoxy discs were placed in pH 3 – 8 buffers and a non-coated epoxy reference was also imaged for each case. (H) Plots of ratio normalized to reference at pH 3 – 8 for 6 mm and 11 mm tissue. Reference is plotted as pH 2.5.

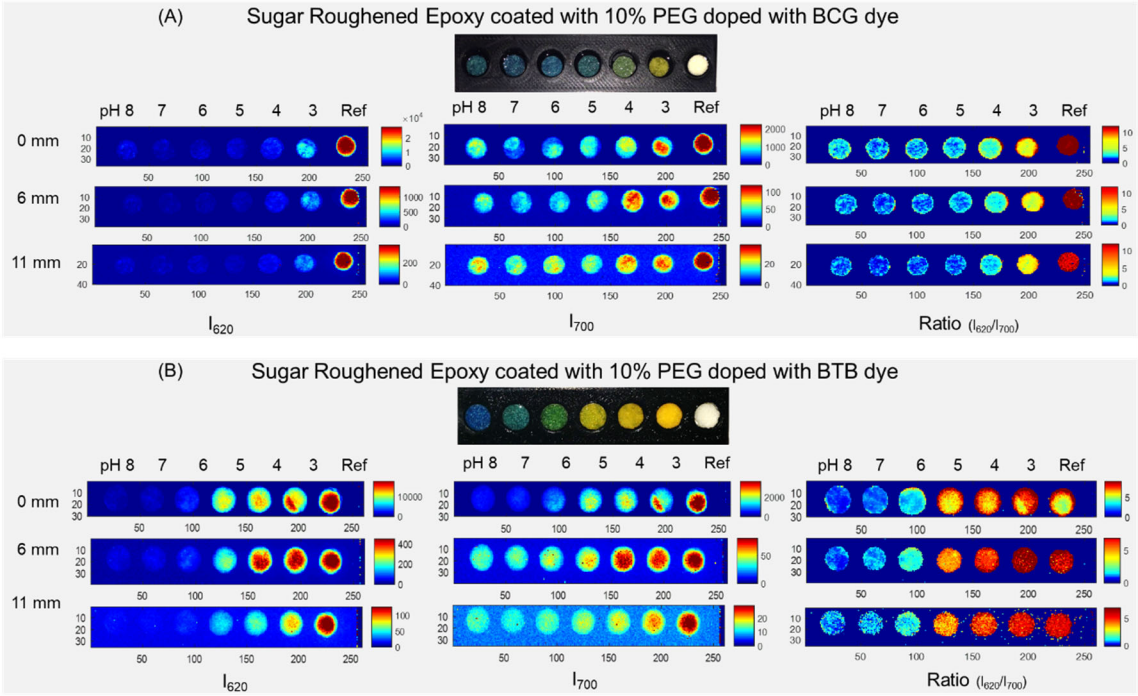

Figure 4.12: Sensor images of signal intensities through chicken tissue. (A) Photograph showing the pH sensor discs made from epoxy-PEG containing the BCG pH dye placed in a 3-D printed holder in pH buffers 8, 7, 6, 5, 4 and 3 and a reference disc without any pH coating. The holder was sandwiched between two pieces of chicken tissue and imaged through 6mm and 11 mm of chicken tissue. XELCI images showing the 620 nm, 700 nm and ratio of 620 to 700 nm signal intensities of the pH sensor discs at respective pH obtained without tissue and through 6 and 11 mm of chicken tissue. (B) Same as (A) except the pH sensor discs were made from epoxy-PEG containing BTB pH dye.

For both, the ratiometric and raw signal intensities, the reference discs appear brighter than the hydrogel coated discs. The 620 and 700 nm raw signal intensities decrease when passing through thicker (11 mm vs 6 mm) tissue due to attenuation and scattering by the tissue. Sample discs that are at acidic pH also appear brighter (depending on the pH range of the dye used) than those at higher pH due to increased absorption of the scintillator emission by the pH dye at higher pH, this is especially evident for the 620 nm images as the pH dyes absorb the 620 nm emission while the 700

nm emission remains unaffected by the pH indicating dyes. The 700 nm images are used to correct for any attenuation or variations caused due to tissue and sample preparation in the resulting ratiometric images obtained by dividing the pH modulated 620 nm signal by the pH independent 700 nm signal. Figure 4.11D and 4.11H show the plotted normalized ratios for pH 3,4,5,6,7, 8 and the reference disc through 6 mm and 11 mm thick tissue. The normalized plots for both tissue thicknesses for each dye show good overlap. Plots of the 620 nm and 700 nm signal intensities through porcine tissue for both Epoxy-PEG-BCG and Epoxy-PEG-BTB coatings are shown in Figures 4.13 and 4.14. For the BCG containing discs, the effective range of sensor is between pH 3 and 5. This can also be seen from the color response at different pH (Figure 4.11A), the discs appear yellow, green and blue at pH 3, 4 and 5 respectively, and above pH 5, all discs look blue. In order to make the pH sensing range to be applicable to physiological pH, epoxy-PEG films were prepared using a different pH dye, bromothymol blue (BTB). This extends the pH sensing range from pH 5 to 8 making it more biologically relevant. Figure 4.11E shows the prepared discs with BTB in the respective buffer solutions; the discs appear yellow in color for pH 3, 4 and 5 changing to green at pH 6, bluish-green at pH 7 and blue at pH 8. These color changes associated with pH can be seen in the MATLAB constructed ratiometric images (Figure 4.11F-G) and the plotted ratios of the underlying signal intensities (Figure 4.10H) even through 6 and 11 mm of porcine tissue. These color changes are impossible to see through the tissue either by the eye or plain radiography. However, XELCI enables us to see these color changes clearly through thick tissue.

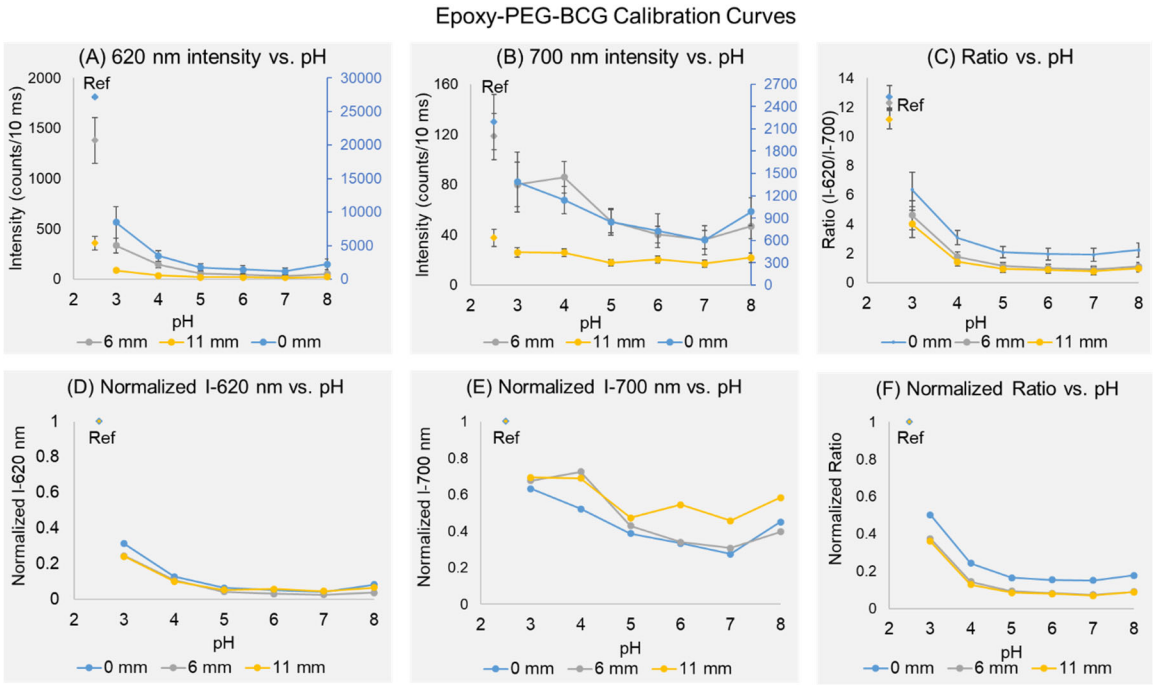

Figure 4.13: Plots of signal intensities as a function of pH through chicken tissue for the sensor discs prepared from epoxy-PEG-BCG. (A) 620 nm light intensity at pH 3, 4, 5, 6, 7 and 8 and ref disc after passing through 0 mm, 6 mm and 11 mm of chicken tissue. (B) 700 nm light intensity at pH 3, 4, 5, 6, 7 and 8 and ref disc after passing through 0 mm, 6 mm and 11 mm of chicken tissue. (C) Ratio of 620 and 700 nm intensities at pH 3, 4, 5, 6, 7 and 8 and ref disc after passing through 0 mm, 6 mm and 11 mm of chicken tissue. (D-E) Plots in (A-C) normalized to respective reference intensities. Note: Error bars represent the pixel-to-pixel standard deviation within a disc. Reference disc plotted arbitrarily at pH 2.5

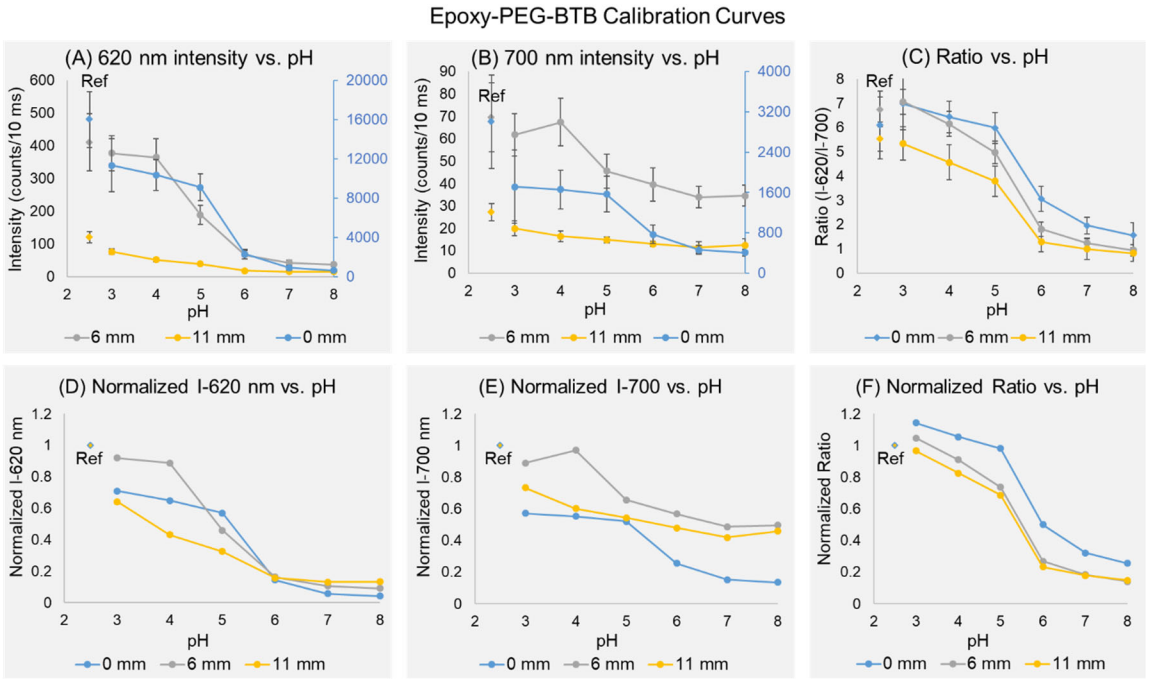

Figure 4.14: Plots of signal intensities as a function of pH through chicken tissue for the sensor discs prepared from epoxy-PEG-BTB. (A) 620 nm light intensity at pH 3, 4, 5, 6, 7 and 8 and ref disc after passing through 0 mm, 6 mm and 11 mm of chicken tissue. (B) 700 nm light intensity at pH 3, 4, 5, 6, 7 and 8 and ref disc after passing through 0 mm, 6 mm and 11 mm of chicken tissue. (C) Ratio of 620 and 700 nm intensities at pH 3, 4, 5, 6, 7 and 8 and ref disc after passing through 0 mm, 6 mm and 11 mm of chicken tissue. (D-E) Plots in (A-C) normalized to respective reference intensities. Note: Error bars represent the pixel-to-pixel standard deviation within a disc. Reference disc plotted arbitrarily at pH 2.5

4.4.5. pH Mapping of Biofilm

Two orthopedic plates were coated with the same epoxy-PEG coating but one containing the BCG dye and another with the BTB dye (Figure 4.15A&B). These plates were then dipped in two pH buffers to create a pH difference on one half of the plate and XELCI images obtained without any covering and then covered by a piece of 1 cm porcine tissue. The 620 nm images in Figure 4.15 show the reduction in signal intensity at high pH while a brighter signal was measured for the half exposed to low pH, these

signal intensities are indicative of the pH change. The 700 nm images remain unaffected by pH and show the variations in the coating as well the attenuation caused by the tissue. Taking a ratio of 620 nm/700 nm gives a pH map of the surface and the pH difference between the two halves of the plate can be clearly seen in ratio images for both with and without tissue even though the raw intensities are much attenuated for the images through tissue as compared to the respective images without tissue.

After successfully imaging the pH difference on the surface of the coated orthopedic plates (Figure 4.15A&B), we wanted to image the pH changes caused by the formation of a biofilm on the plate surface to mimic the case of implant-associated infections. For this purpose, a biofilm was grown from *S. aureus*, the predominant strain found associated with implant associated infections, on one half of each of the epoxy-PEG coated plates, one containing the BCG pH dye (pH range 3-5) and other containing the BTB pH dye (pH range 5-8). The other halves of the plates were covered with agar containing sterile PBS to simulate physiological pH. After growing the biofilm for 24 hours, the pH dropped and became acidic in the half covered by the biofilm. This pH change can be seen in the Figure 4.15D where the part of the plate covered in biofilm appears green while the part covered in PBS is blue. Referring to the calibration curve for the BTB dye, green color indicates a pH of about 6 and blue between pH 7 and 8. This change in pH, however, is not visible in Figure 4.15C where both regions of the plate, with and without biofilm appear blue in color. The plate coating in Figure 4.15C with BCG dye does not respond appreciably to changes in pH above 5 and therefore was not able to detect the pH change produced by the biofilm. Selecting the pH dye to get the

maximum response in the desired pH range is the key for detecting pH changes. Another approach can be combining both the pH dyes in the same coating to create a larger pH sensing range to suit the application. The low pH produced by the biofilm on the epoxy-PEG-BTB coated plate can also be clearly seen in the respective XELCI images in Figure 4.15D. The intensity decreases with increasing tissue thickness, for example, the 700 nm images in Figure 4.15D, maximum intensity for no tissue was 20,000 counts/10ms compared to 1,900 counts/10ms through 1 cm tissue for the same sample. However, good imaging resolution was still obtained when the sample was imaged through 1 cm thick porcine breast and part of the plate covered by the biofilm can be distinctly seen in the images. This demonstrates the successful use of the coating and the imaging technique to map pH changes indicative of infection associated with orthopedic implants.

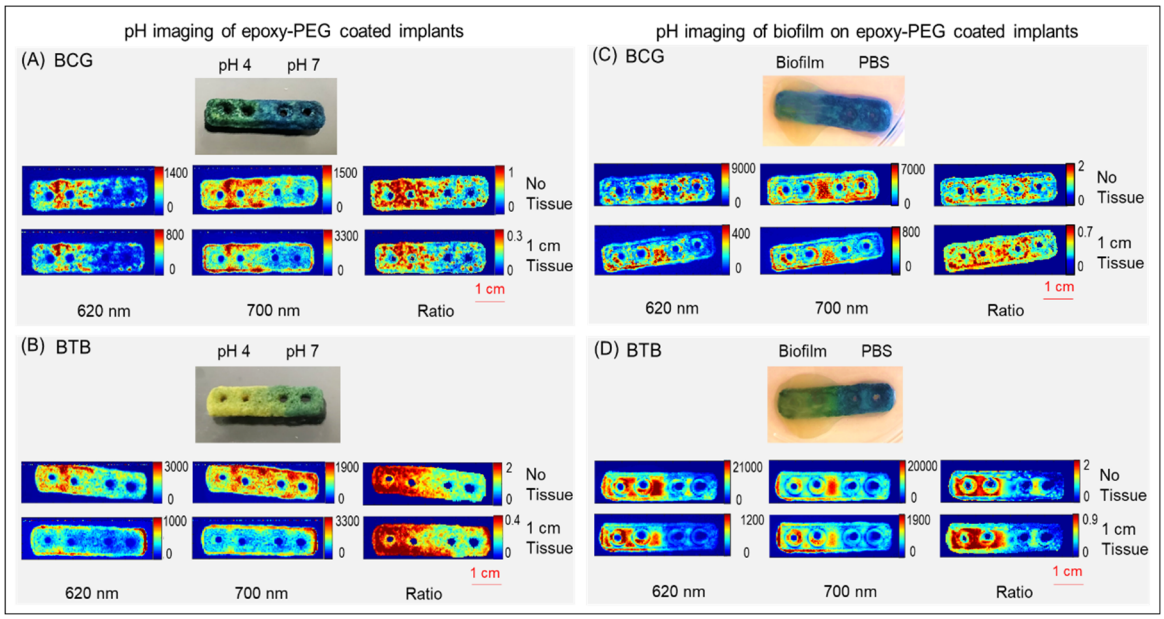

Figure 4.15: pH imaging of epoxy-PEG coated veterinary orthopedic plates. A) Photograph of a plate coated with the epoxy-PEG polymer containing Bromocresol green (BCG) pH dye with one half of the plate dipped in pH 4 buffer (green) and the other half dipped in pH 7 buffer (blue). XELCI images of the plate at 620 nm, 700 nm and ratio of both without tissue and through 1 cm of porcine tissue. B) Photograph of a plate coated with the epoxy-PEG polymer containing Bromothymol blue (BTB) pH dye with one half of the plate dipped in pH 4 buffer (yellow) and the other half dipped in pH 7 buffer (green). XELCI images of the plate at 620 nm, 700 nm and ratio of both without tissue and through 1 cm of porcine tissue. C) Photographs of an epoxy-PEG-BCG coated plate 24 hours after growing a biofilm on the left half and keeping the right half in agar containing PBS (pH 7.4). XELCI images (at 620 nm, 700 nm and ratio of both) of the plate after 24 hours of biofilm growth with no tissue and covered with 1 cm of porcine tissue. D) Photographs of an epoxy-PEG-BTB coated plate 24 hours after growing a biofilm on the left half (green) and keeping the right half (blue) in agar containing PBS (pH 7.4). XELCI images (at 620 nm, 700 nm and ratio of both) of the plate after 24 hours of biofilm growth with no tissue and covered with 1 cm of porcine tissue.

4.5. CONCLUSION

We developed a conformal coating for XELCI imaging of orthopedic plates. The use of the epoxy-PEG coating prevented the sensor from peeling off the plate surface and improved the robustness and handling under debridement and friction conditions. We successfully demonstrated mapping of pH changes on the sensor coated orthopedic plates during formation of a biofilm and formulated a calibration curve. Biocompatibility tests

of epoxy on mammalian cells and bacterial cells did not show significant toxicity specially for pre leached epoxies. A combination of pH dyes can be used for applications requiring sensing over an extended pH range such as demonstrated using BCG and BTB in these epoxy-PEG coatings. These coatings can be modified to find potential applications requiring surface characterization and not just limited to mapping orthopedic infections. With good initial imaging results, further testing will be done using medical grade epoxy to allow for imaging implant surfaces in vivo to monitor pH changes that could indicate possible biofilm formation. Early diagnosis of bacterial growth could help to effectively treat infection and reduce the number of implant removals and replacement surgeries each year.

4.6. REFERENCES

(1) Zalavras, C. G.; Christensen, T.; Rigopoulos, N.; Holtom, P.; Patzakis, M. J. Infection Following Operative Treatment of Ankle Fractures. *Clin. Orthop.* **2009**, *467* (7), 1715–1720. https://doi.org/10.1007/s11999-009-0743-8.

(2) Mody, R. M.; Zapor, M.; Hartzell, J. D.; Robben, P. M.; Waterman, P.; Wood-Morris, R.; Trotta, R.; Andersen, R. C.; Wortmann, G. Infectious Complications of Damage Control Orthopedics in War Trauma. *J. Trauma* **2009**, *67* (4), 758–761. https://doi.org/10.1097/TA.0b013e3181af6aa6.

(3) Vertes, A.; Hitchins, V.; Phillips, K. S. Analytical Challenges of Microbial Biofilms on Medical Devices. *Anal. Chem.* **2012**, *84* (9), 3858–3866. https://doi.org/10.1021/ac2029997.

(4) Bryers, J. D. Medical Biofilms. *Biotechnol. Bioeng.* **2008**, *100* (1), 1–18. https://doi.org/10.1002/bit.21838.

(5) Wang, F.; Raval, Y.; Tzeng, T.-R. J.; Anker, J. N. X-Ray Excited Luminescence Chemical Imaging of Bacterial Growth on Surfaces Implanted in Tissue. *Adv. Healthc. Mater.* **2015**, *4* (6), 903–910. https://doi.org/10.1002/adhm.201400685.

(6) Chen, H.; Rogalski, M. M.; Anker, J. N. Advances in Functional X-Ray Imaging Techniques and Contrast Agents. *Phys. Chem. Chem. Phys.* **2012**, *14* (39), 13469–13486. https://doi.org/10.1039/C2CP41858D.

(7) Wang, F.; Raval, Y.; Chen, H.; Tzeng, T.-R. J.; DesJardins, J. D.; Anker, J. N. Development of Luminescent PH Sensor Films for Monitoring Bacterial Growth through Tissue. *Adv. Healthc. Mater.* **2014**, *3* (2), 197–204. https://doi.org/10.1002/adhm.201300101.

(8) Uzair, U.; Benza, D.; Behrend, C. J.; Anker, J. N. Noninvasively Imaging PH at the Surface of Implanted Orthopedic Devices with X-Ray Excited Luminescence Chemical Imaging. *ACS Sens.* **2019**, *4* (9), 2367–2374. https://doi.org/10.1021/acssensors.9b00962.

(9) Jingbao Lian, X. S.; Jingbao Lian, X. S. Preparation of Gd_2O_2S:Pr Scintillation Ceramics by Pressureless Reaction Sintering Method. *J. Mater. Sci. Technol.* **2009**, *25* (02), 254–258.

(10) Kim, H.-W.; Koh, Y.-H.; Li, L.-H.; Lee, S.; Kim, H.-E. Hydroxyapatite Coating on Titanium Substrate with Titania Buffer Layer Processed by Sol–Gel Method. *Biomaterials* **2004**, *25* (13), 2533–2538. https://doi.org/10.1016/j.biomaterials.2003.09.041.

(11) Bailey, B. M.; Nail, L. N.; Grunlan, M. A. Continuous Gradient Scaffolds for Rapid Screening of Cell–Material Interactions and Interfacial Tissue Regeneration. *Acta Biomater.* **2013**, *9* (9), 8254–8261. https://doi.org/10.1016/j.actbio.2013.05.012.

(12) Bailey, B. M.; Fei, R.; Munoz-Pinto, D.; Hahn, M. S.; Grunlan, M. A. PDMSstar–PEG Hydrogels Prepared via Solvent-Induced Phase Separation (SIPS) and Their Potential Utility as Tissue Engineering Scaffolds. *Acta Biomater.* **2012**, *8* (12), 4324–4333. https://doi.org/10.1016/j.actbio.2012.07.034.

(13) Chiu, Y.-C.; Larson, J. C.; Isom, A.; Brey, E. M. Generation of Porous Poly(Ethylene Glycol) Hydrogels by Salt Leaching. *Tissue Eng. Part C Methods* **2009**, *16* (5), 905–912. https://doi.org/10.1089/ten.tec.2009.0646.

(14) Ejserholm, F.; Stegmayr, J.; Bauer, P.; Johansson, F.; Wallman, L.; Bengtsson, M.; Oredsson, S. Biocompatibility of a Polymer Based on Off-Stoichiometry Thiol-Enes + Epoxy (OSTE+) for Neural Implants. *Biomater. Res.* **2015**, *19* (1), 19. https://doi.org/10.1186/s40824-015-0041-3.

(15) Cintra, L. T. A.; Benetti, F.; de Azevedo Queiroz, Í. O.; Ferreira, L. L.; Massunari, L.; Bueno, C. R. E.; de Oliveira, S. H. P.; Gomes-Filho, J. E. Evaluation of the Cytotoxicity and Biocompatibility of New Resin Epoxy–Based Endodontic Sealer Containing Calcium Hydroxide. *J. Endod.* **2017**, *43* (12), 2088–2092. https://doi.org/10.1016/j.joen.2017.07.016.

(16) Bagheri, Z. S.; Giles, E.; El Sawi, I.; Amleh, A.; Schemitsch, E. H.; Zdero, R.; Bougherara, H. Osteogenesis and Cytotoxicity of a New Carbon Fiber/Flax/Epoxy Composite Material for Bone Fracture Plate Applications. *Mater. Sci. Eng. C* **2015**, *46*, 435–442. https://doi.org/10.1016/j.msec.2014.10.042.

5. MAPPING REAL TIME pH CHANGES ON THE SURFACE OF IMPLANTED ORTHOPEDIC DEVICES IN LIVE RABBIT MODELS USING X-RAY EXCITED LUMINESCENCE CHEMICAL IMAGING — PART I (PRELIMINARY STUDIES WITH SINGLE PLATE REGION)

5.1. ABSTRACT

Implant-associated infection is a leading cause of fixation failures and is often challenging to detect due to lack of symptoms and specific tests to detect localized infection. Low pH is believed to be associated with bacterial infections and can be used to indicate presence of a biofilm as indicated by in vitro studies. We developed a pH sensor and a dedicated imaging system to noninvasively study, detect and monitor implant-associated infection and tested the sensor performance in preliminary in vivo studies. In our approach, an orthopedic plate is coated with the pH sensor and implanted in an animal model enabling imaging of the surface pH with the X-ray excited luminescent chemical imaging (XELCI). Two versions of the pH sensor were tested for comparison. The major goal was to develop a non-invasive method to image chemical concentrations near implant surfaces in order to study implant-associated infection by establishing a baseline for how pH changes in time for normal wound healing and comparing this with infection by inoculation with *gfp* modified *Staphylococcus aureus*. To compare normal wound healing with infection, two animals were kept as complete control and 4 rabbits were inoculated with different concentrations of the inoculum to induce infection. Even though we did not observe a pH change during infection, we were

able to successfully image the implanted sensors through in the live animal and gained useful insights to optimize the sensor and the imaging system.

5.2. INTRODUCTION

Orthopedic implants such as intramedullary nails, plates, screws and external fixator pins are routinely used for fracture fixation together with increasing number of prosthetic devices due to growing number of aging population having hip, shoulder and knee prostheses.[1] A large number (about 5%) of these devices get infected and cause complications and financial burden. Chances of infection in a revision prosthetic surgery are 5 to 40 fold higher than the first surgery and treatment cost of an infected prosthetic joint cost more than $50,000 per episode.[2] Implant associated infection is usually irreducible post-surgical infection may be caused by bacterial contamination during surgery or subsequent adhesion of opportunistic microorganisms (e.g., staphylococcal species) onto implant surface.[3] According to the onset of symptoms after implantation, infection can be classified as Early Postoperative (1-4 weeks, usually acquired during trauma or implant surgery, caused by highly virulent organisms such as *Staphylococcus aureus* or Gram-negative bacilli), Delayed or Chronic (> 1 month, usually acquired during trauma or implant surgery, caused by low virulence organisms). Infection can also be Hematogenous (usually occurring more than 2 years after surgery, caused by microbial spread through bloodstream from a distant focus of infection) or Contiguous (by direct or lymphogenic spread from an adjacent infectious focus or penetrating trauma).[4,5]

Diagnosis and treatment of implant-related infection can be challenging and a combination of clinical, laboratory and microbiological findings together with imaging studies are used for diagnosis of infection. Hematologic tests such as C-reactive protein (CRP) and erythrocyte sedimentation rate (ESR) are generally used to diagnose implant associated infection. These are inexpensive and non invasive tests but CRP and ESR are nonspecific inflammation markers which may be elevated by chronic inflammatory conditions such as rheumatoid arthritis, surgical intervention or other illness. Moreover, blood tests indicate systemic infection and cannot catch localized infection during the early stages. So far, imaging plays an inferior role in early infection but is somewhat useful in delayed and late infections. These methods also lack chemical specificity and cannot provide pH measurements.

This research is aimed at studying pH changes on or near the implant surface in vivo during infection. For this, we developed a preliminary pH sensor and an x-ray excited luminescence imaging (XELCI) technique to study the pH changes during infection. The preliminary pH sensor was tested in vitro and ex vivo to map pH changes through chicken and human cadaveric tissue. This chapter is focused on the preliminary in vivo testing that was performed to evaluate sensor performance in a live animal model. The pH sensor relies on the pH dependent absorbance of the x-ray irradiated luminescence from scintillator particles by a hydrogel film loaded with a pH sensitive dye. The pH sensor is coated onto a plate that is implanted in the animal and interrogated point by point using XELCI. We used rabbits for the animal model studies. A photo of the experimental setup and the schematic of the imaging technique is shown in Figure

5.1. The animal is placed on the x-y-z movable stage under anesthesia and the sensor region (hind leg in this case) is roughly positioned under the x-ray beam using laser points to help determine the position. The X-ray is fitted with a polycapillary lens to focus the x-ray beam. A light guide collects the signal from the x-ray excited luminescence region and is filtered into the 620 and 700 nm wavelengths of interest before reaching the detector that is the photomultiplier tubes (PMTs). The data is acquired using a custom labview program and processed with a custom matlab script with real time data shown on the computer screen.

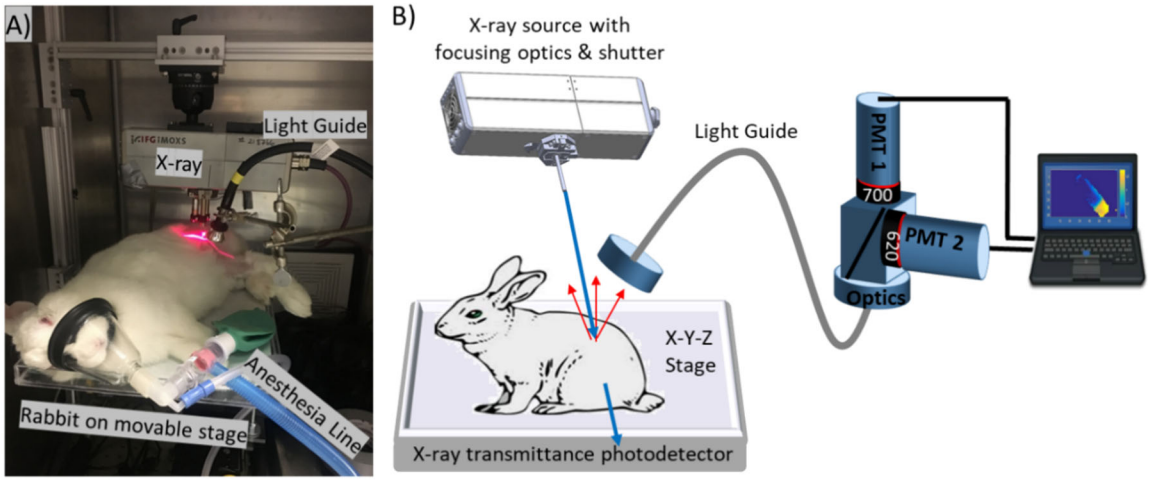

Figure 5.1: XELCI experimental setup. A) Photograph of the XELCI setup with a rabbit undergoing imaging under anesthesia. The sample region is positioned under the x-ray beam using a laser cross beam (two red lines in the photo). B) Schematic drawing of the XELCI setup. The animal is placed on an x-y-z motorized stage and the implanted sensor is irradiated with a focused X-ray beam. The luminescence signal is transmitted via the light guide to two photomultiplier tubes (PMTs), measuring light intensity at 620 nm and 700 nm respectively. The intensities and ratios are monitored as the stage scans, with real time image shown on the computer screen.

In vivo testing was comprised of 15 rabbit model studies and is divided into different phases depending on the approach such as preliminary studies, implant type, sensor type and type of infection (open face or cavity) studied. This chapter is focused on the preliminary studies done in Phase A with a single plate region implant and consisted of preliminary experiments conducted to determine biocompatibility and toxicity (if any) of the sensor as well as to test for imaging of the pH on the surface of an implant in vivo.

5.2.1. Phase A: Preliminary study

A preliminary study was conducted with 6 rabbits using two types of sensors, a Vinyl-PEG sensor (Group 1) and a basic PEG hydrogel sensor (Group 2), with 3 animals per group. One animal was kept as control in each group to avoid any possible spread of infection (hematogenous infection) from infected to non-infected leg in the same animal. The sensor coated single region plate was implanted in animal (rabbit) model and inoculated with bacteria culture to induce infection by injecting/spraying the sensor and surrounding tissue with bacteria. Keeping one leg of the animal as control (no infection) and one leg infected with bacteria culture. Two levels of inoculation were tested to get a baseline for the concentration of bacteria required to induce infection without causing fatality to the animal. One rabbit in each group was inoculated with 500 cfu of *S. aureus* and one rabbit inoculated with 5000 cfu of *S. aureus*. The study lasted 10 days (excluding surgery day) with both groups staggered one day apart. The prepared sensors were imaged using XELCI prior to surgery and after surgery in the live animal under anesthesia at least twice a week. At the end of the study, the animals were euthanized following the animal use protocol and postmortem study conducted for each. The goal of

this study was to develop a protocol and ensure practice for imaging of the live animal, to evaluate sensor performance and biocompatibility, and to determine suitability of the imaging system for in vivo live animal imaging for surface specific pH determinations of the implanted sensors. This section describes the details of the in vitro testing conducted to characterize the sensor and the preliminary rabbit studies to determine system suitability.

5.3. METHODS

5.3.1. Sensor Coated Orthopedic Implant

The sensor coated orthopedic implant was prepared by coating a metal plate with the two sensor layers, a bottom layer of scintillator particles (Gd_2O_2S:Eu) encapsulated in polydimethylsiloxane (PDMS), and a pH-sensitive top layer synthesized from biocompatible hydrogel incorporating the pH-indicator dye.

5.3.1.1. Metal Implant

Titanium sheet metal, (0.020 inch thick Ti-6Al-4V ELI, implant grade 6-4 Titanium, M. Vincent & Associates, MN, USA) was cut into 20 x 6 mm plates, polished with 240 grit sand paper, rinsed with alconox detergent and water, and sonicated in acetone followed by ethanol for 15 minutes each.

5.3.1.2. Scintillator layer

Silicone elastomer and curing agent (SYLGARD™ 184 Silicone Elastomer base and curing agent, Dow Corning, Midland, Michigan, United States) were mixed in 10:1 (w/w) ratio and ~8.0 µm diameter Gd2O2S:Eu scintillator particles (UKL63/N-R1,

Phosphor Technologies Inc., Stevenage, England) were added in 5:1 (w/w) ratio to form a final mixture of 5 g scintillator particles per 1 g of PDMS. This mixture was spread directly onto the titanium plates covering the full plate and cured in the oven at 100 °C to form about 0.5 mm thick scintillator-PDMS layer on the titanium plate.

5.3.1.3. pH sensitive layer

The pH sensitive film consisted of a PEG hydrogel with BCG dye (pH range 3-6) approximately 200 μm thick. Details of synthesis, reversibility and leaching of the PEG hydrogel are given in Chapter 2. In summary, the hydrogel film consisted of a solution containing 79% (w/w of sol.) 700 MW polyethylene glycol diacrylate (PEGDA), 9.9% (w/w of sol.) glycerol, 9.9% (w/w of sol.) water, 0.8% (w/w of sol.) photoinitiator (2,2-dimethoxy-2-phenylacetophenone) and 0.4% (w/w of sol.) bromocresol green (pH-indicating dye). This mixture was stirred on a magnetic plate for 30 minutes and the resulting solution was polymerized as follows:

For Group 1 (Vinyl-PEG Sensors), a thin film was prepared from a commercial vinyl adhesive (Vinyl, Fabric and Plastic Clear Fabric Repair Adhesive, Loctite® Brand, Henkel Corporation, OH, USA). Vinyl adhesive was chosen because of its flexibility and low toxicity (Table S7, Toxicity study 1 in Chapter 4) These films were dip coated in the above hydrogel solution of the above mentioned pH sensitive layer, cured under UV for 2 minutes and cut into 14x6 mm pieces. The resulting Vinyl-PEG films were glued onto the scintillator layer (cured on the titanium plates) using superglue.

For Group 2 (PEG Sensors), the polymerizable hydrogel solution was drop coated and sandwiched between two clean cover slips and cured under UV for 2 minutes. The

films were immersed in water to swell and delaminate from the coverslips and washed several times before cutting into 12x6 mm pieces. This PEG hydrogel was glued onto the scintillator layer (cured on the titanium plates) using superglue.

5.3.2. Sensor Characterization

5.3.2.1. Mechanical Integrity for Debridement

The PEG hydrogel film was tested for simulation of high pressure irrigation during irrigation and debridement (I&D) by placing it under running tap water and increasing the water flow to maximum. The flow of water was determined by measuring the amount of time required to fill a 1000 mL beaker at given flow.

5.3.2.2. Confocal imaging of biofilm on sensor

pH indicating sensor films (PEG hydrogel) were fixed to well trays using agarose. Green fluorescent protein (gfp) tagged strain of *Staphylococcus aureus* in tryptic soy broth was cultured on sensor films and imaged after 24 hours using confocal laser scanning microscope (Leica SPE Confocal Microscope, Leica Microsystems Inc., IL, USA).

5.3.3. In vivo studies

All in vivo studies were conducted on the New Zealand White Rabbit. One leg of the animal was kept as control (no inoculation) and one leg was infected. Surgery was performed by the Clemson University veterinarian and all animal studies were conducted at the Clemson University Godley-Snell Research Center after approval of the Institutional Biosafety Committee (IBC) and animal use protocols. Animal anesthesia

during imaging and euthanasia at termination was also administered by the Godley-Snell Research Center staff. All bacterial studies were carried out by Dr. Tzeng's lab in the microbiology department.

5.3.3.1. Implantation and Inoculation

The prepared orthopedic device was implanted in the rabbit femur. For each hind leg of the animal, a 2 cm incision was made and the implant was attached to the femur with either medical glue (cyanoacrylate) or stainless steel screws or both, and the incision closed with sutures. Inoculation was done during surgery after fixation of the implant on the bone. The implant and surrounding tissue was inoculated with either 500 or 5000 cfu of *Staphylococcus aureus*.

5.3.3.2. Imaging

After surgery, plain X-rays were taken, under isoflurane and a preliminary XELCI image taken of each leg. The implant pH was imaged in vivo using our novel imaging modality, X-ray excited luminescence chemical imaging (XELCI), at least three times per week for two weeks. Blood (up to 1 mL) was drawn on imaging days and sent to a test lab to test for inflammatory markers such as C-reactive protein and sedimentation rate.

5.3.3.3. Termination and Postmortem

After two weeks, rabbits were euthanized with commercial euthanasia solution and a terminal 5 ml blood sample obtained. Postmortem studies included retrieval of the implanted the sensors, visual inspection of the implant and surrounding tissue, culturing of bacteria from the surrounding tissue and confirming reversibility of the retrieved pH

sensor films. The rabbit femurs (some with implant attached and others without implant) were stored in freezer for microCT imaging and in formalin for histological examination. MicroCT (MicroCT SkyScan 1176, Bruker, MA, USA) scans were done at 35 μm resolution with a source voltage of 80kV and current 313 μA.

5.4. RESULTS AND DISCUSSION

We first describe the design of the sensor modified orthopedic implant used in the preliminary studies followed by in vitro sensor characterization including reversibility, mechanical and biocompatibility. Here, we briefly mention the reversibility of the sensor; a complete spectroscopic characterization of the preliminary PEG sensor including spectra of the aqueous pH dye (Bromocresol green) and spectra of the pH dye in the gel matrix (PEG) of the sensor in addition to the signal attenuation of the sensor at different pH is already discussed in Chapter 3 where the sensor signal was characterized in detail through different types of tissue. Details of the evaluation of sensor material for mechanical integrity and biocompatibility demonstrated through in vitro biofilm formation are discussed here. The in vivo section describes the classification of the animal studies into two groups with detailed observations for the individual rabbit studies in each group and a comprehensive discussion of the results from each group of experiments. This is followed by combined postmortem evaluations for both groups including details of the postmortem bacterial count, sensor reversibility and leaching in vivo, histological examination and postmortem imaging.

5.4.1. Implant Design

The implant was made from a piece of medical grade titanium sheet metal cut into a rectangular plate and the sensor films glued to the plate. A schematic of the implant is given in Figure 5.2. The metal plate was 20 x 6 mm and covered completely by scintillator film. The pH sensitive film partially covered the scintillator film leaving a 6 x 4 mm white reference region. The pH sensitive area was 14 x 6 mm consisting of both the scintillator and pH sensitive films.

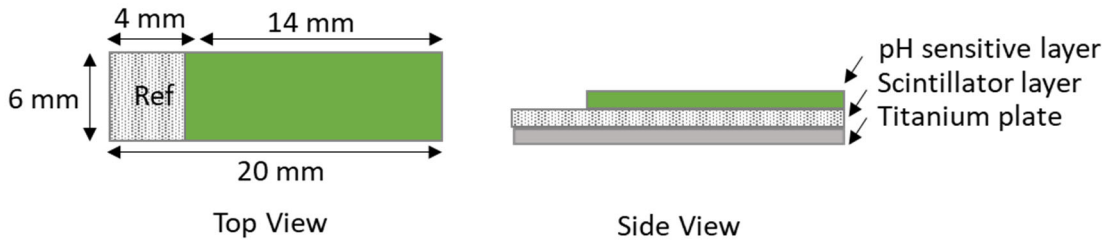

Figure 5.2: Sensor schematic with top and side views. The sensor consists of a titanium plate completely covered with scintillator layer and partially covered in pH sensitive layer. The part of the scintillator film not covered by the pH sensitive layer is the reference region.

5.4.2. Sensor Characterization

The sensor was characterized for pH response, reversibility, biocompatibility and biofilm growth. The details of these are given below.

5.4.2.1. Reversibility

The reversibility study for the preliminary PEG hydrogel sensor with BCG dye is given in Figure 3.5 in Chapter 3. The leaching curves for the dye-doped PEG films (sensor version 1) in PBS and standard buffer 4 are shown Figure 3.6 in Chapter 3.

Briefly, there was significant leaching during the water conditioning treatment (1hr). More leaching was observed in the PBS leachates than in pH 4 buffer leachates.

5.4.2.2. Mechanical Integrity for Debridement

The film need to be able to withstand wound lavage, and irrigation and debridement procedures or accidental scratching during implant insertion. Directed wound irrigation is often used to remove the biofilms and necrotic tissue with solutions delivered to the wound by gravity flow (1-2 psi), low-pressure irrigation (5-10 psi), or high-pressure irrigation (>20 psi).[6] The ideal irrigation technique and pressure required for optimal outcome are still undetermined in the literature.[7] Volumes of 50-100 mL per centimeter of laceration length or per square centimeter of a wound are commonly reported in the literature.[7] Increasing the amount of cross linker and thickness of the film improves the mechanical stability and makes the structure more rigid. We did a testing of the pH indicating film for debridement by placing it under running tap water and increasing the water flow as shown in figure 5.3. The film was resistant to considerable amount of flow (0.1 to 0.25 litre/sec) but ultimately broke off at points of weak attachment under higher flow (> 0.25 litre/sec).

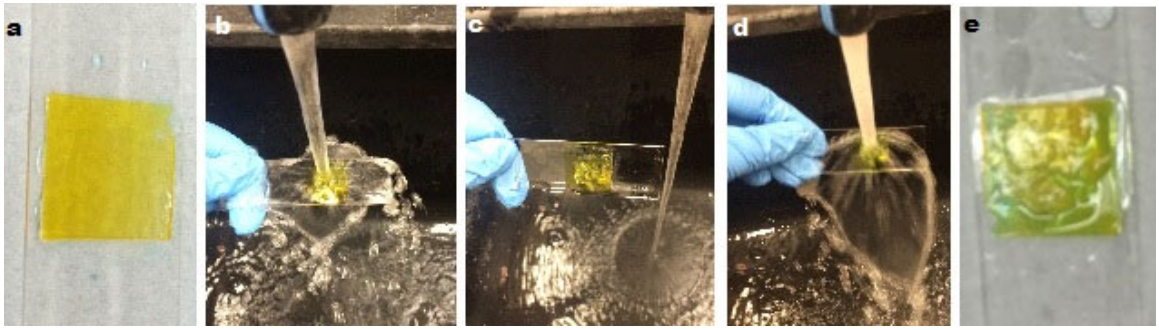

Figure 5.3: Preliminary mechanical testing of PEG film containing 5% PETA for withstanding debridement. The film was attached to a glass slide using super glue (a) and subjected to increasing flow of tap water (b= 0.1litre/sec & d-0.25 litre/sec). c & e shows the intact film after the testing. It ultimately broke off at weak points of attachment under higher flow (> 0.25 litre/sec).

5.4.2.3. In Vitro Biofilm Formation

In order to measure the pH of a biofilm or bacterial culture causing the infection, it is important to know if the biofilm can form on the sensor surface or not. To test this, we studied the formation of biofilm on our sensor films by culturing bacteria (*gfp* tagged *Staphylococcus aureus*) on the pH sensing films. *Staphylococcus aureus* is the primary strain associated with infected metal implants whereas coagulase negative strains such as staphylococcus epidermidis are commonly found in infected polymer implants.[8] The use of *gfp* tagged strain of *S. aureus* allowed to visualize the biofilm coverage on the sensor film. The formation of biofilm was imaged using confocal microscopy which allows the imaging of different thicknesses (z-stacks) of the biofilm. Biofilm coverage as calculated from the image was 54% after 24 hours. Figure 5.4 shows the confocal scanning laser microscopy images (side, volume and top views) of the biofilm grown on PEG sensor films after 24 hour incubation with *gfp* tagged *Staphylococcus aureus*.

Hunter et al showed the pH heterogeneity of the biofilm using a fluorescent pH indicator with values ranging from pH 5.6 (within the biofilm) to pH 7.0 (bulk fluid).[9] This heterogeneous pH is thought to play a strong role in antibiotic resistance, as it affects the antibiotic chemistry and bacterial metabolism and because low pH is an indication of a poorly perfused region with likely lower antibiotic penetration and dormant bacteria.

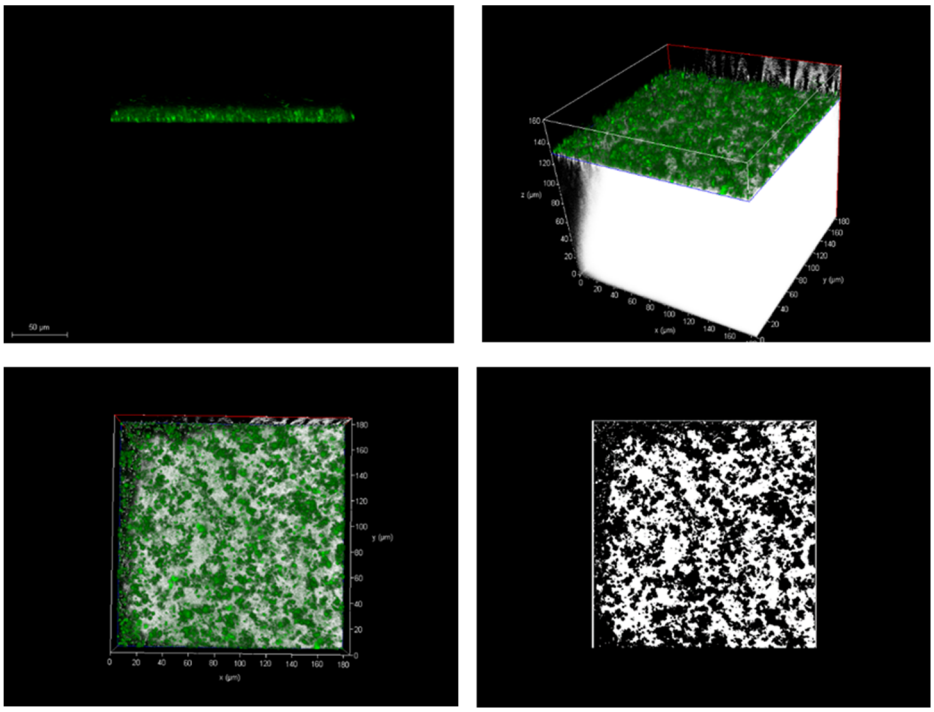

Figure 5.4: Confocal scanning laser microscopy images (side, volume and top views) of biofilm grown on PEG sensor films after 24 hour incubation with gfp tagged bacterial culture (*Staphylococcus aureus*). Thickness of the biofilm from the image was 14.7 um (49 slices) with a total coverage of 54%.

5.4.2.4. Sensor Biocompatibility

We have designed the sensor using biocompatible materials minimizing the toxicity associated with the leaching of the indicator dye, photoinitiator and scintillator particles. The gadolinium particles enclosed in PDMS (Polydimethylsiloxane) do not leach out as tested by incubation in 1 M sulfuric acid for 5 days.[10] Also gadolinium compounds are used as contrast agents in MRI and the amount of Gd used in the sensor (18 mg of Gd_2O_2S:Eu per 1 cm^2 of area) is less than the recommended dose for MRI (0.1 mM of Gd-chelate per kg of body weight).[11] LD_{50} (the median lethal dose) of free Gd ion is 100-200 mg/kg as determined by rodent studies and chelation increases the LD_{50} with regard to the free ion by at least a factor 100.[11] Leaching of the photoinitiator from the sensor film is unlikely as photo initiators are quickly consumed under exposure to oxygen and UV light. To ensure this, the initiator is given enough UV exposure to allow complete reaction of radicals and the film is thoroughly washed with PBS as a pre-treatment step. The pH dye used in this design has not been found to be a carcinogen nor produce genetic, reproductive, or developmental effects. Only about 1mg of dye per gram of the polymer solution is being used and only a fraction of the dye leaches out of the hydrogel.

5.4.3. In Vivo Study

The in vivo testing of two types of sensors was conducted in two groups. The Vinyl-PEG sensors were tested in Group 1 and the PEG hydrogel sensors were tested in Group 2. Each group had 3 animals. Group 1 consisted of rabbit 1, 2 and 3, and Group 2 consisted of rabbit 4, 5 and 6. Rabbit 1 and 4 were complete control animals. For all

other rabbits, left leg was kept as control (not infected) and right leg was inoculated to induce infection. Group 2 surgeries were performed one day after group 1 surgeries. XELCI imaging was done on day of surgery (day 0) if time allowed and then on day 1, 3, 7 and 10 for group 1 and on day 2, 7 and 9 for group 2. Group 1 study was terminated on day 10 and group 2 on day 9 after the surgery. Following are the postmortem observations for each rabbit.

5.4.3.1. Group 1 Studies

Vinyl-PEG sensors were used in group 1 and found to cause inflammation as well excessive leaching of the dye from the sensor based on the following observations for the Preliminary Rabbits 1 - 3.

Preliminary Rabbit 1 (PR 1): This was the complete control animal. For the right leg (PR 1R), the tissue covering the implant was measured to be about 8.8 mm thick. There was not much inflammation or serous fluid present but most of the dye seemed to have leached out of sensor. For the left leg (PR 1L), serous fluid was observed near implant and inflammation was obvious. The implant was no longer attached to the bone but was held in place by muscle tissue an most of dye seems to have leached as well. The sensor was removed and sensitivity tested by immersing in pH 4 buffer but no visible color change could be seen due to excessive leaching of the dye.

Preliminary Rabbit 2 (PR 2): The right leg (PR 2R) was inoculated with 500 cfu of *S. aureus* during surgery. The tissue covering the implant was measured to be about 13 mm thick. No significant inflammation or serous fluid was seen but the incision looked

irritated (red). The left leg (PR 2L) was control but a lot of inflammation and serous fluid was observed around the implant.

Preliminary Rabbit 3 (PR 3): The sensors could not be imaged on last day before euthanasia due to shortage of time. X-Ray images were taken after euthanasia. Right leg (PR 3R) was inoculated with 5000 cfu *S. aureus* during surgery. The tissue covering the implant was measured to be about 6.5 mm thick. Abscess growth with lots of white blood cell accumulation was obvious indicating infection. Left leg (PR 3L) was kept as control and the tissue looked healthy with no significant inflammation or serous fluid.

Figure 5.5 is representative of the Group 1 studies and shows the results form preliminary rabbit 3 (PR#3) study. A photograph of the sensor coated plate to be implanted is given in Figure 5.5A and shows the white reference and the green pH sensitive regions. The sensor coated implants were sterilized in 70% ethanol and implanted on the left and right rabbit femurs using medical superglue (Figure 5.5B). The placement of both implants can be clearly seen in the x-ray image taken after surgery (Figure 5.5C) but we cannot differentiate the reference and senor regions on the implant in the x-ray image. Figure 5.5D shows the XELCI images for the 620 nm, 700 nm and the ratio (620/700) intensities of the sensor coated implants in both legs taken on Day 8 of the experiment through tissue in the live rabbit. The reference region in the implant can be easily differentiated in the XELCI images of the implants in both legs especially in the ratio images. However, we did not see a pH difference between the infected (right) and control (left) legs as we expected during infection and the absence of the pH difference was confirmed during postmortem examination as both the retrieved sensors looked alike.

Postmortem images (Figure 5.5F) show pale colored sensors indicating leaching of the dye. The presence of white pus near the inoculated implant in right leg indicated infection while no pus was observed in the control (not infected) leg.

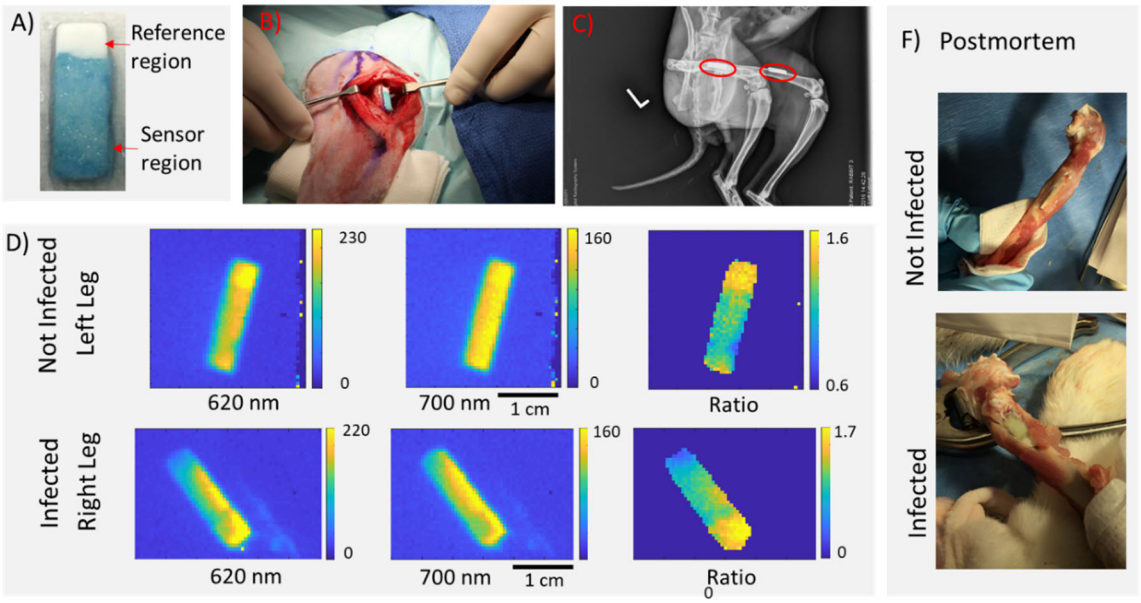

Figure 5.5: Example of a preliminary rabbit study from group 1 (PR#3). A) Photograph of the pH sensor coated plate with reference (white) and sensor (green) regions. B) Sensor in (A) implanted on the rabbit femur during surgery. C) X-ray image showing the implanted sensors (circled) on the rabbit femurs. D) In-vivo XELCI images of the implants at 620 nm intensity, 700 nm intensity and the ratio (I-620/I-700) in both legs (control and infected) through tissue in live rabbit. E) Postmortem photographs of the control (not-infected) and infected rabbit femurs showing the fixed implants. Note the presence of white pus surrounding the implant in the infected leg.

5.4.3.2. Group 2 Studies

PEG sensors were used for group 2 studies. Based on the postmortem observations, it was found that the tissue does not attach to these implants as much as it does to vinyl-PEG sensors used in group 1. Detailed observations for the group 2 Preliminary Rabbits 4-6 are given below.

Preliminary Rabbit 4 (PR 4): This was the complete control animal. For the right leg (PR 4R), the tissue covering the implant was measured to be about 7 mm thick. A little inflammation and serous fluid was present and the sensor was green in color indicating in-situ pH and no significant leaching. For the left leg (PR 4L), the tissue covering the implant was measured to be about 10 mm thick. There was slight swelling at incision site. The sensor green in color and removed for sensitivity testing and immersed in pH 4 buffer. The sensor response to pH change was slow (at least three hours for visible color change) but still responding.

Preliminary Rabbit 5 (PR 5): The right leg (PR 5R) was inoculated with 500 cfu of *S. aureus* during surgery. The tissue covering the implant was measured to be about 7.8 mm thick. A lots of white pus was present and infection was apparent. The sensor gel appeared green in color indicating in-situ pH and no significant leaching. The left leg (PR 5L) was control and the tissue and incision site looked healthy. Thickness of tissue around the implant was about 8.7 mm. The implant looked green in color.

Preliminary Rabbit 6 (PR 6): Right leg (PR 6R) was inoculated with 5000 cfu *S. aureus* during surgery. The tissue covering the implant was measured to be about 7.8 mm thick. Presence of pus with lots of white blood cell accumulation was obvious indicating infection but the implant indicated physiological pH (green in color). Left leg (PR 6L) was kept as control. The tissue around the implant was about 11 mm thick and looked healthy.

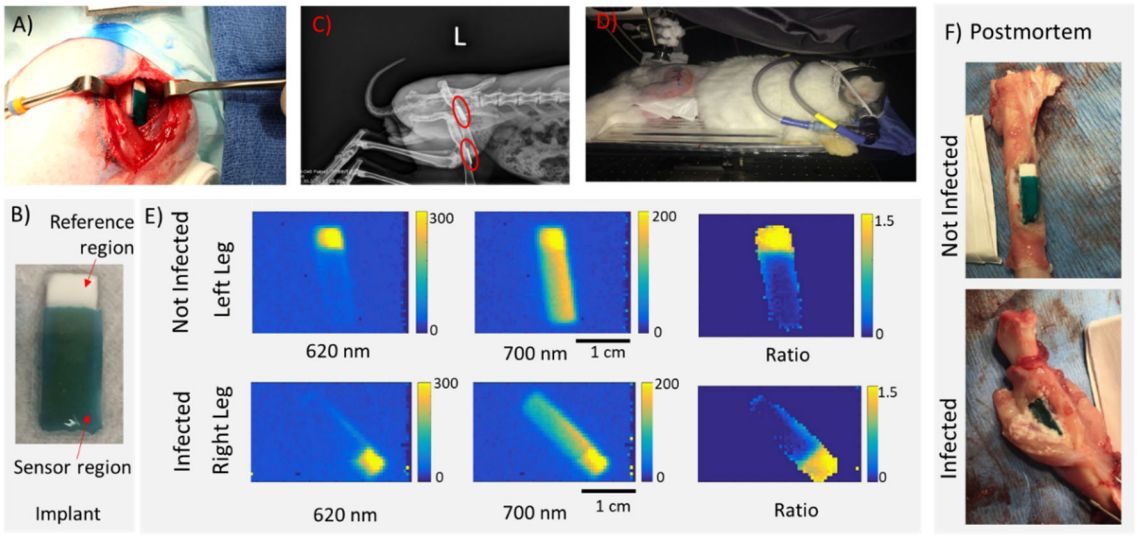

Figure 5.6: Example of a preliminary rabbit study from group 2 (PR#6). A) Sensor implanted on the rabbit femur during surgery. B) Photograph of the pH sensor coated plate with reference (white) and sensor (green) regions taken before surgery. C) X-ray image showing the implanted sensors (circled) on the rabbit femurs. D) Photograph of the rabbit undergoing XELCI imaging under anesthesia. E) In-vivo XELCI images of the implants at 620 nm intensity, 700 nm intensity and the ratio (I-620/I-700) in both legs (control and infected) through tissue in live rabbit. F) Postmortem photographs of the control (not-infected) and infected rabbit femurs showing the fixed implants. Note the presence of white pus surrounding the implant in the infected leg.

An example of a preliminary rabbit study from group 2 is given in Figure 5.6 for the preliminary rabbit 6 (PR#6). A photograph of the sensor coated plate to be implanted is given in Figure 5.6B and shows the white reference and the dark green pH sensitive regions. The sensor coated implants were sterilized in 70% ethanol and implanted on the left and right rabbit femurs using medical superglue. Photograph of the right leg during surgery when the sensor is being implanted is shown in figure 5.6A and both implants are clearly visible in the x-ray image in figure 5.6C. Photograph of the anesthetized rabbit undergoing XELCI imaging on the right leg is also shown in figure 5.6D. XELCI images in figure 5.6E show the clearly distinguished reference and sensor regions of the implant in both legs. The yellow regions indicate high signal intensity as expected for the

reference region and can also be indicative of low pH if present in the sensor region (other than the reference). The darker regions indicate low signal intensity and high pH. Postmortem images (figure 5.6F) confirmed dark green colored sensors indicating high pH (and no significant leaching) for both right and left leg implants. Presence of white pus near the inoculated implant (right leg) indicates infection but a pH drop was not observed.

5.4.4. Postmortem Evaluation

Postmortem study included visual inspection of the tissue and bone and retrieval of implants. The retrieved implants (explants) were then tested for reversibility and visually inspected any possibly leaching of the dye. Tissue samples surrounding the implants were taken to confirm presence of bacteria.

5.4.4.1. Postmortem Bacterial Count

The tissue surrounding the implants was observed for any signs of inflammation, irritation and presence of pus to indicate infection. To confirm that the infection was established or not, bacteria was cultured from the surrounding tissue samples and results are given in the table below. Inflammation of the surrounding tissue was observed for the control rabbit, PR 1 in Group 1 indicating possibility of biocompatibility issues for the Vinyl-PEG sensors. The recovered bacteria confirmed the presence of infection in the infected legs of PR 3 and PR 6 inoculated with 5000 cfu in both groups while the infection was confirmed in only group 2 rabbit, PR 5, inoculated with 500 cfu but not for PR 2 inoculated with same concentration. This indicated the need for at least 5000 cfu of

initial bacterial concentration to induce infection. The rabbits inoculated with 5000 cfu did not develop any severe illness and the study demonstrated the safe use of this high concentration. No bacteria was recovered from the control rabbits, PR 1 and PR 4 and also from the control legs of the infected rabbits confirming the absence of hematogenous infection. A summary of the postmortem observations including bacteria recovery from the retrieved implants and the surrounding tissue, signs of infection in the tissue and the initial concentration of the inoculation used for the preliminary rabbit studies is given in Table 5.1.

#	Implant type	Inoculation		Sign of infection in tissue (Infected Leg)	Sign of infection in tissue (Control leg)	Bacteria recovered from tissue (Infected Leg)	Bacteria recovered from tissue (Control Leg)
		Right leg (Infected)	Left leg (Control)				
PR 1	Metal plate + Glued Vinyl Sensor	NA	NA	-	Inflammati-on	-	-
PR 2	Metal plate + Glued Vinyl Sensor	500 cfu	NA	-	Inflammati-on	-	-
PR 3	Metal plate + Glued Vinyl Sensor	5000 cfu	NA	Abscess growth	-	1.36E+05 cfu/g	-
PR 4	Metal plate + Glued PEG Sensor	NA	NA	-	-	-	-
PR 5	Metal plate + Glued PEG Sensor	500 cfu	NA	Abscess growth	-	2.17E+04 cfu/g	-
PR 6	Metal plate + Glued PEG Sensor	5000 cfu	NA	Abscess growth	-	1.78E+04 cfu/g	-

Table 5.1: Summary of bacteria recovered from tissue culture and retrieved implants for preliminary rabbit studies.

5.4.4.2. Sensor Reversibility and Leaching

The pH sensors were responding to changes in pH and were reversible after retrieval from the animal. The Vinyl-PEG sensors used in Group 1 had excessive leaching of the dye that was visually obvious while the PEG sensors used in Group 2 did not seem to have any significant leaching and looked saturated with the dye. The sensors were tested immediately after retrieval for reversibility in pH 4 buffer and stored in same for about a month. They were later immersed in PBS and no visible color change was observed for 2 hours since the sensors got saturated with salts from acidic pH buffer

storage as confirmed by drop in pH of the PBS solution they were immersed in. The sensors were rinsed with water followed by re-immersion in PBS and photos taken at different time intervals as shown in figure 5.7. The sensors started changing color (yellow to green) on the edges as soon they were immersed in fresh PBS and it took a maximum of 17 hours for the complete color change. The sensors were then immersed in pH 5 buffer followed by pH 4 buffer with the time taken for complete color change from PBS to pH 5 buffer being 8 hours maximum and from pH 5 to pH 4 buffer at 5 hours maximum. The response times for the retrieved sensors stored in acidic buffer were much slower (hours vs minutes) than those observed during sensor characterization studies. These observations suggest the need to store the sensors in low salt concentrations such as 10 - 100x diluted PBS and to rinse the sensors with water before use.

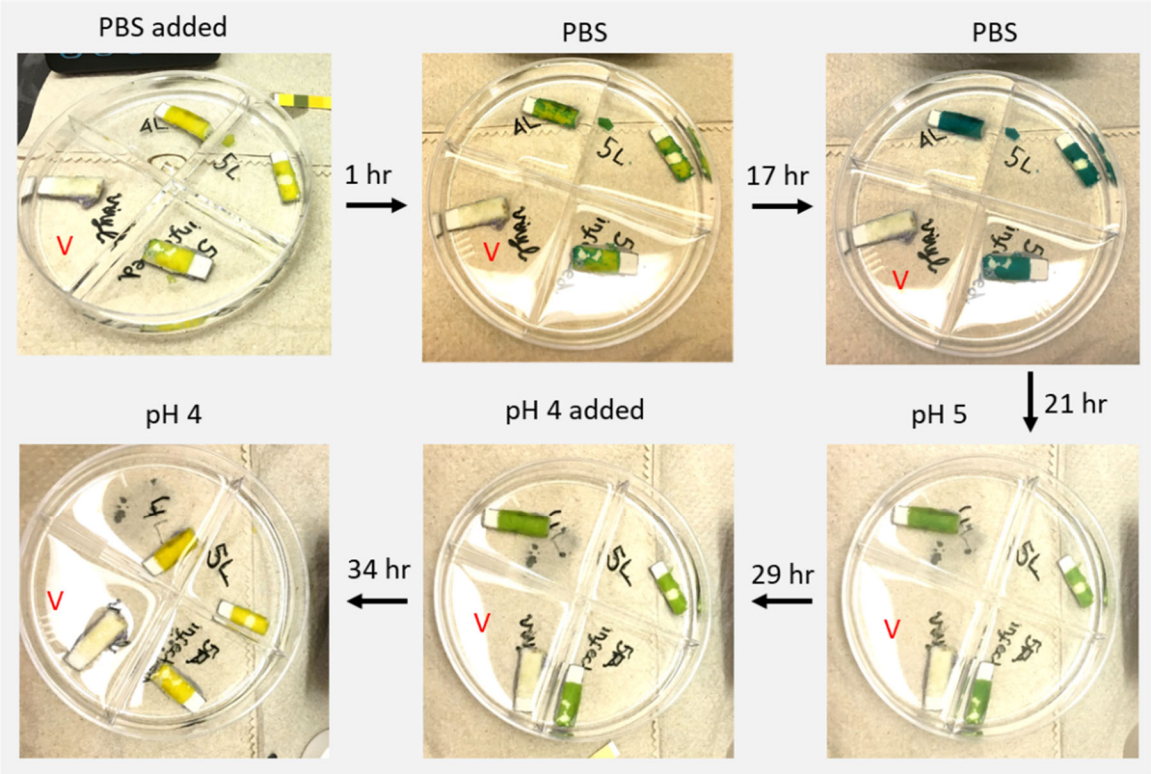

Figure 5.7: Reversibility check of the retrieved implants. One implant from Group 1 (Vinyl-PEG) indicated by a 'V' in the petri dish and three implants from Group 2 (PEG only) were initially stored in pH 4 buffer after retrieval. These were immersed in phosphate buffered saline (PBS), pH 7.2 till a complete color change was obtained (max. 17 hrs) followed by immersion in pH 5 buffer (for 4 hrs) and pH 4 buffer (5 hrs). Time given is the total time elapsed since the sensors were first put in PBS. Note the excessive leaching of dye from the vinyl sensor.

5.4.4.3. Histology and Imaging

The rabbit femurs (some with implant attached and others without implant) were stored in freezer for microCT imaging and in formalin for histological examination. MicroCT was performed on PR 1, Right Femur (implant intact) and PR 4, Left femur (implant detached) to look for any abnormalities in the bone structure. MicroCT images of for PR 1 of the bone and attached implant are given in figure 5.8. The bone looks intact with no signs of erosion and the different layers of the implant (metal plate,

scintillator and hydrogel) are clearly visible in the microCT images. The microCT 3D images provide excellent spatial details of the bone and the individual implant layers but no chemical observations could be made as in the case of XELCI images.

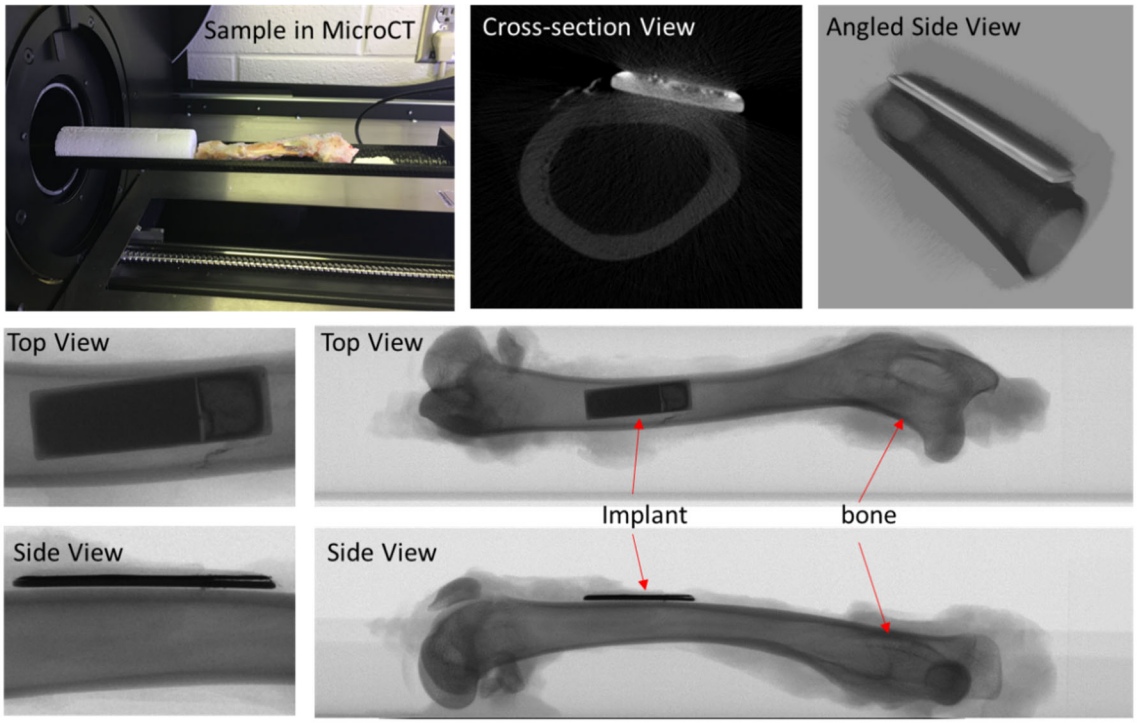

Figure 5.8: MicroCT imaging of the implant fixed on a rabbit femur (PR 1, right leg) showing the imaging set up and different views from the reconstructed microCT images.

The following samples were reserved in formalin for preparation of histology slides: PR 2 right and left femur, PR 3 right and left femur, PR 4 right femur, PR 5 right femur, PR 6 right and left femur. The prepared slides were stained using H&E (Haemotoxylin and Eosin) stain where eosin is an acidic dye and stains basic structures red or pink while haematoxylin is stains the acidic structures a purplish blue. The prepared slides are shown in figure 5.9 and and we did not observe any evidence of major

toxicity. The sensor was still intact and the bone cortex, cavity and layers of the implant (metal plate, scintillator and hydrogel) can be clearly seen in the histology slices. The slides were also imaged with a fluorescence microscope using settings for GFP and DsRed to locate the *gfp* tagged *S. aureus* in the slides. We were not able to confirm the presence of *gfp* tagges *S. aureus* as the images showed much bigger fluorescence spots than expected for the size of *S. aureus* (usually between 0.5 – 2.0 µm). All the samples showed fluorescence with both settings as shown indicating autofluorescence. No clear fluorescence from GFP could be attributed to the chemicals used during slides' fixation and the signal is usually weakened after a few weeks. Therefore, the samples for GFP imaging should not be treated with any chemicals and imaged as soon as possible.

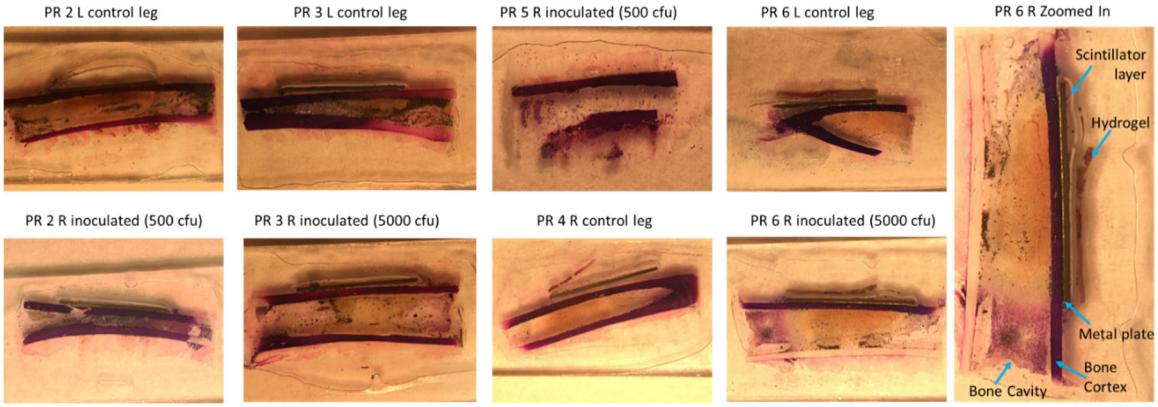

Figure 5.9: Histology slides from select preliminary rabbit studies and a zoomed in image of one of the slides (from PR 6, Right Leg) showing sections of bone (cortex and cavity) and sensor (metal plate, scintillator layer and hydrogel).

5.5. CONCLUSION

The preliminary rabbit study was conducted with 6 rabbits divided into two groups with two versions of the preliminary sensor. Group 1 studies were done with a Vinyl-PEG sensor and group 2 studies used a PEG sensor. The purpose of this preliminary study was to establish a protocol for future in vivo studies and to evaluate sensor performance and suitability to optimize it for future studies. The Vinyl-PEG sensor used in Group 1 had excessive leaching and possible biocompatibility issues as observed by tissue inflammation in the control rabbit and found to be not suitable for in vivo studies. Even though we could not observe a pH change despite clear signs of infection, PR 5 and PR 6, the PEG sensor used in Group 2 showed promising results as no leaching was observed and the tissue in the control rabbit (PR 4) was completely healthy. Therefore, the PEG sensor used in Group 2 studies should be optimized for increased sensitivity within the biological range of pH (pH 6.0 – 7.4) and used for further studies. The slow reversibility response of the sensor necessitates the need for pre-conditioning of the senor gels by cycling between high and low pH buffer solutions. The sensor gels should be stored in low salt concentrations such as 10 - 100x diluted PBS and rinsed with distilled water before use. Two levels of inoculant concentration were also tested to establish a minimum concentration of inoculant required to successfully establish infection without proving to be fatal for the animal. A minimum concentration of 5000 cfu was determined to be used for future inoculations to induce infection as we could not confirm infection in one of the two rabbits tested with a lower amount of inoculant (500 cfu). Since no bacteria was recovered from the control legs of the infected

rabbits negating the possible spread of infection from infected to non-infected leg in the same animal, we can eliminate the use of a control animal (with both legs as control) for future pilot studies and designation of one leg as non-infected in each animal should suffice as control.

With regards to the imaging protocol, conducting simultaneous XELCI imaging of 6 rabbits was found to be impractical (even though possible) given the slow rate of scan and multiple number of scans needed to determine the exact location of the implant in the live rabbit for imaging. Therefore, future studies will be broken into smaller groups and the XELCI imaging to be improved to allow for faster scanning and increasing the amount of signal collected to yield high resolution images. Current scans were done with 500 μm pixel size compared to the 250 μm scans for the ex vivo studies to increase scan speed at the cost of image resolution. MicroCT imaging provided high resolution 3D images of the bones with implant details but yields no chemical information such as pH and is time consuming. Therefore, microCT imaging should be performed only if radiographic images don't reveal sufficient details in cases where bone erosion is suspected or a comparison is needed. We could not observe fluorescence from the *gfp* tagged *S. aureus* under fluorescence microscopy imaging due to longer time lapse between the imaging and sample collection, and due to the chemical treatment of the sample for slide fixation.

Based on these conclusions from the preliminary rabbit studies conducted in Phase A, the PEG sensor and implant design will be optimized. There is also a clear need for improving the signal collection to reduce the time required for XELCI imaging.

5.6. REFERENCES

(1) Kozak, L. J.; Hall, M. J.; Owings, M. F. National Hospital Discharge Survey: 2000 Annual Summary with Detailed Diagnosis and Procedure Data. *Vital Health Stat. 13.* **2002**, No. 153, 1–194.

(2) Trampuz, A.; Zimmerli, W. Prosthetic Joint Infections: Update in Diagnosis and Treatment. *Swiss Med. Wkly.* **2005**, *135* (17–18), 243–251. https://doi.org/2005/17/smw-10934.

(3) Arciola, C. R.; Alvi, F. I.; An, Y. H.; Campoccia, D.; Montanaro, L. Implant Infection and Infection Resistant Materials: A Mini Review. *Int. J. Artif. Organs* **2005**, *28* (11), 1119–1125. https://doi.org/10.1177/039139880502801109.

(4) Widmer, A. F. New Developments in Diagnosis and Treatment of Infection in Orthopedic Implants. *Clin. Infect. Dis. Off. Publ. Infect. Dis. Soc. Am.* **2001**, *33 Suppl 2*, S94-106. https://doi.org/10.1086/321863.

(5) Trampuz, A.; Zimmerli, W. Diagnosis and Treatment of Infections Associated with Fracture-Fixation Devices. *Injury* **2006**, *37 Suppl 2*, S59-66. https://doi.org/10.1016/j.injury.2006.04.010.

(6) Flow Investigators. Fluid Lavage of Open Wounds (FLOW): Design and Rationale for a Large, Multicenter Collaborative 2 x 3 Factorial Trial of Irrigating Pressures and Solutions in Patients with Open Fractures. *BMC Musculoskelet. Disord.* **2010**, *11*, 85. https://doi.org/10.1186/1471-2474-11-85.

(7) Chatterjee, J. S. A Critical Review of Irrigation Techniques in Acute Wounds. *Int. Wound J.* **2005**, *2* (3), 258–265. https://doi.org/10.1111/j.1742-4801.2005.00123.x.

(8) Barth, E.; Myrvik, Q. M.; Wagner, W.; Gristina, A. G. In Vitro and in Vivo Comparative Colonization of Staphylococcus Aureus and Staphylococcus Epidermidis on Orthopaedic Implant Materials. *Biomaterials* **1989**, *10* (5), 325–328. https://doi.org/10.1016/0142-9612(89)90073-2.

(9) Hunter, R. C.; Beveridge, T. J. Application of a PH-Sensitive Fluoroprobe (C-SNARF-4) for PH Microenvironment Analysis in Pseudomonas Aeruginosa Biofilms. *Appl. Environ. Microbiol.* **2005**, *71* (5), 2501–2510. https://doi.org/10.1128/AEM.71.5.2501-2510.2005.

(10) Wang, F.; Raval, Y.; Chen, H.; Tzeng, T.-R. J.; DesJardins, J. D.; Anker, J. N. Development of Luminescent PH Sensor Films for Monitoring Bacterial Growth Through Tissue. *Adv. Healthc. Mater.* **2014**, *3* (2), 197–204. https://doi.org/10.1002/adhm.201300101.

(11) Penfield, J. G.; Reilly, R. F. What Nephrologists Need to Know about Gadolinium. *Nat. Clin. Pract. Nephrol.* **2007**, *3* (12), 654–668. https://doi.org/10.1038/ncpneph0660.

6. MAPPING REAL TIME pH CHANGES ON THE SURFACE OF IMPLANTED ORTHOPEDIC DEVICES IN LIVE RABBIT MODELS USING X-RAY EXCITED LUMINESCENCE CHEMICAL IMAGING—PART II (STUDIES WITH PARTITIONED PLATE REGIONS).

6.1. ABSTRACT

We developed a pH sensor to map real time pH changes on the surface of implanted orthopedic devices using X-ray excited luminescence chemical imaging to detect and monitor implant-associated infection. We designed a partitioned plate with designated sensor regions to be implanted in the rabbit to study pH changes with and without infection. The sensor modified orthopedic plates were implanted in the rabbits and imaged for two weeks followed by confirmation of the imaging results by postmortem evaluations. We conducted 15 rabbit studies that are classified into single plate region (Part I) and partitioned plate regions (Part II). These are further divided into Phase A, B, C and D for clarification with Phase A comprising of all the single plate region studies discussed in Part I. Based on the results of the preliminary studies in Phase A, we optimized the sensor gels to be able to better monitor small changes in physiological pH with a working pH range of pH 6 – 8. We also modified the X-ray excited luminescence chemical imaging (XELCI) system by using a solid light guide to capture more light and increase the signal to noise ratio. The optimized sensor and the modified XELCI system were tested to make sure the system works properly in live rabbits. We studied different case scenarios of infection on the implant surface, in a cavity and the rate of neutralization of pH with and without a biofilm.

6.2. INTRODUCTION

The major goal of this research is to develop a non-invasive method to image chemical concentrations near implant surfaces in order to study implant infection by establishing a baseline for how pH changes in time for normal wound healing and comparing this with infection by inoculation with *gfp* modified *Staphylococcus aureus*. Preliminary in vivo experiments were conducted to determine biocompatibility, toxicity and pH response of the sensor as well as to test for imaging of the pH on the surface of an implant in vivo. The PEG-vinyl sensor used in Group 1 studies of Phase A, had excessive leaching issues while the PEG sensor used in Group 2 studies of Phase A showed promising results however we did not observe a pH change during infection. The preliminary sensor was designed based on the observations from initial in vitro studies that showed a large drop in pH during biofilm formation, but the preliminary in vivo studies proved otherwise. The PEG sensor was optimized to respond to a pH range close to the physiological pH range. The sensors used in Phase A studies had a working pH range of pH 3-6 compared to the optimized sensor with a working pH range of pH 6-8. The implant was redesigned to include partitions for different sensor regions in Phase B followed by a lid in Phase C to form a cavity. The optimized sensor was tested in pilot rabbit studies in Phase B to make sure that the sensor works properly in live rabbits and to allow us to modify it if it does not. The imaging system was also optimized to collect more signal that reduced the background and decreased the imaging time. In vivo experiments were conducted with the optimized sensor and the modified imaging system in Phase C to test for imaging of the pH on the surface of an implant in vivo in different

case scenarios of infection including open plate and cavity simulations. The sensor was implanted in animal (rabbit) model and inoculated with bacteria culture to induce infection. Keeping one leg of the animal as control (no infection) and one leg infected with bacteria culture. The studies lasted 10 days with one exception (R8) where the study was terminated earlier to see the intermediate pH change. We measured and compared the average pH value, spatial distribution, and time course between infected and non-infected legs postmortem. A summary of all the rabbit studies is given in Table 6.1. Phase A studies were discussed in detail in chapter 5. This chapter describes in detail, the studies conducted in Phase B and C as outlined in the summary below and each study is explained in detail in the respective phase. Phase D study is briefly described in Chapter 7 to serve as a model for future work. This chapter provides a general introduction of the studies followed by a general methods section detailing procedures that are applicable to both Phase B and C such as sensor synthesis, design of in vivo studies, implant preparation and inoculation. The studies performed in Phase B and C have their separate sections for methods, results and discussion, and conclusions. Phase B is focused on characterization and evaluation of the optimized sensor in vitro and in vivo, and Phase C assesses different infection scenarios in vivo.

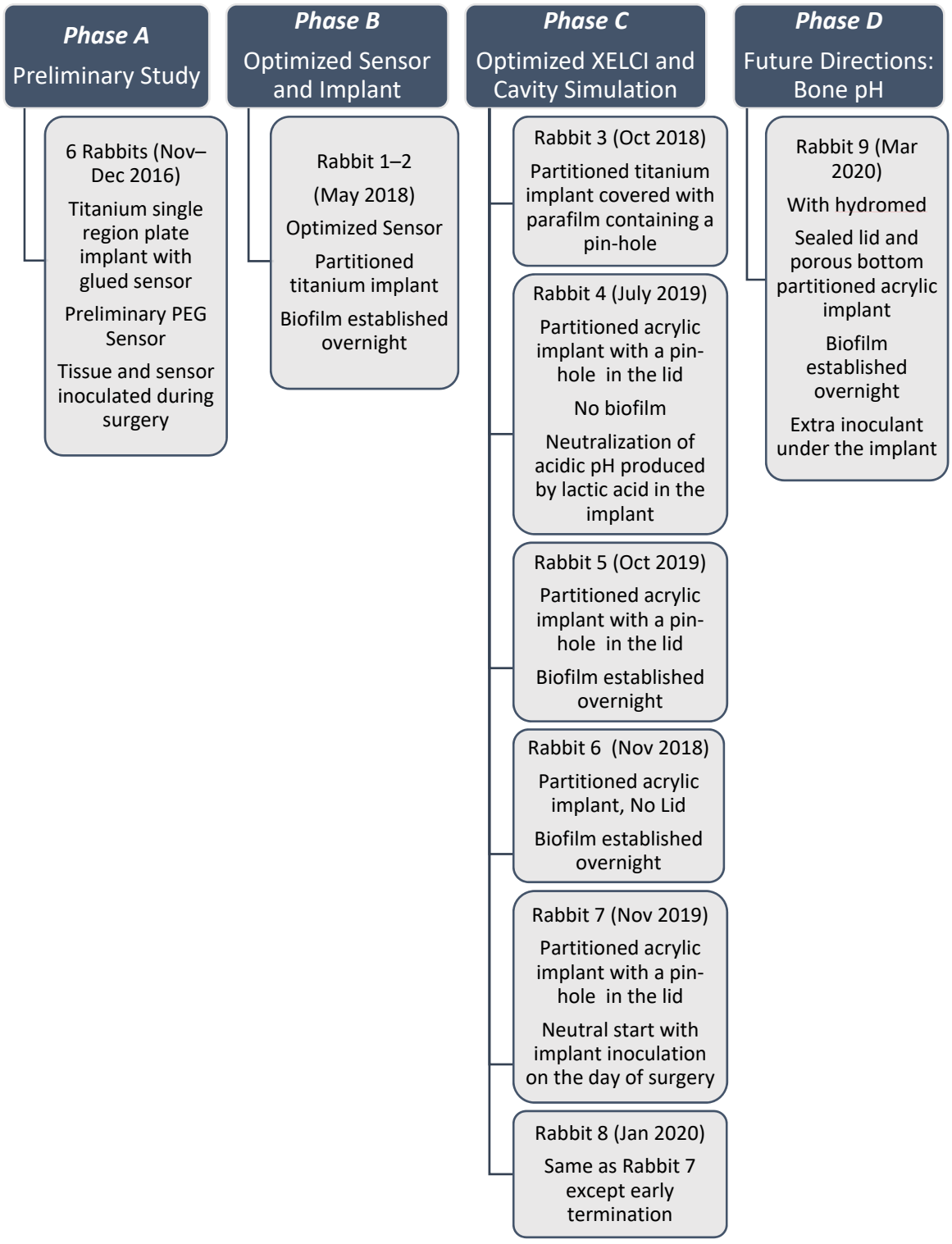

Table 6.1: Summary of rabbit studies.

6.3. GENERAL METHODS

6.3.1. Sensor fabrication

The sensor consists of two layers. A bottom layer of scintillator particles (Gd2O2S:Eu) encapsulated in polydimethylsiloxane (PDMS), and a pH-sensitive top layer synthesized from biocompatible hydrogel incorporating the pH-indicator dye.

6.3.1.1. Scintillator layer

PDMS layer: Silicone elastomer and curing agent (SYLGARD™ 184 Silicone Elastomer base and curing agent, Dow Corning, Midland, Michigan, United States) were mixed in 10:1 (w/w) ratio and ~8.0 μm diameter Gd2O2S:Eu scintillator particles (UKL63/N-R1, Phosphor Technologies Inc., Stevenage, England) were added in 4:1 (w/w) ratio to form a final mixture of 4 g scintillator particles per 1 g of PDMS. This mixture was spread on a glass slide and cured in the oven at 100 °C to form about 0.4 mm thick scintillator-PDMS layer that was cut into desired shape.

6.3.1.2. pH sensitive layer

The optimized sensor used in later studies contained PEG-PAAm hydrogel with BTB dye (pH range 6-8) approximately 400 μm thick. To prepare the pH indicator hydrogel film, a polymerizable solution was prepared by mixing the neutral monomer: acrylamide (AAm) (35 wt%), the chemical cross-linker: polyethylene glycol diacrylate average Mn 700 (PEGDA) (35 wt%), and the UV initiator, 2,2-dimethoxy-2-phenyl acetophenone (DMPA) (1 wt%), a pH indicating dye, bromothymol blue (BTB) (0.5 wt%) together in deionized (DI) water. To synthesize the hydrogel, all the chemical

ingredients were used as received and all of them were taken by mass in a container and the solution was mixed well using a 360° rotator for 2-3 hours and a vortex mixture. Finally, a clear solution was obtained which was kept in an opened glass vial for 1-2 hr under the nitrogen environment in a Cleatech® 2100-4-C glove box (Cleatech, LLC, Santa Ana, CA) before use to synthesize the pH indicating hydrogel film. Next, the polymerizable mixed solution was poured into the reaction cell, where a rectangular silicone rubber frame of 400-micron thickness was sandwiched between a pair of parallel flint glass plates. To construct the reaction cell a pair of flint glass plates, a silicone rubber film, and binder clips were used. Before each use, the glass plates were soaked in a glass cleaner solution of 50 g/L NaOH in 50 % EtOH. In the following, a photo-polymerization reaction was performed using UV irradiation (365 nm) from both sides of the reaction cell for 10 minutes. After completion of the polymerization, a 0.4 mm (approximately) thick Polyethylene glycol – Polyacrylamide (PEG-PAAm) hydrogel film was obtained. The hydrogel film was removed from the reaction cell and subsequently immersed in DI water to remove the unreacted monomers and initiators and for spontaneous hydration. The DI water in the hydrogel container was replaced with fresh once daily for 3 days to satisfactorily remove the unreacted chemicals and excessive/unadhered dye molecules in the hydrogel film. The well washed and hydrated hydrogel film was finally transferred in pH 7.4 PBS solution and cut to desired size.

6.3.2. In Vivo Studies

All in vivo studies were conducted on the New Zealand White Rabbit. One leg of the animal was kept as control (no inoculation) and one leg was infected. Surgery was

performed by the Clemson University veterinarian and all animal studies were conducted at the Clemson University Godley-Snell Research Center after approval of the Institutional Biosafety Committee (IBC) and animal use protocols. Animal anesthesia during imaging and euthanasia at termination was also administered by the Godley-Snell Research Center staff. All bacterial studies were carried out by Dr. Tzeng's lab in the microbiology department.

6.3.2.1. Orthopedic Implant

The implant consisted of a partitioned orthopedic plate with designated chambers for reference, control and infected regions and were machined out of either titanium or acrylic. The control and infected regions were covered with a scintillator film and a pH indicating film. Reference region consisted of just the scintillator film without the pH film except otherwise indicated. The design of acrylic implants was improved to contour to the bone shape of the rabbit after making measurements of several rabbit femurs.

6.3.2.2. Inoculation and Implantation

For Rabbit 1, 2, 3, 5, 6 and 9, the biofilm was established overnight on the infected region of the sensor using an initial bacterial concentration of 5000 cfu. *Staphylococcus aureus* was cultured in 1.5% TSA on the pH-sensing film causing the pH to drop in the TSA and the pH film to change colors. The pH film was placed on an X-ray scintillator film (Gd2O2S:Eu in PDMS) which was fixed in an orthopedic implant; sterile pH sensor regions and uncoated scintillator films were also placed in the designated chambers of the implant.

There was no inoculation for Rabbit 4, instead the acidic pH was produced using lactic acid in the infected region. For Rabbit 9, there was extra inoculation on the underside of the implant by depositing a thin film of 0.7% TSA with bacteria, sterile 0.7% TSA was also deposited on underside of control implant.

For Rabbit 7 and 8, *S. aureus* was cultured in the same manner as mentioned above except that it was cultured fresh on the day of surgery and the biofilm did not have a chance to establish overnight. As a result, the sensor color did not change, and it was implanted with a close to neutral pH as compared to the established acidic pH for R1-6. Table 6.2 summarized the contents of each chamber for both left and right implants for all rabbit studies.

The prepared orthopedic device was then implanted in the rabbit femur. For each hind leg of the animal, a 2 cm incision was made and the implant was attached to the femur with either medical glue (cyanoacrylate) or stainless steel screws or both, and the incision closed with sutures.

Rabbit #	Right leg control		Left leg infected	
	Big chamber	Small chamber	Big chamber	Small chamber
R1	TSA	TSA	TSA	TSA + B
R2	TSA	TSA	TSA + B	TSA
R3	TSA	TSA	TSA + B	TSA
R4	TSA	0.7% Agarose	TSA + Lactic acid, pH:5	0.7% Agarose
R5	TSA	0.7% Agarose	TSA + B	0.7% Agarose
R6	TSA + 1% Glucose	0.7% Agarose	TSA + 1% Glucose + B	0.7% Agarose
R7	TSA + 1% Glucose	0.7% Agarose	TSA + 1% Glucose + B	0.7% Agarose
R8	TSA + 1% Glucose	0.7% Agarose	TSA + 1% Glucose + B	0.7% Agarose
R9	TSA + 1% Glucose	0.7% Agarose	TSA + 1% Glucose + B	0.7% Agarose

Table 6.2: Summary of inoculation chamber by chamber for Rabbit studies 1 – 9. TSA: Tryptic Soy Agar, B: Bacteria (*S. aureus* 5000 cfu).

6.3.2.3. Imaging

After surgery, plain X-rays were taken under isoflurane followed by XELCI image of each leg. The implant pH was imaged in vivo using our novel imaging modality, X-ray luminescence chemical imaging (XELCI), at least three times per week for two weeks. Blood (up to 1 mL) was drawn on imaging days to look for inflammatory markers such as C-reactive protein.

6.3.2.4. Termination and Postmortem

After two weeks, rabbits were euthanized with commercial euthanasia solution and a terminal 5 ml blood sample obtained. Postmortem studies included retrieval of the

implanted the sensors, pH measurements of the implant and surrounding tissue using either a pH microelectrode (Orion™ 9863BN Micro pH Electrode, Thermo Fisher Scientific, USA, or Ultra-M micro pH electrode PHR-146XS, Lazar Research Laboratories, Inc. CA, USA) or commercial pH strips (Whatman® pH indicator papers, Integral Comparison Strip, 6.0 to 8.1 range, Global Life Sciences Solutions USA LLC), culturing of bacteria from the surrounding tissue, imaging of the retrieved implants using XELCI and confirming reversibility of the retrieved pH sensor films.

The sensor consists of two layers. A bottom layer of scintillator particles (Gd2O2S:Eu) encapsulated in polydimethylsiloxane (PDMS), and a pH-sensitive top layer synthesized from biocompatible hydrogel incorporating the pH-indicator dye.

6.3.2.5. Scintillator layer

PDMS layer: Silicone elastomer and curing agent (SYLGARD™ 184 Silicone Elastomer base and curing agent, Dow Corning, Midland, Michigan, United States) were mixed in 10:1 (w/w) ratio and ~8.0 μm diameter Gd2O2S:Eu scintillator particles (UKL63/N-R1, Phosphor Technologies Inc., Stevenage, England) were added in 4:1 (w/w) ratio to form a final mixture of 4 g scintillator particles per 1 g of PDMS. This mixture was spread on a glass slide and cured in the oven at 100 °C to form about 0.4 mm thick scintillator-PDMS layer that was cut into desired shape.

6.3.2.6. pH sensitive layer

The optimized sensor used in later studies contained PEG-PAAm hydrogel with BTB dye (pH range 6–8) approximately 400 μm thick. To prepare the pH indicator

hydrogel film, a polymerizable solution was prepared by mixing the neutral monomer: acrylamide (AAm) (35 wt%), the chemical cross-linker: polyethylene glycol diacrylate average Mn 700 (PEGDA) (35 wt%), and the UV initiator, 2,2-dimethoxy-2-phenyl acetophenone (DMPA) (1 wt%), a pH indicating dye, bromothymol blue (BTB) (0.5 wt%) together in deionized (DI) water. To synthesize the hydrogel, all the chemical ingredients were used as received and all of them were taken by mass in a container and the solution was mixed well using a 360° rotator for 2–3 hours and a vortex mixture. Finally, a clear solution was obtained which was kept in an opened glass vial for 1–2 hr under the nitrogen environment in a Cleatech® 2100-4-C glove box (Cleatech, LLC, Santa Ana, CA) before use to synthesize the pH indicating hydrogel film. Next, the polymerizable mixed solution was poured into the reaction cell, where a rectangular silicone rubber frame of 400-micron thickness was sandwiched between a pair of parallel flint glass plates. To construct the reaction cell a pair of flint glass plates, a silicone rubber film, and binder clips were used. Before each use, the glass plates were soaked in a glass cleaner solution of 50 g/L NaOH in 50 % EtOH. In the following, a photo-polymerization reaction was performed using UV irradiation (365 nm) from both sides of the reaction cell for 10 minutes. After completion of the polymerization, a 0.4 mm (approximately) thick Polyethylene glycol–Polyacrylamide (PEG-PAAm) hydrogel film was obtained. The hydrogel film was removed from the reaction cell and subsequently immersed in DI water to remove the unreacted monomers and initiators and for spontaneous hydration. The DI water in the hydrogel container was replaced with fresh once daily for 3 days to satisfactorily remove the unreacted chemicals and

excessive/unadhered dye molecules in the hydrogel film. The well washed and hydrated hydrogel film was finally transferred in pH 7.4 PBS solution and cut to desired size.

6.3.3. In vivo studies

All in vivo studies were conducted on the New Zealand White Rabbit. One leg of the animal was kept as control (no inoculation) and one leg was infected. Surgery was performed by the Clemson University veterinarian and all animal studies were conducted at the Clemson University Godley-Snell Research Center after approval of the Institutional Biosafety Committee (IBC) and animal use protocols. Animal anesthesia during imaging and euthanasia at termination was also administered by the Godley-Snell Research Center staff. All bacterial studies were carried out by Dr. Tzeng's lab in the microbiology department.

6.3.3.1. Orthopedic implant

The implant consisted of a partitioned orthopedic plate with designated chambers for reference, control and infected regions and were machined out of either titanium or acrylic. The control and infected regions were covered with a scintillator film and a pH indicating film. Reference region consisted of just the scintillator film without the pH film except otherwise indicated. The design of acrylic implants was improved to contour to the bone shape of the rabbit after making measurements of several rabbit femurs.

6.3.3.2. Inoculation and implantation

For Rabbit 1, 2, 3, 5, 6 and 9, the biofilm was established overnight on the infected region of the sensor using an initial bacterial concentration of 5000 cfu.

Staphylococcus aureus was cultured in 1.5% TSA on the pH-sensing film causing the pH to drop in the TSA and the pH film to change colors. The pH film was placed on an X-ray scintillator film (Gd2O2S:Eu in PDMS) which was fixed in an orthopedic implant; sterile pH sensor regions and uncoated scintillator films were also placed in the designated chambers of the implant.

There was no inoculation for Rabbit 4, instead the acidic pH was produced using lactic acid in the infected region. For Rabbit 9, there was extra inoculation on the underside of the implant by depositing a thin film of 0.7% TSA with bacteria, sterile 0.7% TSA was also deposited on underside of control implant.

For Rabbit 7 and 8, *S. aureus* was cultured in the same manner as mentioned above except that it was cultured fresh on the day of surgery and the biofilm did not have a chance to establish overnight. As a result, the sensor color did not change, and it was implanted with a close to neutral pH as compared to the established acidic pH for R1–6. Table 6.2 summarized the contents of each chamber for both left and right implants for all rabbit studies.

The prepared orthopedic device was then implanted in the rabbit femur. For each hind leg of the animal, a 2 cm incision was made and the implant was attached to the femur with either medical glue (cyanoacrylate) or stainless steel screws or both, and the incision closed with sutures.

Rabbit #	Right leg control		Left leg infected	
	Big chamber	Small chamber	Big chamber	Small chamber
R1	TSA	TSA	TSA	TSA + B
R2	TSA	TSA	TSA + B	TSA
R3	TSA	TSA	TSA + B	TSA
R4	TSA	0.7% Agarose	TSA + Lactic acid, pH:5	0.7% Agarose
R5	TSA	0.7% Agarose	TSA + B	0.7% Agarose
R6	TSA + 1% Glucose	0.7% Agarose	TSA + 1% Glucose + B	0.7% Agarose
R7	TSA + 1% Glucose	0.7% Agarose	TSA + 1% Glucose + B	0.7% Agarose
R8	TSA + 1% Glucose	0.7% Agarose	TSA + 1% Glucose + B	0.7% Agarose
R9	TSA + 1% Glucose	0.7% Agarose	TSA + 1% Glucose + B	0.7% Agarose

Table 6.3: Summary of inoculation chamber by chamber for Rabbit studies 1–9. TSA: Tryptic Soy Agar, B: Bacteria (*S. aureus* 5000 cfu).

6.3.3.3. Imaging

After surgery, plain X-rays were taken under isoflurane followed by XELCI image of each leg. The implant pH was imaged in vivo using our novel imaging modality, X-ray luminescence chemical imaging (XELCI), at least three times per week for two weeks. Blood (up to 1 mL) was drawn on imaging days to look for inflammatory markers such as C-reactive protein.

6.3.3.4. Termination and postmortem

After two weeks, rabbits were euthanized with commercial euthanasia solution and a terminal 5 ml blood sample obtained. Postmortem studies included retrieval of the

implanted the sensors, pH measurements of the implant and surrounding tissue using either a pH microelectrode (Orion™ 9863BN Micro pH Electrode, Thermo Fisher Scientific, USA, or Ultra-M micro pH electrode PHR-146XS, Lazar Research Laboratories, Inc. CA, USA) or commercial pH strips (Whatman® pH indicator papers, Integral Comparison Strip, 6.0 to 8.1 range, Global Life Sciences Solutions USA LLC), culturing of bacteria from the surrounding tissue, imaging of the retrieved implants using XELCI and confirming reversibility of the retrieved pH sensor films.

6B. PHASE B: OPTIMIZED SENSOR AND IMPLANT

Based on observations from Phase A studies, the sensor was optimized and updates made to the XELCI system. The implant was redesigned and machined out of titanium with designated chambers for each sensor region such as reference, control and infection instead of a simple piece of sheet piece cut into a rectangular plate. The pH indicating sensor gel was optimized to respond to a pH range between pH 6.0 and 8.0 to better match the changes occurring close physiological pH and synthesized from a cross linked polymer network of diacrylated polyethylene glycol (PEG) and polyacrylamide (PAAm) with bromothymol blue (BTB) as the pH indicating dye. The imaging system was updated with a bigger y-motor capable to travel longer distance as compared to earlier version of the system (150 mm vs. 50 mm). The MATLAB code used for data analysis was also updated to improve the signal to noise ratio in the final images. Two pilot rabbit studies were conducted to evaluate in vivo performance of the optimized sensor. Both studies lasted 10 days after surgery and surgery day was counted as Day 0. The two rabbit studies were conducted 3 weeks apart to avoid any overlap and time conflicts as experienced in Phase A.

6B.1. METHODS

6B.1.1. Sensor synthesis and characterization

6B.1.1.1. Sensor synthesis

The orthopedic implant was machined out of titanium and had partitions for each sensor region. The scintillator and pH indicating layers were prepared as mentioned in the general methods and placed in the respective chambers of the implant.

6B.1.1.2. Spectra (extinction & absorbance)

Spectra were obtained for the pH dye free in solution and encapsulated in the hydrogel at different pH as described in Chapter 3. Briefly, for the free dye, a solution of the dye was prepared in ethanol (1 mg/ml) and 20 µl of this dye solution was added to 2 ml of standard buffers of pH 3 -8 and spectra obtained. For the dye in gel spectra, a piece of the pH sensitive hydrogel was placed in a customized holder placed on the stage of an inverted microscope (DMI 5000, Leica Microsystems, Germany). The gel was immersed sequentially in pH buffers from pH 5 to 8 for 30 minutes each and spectra for each pH was collected by a 5x objective lens and focused to a spectrometer (DNS 300, DeltaNu, Laramie, WY, United States), equipped with a cooled CCD camera (iDUS-420BV, Andor, South Windsor, CT, United States). To measure the attenuation of the scintillator emission signal by the pH dye, the sensor (a piece of pH film covered by scintillator film) immersed in standard buffer solution was placed on the stage of an inverted microscope and irradiated with a focused x-ray beam. The pH modulated emission of the scintillator film was collected by a 5x objective lens and focused to a spectrometer as described

above. Spectra were collected for each pH after immersing the pH film in the respective buffers.

6B.1.1.3. Reversibility

For reversibility study, a 5 mm pH film was fixed to a sample holder and cycled between pH 6 and phosphate saline (~pH 7.2) buffers. Spectra was acquired on the same spectrometer every 1 second for a total of 40 minutes in each buffer and repeated for 5 cycles.

6B.1.1.4. Calibration Curves

A sample of pH film containing the pH dye, was prepared as described in the synthesis section and cut into 5 mm discs using a hole punch. These discs were equilibrated overnight in pH 6.0, 6.5, 7.0, 7.5 and 8.0 buffers to achieve the color change response associated with the respective pH. A reference disc was also prepared that consisted of just the scintillator layer without any pH film. These discs were then placed in 3D printed holder containing the different pH buffers. Reference disc was placed in PBS. This was then imaged using XELCI with no tissue and through 6 mm and 11 mm of chicken tissue, and the 620 nm and 700 nm intensity images were obtained. The raw data (620 nm PMT counts, 700 nm PMT counts, and stage position vs. time) was processed using a MATLAB script to form the 620 nm, 700 nm, and ratio images vs. stage position. The signal was averaged over each disc and normalized to the reference signal.

6B.1.1.5. Evaluation of optimized sensor to measure pH during biofilm formation

A piece of the optimized sensor gel and a pH indicating strip (MColorpHast pH Indicator Test Strips (non-bleeding), EMD Millipore, Germany) was placed in a petri dish and covered with tryptic soy broth (TSB) containing 1% glucose and inoculum (1+E04 *Staphylococcus aureus* cells/ml). A control was also prepared with sterile TSB without inoculum. The samples were incubated at 37°C and a picture was taken every hour to see if the color of gel has changed.

6B.2. RESULTS AND DISCUSSION

We first describe the design of the sensor modified orthopedic implant used in Phase B studies and the detailed in vitro characterization of the optimized sensor including spectra of the aqueous pH dye (Bromothymol blue) and spectra of the pH dye in the gel matrix (PEG-PAAm) of the sensor, signal attenuation of the sensor at different pH and the calibration curves through different tissue thickness. An evaluation of the optimized sensor to measure pH during biofilm formation is also provided. The in vivo section discusses the results of the two pilot rabbit studies followed by postmortem thermal and fluorescence (IVIS) imaging.

6B.2.1. Sensor Characterization

The sensor film needs to be reversible in a short period of time to rapidly detect changes occurring in the pH of the biofilm and on implant surface. For this purpose, the gel in which the dye is entrapped should be H+ permeable for the H+ ion to diffuse through rapidly but keep the dye molecules from leaching out. Initially we used a PEG

based sensor with bromocresol green dye and later we improved the composition to PEG-PAAM hydrogel with bromothymol blue dye as indicator. The change to a new gel composition was to minimize the leaching of the dye and to improve the resilience of the hydrogel films during handling by making thicker films (400 µm vs 200 µm). The shift to a different pH dye (BTB instead of BCG) was after the observation from preliminary pre-pre-pilot rabbit studies where we did not observe a pH drop necessitating for development of a pH sensor with increased sensitivity from pH 6 to 7.4 (close to in situ pH).

6B.2.1.1. Implant Design

The implant was designed to have partitions to hold the sensor layers without the need of any glue. For this, the plate was made into partitioned wells or chambers 1 mm deep with a designated chamber for each sensor region (figure 6.1). The two 2 x 5 mm chambers on each end of the plate were for sensor reference regions while the two middle ones were for control and infected regions. We expected to see the spread of infection and the associated acidic pH from the infected chamber to the control chamber. The two middle chambers were unequal in size with the big chamber measuring 10 x 5 mm and the small chamber measured 6.5 x 5 mm.

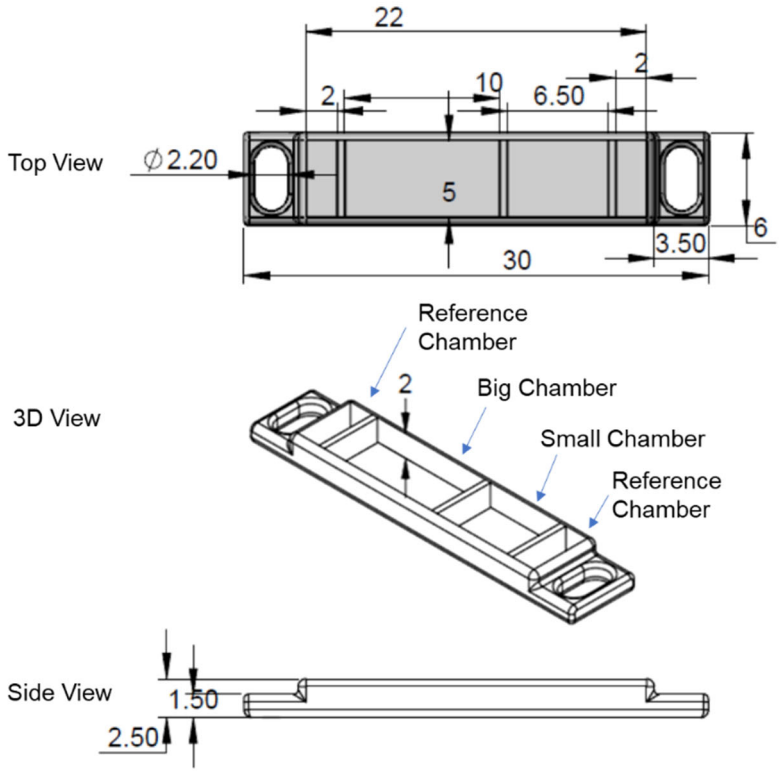

Figure 6.1: SOLIDWORKS drawing of the implant with dimensions in millimeters. The design includes individual chambers for different sensor regions; the two 2x5 mm chambers on each of the implant are reserved for reference region while the two middle chambers are for pH sensitive regions.

6B.2.1.2. Spectra

The shift to bromothymol pH indicating dye was due to its pKa 7.1 that is closer to physiological pH (~7.4). Spectra of the aqueous dye solution and the dye-in-gel at different pH buffers in given in figure 6.2 along with the attenuation of scintillator luminescence after passing through the gel containing the pH dye in different pH. The aqueous solution of the dye has a broader range of pH from pH 5 to 8 with the highest change in absorbance (a factor of 4.3x) from pH 6 to 7 that is ideal for detecting small pH changes close to the physiological pH. The absorbance spectra of the dye

encapsulated in the sensor gel also shows good response and changes by a factor of 1.5x in going from pH 6.5 to 7.0, a change of 1.4x from pH 6.0 to 6.5, 2.8x from pH 7.0 to 7.5 and a change of 1.5x in going from pH 7.5 to 8.0. The 620 nm luminescence intensity of the x-ray irradiated scintillator film decreases due to absorbance by the pH sensitive layer as the pH increases but the 700 nm intensity remains unaffected as shown in figure 6.2C. The ratio of 620 nm and 700 nm intensities as a function of pH are plotted as an inset in figure 6.2C.

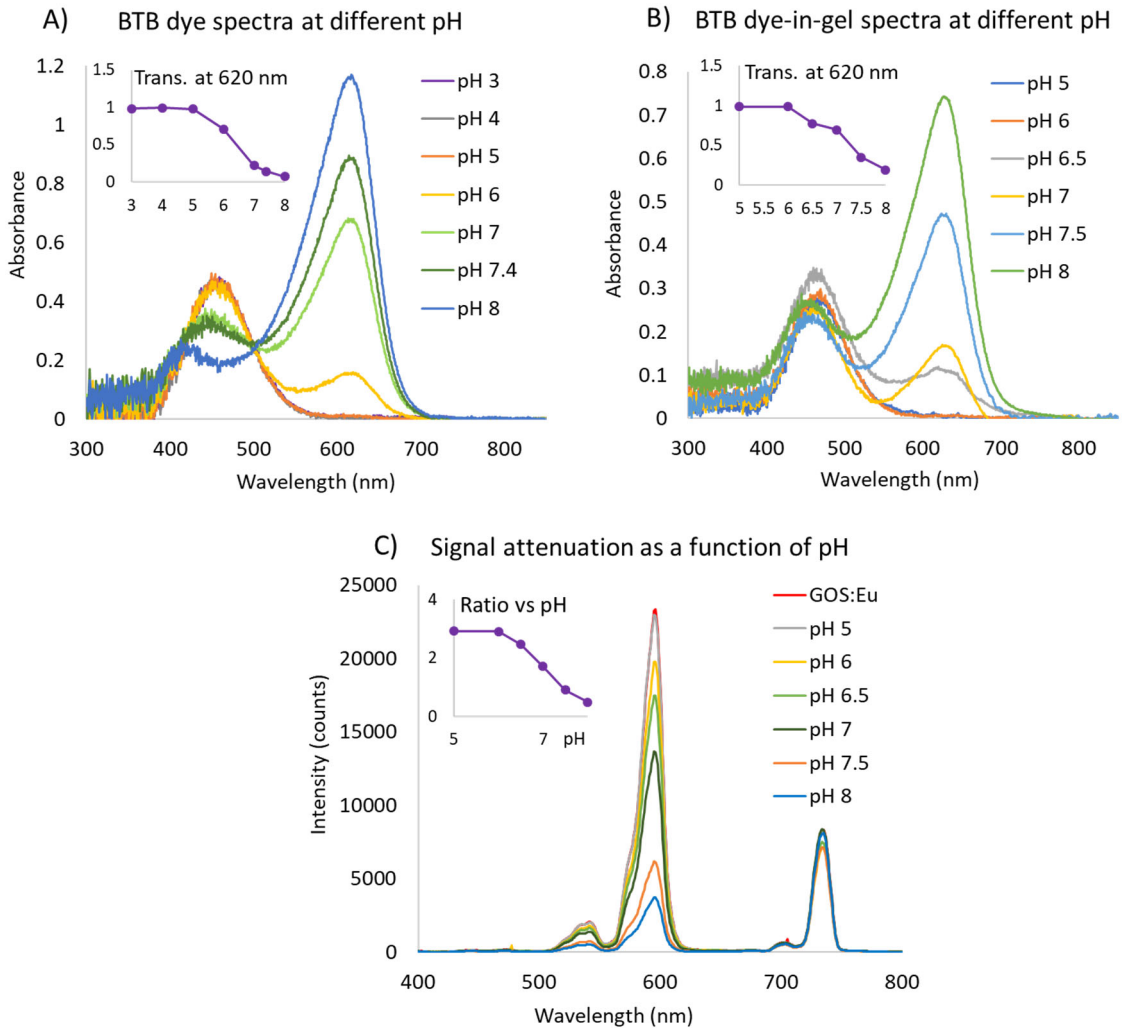

Figure 6.2: Absorbance as a function of pH. A) Absorption spectra of the pH dye in free form (aqueous solution) taken at different pHs (pH 3-8). Inset: Transmittance of BTB dye at 620 nm in different pH. B) Absorption spectra of the BTB pH dye encapsulated in the PEG-PAAm hydrogel taken at different pHs (pH 6-8). Inset: Transmittance of BTB dye in gel at 620 nm in different pH. C) Scintillator radioluminescence spectra of Europium doped Gadolinium oxysulfide (GOS:Eu) after passing through the Bromothymol blue pH dye in PEG-PAAm hydrogel at different pHs. Inset: Ratio of 620 and 700 nm intensities plotted for each pH.

6B.2.1.3. Response Time and Reversibility

The optimized PEG-PAAm films were about 400 µm thick and provided an ideal pH range with the Bromothymol blue pH indicating dye. Two different dye

concentrations were tested and final concentration optimized for a clear color change response without saturating the absorption spectra. The thicker films were easier to handle and synthesize without compromising the response time. A reversibility study done to measure the response time of the films when they were cycled between two different pH (6 and 7.2). The observed response time was slow when going towards basic pH (pH 6 to 7.2) than when the solution is changed to acidic pH (pH 7.2 to 6). This is consistent with previous studies with the PEG-BCG sensors that showed a similar response (Figure 3.5 in Ch 3). The sensor is reversible and has an average τ90% time constant of approximate 30 minutes going from pH6 to pH 7.2 and 5 minutes going from pH 7.2 to pH 6, which is adequate for most in vivo applications where pH shifts over hours.

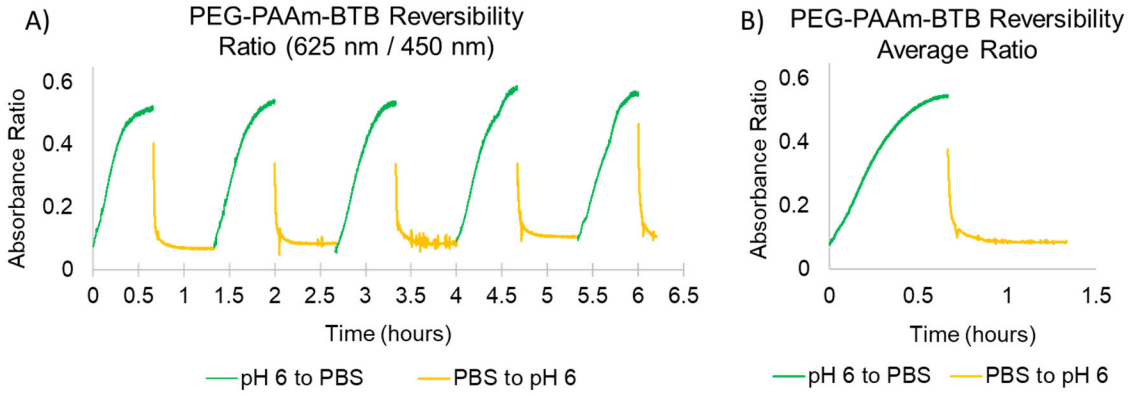

Figure 6.3: Reversibility study of the optimized pH sensor film, PEG-PAAm hydrogel with bromothymol blue pH dye (PEG-PAAm-BTB). (A) pH film was cycled between PBS (pH 7.2) and pH 6 buffer and spectra recorded every 1 second for 40 minutes in each buffer. (B) Average absorbance ratio of the 5 cycles in (A). Gaps correspond to times when the pH buffers were being changed and spectra acquisition was paused to prevent artefacts during pipetting of buffer solutions.

6B.2.1.4. Calibration Curve

Calibration curves were acquired for the optimized sensor through 0, 6 and 11 mm of tissue. XELCI images and plots of individual intensities at 620 and 700 nm and ratio of 620 and 700 nm intensities are shown in figure 6.3. The ratiometric XELCI images for the sensor discs at different pH agree with the color change observed in the photograph of these sensor discs. The reference disc appears the brightest due to absence of any pH-dependent absorbance. The sensor discs at acidic pH are brighter than the ones at higher pH as the signal intensity decreases in going from pH 6 to pH 8 due to increased absorbance of the 620 nm intensity by the pH dye at higher pH. The 700 nm intensity remains unaffected by pH as it is not absorbed by the pH dye at any pH and is used to account for signal attenuation due to variable thickness of the tissue in the ratio image. The intensities were normalized to the respective reference intensity and plotted as normalized intensities I-620 (N), I-700 (N) and Ratio (N).

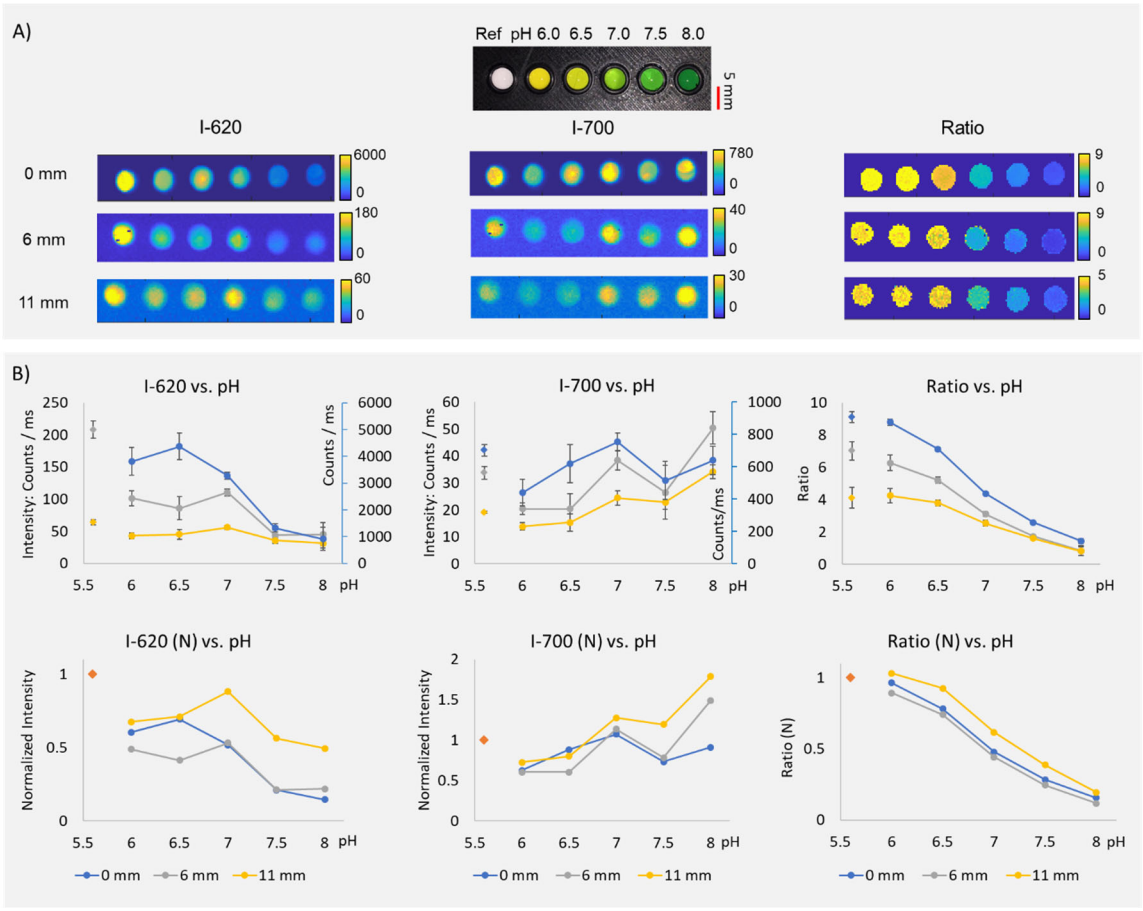

Figure 6.4: Calibration Curves. (A) Photograph showing the pH sensor discs (PEG-PAAm-BTB gel on scintillator film) placed in a 3-D printed holder in pH buffers 6.0, 6.5, 7.0, 7.5 and 8.0 and a reference disc without any pH coating (plotted arbitrarily at pH 5.6). This calibration setup was imaged without tissue and later sandwiched between two pieces of chicken tissue and imaged through 6mm and 11 mm of chicken tissue. XELCI images showing the 620 nm, 700 nm and ratio of 620 to 700 nm signal intensities of the pH sensor discs at respective pH obtained without tissue and through 6 and 11 mm of chicken tissue. (B) Plots of signal intensities as a function of pH through chicken tissue for the sensor discs shown in (A). 620 nm light intensity, 700 nm light intensity and Ratio of 620 and 700 nm intensities at pH 6.0, 6.5, 7.0, 7.5 and 8.0 and ref disc after passing through 0 mm, 6 mm and 11 mm of chicken tissue. Note: Error bars represent the pixel-to-pixel standard deviation within a disc. (N) indicates plots normalized to respective reference intensities.

6B.2.1.5. Evaluation of optimized sensor to measure pH during biofilm formation

In order to evaluate the suitability of the optimized gels to indicate pH during infection, biofilm was grown on the sensor gels and pH response of the gels was evaluated by measuring the pH of the surrounding medium with a commercial pH strip. Since the gel appears green in neutral pH and yellow in acidic pH, we expected the gel color to change from green to yellow with the growth of bacteria on the sensor gel and surrounding media. The gel color did change after 15 hours corresponding with pH change measured by the pH strips from pH 7 to 5 after 15 hours as shown in figure 6.4A-B. pH did not change for the control (B-). The experiment was repeated to see the pH effect due to spread of biofilm from the inoculated (B+) medium to the sterile (B-) medium by using one piece of gel with one half covered with in inoculated medium and one half covered with sterile medium. After 15 hours, the part of gel in inoculated medium was yellow in color and the pH strip measured pH 5 in the inoculated medium while the pH strip indicated pH 7 in the sterile medium but the gel appeared to be greenish yellow indicated acidic pH and spread of bacteria from the inoculated region of the gel to the sterile region. The pH strip indicated neutral pH in sterile medium as this spread was not enough to convert the pH of the sterile medium to acidic in such a short duration.

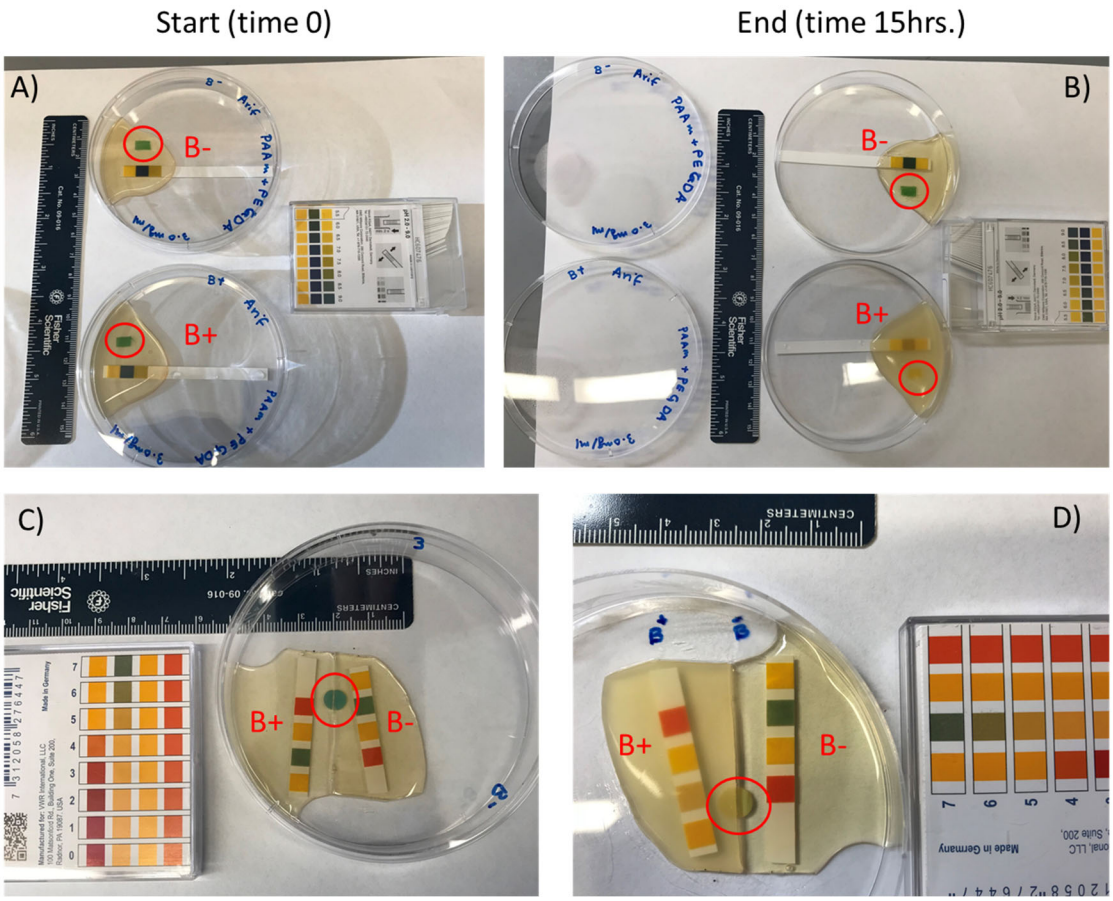

Figure 6.5: Evaluation of optimized sensor to measure pH during biofilm formation. The optimized sensor gels were tested for pH response during in vitro biofilm formation. To confirm the pH of the medium, a piece of pH strip was placed with the sensor gel. B+ means bacteria added, B- means no bacteria, green gel color indicates neutral pH, yellow gel color indicates acidic pH.

6B.2.2. In Vivo Study

Two pilot rabbit studies were performed to evaluate the performance of the optimized sensors. Right leg was kept as control and the left leg was infected. The inoculation was done differently than the Phase A rabbits by establishing a biofilm overnight in one of the implant chambers on the sensor gel as opposed to inoculating the implant and surrounding tissue during surgery.

6B.2.2.1. Pilot Study, Rabbit 1

The sensors were prepared by placing the scintillator layer in the implant chambers. Sealed acidic and physiological pH references were prepared to allow for easier comparison of pH of the implanted sensor during imaging. For the reference chambers, the gels were soaked in acidic (pH 4) and basic (pH 8 or PBS) and dried in oven at 45°C for 5 hours. These dried reference gels were laminated and placed on top of the scintillator film in reference chambers and covered with PDMS and cured at 60°C for 2 hours. The acidic reference was placed in the reference chamber next to small chamber and physiological pH reference was placed in the reference chamber next to big chamber. Hydrated sensor gels (in PBS) were placed in the big and small chambers on top of the scintillator film. For the control implant (placed on right leg), a layer of sterile TSA was added on top of the sensor gels. For the inoculated implant (placed on left leg), a layer of sterile TSA was added on top of sensor gel in big chamber and a layer of inoculated TSA was added on top of sensor gel in small chamber to induce infection (Figure 6.5A). We expected to see the spread of infection from small to big chamber and a change in pH of both chambers in the infected leg over the course of the experiment as observed in the in vitro study. X-ray image of the implant show all the chambers, but no pH sensitive information can be deduced from the x-ray images. A XELCI image of the implants was taken before surgery (pre-op) without any tissue. The implants were fixed to the femur using two 8 x 2 mm stainless steel screws with pilot holes drilled in the bone. X-ray images of rabbit legs were obtained after surgery and the animal was imaged with XELCI

under anesthesia after the surgery and on day 1, 2, 4 , 7, 9 and 10 after the surgery. The XELCI images are shown in figure 0.5E-F for both legs. All four chambers are clearly distinct in all the images. The inoculated region (yellow) of the left implant is clearly acidic in the pre-op image and seems to be neutralized and look the same as the control region in rest of the images. The pre-op and postmortem XELCI images of the sensor taken without tissue are sharp and clear but the in vivo images still show a lot of noise and are not as sharp. This indicates the need to improve the signal collecting optics to increase the signal to noise ratio. Imaging also depends on the placement of the rabbit to position the implanted sensors perpendicular to the x-ray beam and placement of the collecting light guide to collect signal. Week 2 images are clearer than week 1 images. Both reference regions can be seen in the images with the acidic reference appearing brighter (yellow) than the basic reference in most of the images, however in Day 9, 10 and postmortem images of the left implant, both references appear to be equally bright. This could be due to variable tissue thickness covering both ends of the implant and the use of two different references is not useful in such a case. Use of two homogeneous references on each side can help determine the pH-independent effect of tissue thickness.

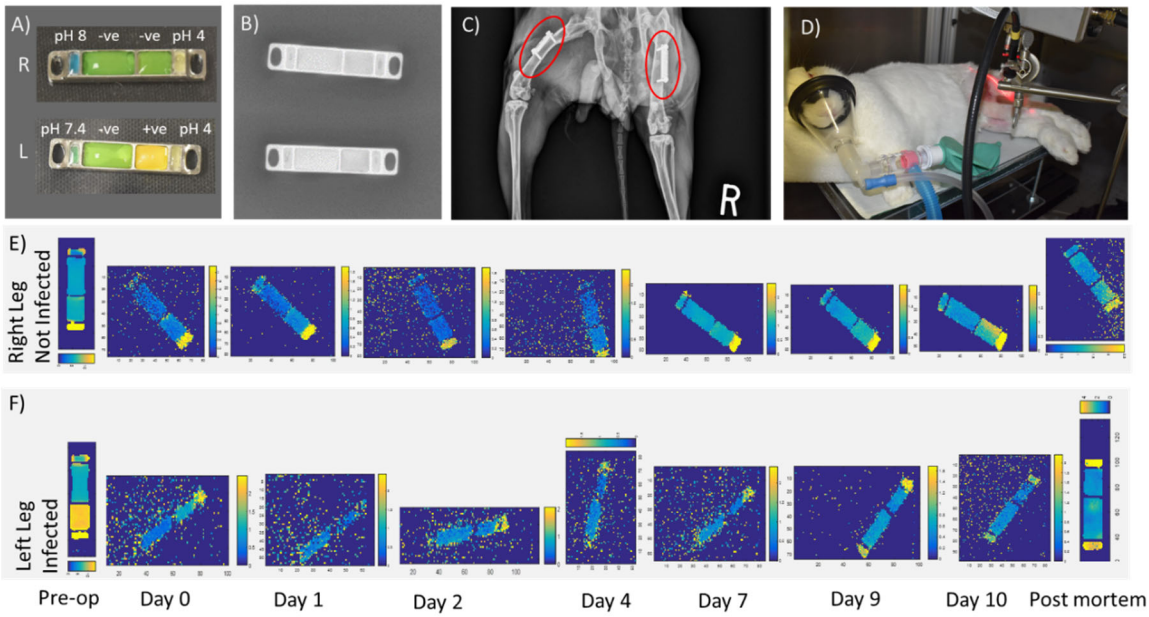

Figure 6.6: Rabbit 1 Study. A) Photographs of the pH sensitive plates implanted in the right leg (non infected) and left leg (infected) of the rabbit with two references (acidic and physiological pH), control sensor regions (green) and inoculated sensor region (yellow). B) X-ray images of the orthopedic plates to be implanted during surgery. C) X-ray image of the rabbit showing the implants fixed with screws on both femurs of the rabbit. D) Rabbit undergoing XELCI imaging under anesthesia. E) In-vivo XELCI images (ratio) of the pH sensitive implant through tissue in live rabbit images over a period of 10 days followed by postmortem implant imaging. F) In-vivo XELCI images (ratio) of the pH sensitive implant through tissue in live rabbit imaged over a period of 10 days followed by postmortem implant imaging.

Postmortem observations were made on termination of the study on Day 10. The incision made for surgery was opened and tissue examined for signs of infection. The tissue was removed to expose the implanted sensors and photos taken to document the color of the implant. Figure 6.6 shows a comparison of the implanted sensors at start (Day 0) and end (Day 10) of the experiment. Both chambers, big and small, of both right and left implants appeared green in color. The references were still intact. Tissue of the control leg looked healthy while the tissue surrounding the inoculated implant was clearly infected as evident by the presence of white pus pockets under the skin at incision site

and covering the implant. Thickness of the muscle tissue covering the implant for the right leg measured at portion of maximum thickness using calipers was 12.8 mm and skin was 3.1 mm, giving a total thickness of 15.9 mm. Thickness of both muscle and skin tissue covering the implant on left leg was 13 mm. thickness. The gel in both implants turned darker green after being exposed to air. The retrieved gels responded to pH 6 buffer and were reversible.

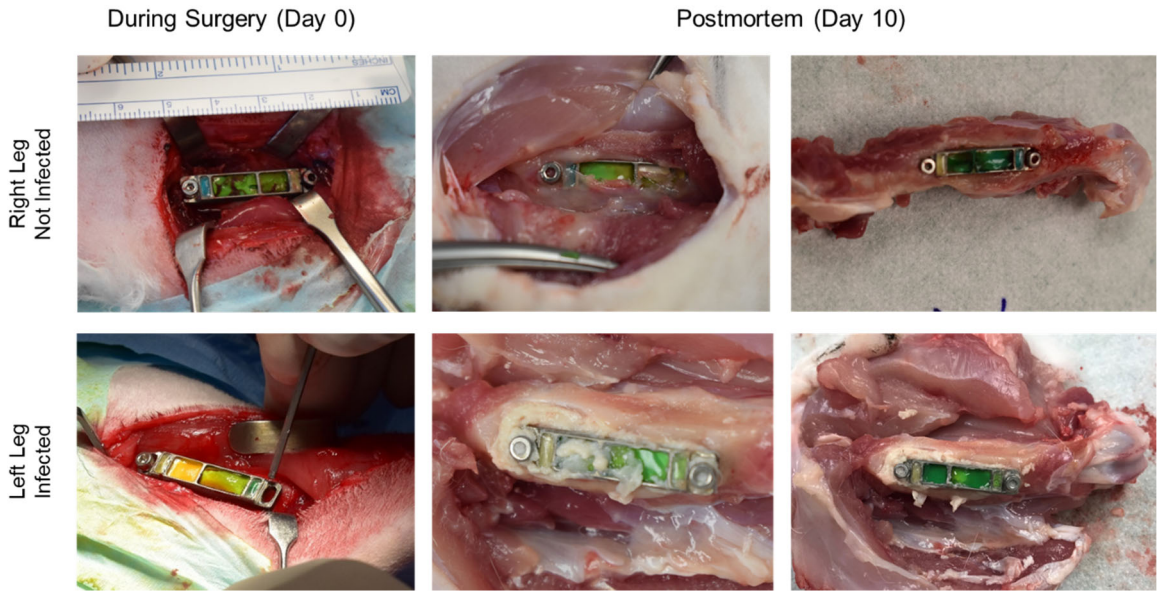

Figure 6.7: Postmortem implant retrieval. Photographs of the pH sensitive implant during surgery (Day 0) and postmortem photographs of the same on Day 10 for both infected and control legs. The pH sensor implanted in the infected leg had a yellow color due to biofilm growth at start of experiment. Postmortem images show both implants to be green in color indicating neutral pH despite presence of white pus in the infected leg indicating infection.

6B.2.2.2. Pilot Study, Rabbit 2

The pH sensors were prepared as for rabbit 1 sensors except the two references on each end of the implant were the same and contained only the scintillator layer and no pH gel to account for any pH-independent signal attenuation. Both the big and small chambers were control in the right implant while only the small chamber was control and the big chamber was inoculated in the left implant as shown in the implant photographs in Figure 6.7A-B. Thickness of the tissue was 13 mm for right leg and 16 mm for left leg measured from top of implant surface during surgery. X-ray images of the implanted sensors were taken after surgery and the animal was imaged with XELCI under anesthesia after the surgery and on day 1, 2, 3 , 6, 9 and 10 after the surgery. All the sensor regions, infected, control and reference regions can be distinctly seen in all XELCI images. The inoculated region of the left implant is a bright yellow in the pre-op scan and still appears to be acidic after surgery in Day 0 scan but appears to be neutralized on Day 1. Both references also appear yellow, however, in some images such as Day 6 for the infected implant, the reference next to big chamber appears brighter than the reference next to small chamber and we also see decreased signal for the small chamber indicating possible attenuation by tissue and angle dependence of the collector and rabbit positioning.

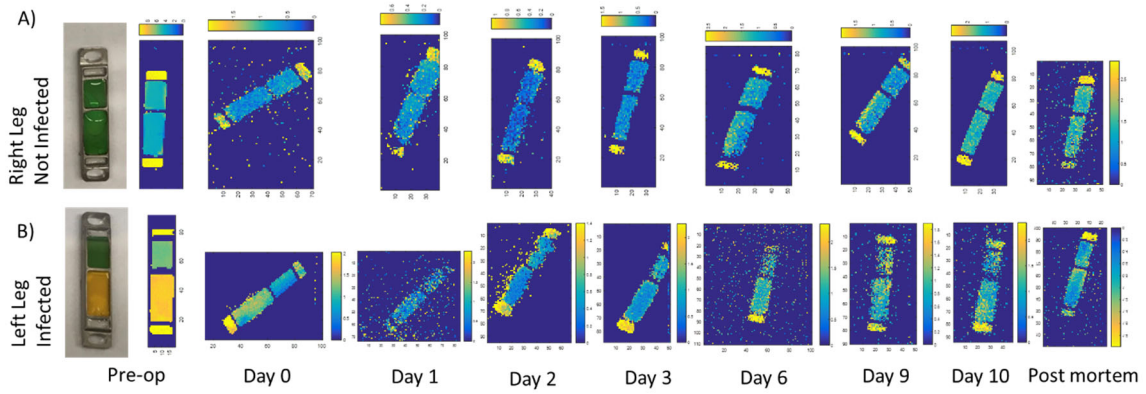

Figure 6.8: Rabbit 2 Study. A) Photograph of the pH sensitive plate implanted in the right femur (non infected leg) of the rabbit with two reference (white) and two control (green) chambers. In-vivo XELCI images (ratio) of the pH sensitive implant through tissue in live rabbit imaged over a period of 10 days followed by postmortem implant imaging. B) Photograph of the pH sensitive plate implanted in the left femur (infected leg) of the rabbit with two reference (white), control (green) and infected (yellow) chambers. In-vivo XELCI images (ratio) of the pH sensitive implant through tissue in live rabbit imaged over a period of 10 days followed by postmortem implant imaging.

The skin was separated and implants exposed to see sensor condition and measure pH immediately after euthanasia. Postmortem observation of the implants confirmed neutralization of the pH as indicated by XELCI images. The tissue and skin flap was placed back and both legs imaged again to obtain post mortem XELCI and microCT images. Th right leg tissue looked healthy and the sensor gels were green in color and intact in the chambers. pH of the tissue surrounding the implant in the right leg was pH 7.8 as measured by pH strips, the microelectrode indicated an initial pH of 7.81 but the stabilized reading was pH 7.29. Infection was evident in the left leg as indicated by presence of heavy pus around and on top of the implant, and the sensor gels were found to dislocated and out of the implant upon opening. This could have happened during the disarticulation process as the last XELCI image obtained before euthanasia showed the

sensor to be intact. The color of the gels indicated pH 7 compared to the calibration curve but the gel color turned dark green a few minutes after exposure to air. Some serous fluid was present in the left implant sensor chamber and pH of the fluid was pH 6.91 as measured by microelectrode and between pH 6.9 – 7.2 as confirmed by the pH paper strip. pH of the tissue and pus surrounding the plate was (1) pH 7.6 by microelectrode and (2) pH 7.8 by pH strip. Figure 6.8 shows photographs of the implant during surgery (Day 0) and postmortem (Day 10) and pH measurements of the tissue with a microelectrode and pH strips. The retrieved gels were reversible and responded within 5 minutes when placed in pH PBS, pH 6.5 and pH 6.0 buffers as shown in figure 6.9.

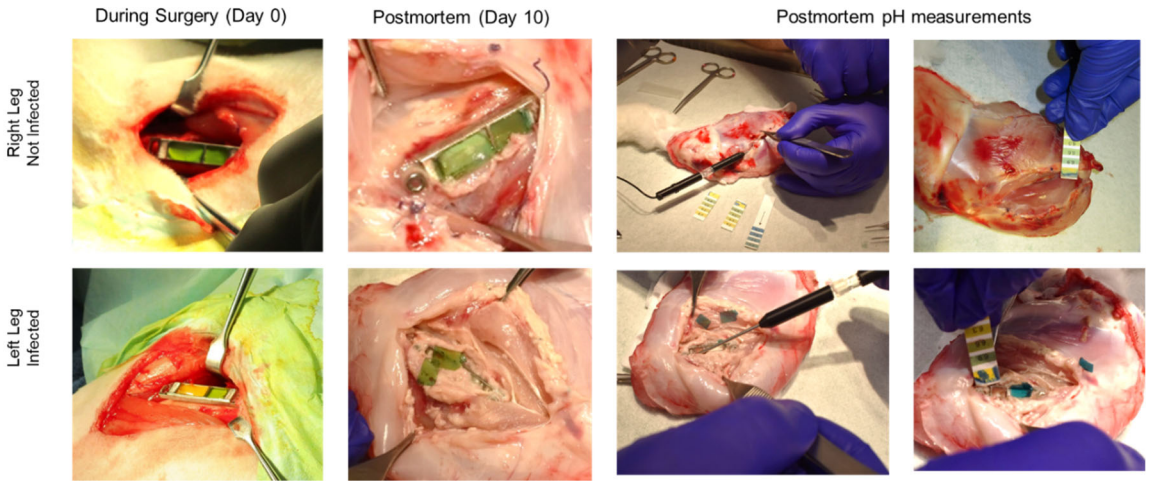

Figure 6.9: Postmortem implant retrieval. Photographs of the pH sensitive implant during surgery (Day 0) and postmortem photographs of the same on Day 10 for both infected and control legs. The pH sensor implanted in the infected leg had a yellow color due to biofilm growth at start of experiment. Photos taken during postmortem pH measurements of the surrounding tissue with a pH microelectrode and pH indicating paper strips.

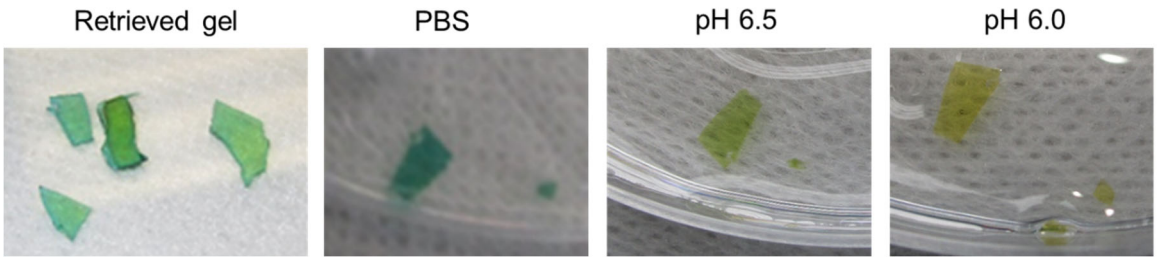

Figure 6.10: Reversibility check of the retrieved sensor gels. These were immersed in phosphate buffered saline (PBS), pH 7.2 till a complete color change for 5 minutes followed by immersion in pH 6.5 buffer (5 minutes) and pH 6.0 buffer (5 minutes).

6B.2.2.3. Thermal Imaging

Thermal images of the animal were taken to see if the infection would raise the body temperature as expected during infection. Images were taken before and after XELCI imaging. The temperature of the leg was higher than rest of the body for both cases as visible by the hot spots (brighter) in the leg area in the thermal images shown in figure 6.10. This is due to the absence of fur in the shaved leg area and the direct association of higher temperature in the leg area cannot be established with presence of infection or inflammation. Left Leg was about 2°C warmer than right leg after imaging (36.4 vs. 34.7 °C max). There was not much difference in temperature of the left leg before and after imaging in contrast to the right leg that was 3°C warmer after the imaging than before imaging. However, these observations cannot be validated as the thermal camera was not calibrated and had a background of about 2°C that varied largely between the shaved and fur areas and is not useful for application to measuring small temperature differences.

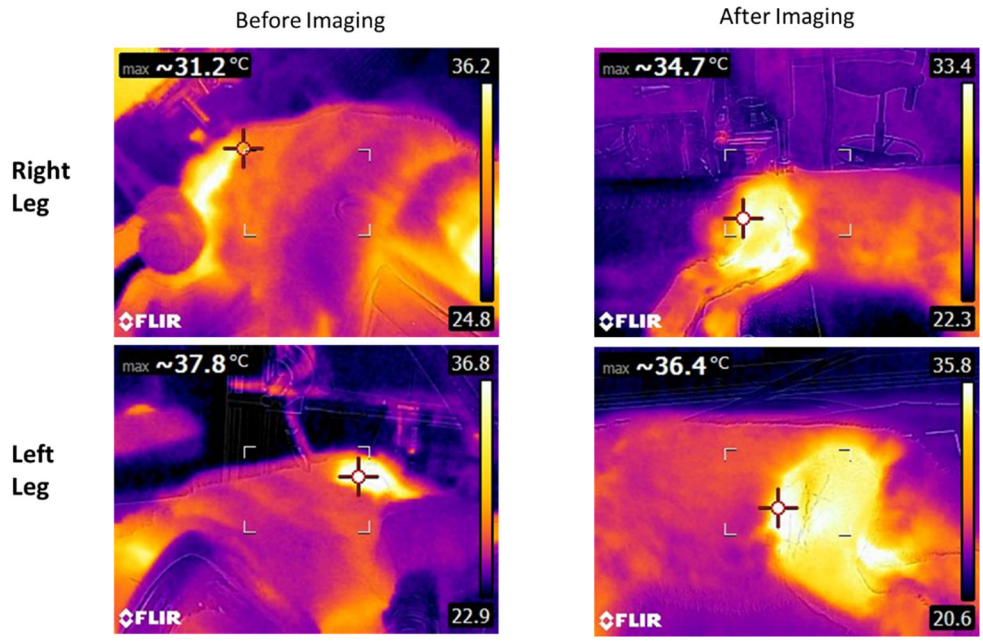

Figure 6.11: Thermal images of the rabbit taken during and after XELCI imaging with a FLIR camera. The hind legs appear to be warmer than rest of the animal body.

6B.2.3. Postmortem Evaluation

6B.2.3.1. Postmortem Bacterial Count

Bacteria was recovered from the tissue samples collected for the infected leg confirming infection and no bacteria was recovered from the tissue collected from right leg confirming no spread of infection to the control leg.

6B.2.3.2. Imaging

Bioluminescence imaging of the retrieved implants still fixed on the bone with tissue intact was done using in vivo imaging system (IVIS) with the GFP emission filter and excitation wavelength of 465 nm, the images are shown in Figure 6.11 for both legs. A lot of autofluorescence from the rabbit skin and fur inhibited obtaining good images of

the right leg but reasonable images of the left leg were obtaining by covering the skin with cardboard and exposing only the implant area. Fluorescence was observed in the pus surrounding the implant in the left leg. MicroCT scan was also done for both legs and some of the images shown in figure 6.12.

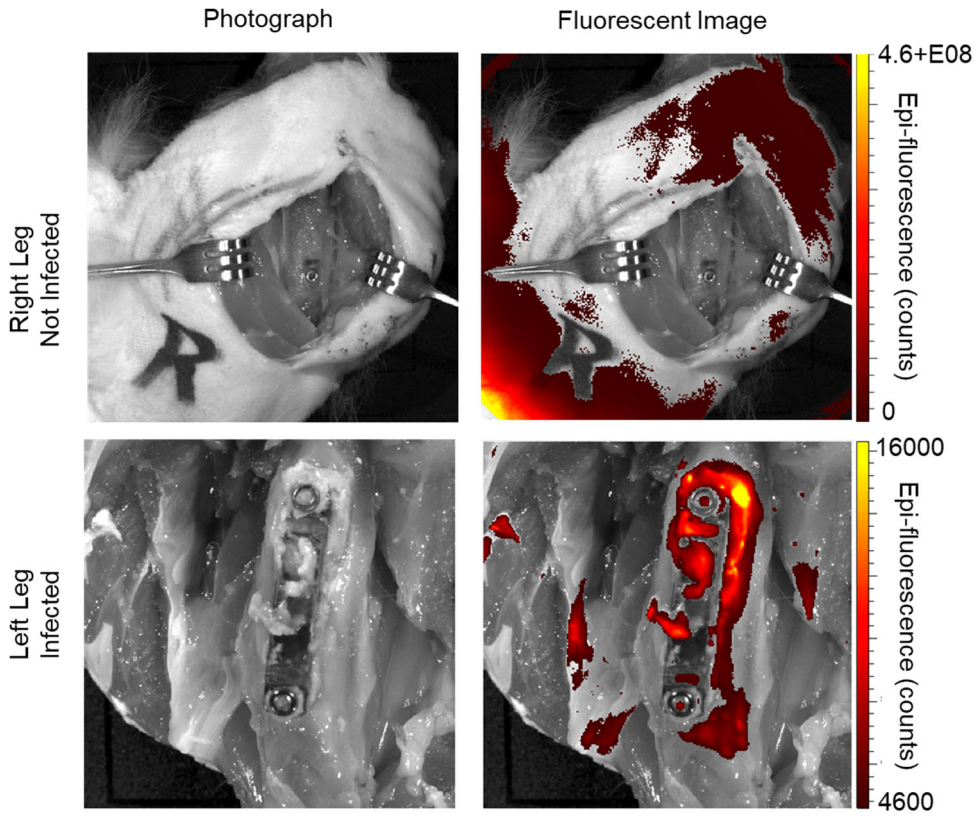

Figure 6.12: Postmortem photographs and fluorescent IVIS images of implants still fixed on the femur with surrounding tissue.

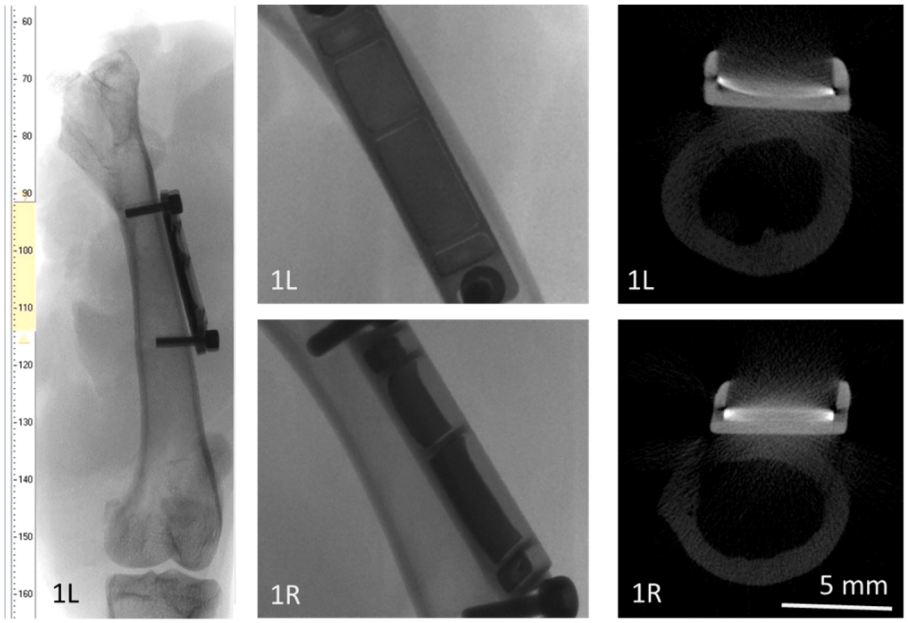

Figure 6.13: MicroCT imaging of the implant fixed on a rabbit 1 femurs (1R: right leg, 1L: left leg) showing different views taken from the reconstructed microCT images.

6B.2.3.3. Blood Tests

Blood was drawn over the course of the experiment and sent for testing of erythrocyte sedimentation rate (ESR), C-reactive protein (CRP) and white blood cell (WBC) count. The results are summarized in table 6.3. These tests are considered general markers of infection and often used to confirm infection, but these can also indicate inflammation as observed after surgery. In a comprehensive analysis of CRP and ESR in patients undergoing orthopedic implant removal with and without infection, Piper KE et al concluded that CRP and ESR have poor sensitivity for diagnosis of shoulder implant infection.[1] The results of the blood tests for this rabbit study were indecisive regarding presence of infection even though we did see a slight increase in the WBC on Day 6 and 9 and then it went back to normal range. The sedimentation range also showed an upward

trend after surgery but remained within the expected range and went back down on Day 6. CRP remained less than 0.03 for the course of the experiment.

Day No.	Sedimentation Rate		CRP		WBC R2
	R1	*R2*	*R1*	*R2*	
0	1	1	<0.03	<0.03	7.9
1	6	NA	<0.03	<0.03	NA
2	5	13	<0.03	<0.03	7.2
3	NA	16	<0.03	<0.03	10.4
6	2	NA	<0.03	<0.03	12.4
9	1	5	<0.03	<0.03	12.2
10	NA	3	<0.03	<0.03	7.9
Ref range	0-20		<=0.49		3.50-10.80
Units	mm/hr		mg/dL		K/microL

Table 6.4: Results from blood tests of rabbit 1 and 2 drawn on different days of the study. The blood was tested for sedimentation rate, C-reactive protein (CRP) and white blood cells (WBC).

6B.3. CONCLUSION

The PEG sensor was optimized to respond to a pH range close to the physiological pH range with a working pH range of pH 6-8 and the implant was redesigned to include partitions with designated sensor regions. Each implant had a control region, testing region and two reference regions. The optimized sensor was tested in a pilot rabbit study with 2 rabbits to make sure that the sensor works properly in live rabbits and to allow us to modify it if it does not. XELCI images of the sensor taken without tissue were sharp and clear but the in vivo images showed a lot of noise and were

not as sharp indicating the need to improve the signal collecting optics to increase the signal to noise ratio. We found that the placement of the rabbit affects the final images obtained with XELCI as the implanted sensors need to be perpendicular to the x-ray beam and placement of the collecting light guide at the proper angle to collect signal is also important. We used two heterogenous references on each side of the implant in Rabbit 1 with one reference at acidic pH and one reference at basic pH. This was not very helpful especially where the tissue covering the implant was not uniform. Therefore, the use of two homogeneous references (without the pH indicating film) on each side can help determine the pH-independent effect of tissue thickness. Rabbit 2 implants had two homogenous reference regions on each side allowing for a better estimation of variation in the signal across the implant.

Real time changes in pH on the implant surface can be non-invasively visualized using XELCI as observed by the neutralization of acidic pH in the infected implant by body fluids. The XELCI images agreed with the postmortem observation and the pH of the sensor was in fact neutralized. The sensors were readily reversible and responded to changes in pH after retrieval. Blood tests such as CRP are not reliable to indicate localized infection, and sedimentation rate and white blood cell count was also affected by inflammation after surgery. We saw an upward trend in the WBC and ESR after surgery but it went back to normal range whereas the CRP remained less than 0.03 for the course of the experiment. Even though infection was evident and highly localized, a pH drop was not observed. This is in contrast with the in vitro studies where the pH dropped from pH 7 to pH 5 within 15 hours and can be explained by neutralization of the pH by

body fluids. The in vitro experiments were conducted in controlled condition with no exchange of external fluids and the acidic products created by bacterial metabolism during biofilm growth turned the pH of the surrounding medium to acidic. The surrounding medium was buffered (PBS) but ultimately the acidity overcame the buffering capacity of the surrounding medium that was not replenished. This is not the case in in vivo where the implant was part of a dynamic system with constant exchange of body fluids that washed away the acidity created by bacterial metabolism and restored the pH. For Phase C experiments, these observations lead to developing a simulation for a closed system such as a cavity where the exchange of fluids is more controlled and observe either the accumulation of acidic products or the slow wash out of the acidic products by the body fluids.

6C. PHASE C: OPTIMIZED XELCI AND CAVITY SIMULATIONS

After confirming the in vivo performance of the optimized sensor in Phase B studies, further in vivo experiments were conducted in Phase C to study different case scenarios of infection such as in the cavity or open face implant. Studies performed in Phase C can be broadly grouped into two categories, one group can fall into studies performed with the optimized imaging system that allowed for greater signal collection with better images, and the other group consisted of comparison of open system (open face implant, no lid) with closed system (cavity simulations) where the implant surface was partially sealed to simulate a cavity in close proximity of the bone surface. The studies in both groups have some overlap, for example, one cavity simulation was performed with the non-optimized imaging system while all other cavity simulations were performed with the optimized system. The open system studies performed in Phase B were also repeated with the optimized system to obtain a direct comparison with closed system studies imaged with the optimized system. The order of these studies was not strictly systematic when explained in a chronological order but the rabbits were numbered based on the timing of when that study was performed. The studies are explained in the systematic order and include the following:

I. Pilot study, Rabbit 3, cavity simulation with parafilm, non-optimized XELCI

II. Rabbit 6, open system with biofilm, optimized XELCI

III. Rabbit 5, cavity simulation with biofilm, optimized XELCI

IV. Rabbit 4, cavity simulation with lactic acid, optimized XELCI

V. Rabbit 7, neutral start, cavity simulation, optimized XELCI

VI. Rabbit 8, neutral start, cavity simulation, early termination, optimized XELCI

6C.1. METHODS

6C.1.1 Sensor design and characterization

6C.1.1.1. Sensor assembly

The orthopedic implant was machined out of either titanium or acrylic and had partitions for each sensor region. The scintillator layer and pH sensitive layer (PEG-PAAm hydrogel with BTB) were prepared as mentioned earlier in the general methods. Both layers were placed in each chamber of the implant. For cavity simulations, implant's top surface was covered with an acrylic lid (Acrylic Precision Thin Sheet 0.4 mm thick, Emco Industrial Plastics, Inc., NJ, USA) fixed using screws (M1.4 x 2.8 mm). The lid was cut using a laser cutter at the Clemson Makerspace.

6C.1.1.2. Calibration curve

Calibration curve for the optimized XELCI with the optimized sensor (PEG-PAAm-BTB hydrogel) was obtained in the same way as the calibration curve mentioned in Phase B except that the optimized imaging system that included a ¾ inch acrylic light guide splitting into two PMTs with PMT1 without any filter and PMT2 with an optical filter for 700 nm. The raw data (PMT1 counts, PMT2 counts, and stage position vs. time) was processed using a MATLAB script to form the 620 nm, 700 nm, and ratio images vs.

stage position. The signal was averaged over each disc and normalized to the reference signal.

6C.1.2 Simulation of the body condition in vitro

For all in vitro studies involving bacteria, B+ gels consisted of Staphylococcus aureus (5000 cfu) was grown on the gel in TSA and B- gels (control) consisted of the gel and sterile TSA except noted otherwise.

6C.1.2.1. Neutralization Study

Both B+ and B- gels were incubated in a petri dish at 37°C for 15 hrs. The TSA surrounding the gels was trimmed around the edges and 0.7% agarose (dissolved in PBS) was added to the petri dish and incubated at 37°C. Images were taken every hour.

6C.1.2.2. Cavity simulation — parafilm study

The prepared implants with B+ and B- gels were covered with a layer of parafilm (1 layer) with a small hole made with a needle in the parafilm covering. 0.7% agarose (dissolved in PBS) was added to the petri dish and incubated at 37°C.

6C.1.2.3. Cavity simulation — lid hole size study

The implants were prepared with the B+ gels in the big chamber and B- gels in small chambers on top of the scintillator layer and 0.7% agarose (dissolved in PBS) was added on the implants kept in petri dish. Lids with different size pinholes (0.25, 0.50, 0.75 and 1.0 mm) were tested. One control implant with 1 mm pinhole lid was kept in just PBS solution (instead of agarose) and one control implant was prepared without a lid

and kept in 0.7% agarose dissolved in PBS. The study was repeated with hydrochloric acid (HCl) to produce acidic pH instead of the bacteria in the B+ gels (sensor gels covered in sterile TSA and HCl added).

6C.1.2.4. Implant inoculation for in vivo study

For study I, II and IV, biofilm was established overnight by covering the sensor gel with tryptic soy agar (TSA, 40 mg/ml) containing the inoculum (5000 cfu *S. aureus*) a night before surgery to get an acidic pH. The control was prepared with sterile TSA. For study V and VI, the sensor gel was covered with tryptic soy agar (TSA, 40 mg/ml) containing the inoculum (5000 cfu *S. aureus*) just before the surgery to start the experiment with neutral pH. The control was prepared with sterile TSA.

6C.2. RESULTS AND DISCUSSION

We first describe the changes made to the optimized XELCI system and the calibration curve acquired with the modified system using the same sensors as described in Phase B. The re-design of the sensor modified orthopedic implant used in most of the Phase C studies is discussed next followed by the in vitro experiments conducted to simulate body condition and determine the effect of diffusion in a cavity affecting the rate of neutralization of pH with and without a biofilm. These experiments were repeated in vivo and are described in detail along with the postmortem observations for each study.

6C.2.1 Optimized imaging system

The XELCI system was optimized for better signal collection and to increase the signal to noise ratio for better imaging of the pH changes on the implant surface in vivo. The liquid light guide (core diameter: 7.6 mm, length: 1 m) was replaced with a bigger and shorter (diameter: 2 cm, length: 16 inches) solid light guide made from acrylic. Increasing the diameter of the collection optics increased the signal collection at least by a factor of three thus improving the signal to noise ratio. The acrylic light guide was split on the other end to couple to two PMTs (photomultiplier tubes). PMT1 collected all wavelengths while PMT2 had an optical filter to pass the 700 nm light and filter out 580–660 nm. Earlier versions of the XELCI had both PMTs equipped a filter with PMT1 collecting the 620 nm and PMT2 collecting the 700 nm light. The MATLAB code to plot the data as images representative of the 620 nm, 700 nm and the ratio intensities was modified to reflect this change of light collection filters and a new calibration curve was acquired as shown in figure 6.13. We can clearly differentiate the sensor discs at different pH especially pH 6.5, 7.0 and 7.5 that are physiologically most relevant. The XELCI images look almost the same as for the previous calibration curve with the same sensor gels acquired using a liquid light guide given in figure 6.3 except that the signal intensities for 620 and 700 nm are much higher for the data collected using the acrylic light guide (figure 6.13). The signal was saturating when collected without tissue with the optimized XELCI system, to avoid the saturation of the PMTs, X-ray intensity was reduced by 10x to obtain the data for no tissue (0 mm). If we compare the average reference intensities for the 700 nm images, we see an increase of 88x and 26x for signal

through 6 and 11 mm of tissue respectively (I-700 reference disc intensities for 6 mm tissue with ALG is 3000 and LLG is 34 counts/10ms and I-700 max intensities for 11 mm tissue with ALG is 500 and LLG is 19 counts/10ms).

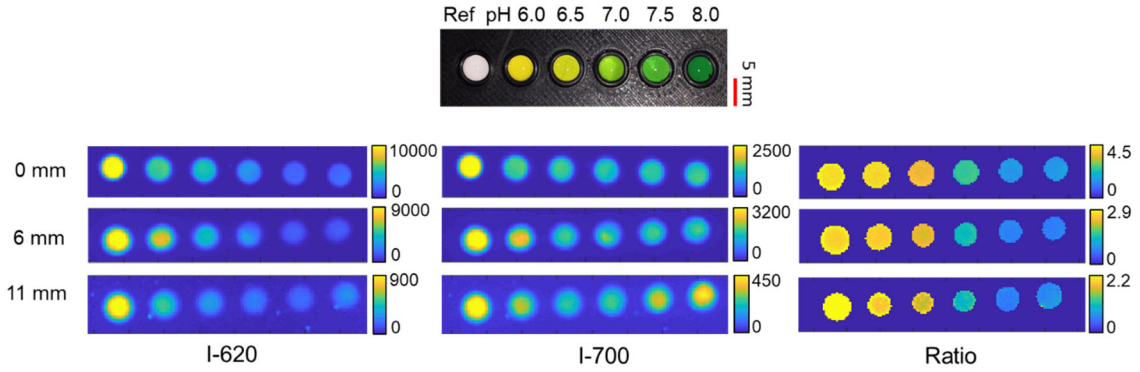

Figure 6.14: Calibration Curve for PEG-PAAm-BTB sensors acquired using optimized XELCI with acrylic light guide. Photograph showing the pH sensor discs (PEG-PAAm-BTB gel on scintillator film) placed in a 3D printed holder in pH buffers 6.0, 6.5, 7.0, 7.5 and 8.0 and a reference disc without any pH coating. This calibration setup was imaged without tissue and later sandwiched between two pieces of chicken tissue and imaged through 6mm and 11 mm of chicken tissue. XELCI images showing the 620 nm, 700 nm and ratio of 620 to 700 nm signal intensities of the pH sensor discs at respective pH obtained without tissue and through 6 and 11 mm of chicken tissue.

6C.2.2 Implant design

Study I was carried out using the metal implant with partitions as explained in Phase B and the big chamber (in infected implant only) was covered using a layer of parafilm with a hole poked in it using a needle to form a cavity. The implant was redesigned for later studies with the bottom side of the implant contoured to the bone shape of the rabbit for a better fit and included a transparent lid to cover the implant surface to simulate a cavity. The entire implant with the lid was machined out of acrylic

and a schematic as well a detailed drawing is given in figure 6.14. The lid design was mostly open on top of the control region and had a 1 mm hole on top of the infected region to allow slow exchange of fluids. The shift to acrylic implants was made after biocompatibility testing of the materials. Bacterial growth was observed on the surfaces of polycarbonate and acrylic sheets tested. However, there was a clear zone (inhibition zone) surrounding surgical glue that was also tested and it indicated that the bacteria did not grow near the surgical glue so we decided to use screws to hold the lid in place instead of the glue. The implants were however fixed to the bone using surgical glue as it was more convenient than fixing them using screws that involved drilling a pilot hole and potential risk of fracture in the fragile rabbit bones.

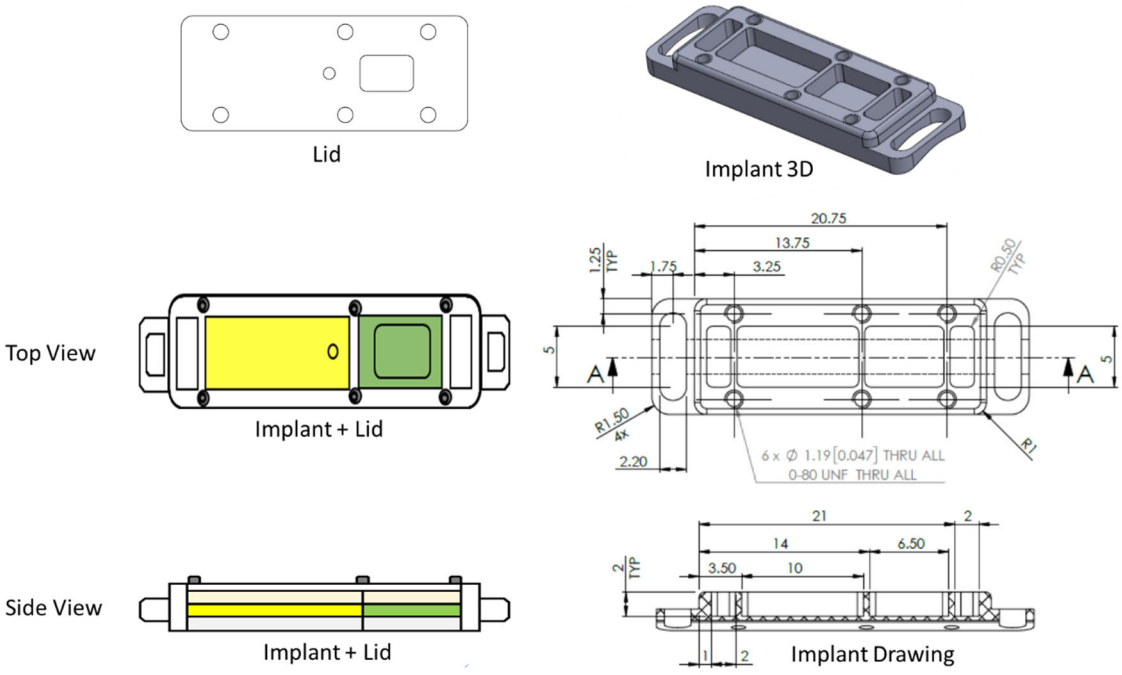

Figure 6.15: Schematic of the acrylic implant with lid. The design includes individual chambers in the implant for different sensor regions; the two 2x5 mm chambers on each side of the implant

are reserved for reference region while the two middle chambers are for pH sensitive regions (yellow = infected, green = control). The lid has an opening on top of the small chamber and a pin hole in the section covering the big chamber and 6 peripheral holes for screws to fix it to the implant. All dimensions are in millimeters.

6C.2.3 Simulation of the body condition in vitro

Phase B studies indicated a need for simulation of the body condition in vitro by allowing for fluid exchange between the sensor and the surrounding medium. Phosphate saline buffer is used to replicate the physiological pH and salt concentrations present in the body. The following studies were carried out to see the effect of surrounding medium on the pH of the sensor gels and to estimate the time it takes to neutralize the acidic pH in both open and closed (cavity) systems.

6C.2.3.1. Neutralization study

A neutralization study was carried out for the open system with two gels in tryptic soy agar (TSA). One gel contained bacteria (B+) and the other one was control (B-). Both gels were initially in PBS (green in color) and growth of bacteria on B+ gel produced acidic pH making the gel color yellow. The TSA around the gels was trimmed, with the agar cut close to the gels in one set of experiment (Figure 6.15A) and the agar cut farther from the gel in the second set of experiment (Figure 6.15B). Agarose 0.7% dissolved in PBS was added as the surrounding pH and the effect of the pH from the surrounding PBS neutralizing the acidic pH of the B+ gel was observed. Color of the B+ gels changed from yellow to green in both experiments but took different amount of time depending on the size of the surrounding agar. The less the surrounding agar, the faster the color change

occurred as evident from the images in figure 0.15. pH of the B+ gel with a larger area of agar neutralized between 8 and 24 hours whereas the B+ gel with a smaller area of agar started to neutralize within the first 5 hours.

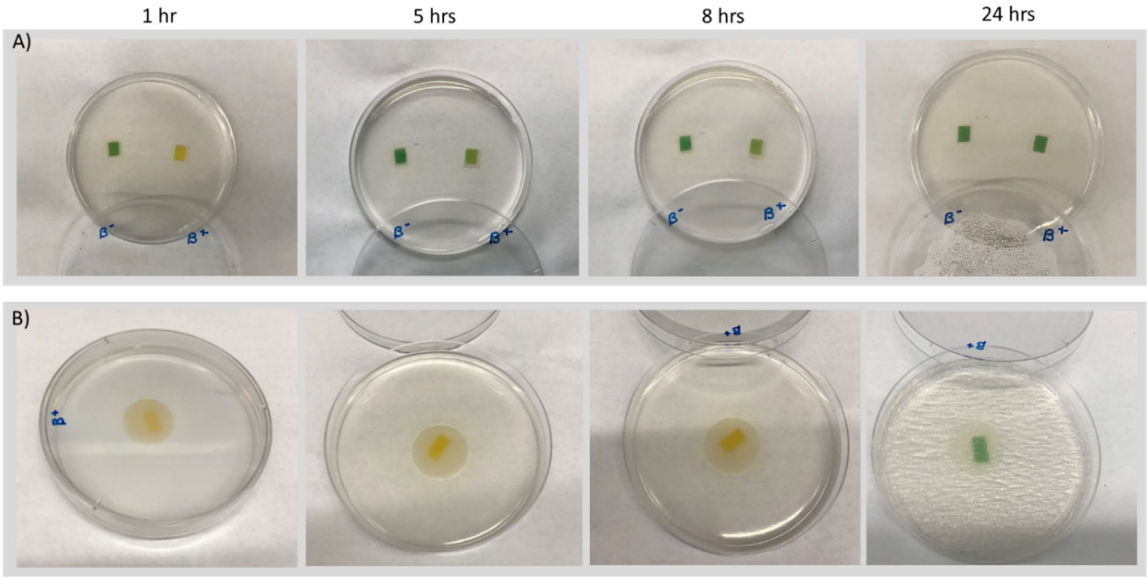

Figure 6.16: Simulation of body condition in vitro. A) The B+ and B- gels covered with tryptic soy agar (TSA) were placed in 0.7% agarose (dissolved in PBS) and color change of the gels due to neutralization by PBS was observed over time. B) B+ gel covered in a larger area of TSA placed in 0.7% agarose (dissolved in PBS) and color change of the gel due to neutralization by PBS was observed over time. Note: B+ contain bacteria in TSA, B- contain sterile TSA. Yellow color indicates acidic pH, green color indicates neutral to basic pH.

6C.2.3.2. Cavity simulation — parafilm study

The neutralization study was repeated for a cavity simulation by the covering the B+ gel in agar with a layer of parafilm containing a small hole to restrict the rate of fluid exchange. The parafilm covering delayed the color change as expected and the size of the hole in the parafilm affected the color change speed. Since the gels were placed in the implant chambers, it was difficult to completely cover all the chamber edges specially the

common edge between the two chambers (big and small), that could explain the control gel color change from green to light green near the infected gel at 4 and 7 hours due to spread of bacteria from infected to control gel. But the pH of both gels was neutralized by the surrounding medium (agarose in PBS) after 24 hours as shown in figure 6.16.

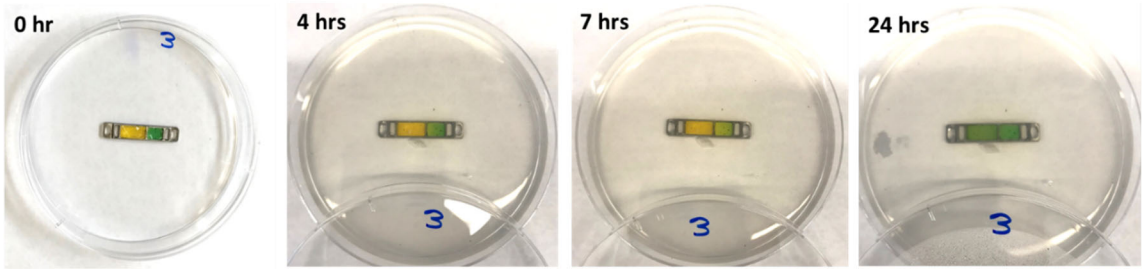

Figure 6.17: In vitro cavity simulation using parafilm. The implant was prepared with B+ (yellow) in big chamber and B- (green) gels in small chamber. The big chamber was sealed with a piece of parafilm with a pinhole. 0.7% agarose (dissolved in PBS) was added to the petri dish and color change of the gels due to fluid exchange between the chambers was observed over time. Note: B+ contain bacteria in TSA, B- contain sterile TSA. Yellow color indicates acidic pH, green color indicates neutral to basic pH.

6C.2.3.3. Cavity simulation — lid hole size

The neutralization study for cavity simulation was repeated using acrylic lids screwed on the implants for better sealing of the edges as compared to the parafilm and the effect of hole size in the lid (on top of the infected chamber) on the rate of pH neutralization due to diffusion of fluids was evaluated. Hydrochloric acid (HCl) was used to produce acidic pH in the B+ gels placed in big chambers. HCl is produced by osteoblasts and is important in context of bone erosion related to orthopedic infections. Figure 6.17A shows the preparation of implants containing green (B-) gels in both chambers and addition of HCl to the big chamber produces acidic pH (pH 5) changing

the gel color to yellow. The implants were fitted with lids having a pin-hole size of either 0.25, 0.5, 0.75 or 1 mm and placed in the petri dish containing 0.7% agarose that was covered with additional PBS solution on top. One implant with a lid containing 1 mm pin-hole was placed in just PBS solution (no agarose). A control was prepared without any lid. The study lasted 5 days with a faster neutralization even for larger hole sizes. For example, it took 4–5 days for gels in the implants with smaller hole sizes (0.25 and 0.5 mm) to change color whereas the color change started on Day 3 for larger hole sizes (0.75 and 1 mm). The control implant without the lid neutralized after 24 hours.

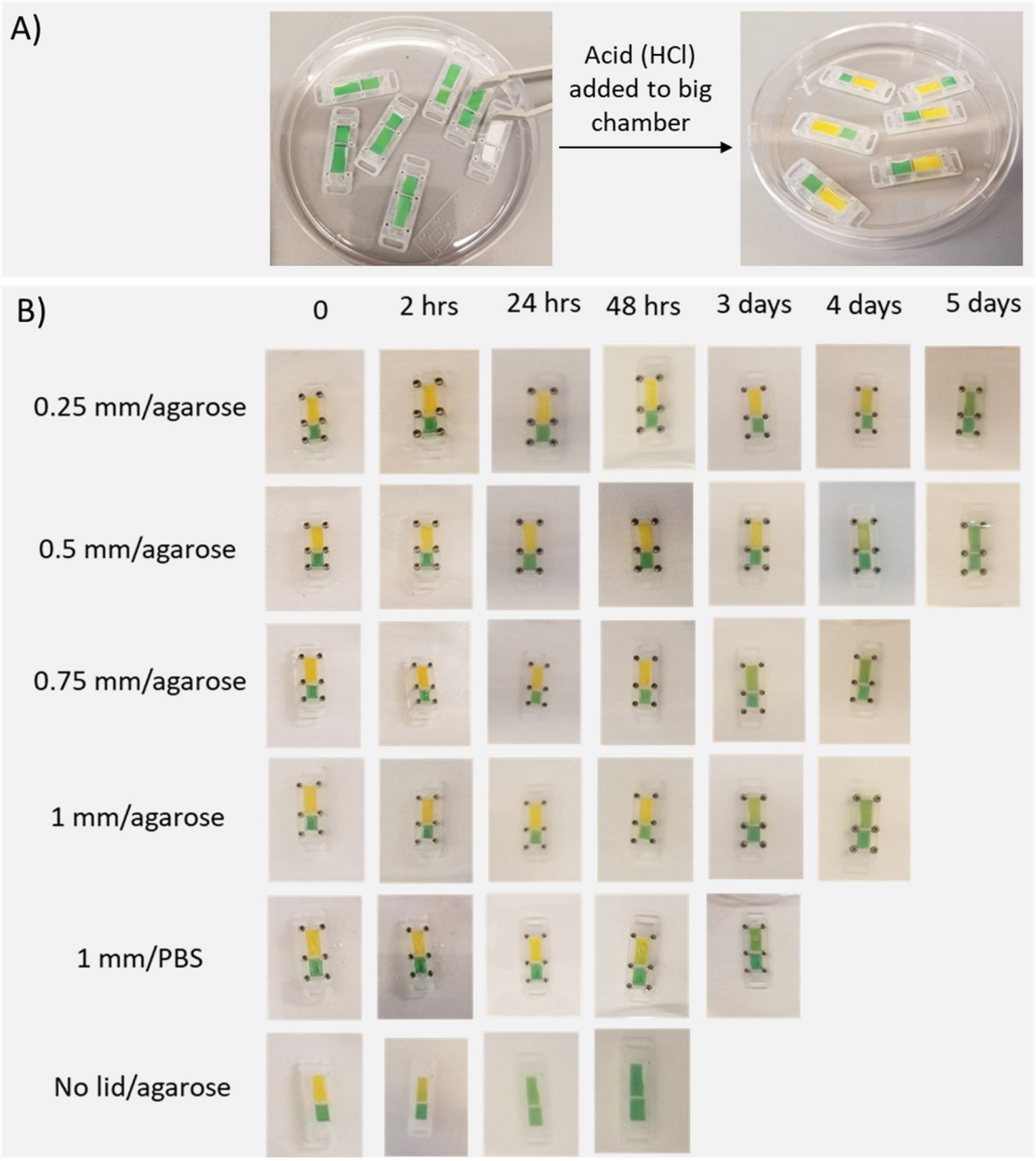

Figure 6.18: In vitro cavity simulation using lids with different size hole. A) The implants were prepared with B- (green) gels in both chamber and HCl was added in big chamber to produce acidic pH (yellow color). A lid with a pinhole was screwed on top of the implant. B) The implants were placed in agarose (0.7% dissolved in PBS) and color change of the gels due to fluid exchange between the chambers was observed over time. Note: B- contain sterile TSA. Yellow color indicates acidic pH, green color indicates neutral to basic pH.

The study was repeated with biofilm growth to produce acidic pH in the B+ gels placed in big chambers. This experiment was performed to demonstrate the effect of diffusion with a biofilm versus the effect of pure diffusion studied with HCl. Figure 6.18A shows a schematic of the experiment with the implant fitted with a lid placed in the petri dish containing 0.7% agarose that was covered with additional PBS solution on top. Implants were prepared with lids having a pin-hole size of 0.25, 0.5, 0.75 and 1 mm. One implant with a lid containing 1 mm pinhole was placed in just PBS solution (no agarose). A control was prepared without any lid. The sensor gels in the control chambers (the control gels, B- were covered with agarose instead of TSA to avoid bacterial growth in the control chamber) stayed green and the infected chamber (B+ gels) stayed yellow even after 48 hours of incubation at 37°C. The B+ gel in the implant with 1mm pin-hole lid placed in PBS solution started changing color on Day 3 and the B+ gel in the implant with 1 mm pin-hole lid placed in agarose turned light green on Day 4 of the experiment. This indicates a faster color change and more fluid exchange for the liquid PBS as compared to the semi-solid agarose. It took 6–7 days for B+ gels in the implants with smaller hole sizes (0.25, 0.5 and 0.75 mm) to change color. The control implant without the lid neutralized after 10 hours. The experiment was concluded on Day 7 with the observation that pin-hole sizes smaller than 1 mm takes longer to neutralize by restricting the rate of fluid exchange with the surrounding medium and that the rate of exchange is faster when the surrounding medium is a liquid such as PBS solution as compared to a semi-solid medium like agarose dissolved in PBS. The neutralization rate was slower for the implants with biofilms as compared to the study done with implants containing acid

(no bacteria), this could be because pure acid does not have a buffering action and there was no biofilm present to keep replenishing the acidic pH in the B+ gels thus resulting in a faster neutralization for the acid implants.

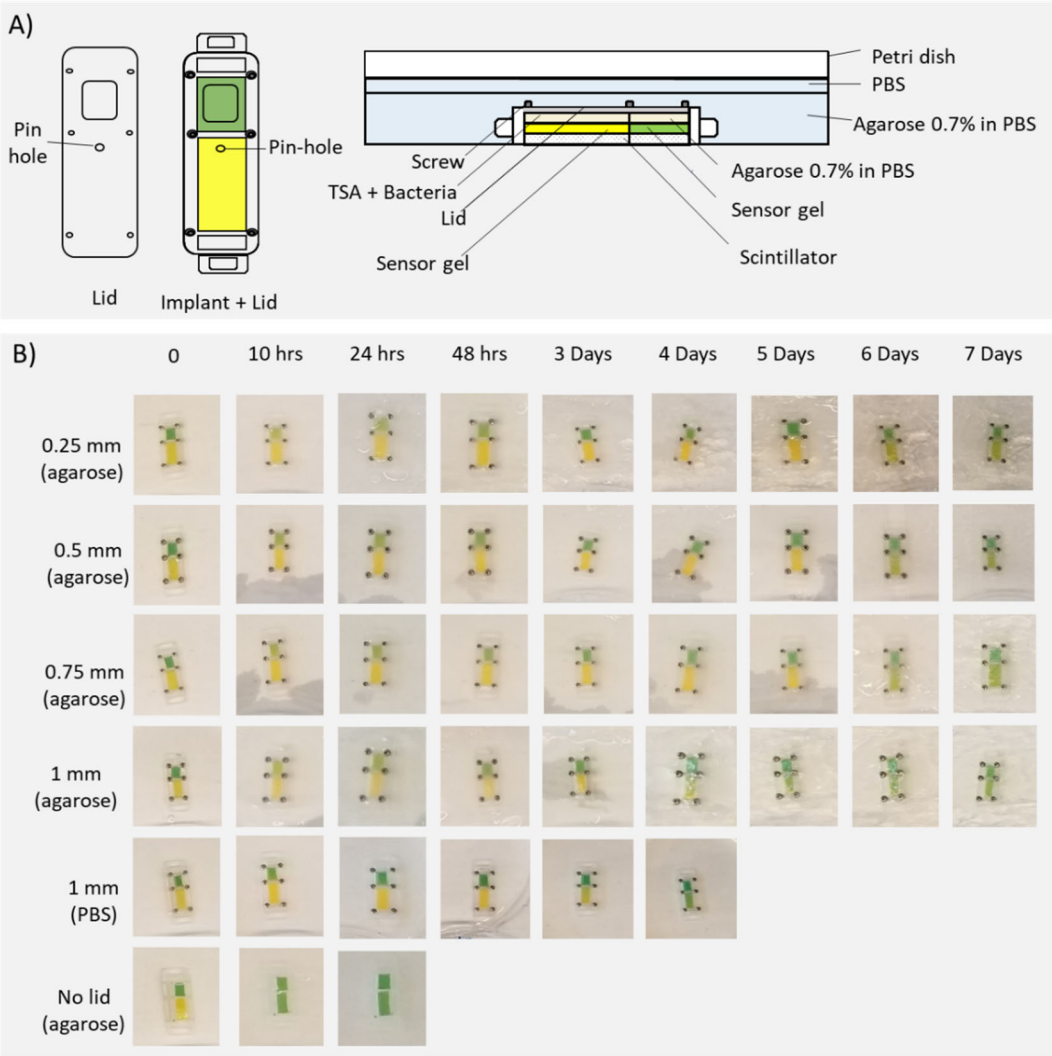

Figure 6.19: In vitro cavity simulation with biofilm using lids with different size hole. A) Schematic of the experiment showing the implant with lid placed in petri dish. The implants were prepared with B+ (yellow) in big chamber and B- (green) gels in small chamber and a lid with a pinhole was screwed on top of the implant. Agarose (0.7% dissolved in PBS) was added to the petri dish and color change of the gels due to fluid exchange between the chambers was observed over time. Note: B+ contain bacteria in TSA, B- contain sterile TSA. Yellow color indicates acidic pH, green color indicates neutral to basic pH.

6C.2.4 In vivo studies

Study I: Pilot study, rabbit 3, cavity simulation with parafilm, non-optimized XELCI

A pilot study was performed to simulate the infection occurring in a confined space or a cavity with restricted exchange of body fluids. Such cavities are commonly found around the infected implants such as an abscess at point of contact of the fixation hardware or due to inflammation of the surrounding the tissue.[2] It is also a known fact observation that biofilms form in regions that are closed or have poor access to the environment such as teeth cavities or infection in the intermedullary region of the femur.[3,4] After in vitro evaluation of the cavity simulation, the study was performed in vivo. The infected chamber in the left implant was covered with parafilm with a hole poked with a needle on the top of the infected chamber to make a cavity for slow fluidic exchange. The control implant did not have a parafilm wrap. Figure 6.19 shows the photographs of the prepared sensor modified orthopedic plates to be implanted in the left and right legs and their X-ray and XELCI images. The X-ray images of the plates clearly show the different chambers as the plates are made from metal but cannot distinguish between the contents of the chamber such as the control and infected gels. The contents of each chamber can be easily identified in the pre-op XELCI scan of the plates based on the different signal intensities: the bright yellow regions are the white reference regions in the photograph of the plates and have the highest signal intensity due absence of the pH sensitive film in the reference regions, the light blue regions in the XELCI images represent the green control gels in the plates that are at physiological pH and attenuate the

signal while the greenish yellow region in the XELCI image of the left implant represent the yellow infected cavity containing a biofilm and is at an acidic pH as indicated by a higher signal intensity due to shift in absorbance of the pH sensitive gel at lower pH. After implantation of the sensor modified orthopedic plates in the rabbit, the infected cavity can still be clearly seen through tissue in the live rabbit (XELCI image Day 0 for left leg). The imaging was continued for 10 days with consecutive imaging for first two days. Due to positioning issues and time constraints, some of the XELCI images does not show the full plate as a full image could not be acquired. Most of the images also appear grainy due to random spikes in the background. Based on Day 1 image of left implant, it looks like the pH in the infected chamber increased as compared to Day 0 image of the same but the reference region also looks less bright than it is in Day 0. Since the control chamber is cut off in the Day 1 image, we cannot compare the pH change but the Day 4 image clearly indicates an in increase in pH of the infected chamber. Day 7 image of the control (right leg) implant appears brighter than rest of the images for the same plate but the reference regions also appear brighter ruling out the possibility of a low pH. This study was done before optimizing the XELCI system and could not provide the best images. Postmortem results were encouraging as we did see a slight drop in pH in the simulated cavity for the first time among all the in vivo studies conducted so far. The infected cavity was at measured to be at pH 6.8 while the control implant was at pH 7.4. Even though we observed a slightly acidic pH in the cavity region but it was not obvious in the XELCI images. This could be due to the possible reflection of the signal from parafilm and reabsorption by the sensor film and the tissue resulting in a decreased signal

giving a false pH since the parafilm is not completely transparent and inhomogeneous due to stretching of the film during application. So there is a need to use a transparent and homogenous material for the covering to form a cavity. Also the parafilm cover was not applied to the control implant and does not provide a good comparison between control and infected implants.

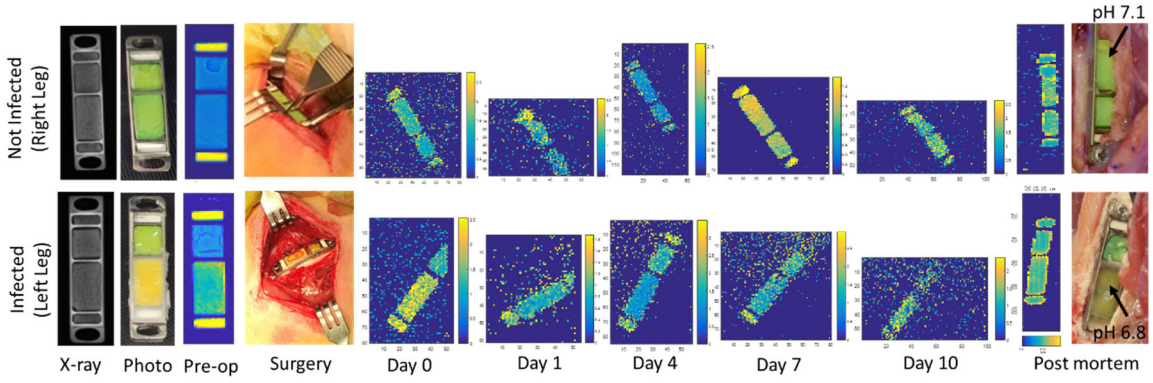

Figure 6.20: Study I Summary. Photographs, X-ray images and pre-op XELCI images of the sensor modified orthopedic plates implanted in the right femur (control leg) and the left femur (infected leg) of the rabbit. The control implant has two reference (white) and two control (green) chambers. The infected implant has two reference (white), one control (green) and one infected (yellow) chamber wrapped in parafilm. In-vivo XELCI images (ratio) of the sensor modified orthopedic plates through tissue in live rabbit imaged over a period of 10 days followed by postmortem implant imaging and implant retrieval.

Postmortem photograph of the left implant shows a color difference between the infected chamber having a yellow green appearance and the more green control chamber (figure 6.20). Both chambers in the right (not infected) implant appear to be the same color. Initial photos of the implants before surgery are also shown alongside the postmortem photographs of the implant for a direct comparison of pre-op and postmortem condition of the implants and the right implant looks almost identical in both photographs except for a small yellow region on one end in the postmortem image. The

hole in the parafilm in the left implant as also visible as an indentation in the postmortem image. Sensor pH in the infected cavity was measured at the hole using a microelectrode and found to be slightly acidic (pH 6.8) that is also indicated by the gel color. pH of the sensor gel in the control implant was 7.4. Infection is also obvious by presence of the white pus around the left implant while the tissue surrounding the control implant was healthy. The amount of pus observed in around the infected implant is much less than what was observed in previous studies in Phase B where the open face implant was completely covered in a white layer of pus. This can be related to the highly localized nature of infection due to confinement in a cavity. pH of the surrounding healthy tissue away from the implant region was also measured for reference and measured to be around the physiological pH of 7.4.

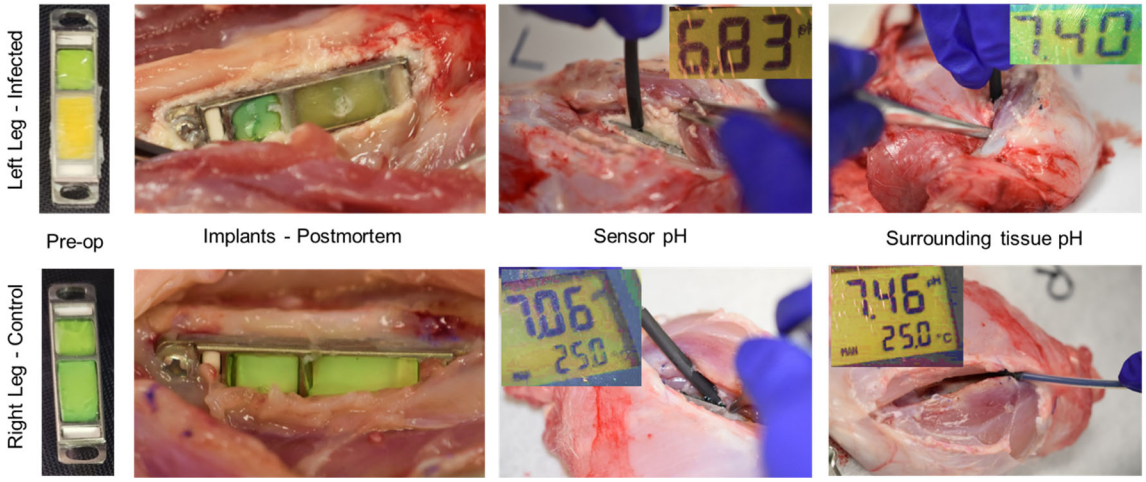

Figure 6.21: Postmortem pH measurements (Study I). Photographs of the sensor modified orthopedic plates before surgery (pre-op) and postmortem photographs of the same for both infected and control legs. The pH sensor implanted in the infected leg had a yellow color due to biofilm growth at start of experiment. Photos taken during postmortem pH measurements of the implanted sensors (big chambers) and the surrounding tissue with a pH microelectrode. The measured pH is shown as an inset in the respective photograph.

Post mortem IVIS and microCT images were also obtained and the IVIS images for the left implant (with GFP emission filter and 465 nm excitation) are shown in figure 6.21. We see bright fluorescent spot around the infected implant at the lighter region in the black and white photograph where white pus was present confirming bacterial activity. The surrounding tissue and rabbit skin was covered with a piece of black cardboard to avoid autofluorescence in the images from the fluids present on rabbit skin.

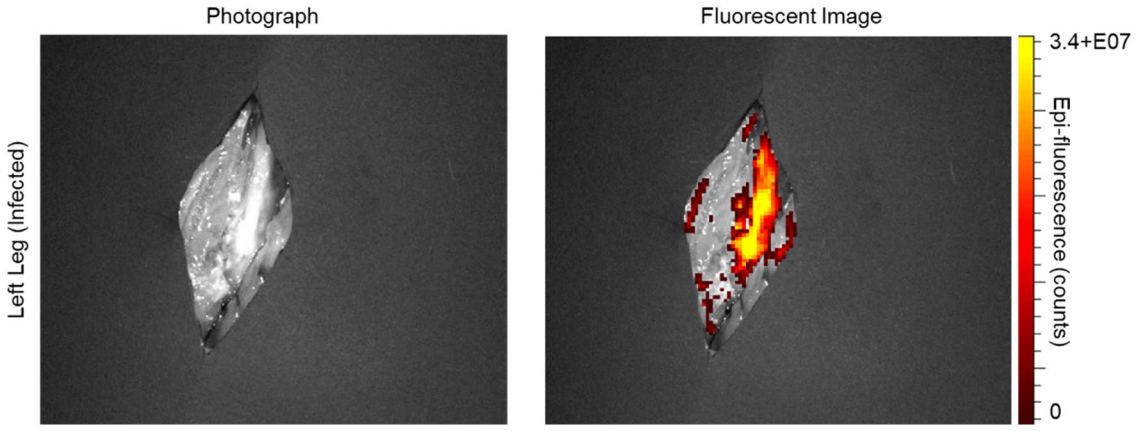

Figure 6.22: Postmortem photograph and fluorescent IVIS image of the left implant still fixed on the femur with the surrounding tissue covered with black cardboard.

Study II: Rabbit 6, open system with biofilm, optimized XELCI

Earlier studies indicated a need to increase the signal collection in the XELCI system to improve the in vivo imaging of the implants. The liquid light guide that served as the collection optics was replaced by a bigger diameter and shorter length solid light guide to collect signal from a larger area as it was initially restricted to a smaller acceptance angle of the smaller diameter liquid light guide. This dramatically improved

the signal collection resulting in sharper XELCI images and shorter scan time as the implants can be quickly located as a lot more signal could be collected through tissue. The images taken without any tissue started to show saturation, so we had to decrease the x-ray intensity to obtain images of the sensor without any tissue covering. To test the optimized XELCI system for in vivo imaging, we repeated the Phase B studies with an open face implant. The implant was machined from acrylic as shown earlier in figure 6.14. The pre-op scan and photographs of the sensor modified acrylic orthopedic plates implanted in the right (control) and left (infected) legs are given in figure 6.22. The reference, control and infected regions of the implant can be clearly distinguished in the XELCI images. The low pH in the infected chamber of the left implant started neutralizing soon after surgery as can be seen in Day 0 image of the left implant and completely neutralized on Day 1 (within 24 hours). Postmortem, both the implants had green color sensors indicating physiological pH despite clear signs of infection around the left implant. Postmortem XELCI images were taken with the implant still fixed to the bone through the cadaveric rabbit tissue and also without tissue. The XELCI images taken with the optimized system are clear, sharp with a clean background (no speckles) and high signal to noise ratio. The scanning time was also reduced as the implant could be located during one low resolution scan and imaged at a higher resolution for the final scan eliminating the need for multiple scans over a larger area to locate the implant through the tissue.

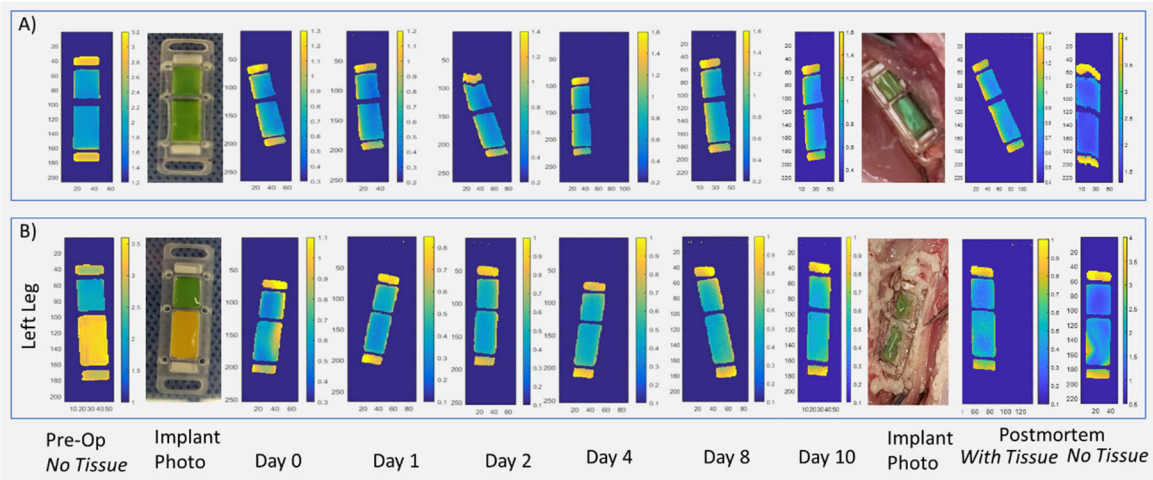

Figure 6.23: Study II Summary. Photographs and pre-op XELCI images of the sensor modified orthopedic plates implanted in the right femur (control leg) and the left femur (infected leg) of the rabbit. The control implant has two reference (white) and two control (green) chambers. The infected implant has two reference (white), one control (green) and one infected (yellow) chamber. In-vivo XELCI images (ratio) of the sensor modified orthopedic plates through tissue in live rabbit imaged over a period of 10 days followed by postmortem implant retrieval and imaging.

Another improvement of the XELCI system was the addition of a mini x-ray camera (an astronomical camera fitted with a scintillator screen, Lodestar Autoguider, Starlight Xpress Ltd, UK) under the sample stage lined up with the x-ray to obtain plain radiographs of the sample being scanned with XELCI in the same orientation as the XELCI images. Both the XELCI image and the radiograph can then be superimposed to provide spatial and chemical details in the same image. The same is also possible for the radiographs taken with the commercial x-ray outside the XELCI scanning system but then the XELCI image may not be in the same orientation as the radiograph. Figure 6.23A shows the radiographs taken with the mini x-ray cam and the superimposed images of the left and right implants. The images line up well and the radiograph provides the additional details, for example the bone where the sensor is implanted can also be seen in

the radiographic image that was not visible in the XELCI image. In Day 0 image of the right leg, we can also see the placement of both legs was close together as the left iplant is also partially visible in the radiograph.

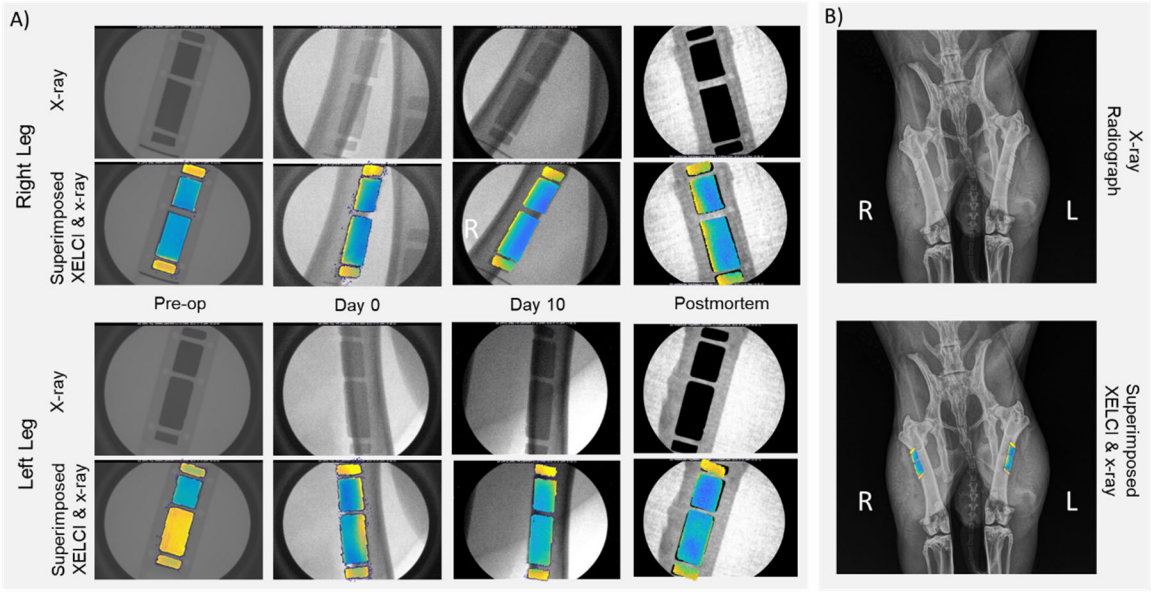

Figure 6.24: Superimposed X-ray and XELCI. A) Plain x-ray images (taken with mini x-ray cam) of the implant in both right and left legs superimposed with XELCI images to provide both spatial and chemical details. B) Top: Plain radiograph of the rabbit (taken with commercial x-ray) showing both implants on right and left femur. Bottom: XELCI and radiograph overlay of the implants.

Postmortem observations confirmed the physiological pH in both sensors as indicated by the green appearance of the sensor gels and pH measurements. Infection was evident in the left implant due to presence of pus as can be seen in the postmortem images in figure 6.24. Photographs of the sensor before and during implantation are also shown for comparison. The right implant did not have any pus but the top clear TSA layer of the sensors turned translucent and had to be removed to reveal the sensor gel color for right implant. The gel in the small chamber turned a darker green upon exposure

to air. pH was measured in the big chambers and the tissue around the implant, the pH was around physiological pH for all except for a spot in the pus surrounding the implant that was measured to be slightly low, pH 6.78–7.01.

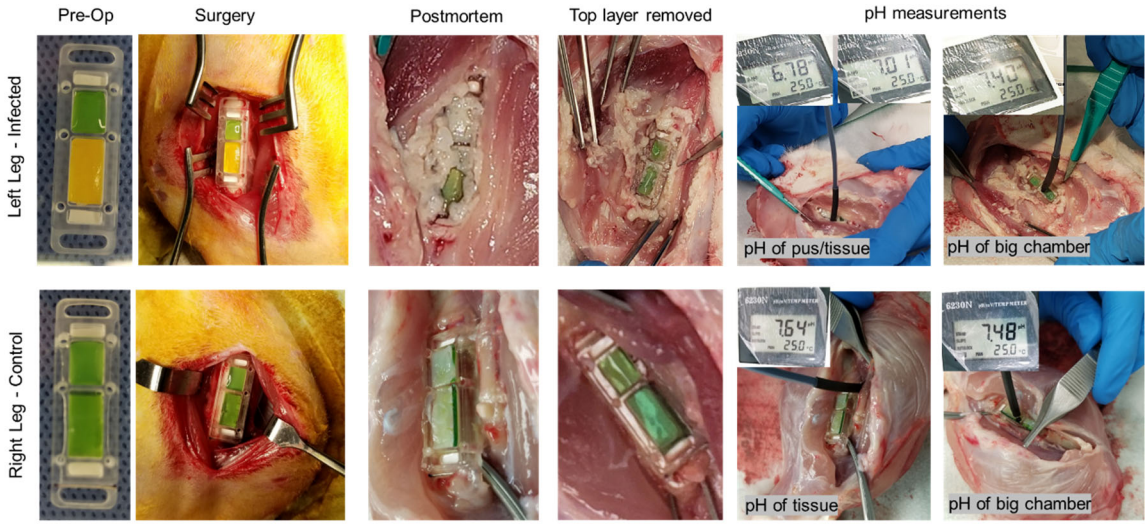

Figure 6.25: Postmortem (Study II). Photographs of the sensor modified orthopedic plates before surgery (pre-op), during surgery and postmortem photographs of the same for both infected and control legs. Photos taken during postmortem pH measurements of the implanted sensors (big chambers) and the surrounding tissue with a pH microelectrode. The measured pH is shown as an inset in the respective photograph.

The gels were taken out of the implant and placed in PBS to equilibrate. A set of reference gels from the same batch were also tested for reversibility together with the retrieved gels for comparison. Both the retrieved and reference gels responded to pH changes in same time and to the same color intensity as shown in figure 6.25. It took them 5–7 minutes for a complete color change from physiological pH to acidic pH and 35 minutes to return from pH 5 buffer to PBS. This agrees with the response time observed in the in vitro reversibility study. Overall, this single rabbit experiment ensured that the

modified imaging system was able to image the pH film in rabbits and we observed neutralization of the acidic pH by the body fluids in the presence of a biofilm.

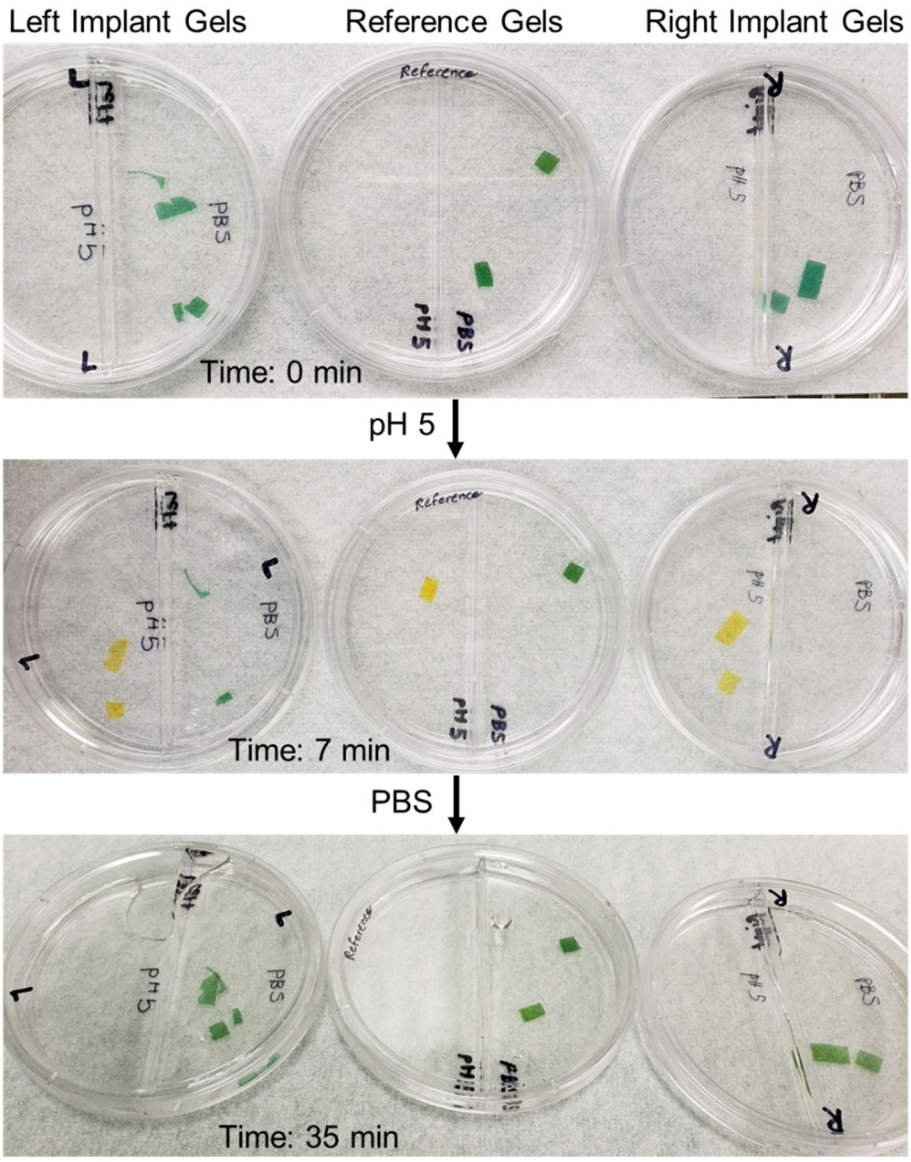

Figure 6.26: Reversibility check of the retrieved sensor gels. The gels taken from the retrieved implants and two reference gels from the same batch (not implanted) were immersed in phosphate buffered saline (PBS), pH 7.2 followed by immersion in pH 5 buffer (7 minutes) and back in PBS (35 minutes). Green color indicate physiological pH, yellow color indicates acidic pH.

Study III: Rabbit 5, cavity simulation with biofilm, optimized XELCI

Even though we observed a slightly acidic pH in the cavity region, but it was not obvious in the XELCI images. This could be due to the possible reflection of the signal from parafilm and reabsorption by the sensor film and the tissue resulting in a decreased signal giving a false pH since the parafilm is not completely transparent and inhomogeneous due to stretching of the film during application. There was a need to use a transparent and homogenous material for the covering to form a cavity. Also, the parafilm cover was not applied to the control implant and does not provide a good comparison between control and infected implants. Therefore, we moved on to the use of an acrylic lid to cover the implants to form a cavity instead of using parafilm. The use of a well-defined lid provided more control than using the parafilm, the hole size and thickness of which can greatly vary between experiments. Study III was performed with a cavity simulation formed by a lid covering the implant, both made of acrylic. The lid was secured to the implant using screws and was open on top of the small chamber and had a defined 1 mm hole on top of the big chamber to allow for slow exchange of fluids allowing to study the effect of diffusion on the pH of the cavity in the presence of an established biofilm. Photographs and the XELCI scans of the implants before surgery are given in figure 6.26. The control implant did not have a biofilm but still had 1 mm hole in the lid. The infected chamber can be clearly seen in pre-op, day 0 and day 1 XELCI ratiometric images to have an acidic pH indicated by the higher signal intensity (yellow color) compared to the control chamber (light blue) that was at physiological pH. We can see the diffusion of body fluids and neutralization of acidic pH close to the hole in the lid

(towards the small chamber) in the XELCI image of the left implant on Day 1 indicated by the greenish blue spot on the edge of the big chamber located towards the small chamber. The pH appeared to be mostly neutralized within 48 hours (Day 2). Compared to the in vitro study of cavity simulation with a biofilm where the neutralization took at least 4 days for the implant with 1 mm pinhole, the in vivo study for the same hole size indicated 2x faster neutralization of the cavity pH (Day 2 in vivo vs. Day 4 in vitro). The control implant did not show much change in pH over 10 days. The implants were retrieved on Day 10 and postmortem images obtained.

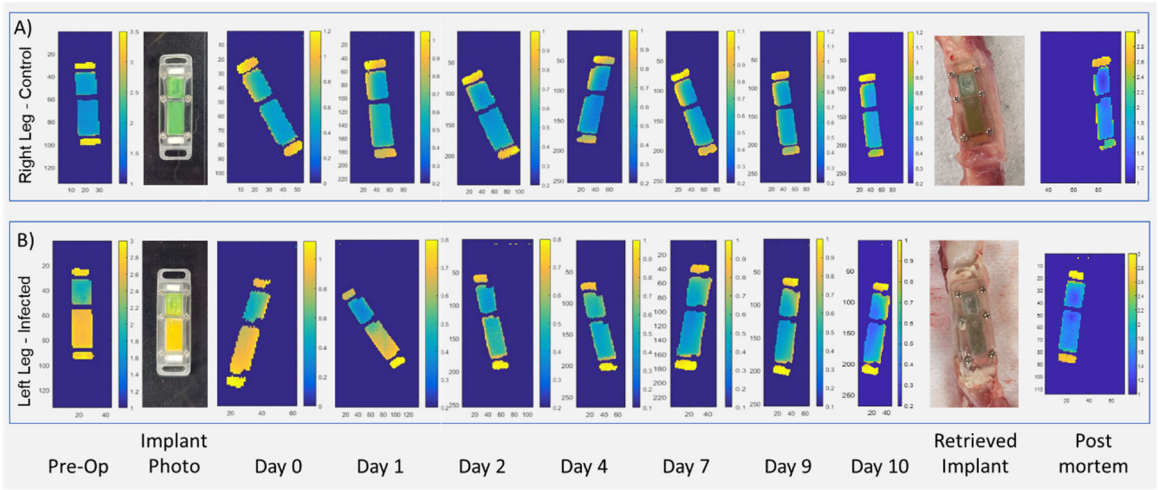

Figure 6.27: Study III summary. Photographs and pre-op XELCI images of the sensor modified orthopedic plates implanted in the right femur (control leg) and the left femur (infected leg) of the rabbit. The control implant has two reference (white) and two control (green) chambers. The infected implant has two reference (white), one control (green) and one infected (yellow) chamber. In-vivo XELCI images (ratio) of the sensor modified orthopedic plates through tissue in live rabbit imaged over a period of 10 days followed by postmortem implant retrieval and imaging.

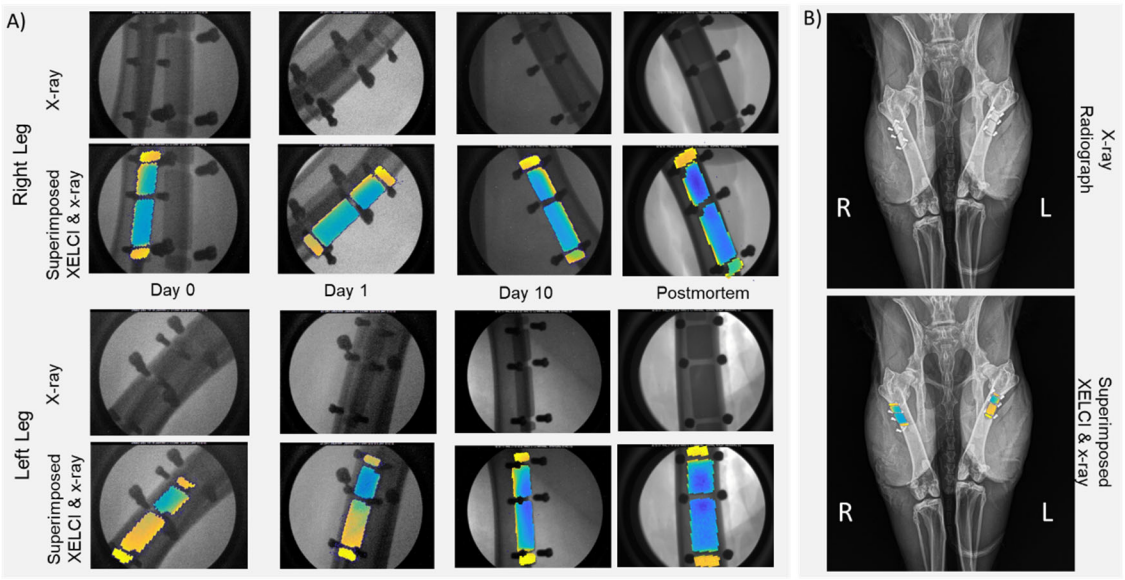

Figure 6.28: Superimposed X-ray and XELCI for Study III. A) Plain x-ray images of the implant in both right and left legs superimposed with XELCI images to provide both spatial and chemical details. B) Top: Plain radiograph of the rabbit (taken with commercial x-ray) showing both implants on right and left femur. Bottom: XELCI and radiograph overlay of the implants.

Superimposed XELCI and x-ray images were also obtained by taking x-rays of the implant in the same orientation during XELCI imaging and some of them are shown in figure 6.27A. This overlay of XELCI images with radiographs provides information with regards to the position of the implant on the bone and we can directly evaluate the bone condition next to the implant to see if there are any signs of implant loosening or fractures in the bone coupled with the chemical information such as pH on the implant surface provided by the XELCI images. Postmortem observations are summarized in figure 6.28 showing a comparison of the implant condition before surgery and postmortem. The tissue surrounding the left implant was clearly infected as can be seen by the abscess growth around the inoculated implant that was absent in the control leg. Accumulation of blood and white blood cells in the agar layer in the implant cavity

affected the visual observation of the color of the gels in the implants but the gels in the big chambers appear to be lighter green than those in the small chambers. pH measurements were made immediately after euthanasia and pH of the surrounding tissue in right leg was between 7.43 and 7.65 while in the left leg, pH was higher in the healthy tissue clear of any pus (pH 7.81) compared to that of the serous fluid and the pus (pH 6.78). The implants' lids were removed and the top agar layer cleared to reveal gel color and pH measured in the implant chambers. The control chambers were at slightly higher pH than the cavity chambers in both implants. However the overall pH was slightly higher in the right implant compared to the left implant. pH in the left implant small chamber was 7.65 and cavity chamber was pH 7.13 while for the right implant, small chamber pH was 7.89 and cavity chamber was at pH 7.31.

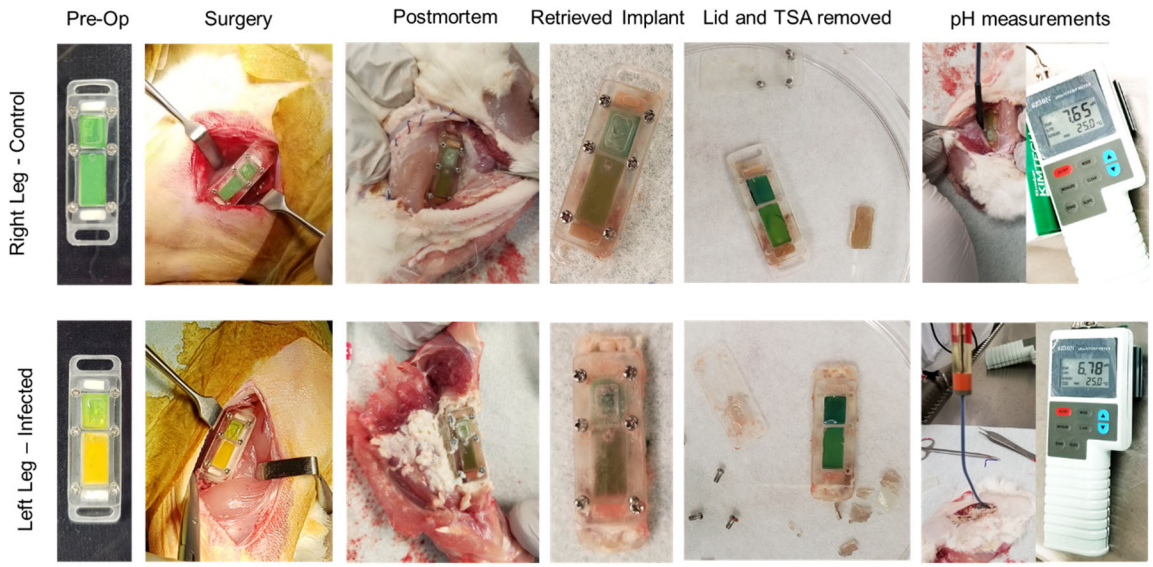

Figure 6.29: Postmortem (Study III). Photographs of the sensor modified orthopedic plates before surgery (pre-op), during surgery and postmortem photographs of the same for both infected and control legs. Photos of the implant with the lid removed and during postmortem pH measurements of the surrounding tissue with a pH microelectrode. The measured pH is shown alongside the respective photograph.

To summarize Study II, we were able to see the effect of diffusion in the presence of biofilm and neutralization of the pH by the body fluids in a cavity simulation. The pH change was non-invasively imaged in vivo in real time using XELCI and sharp, background free images were obtained.

Study IV: Rabbit 4, cavity simulation with lactic acid, optimized XELCI

The study was performed without infection to see the effect of pH neutralization in a cavity without any biofilm. For this experiment, to make sure we have an acidic and neutral region to test the neutralization rate and imaging ability, we used lactic acid to achieve acidic pH 5.0 mixed with phosphate buffered saline, PBS in agar in the implant itself. Lactic acid is produced by bacteria and other cells in the form of lactate that is converted to lactic acid and is a primary end-product of anaerobic respiration.[5,6] The agar was placed in the chamber with a cover placed over it with a small hole to allow slow exchange; we did not expect the pH 5.0 agar to cause any pain; buprenorphine was administered to provide post implantation analgesia. The experiment was run for 10 days. The purpose of the experiment was to serve as a comparison to past and future *Staph aureus* experiments to see how much of the pH effect is from acid generation within the biofilm vs. diffusion of the initially acidic species.

Figure 6.29A shows the imaging setup with the rabbit with the anesthetic mask placed on the stage positioned under the focused X-ray beam lined up with the acrylic light guide to collect the signal from the implant. Optics and implant alignment is done

using a laser cross beam (red lines in the image). The prepared orthopedic plates were imaged before surgery (pre-op images in Figure 6.29C-D), implanted in the rabbit and imaged for 10 days. The pre-op images obtained without any tissue covering saturated due to increased signal collection by the optimized XELCI and that explains why the different chambers of the implant does not look as expected in the pre-op images of the implant especially the left implant where both the small and big chambers appear to be almost equally bright instead of a blue small and yellow big chamber. In vivo images are clear and the different chambers can be distinguished from each other. The intensity of reference regions indicates variations in tissue thickness such as in Day 9 and 10 for right implant where the reference close to the big chamber appears brighter than the reference close to the small chamber. The acidic region in the left implant started to neutralize on Day 0 and on Day 1 there was only a small spot (yellow spot) in the big chamber that was still acidic and rest of the sensor in the big chamber was mostly neutralized. We can see a gradient around the spot (yellow to green to blue) in the big chamber of left implant on Day 1 and Day 2. The small acidic spot was still visible on Day 10 and postmortem implant retrieval showed a small bubble with yellowish gel present in the region of the acidic spot visible in XELCI images. Compared to the results of in vitro simulation of pure diffusion through a 1 mm hole (figure 6.17), the neutralization in vivo was 2x faster (started within 24 hrs in vivo as compared to 48 hours for in vitro). This is consistent with the cavity simulation with a biofilm where the neutralization was 2x faster than the in vitro study. However, unlike the in vitro study where the neutralization was complete on

Day 3, the acidic region in the implant in vivo did not completely and evenly neutralized due to presence of a bubble in the implant that formed soon after implantation in vivo.

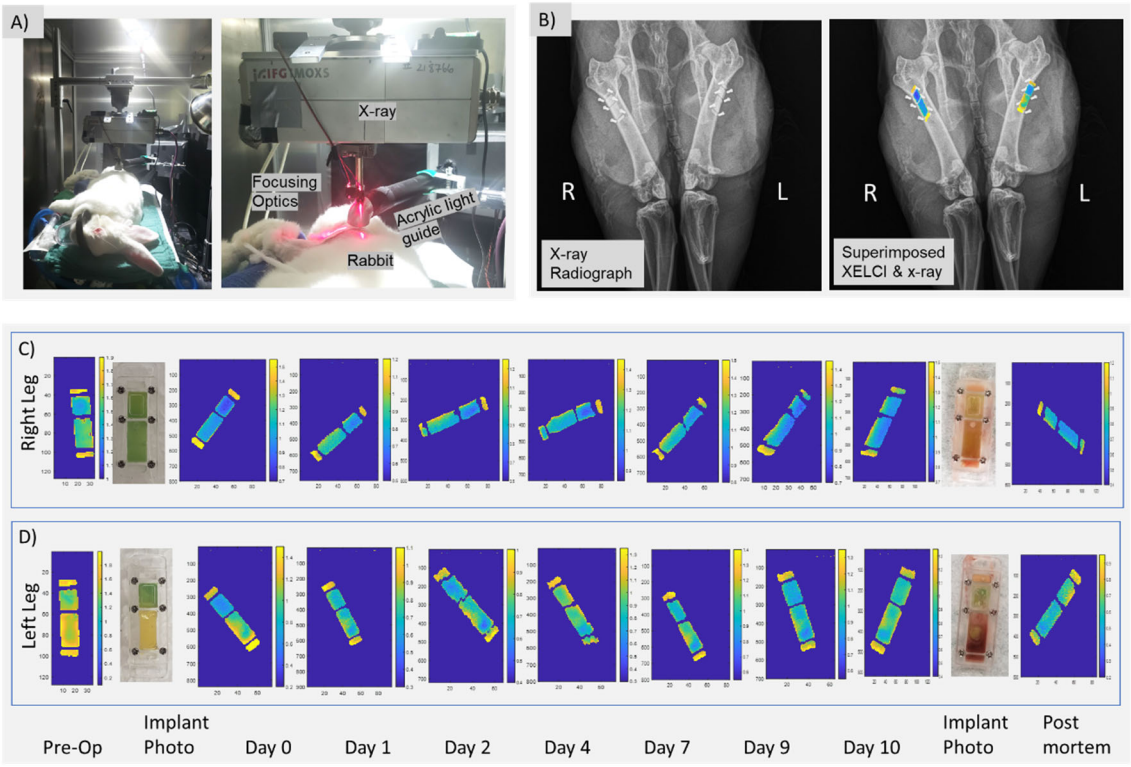

Figure 6.30: Study IV Summary. A) Photograph of the rabbit in the imaging setup followed by a close-up photograph showing the X-ray unit, focusing optics attached to the X-ray unit and the acrylic light guide collecting signal. The focusing optics, light guide and the implant region are all lined up using a laser cross beam. B) Plain radiograph of the rabbit (taken with commercial x-ray) showing both implants on right and left femur followed by the XELCI and radiograph overlay of the implants. C) Photographs and pre-op XELCI images of the sensor modified orthopedic plates implanted in the right femur (control leg) and the left femur (low pH leg) of the rabbit. The control implant has two reference (white) and two control (green) chambers. The low pH implant has two reference (white), one control (green) and one low pH (yellow) chamber. In-vivo XELCI images (ratio) of the sensor modified orthopedic plates through tissue in live rabbit imaged over a period of 10 days followed by postmortem implant retrieval and imaging.

Figure 6.30 shows the implant images before and during surgery compared with postmortem images of the same. There were no signs of infection or inflammation in the

tissue in both legs but pH of tissue in contact with the implant was slightly higher (about 7.8) than rest of the tissue (about 7.2). Postmortem photographs of the implants showed accumulation of blood in the implants especially in the left implant where we also see the bubble with acidic pH in the big chamber surrounded by light green region of gel. The top agar layer in both implants turned translucent with absorption of white blood cells and blood affecting a direct evaluation of the pH sensor gel color underneath. The right control implant also appeared to be slightly acidic based on the visual color of the sensor gel covered in agar but the gel looked more green after that layer was taken off. Implants' lids were taken off and pH measured for each chamber. Right implant had a pH of 7.67 and 7.29 in the small and big chambers respectively. pH of both chambers in left implant was about 7.4. The bubble in the left implant disappeared after taking off the lid and pH neutralized over the big chamber. Both implants were placed in PBS and the gels turned green confirming reversibility and color intensity was same as before the surgery indicating there was no significant leaching of the dye.

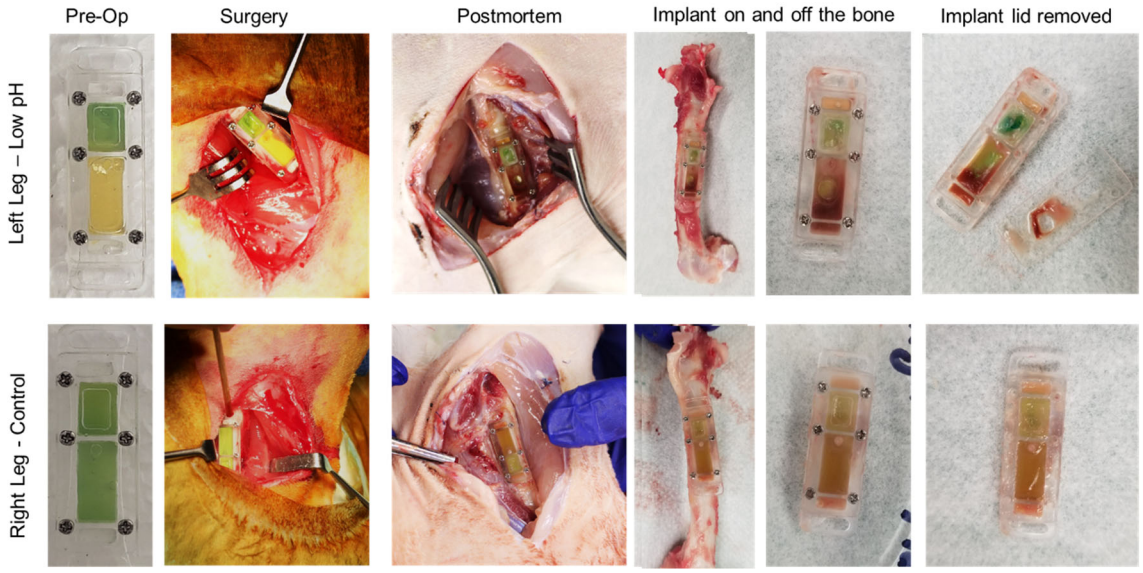

Figure 6.31: Postmortem (Study IV). Photographs of the sensor modified orthopedic plates before surgery (pre-op), during surgery and postmortem photographs of the same for both legs. The implant was taken off the bone and the lid removed.

Study V: Rabbit 7, developing infection (neutral start), cavity simulation, optimized XELCI

We observed the neutralization of the pH from acidic to neutral both in the presence and absence of a biofilm in study III and IV. In case of study III, we started the experiment with an established biofilm where the inoculant had enough time to form a biofilm and produce acidity that was detected by the sensor gel making it turn yellow from green. This acidity was neutralized by the body fluids after implantation with the sensor gel turning back to green. Next, we wanted to see if we could observe this production of acidic byproducts during formation of the biofilm on the sensor gel and see the color changing from green to yellow. For study V, we started the experiment with a neutral pH instead of acidic pH in the infected chamber. This was done by inoculating the

big chamber of the left implant an hour before surgery compared to previous studies where the inoculant had time to establish the biofilm overnight before surgery. As a result, the pH of the infected chamber was still neutral even though we can see in the photograph in figure 6.31B that the inoculant already started working and the gel color in the big chamber in left implant appears lighter green compared to the darker green gel in the control chamber. This slight difference in pH is also visible in the pre-op XELCI scan of the left implant. This study also lasted 10 days and the animal was imaged everyday for the first 72 hours as we expected the first 3 days to be critical for the pH change and then every 2 days after that. Based on the XELCI images, we did not see a big drop in pH over the course of the study but we did see a slight pH difference between the control and infected chambers of the left implant that lasted till Day 8 and seems to be finally neutralized on Day 10. Even though both references had were equally bright in the pre-op scan, the reference next to the small chamber also appears brighter than the reference next to the big chamber indicating a potentially lower pH in the big chamber. A brighter reference indicates more signal is being collected that could be due to a thinner tissue covering one end of the implant and thicker tissue on the other end makes the reference appear less bright. If we apply a signal gradient based on the intensities of the two references, we will expect more signal in the infected region and more signal indicates a lower pH. This also indicates the need to improve the MATLAB script to account for theses changes and apply a gradient. Moreover, having a reference along the length of the implant on both sides can also be useful and will help to make the normalization much easier.

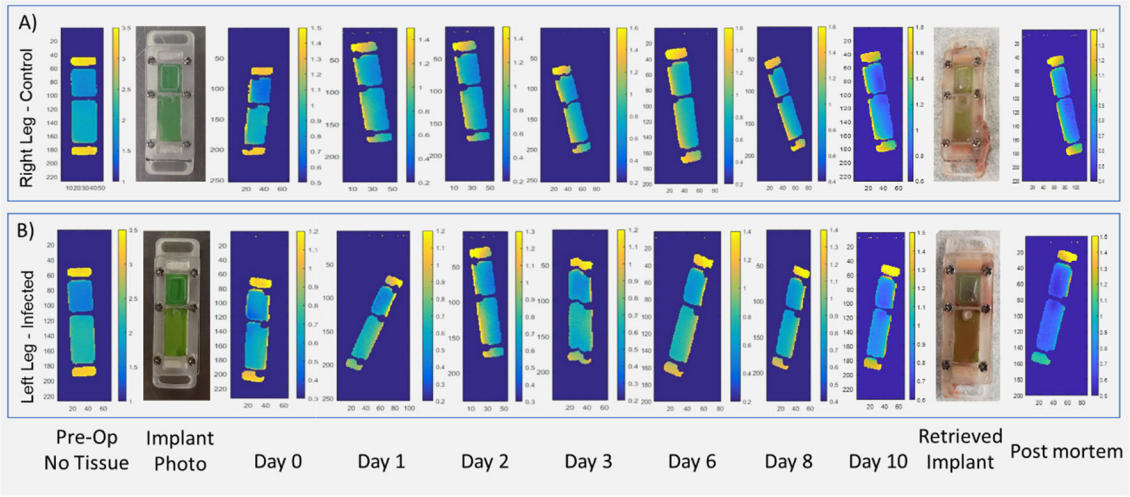

Figure 6.32: Study V Summary. Photographs and pre-op XELCI images of the sensor modified orthopedic plates implanted in the right femur (control leg) and the left femur (infected leg) of the rabbit. The control implant has two reference (white) and two control (green) chambers. The infected implant has two reference (white), one control (green) and one inoculated (light green) chamber. In-vivo XELCI images (ratio) of the sensor modified orthopedic plates through tissue in live rabbit imaged over a period of 10 days followed by postmortem implant retrieval and imaging.

Figure 6.32 shows the overlaid XELCI and X-ray images obtained during the study. If we compare the XELCI images in figure 6.32 with the superimposed x-ray and XELCI images in figure 6.32, we see that the small dark spots on the tilted side of the chamber edges in some of the XELCI images are due to the screws visible in the x-ray images. If the animal is positioned such that the implant is not completely perpendicular to the collection optics, the screws block the visible light signal producing dark spots in the XELCI image. This becomes clear in the superimposed images where the screws line up with the dark spots in the XELCI image as can be seen in Day 1, 8 and 10. This is not the case for the pre-op scan where the implant was imaged directly perpendicular to the optics as the positioning and placement of the implant was much easy and clear when it is

in the petri dish compared to orientation of the animal body to position the implant. Another issue due to this positioning is that more signal is collected from the implant region that is closer to the light guide versus the regions that are tilted away from the light guide. The signal from farther regions must travel through a larger distance in tissue to reach the light guide compared to the signal that is collected from the implant that is perpendicular to the light guide. We also see a bright yellow line across the length of one side of the implant depending on the orientation of the implant. This can be seen on the left side of the right implant and the right side of the left implant in the XELCI images for Day 1, 6 and 8. Again this issue is not seen in the pre-op scan where the implant is perpendicular to the light guide. This is because the sensor consists of two layers and the gel layer does not cover the scintillator layer when viewed from the side, it only covers the top side of the scintillator layer and since the implants are made from acrylic and are transparent, both layers are visible when viewed from the side. Due to the tilted orientation of the implant, we can the see the bright light from the scintillator layer appearing as a bright that is not covered by the signal attenuating gel film.

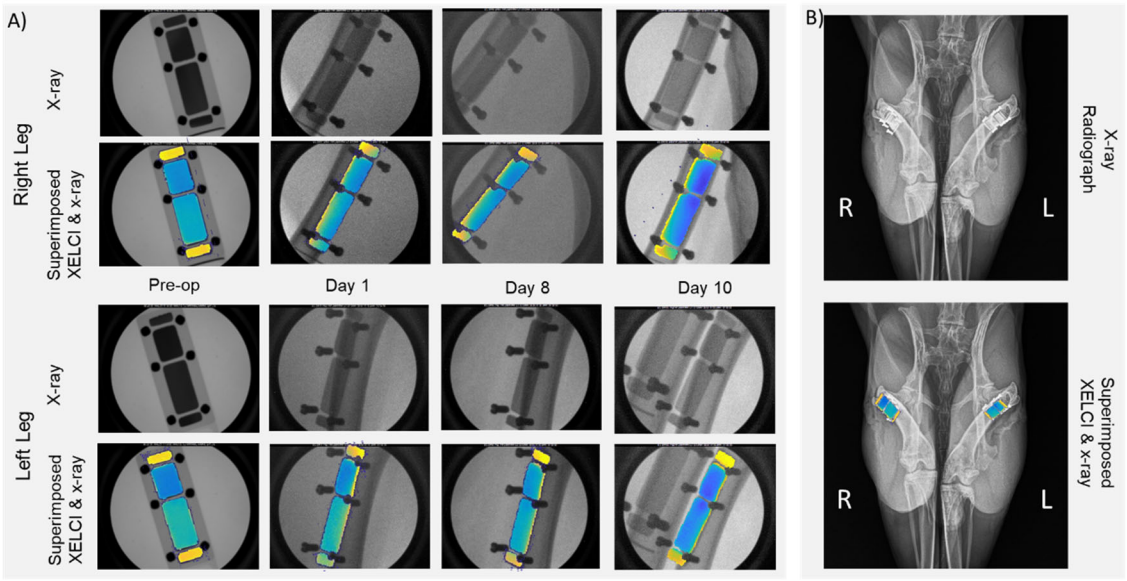

Figure 6.33: Superimposed X-ray and XELCI for Study V. A) Plain x-ray images of the implant in both right and left legs superimposed with XELCI images to provide both spatial and chemical details. B) Top: Plain radiograph of the rabbit (taken with commercial x-ray) showing both implants on right and left femur. Bottom: XELCI and radiograph overlay of the implants.

Postmortem evaluation of the study is summarized in figure 6.33 with a direct comparison of the implant before surgery and postmortem. The tissue in both legs appeared healthy and we did not observe any signs of infection in the tissue surrounding the inoculated implant. The pinhole in the lid of left implant (indicated by the white arrow) appeared to be clogged with a whitish appearance that could be a mixture of white blood cells and pus. To confirm for presence of infection, bacteria was cultured from the implant gels and the surrounding tissue. Bacteria was recovered from the implant but not from the surrounding tissue indicating a very localized infection that was confined only within the implant cavity and did not spread to the surrounding tissue. This also explains why we did not see a big drop in pH as there was not enough bacteria to produce a large amount of acidity especially during neutralization by the body fluids since we did not

start the experiment with an established biofilm. Even though initial concentration of the inoculum is the same (5000 cfu) for both studies III and V, the total concentration of bacteria present at the start of experiment in study III is exponentially greater than that for study V due to the amount of time the initial inoculum had to establish a biofilm overnight and undisturbed in vitro for study III compared to that in the body in study V. Seepage of blood was evident in both implants and top agar layer produced a pseudo color difference between the two chambers in the inoculated implant. Removal of the agar layer revealed the green color of the gels. pH was measured for the surrounding tissue and varied greatly between pH 7.4 and 8 in both legs. The gels were reversible with a response time of 5–7 minutes in going from physiological pH to pH 5 and 35 minutes for pH 5 to PBS consistent with previous reversibility studies of the retrieved gels.

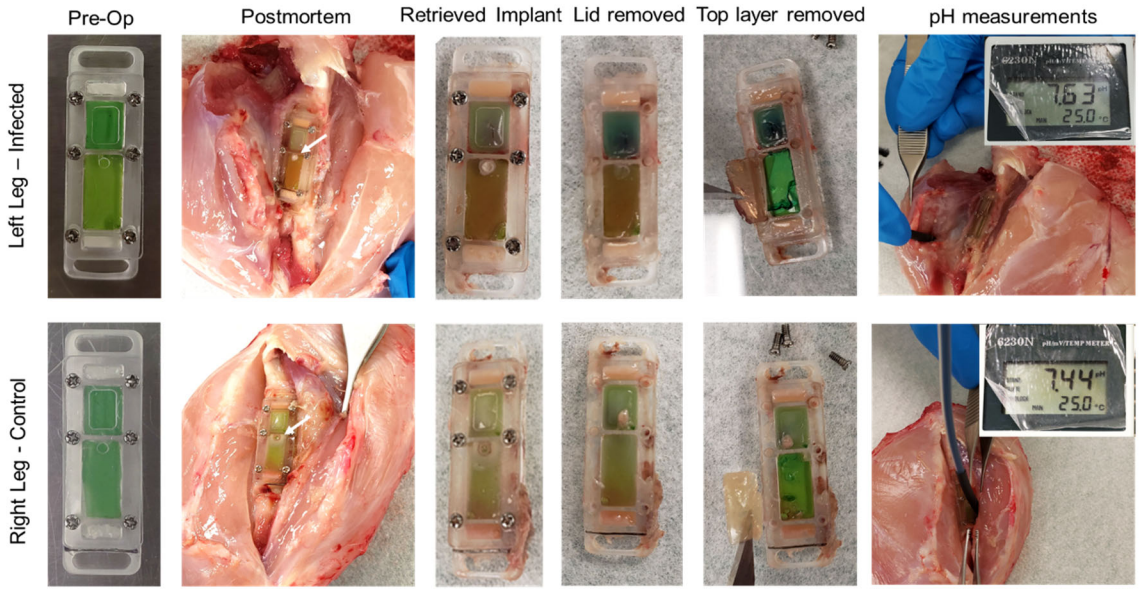

Figure 6.34: Postmortem (Study V). Photographs of the sensor modified orthopedic plates before surgery (pre-op) and postmortem photographs of the same for both legs. Photos of the implant with the lid removed and during postmortem pH measurements of the surrounding tissue with a pH microelectrode. The measured pH is shown alongside the respective photograph.

Study VI: Rabbit 8, developing infection (neutral start), cavity simulation, early termination, optimized XELCI

Study V was repeated with the same neutral start by inoculation just before the surgery but with an early termination of the experiment on Day 3. Th early termination was to evaluate the intermittent implant condition between the start and the usual 10 day study. Previous studies with cavity simulation indicated the possibility of a low pH within the first 48–72 hours and even up to day 8 in study V. A summary of the imaging study is shown in figure 6.34 with the implant photograph and pre-op XELCI scan. The gels in both chambers of the control implant are green in color while the gel in the big chamber (inoculated) of the left implant is a lighter green than the gel in the small chamber (control). Since the inoculation was performed within an hour before the surgery, the biofilm is not established yet giving it a rather neutral pH start. After implantation, there seemed to be an apparent decrease in the pH on day 2 and 3 in the big chamber of both implants. This could be due to blood accumulation and possibility of a clogged hole. Postmortem scans of both implants show a pH difference in the two chambers.

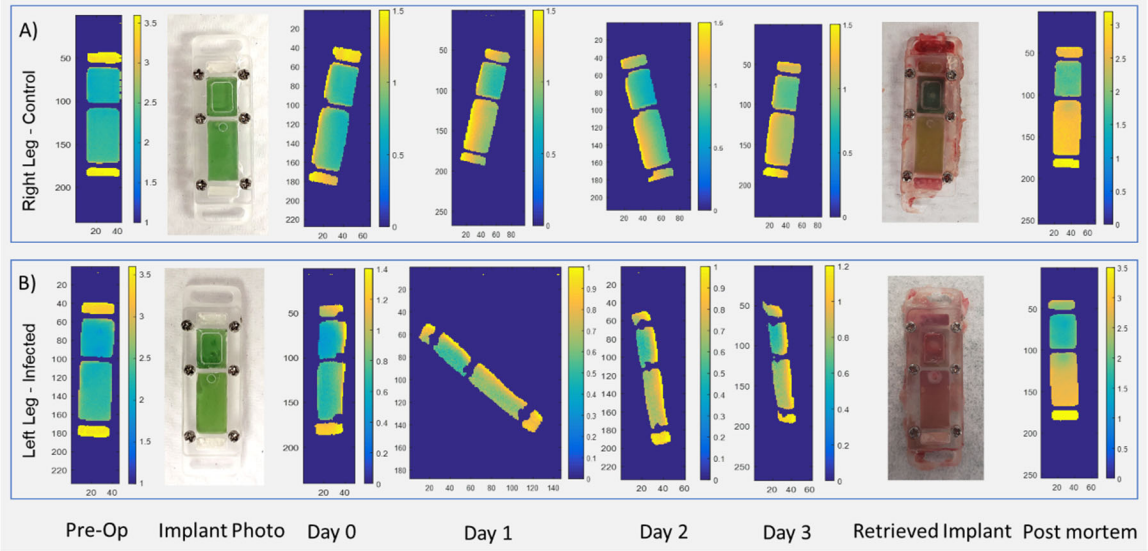

Figure 6.35: Study VI Summary. Photographs and pre-op XELCI images of the sensor modified orthopedic plates implanted in the right femur (control leg) and the left femur (infected leg) of the rabbit. The control implant has two reference (white) and two control (green) chambers. The infected implant has two reference (white), one control (green) and one inoculated (light green) chamber. In-vivo XELCI images (ratio) of the sensor modified orthopedic plates through tissue in live rabbit imaged over a period of 10 days followed by postmortem implant retrieval and imaging.

The retrieved implants confirmed the accumulation of blood in the cavity as can be seen in the postmortem photographs of the implants in figure 6.35. Surprisingly the cavity in the right implant appeared yellow compared to the small chamber in the same implant. For the left implant, both chambers appeared more red than green or yellow with the hole clogged with white pus. The tissue surrounding the implants was completely healthy in both legs with no bacteria recovered from the tissue or the right implant. Bacteria was recovered from the left implant that was inoculated. Since the implants are transparent, side views of the implants reveal the gel color to be green that was hidden under the blood soiled agar. The implant lid was taken off and the agar removed and the underlying gels were green with the big chamber gels lighter green than the control

chamber gels in both implants. Both reference chambers in the right leg also had blood seepage while only one of the reference chambers in the left implant had blood seepage. pH of both implants and surrounding tissue was measured to be between pH 7.2–7.6. Gels were reversible and responded to pH changes within the expected time range established from previous studies. Based on the absorption range of the hemoglobin species (520–620 nm), we would expect the presence of blood to absorb more of the 620 nm light giving a lower signal indicative of higher pH but the XELCI images indicate a low pH in the cavity chambers of both implants that had blood seepage. Even with chambers covered in blood soiled agar in the left implant, XELCI images show a pH difference between both chambers. Further studies need to be performed with extra inoculation around the implant to provide a greater total concentration of the bacteria at the time of surgery comparable to those present in an established biofilm and evaluate the pH changes and confirm results by terminating the study at different time intervals to understand the biology.

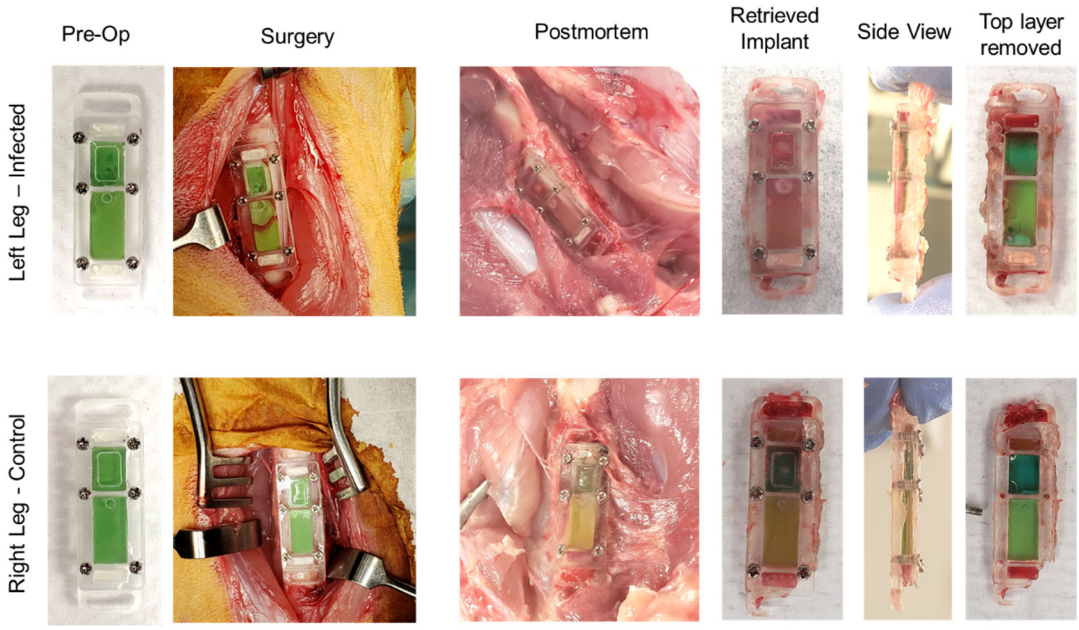

Figure 6.36: Postmortem (Study VI). Photographs of the sensor modified orthopedic plates before surgery (pre-op), during implantation (surgery) and postmortem. Lid and the top agar layer removed to reveal gel color.

6C.2.5 Summary

A summary of the all the rabbit studies conducted in Phase B, C and D is given in table 6.2. The table lists the type of implant, how the acidic pH was produced and the results of bacteria recovery from the retrieved implants and surrounding tissue. We do not see contamination of the control implants and bacteria was consistently recovered from all inoculated implants. Bacteria recovery from the tissue surrounding the infected implant was also positive in most of the cases except for the studies where a biofilm was not established overnight.

Rabbit#	Implant type	Notes	Signs of infection in tissue (Infected leg)	Bacteria recovered from tissue (Infected leg)	Bacteria recovered from tissue (Control leg)	Bacteria recovered from infected explant
R1	Machined metal implant, no lid	Biofilm established overnight before surgery	+	+	-	
R2	Machined metal implant, no lid	Established biofilm	+	+	-	
R3	Machined metal implant, Big chamber covered by parafilm with a pin hole	Established biofilm	+	+	-	
R4	Machined acrylic implant, Lid with 1 mm pinhole on top of big chamber	Lactic Acid	NA	NA	NA	NA
R5	Machined acrylic implant, Lid with 1 mm pinhole	Established biofilm	+	+	-	+
R6	Machined acrylic implant, no lid	Established biofilm	+	+	-	NA
R7	Machined acrylic implant, Lid with 1 mm pinhole	Start neutral, bacteria added on the surgery day	-	-	-	+
R8	Machined acrylic implant, Lid with 1 mm pinhole	Start neutral, bacteria added on the surgery day, euthanizing after 3 days	-	-	-	+
R9	Machined acrylic implant with holes in the bottom, Solid lid without any holes	A layer of 1.5% TSA+B under the infected implant A layer of 1.5% TSA under the control implant	+	+	-	NA

Table 6.5: Summary of bacteria recovered from tissue culture and retrieved implants.

6C.3. CONCLUSION

We studied pH changes with and without infection on the surface of sensor modified orthopedic implants. Different possible scenarios of infection were studied in vitro and in vivo for a comprehensive comparison. A pilot study (study I) was performed to simulate a cavity by covering the infected region of the implant with parafilm and allowing for slow exchange of body fluids. The postmortem results were encouraging and we saw a slight drop in pH in the simulated cavity for the first time with the infected cavity measured to be at pH 6.8 while the control implant was at pH 7.4. This was not very clear in the XELCI images due to the weak signal and possible interference from the parafilm. The XELCI system was optimized to collect more signal by addition of a solid light guide and tested to image the pH neutralization of an open face implant with biofilm (study II). The in vivo XELCI images taken with the optimized system were clear, sharp with a clean background (no speckles) and high signal to noise ratio. The scanning time was also reduced and the implant could be quickly located with a single low resolution followed by a higher resolution final scan. We were able to observe the neutralization of the low pH in the infected chamber of the left implant soon after surgery with the XELCI imaging.

Cavity simulation was repeated with a redesigned implant with a transparent lid. The lid had a pin-hole of 1 mm to allow for slow exchange of fluids and the pin-hole size was selected after an in vitro evaluation of the effect of different hole sizes (0.25 to 1 mm) on the rate of pH neutralization. Cavity simulation was conducted with and without the biofilm to compare the rate of neutralization of pH in the presence and absence of

bacteria (Study III and IV). We were able to see the effect of diffusion in both cases and neutralization of the acidic pH by the body fluids in the presence and absence of a biofilm in a cavity simulation. The pH change was non-invasively imaged in vivo in real time using XELCI and sharp, background free images were obtained. Compared to the results of in the vitro cavity simulation with and without biofilm, the neutralization in vivo was 2x faster than the in vitro study.

Study V was performed to see the pH changes that occur during the case of a developing infection as opposed to an established infection scenario studied earlier. In order to observe the production of acidic byproducts during formation of the biofilm on the sensor gel, the experiment was started with a neutral pH by inoculating the big chamber of the left implant an hour before surgery compared to previous studies where the inoculant had time to establish the biofilm overnight before surgery. We observed only a slight pH difference between the control and infected chambers that was completely neutralized by the end of the study. Postmortem evaluation revealed no visible signs of infection even though we were able to recover bacteria from the inoculated implant but not the surrounding tissue. This study demonstrates the scenario of a highly localized infection that was confined only within the implant cavity and did not spread to the surrounding tissue. Such infections are hard to diagnose with plain radiography or the blood tests. The study was repeated with early termination and the results obtained from XELCI imaging were compared to the actual implant condition. XELCI images showed a pH difference between both chambers, even in the control implant. However, the retrieved implants had issues of blood seepage that introduces a

potential interference for evaluation of the actual pH. To avoid the problem of blood seepage, the edges of the implant lid can be sealed with valap (a mixture of petroleum jelly, lanolin and paraffin) and further studies need to be performed with extra inoculation around the implant to evaluate the pH changes and confirm results by terminating the study at different time intervals to understand the biology. For all in vivo studies, we observed the sensor gels in the retrieved implants turn darker green upon exposure to air. This can be explained based on the amount of carbon dioxide present in the air compared to that in body, especially in deoxygenated blood. The body homeostasis is disturbed after euthanasia and opening of the tissue to retrieve implant. Consequently, the results of postmortem evaluations become questionable especially as more time is elapsed after euthanasia. XELCI can also provide non-invasive postmortem measurements of the pH on the implant surface without the need for implant retrieval.

A problem with the XELCI images has been the variations in signal intensity due to uneven thickness of the tissue covering the implant interfering with the visual interpretation of the pH. The MATLAB script needs to be updated to account for changes in signal intensities due to changes in tissue thickness and orientation of the implant by applying a gradient normalization approach. For this, a reference along the length of the implant on both sides can be useful. We also added plain X-ray imaging to the XECI system to obtain radiographs of the implant in the same orientation as the XELCI scans. This will ultimately be improved to obtain simultaneous x-ray images with the XELCI scans. The superimposed XELCI images with radiographs provide information regarding implant position on the bone and the immediate environment of the implant such as

implant loosening or fractures in the bone coupled with the chemical information such as pH on the implant surface.

6C.4. REFERENCES

(1) Piper, K. E.; Fernandez-Sampedro, M.; Steckelberg, K. E.; Mandrekar, J. N.; Karau, M. J.; Steckelberg, J. M.; Berbari, E. F.; Osmon, D. R.; Hanssen, A. D.; Lewallen, D. G.; Cofield, R. H.; Sperling, J. W.; Sanchez-Sotelo, J.; Huddleston, P. M.; Dekutoski, M. B.; Yaszemski, M.; Currier, B.; Patel, R. C-Reactive Protein, Erythrocyte Sedimentation Rate and Orthopedic Implant Infection. PloS One 2010, 5 (2), e9358. https://doi.org/10.1371/journal.pone.0009358.

(2) Konttinen, Y. T.; Takagi, M.; Mandelin, J.; Lassus, J.; Salo, J.; Ainola, M.; Li, T.-F.; Virtanen, I.; Liljeström, M.; Sakai, H.; Kobayashi, Y.; Sorsa, T.; Lappalainen, R.; Demulder, A.; Santavirta, S. Acid Attack and Cathepsin K in Bone Resorption Around Total Hip Replacement Prosthesis. J. Bone Miner. Res. 2001, 16 (10), 1780–1786. https://doi.org/10.1359/jbmr.2001.16.10.1780.

(3) Chen, C.-E.; Ko, J.-Y.; Wang, J.-W.; Wang, C.-J. Infection after Intramedullary Nailing of the Femur. J. Trauma 2003, 55 (2), 338–344. https://doi.org/10.1097/01.TA.0000035093.56096.3C.

(4) Makridis, K. G.; Tosounidis, T.; Giannoudis, P. V. Management of Infection After Intramedullary Nailing of Long Bone Fractures: Treatment Protocols and Outcomes. Open Orthop. J. 2013, 7, 219–226. https://doi.org/10.2174/1874325001307010219.

(5) Juturu, V.; Wu, J. C. Microbial Production of Lactic Acid: The Latest Development. Crit. Rev. Biotechnol. 2016, 36 (6), 967–977. https://doi.org/10.3109/07388551.2015.1066305.

(6) Jurtshuk, P. Bacterial Metabolism. In Medical Microbiology; Baron, S., Ed.; University of Texas Medical Branch at Galveston: Galveston (TX), 1996.

7. CONCLUSION AND FUTURE WORK

We developed a pH sensor and a novel imaging technique, X-ray excited luminescence chemical imaging (XELCI), to non-invasively monitor chemical changes associated with infection on the surface of modified implanted devices. XELCI imaging combines the penetration depth of the x-rays with optical absorbance of a color changing pH dye to evaluate surface specific pH through tissue. The sensor consists of a layer of scintillator particles that luminescence (620 nm and 700 nm intensities) when irradiated by X-rays and are covered by a layer of pH indicating layer composed of a hydrogel containing a pH dye. The absorbance of the pH dye overlaps with the emission (620 nm intensity) of the scintillator particles and modulates the luminescent signal based on the pH. A brighter signal translates to acidic pH and a weaker signal indicates higher pH. We used spectral (700 nm intensity) and spatial references to account for absorption of the light by the tissue and to estimate pH-independent variations in the signal. The sensor was characterized via a number of in vitro and in vivo evaluations and optimized accordingly. Initially the sensor had a working pH range of 3-6 that was later optimized to pH 6-8 to provide sensitivity close to the physiological pH range. Both the preliminary PEG sensor with the BCG dye and the optimized PEG-PAAm sensor with BTB dye were characterized by comparing the spectra of the free dye in aqueous solution to that of the dye in gel matrix and the attenuation of the scintillator luminescence due to absorbance of the pH dye in the gel at different pHs. The sensors are reversible with a response time between 5 – 35 minutes depending on the pH change.

We determined the effect of different types and thickness of tissue on signal intensity by collecting signal at different pHs through chicken and human cadaveric tissue and in live rabbits. The XELCI system was optimized to collect more signal by replacing the liquid light guide with a bigger diameter solid light guide significantly improving the signal collection, reducing background noise and reducing scan time. The pH sensor films were modified to conformally coat the entire orthopedic plate using an epoxy-based matrix and evaluated for measuring pH changes during biofilm formation in vitro.

For in vivo studies, we used a modified orthopedic plate with partitions for different sensor regions. We implanted the pH sensor modified orthopedic plates in rabbits and imaged the implants for 10 days during the infection. We conducted a total of 15 rabbit studies that were classified into Phase A – D for clarification and distributed over two chapters of rabbit studies (Part I and II). We studied the pH changes that occur during normal healing and infection. Our hypothesis was that as the biofilm formation occurs, pH becomes acidic and the sensor film will change color thus altering the emission ratio of the two intensities that would be detected using XELCI. pH remained close to in situ pH in case of no infection / normal healing (despite the anticipated pH changes after surgery due to inflammation of the tissue). We expected to see a drop in pH with the formation of biofilm and development of infection. However, the in vivo studies conducted so far indicated that the pH did not drop significantly in open plate infections even though there was clear evidence of infection and we observed a very small pH change (from pH 7.4 to pH 7.0) in at least one of the cavity simulation studies.

Our expectations were: (1) the pH would decrease in the case of infection both in vitro and in vivo; (2) Our novel XELCI system would be able to observe this pH change non-invasively in vivo; (3) the pH change would depend upon the environment tested and time, especially whether the infection is well perfused or in a cavity or adjacent to the bone; (4) We would be able to distinguish infection from inflammation associated from injury and surgery by the time course of the pH change and its response to vancomycin.

Our conclusions are: (1) We observed a big pH drop during infection in vitro but surprisingly we did not see a similar drop in the in vivo studies and we now trying to understand the biology. We observed a slight drop in pH during at least one of the cavity simulations where the pH drop persisted over the course of the study. The pH was neutralized in all other studies by termination of the experiment. (2) Our novel XELCI system was able to observe the pH changes non-invasively in vivo and we obtained high resolution images of the implant surface for all studies. We clearly observed pH increase when infected regions were neutralized, and the postmortem results agreed with the XELCI imaging. Additionally, the sensor remained functional after implantation for at least 11 days. This is significant because it is the only imaging technique able to provide noninvasive measurements of pH at the implant surface. (3) pH changes highly depend on the environment such as when the infection is well perfused or in a cavity. We found the neutralization of pH to be slow when studied in a cavity compared to the open face implants. These in vivo results are important because many proposed treatment mechanisms assume that the pH is lower near the infection and our initial readings would suggest that these approaches may be ineffective in some cases as we did not observe the

expected pH drop. However, work remains to better understand the conditions that our experiments have probed, in particular we mean to explore involvement of bone osteoclasts and measurements with thinner sensors probing the pH closer to the surface. In clinical cases, bone erosion is a common indication of infection, and since we did not observe bone erosion in any of our samples perhaps a longer exposure and/or a bone fracture/screw hole might make a difference. We briefly studied the pH neutralization through fluid exchange from underside of the implant close to the bone surface and the study needs further evaluations as described in future work. (4) Given the surprising studies so far, we have not yet studied how antibiotic (vancomycin) treatment affects pH and will have to study this in future.

7.1. IMPLICATIONS

The findings of this dissertation can potentially impact the development of "smart" orthopedic devices to detect, monitor and treat implant associated infection and potentially provide guidance in research on methods to reduce infection. Our expectations were based on the preliminary in vitro studies involving measurement of pH during biofilm formation indicating a pH drop of 2-3 pH units but the in vivo studies specified a very small pH drop of less than 0.5 pH units. This signifies the importance of the in vivo studies to validate the in vitro observations. Most in vitro studies are performed under a controlled environment with known variables while the sample is exposed to a dynamic system with a variety of unknown variables inside the body. One factor to consider can be patient health, for example, an immune compromised patient versus a healthy patient would have a greater chance of getting an infection. Current fixation treatments involve

invasive screws and osteomyelitis is generally found at or around the point of contact of the fixation device. Since the fixation device makes the bone more vulnerable to infection with a potential to form cavity in the bone, there is a need to design minimally invasive devices and to seal any cavities (for example, by using bone cement around the screws) that may form during fixation. Despite evidence of pH as low as pH 5 in cases of implant-associated infection reported in literature,[1] we did not observe such a low pH during the in vivo studies. These observations can also have a significant impact on the development of antibiotics targeting low pH, for example, if the pH does not drop significantly to a certain threshold for the antibiotic to be effective, the treatment will not be feasible. Another question raised by these finding is the target site accessibility. The antibiotic needs to be able to penetrate to the site of localized infection and into the biofilm. In the case of an infection in a cavity that is usually cut off from the rest of the body either due to inflammation of the surrounding tissue or cavity formation due to erosion in the bone, the exchange of body fluids is limited. Biofilms also have a mechanism of avoiding the penetration of certain chemicals by creating a gradient of pH resulting from the variable concentrations of the metabolites within the biofilm, this gradient is supposed to be the key towards developing antibiotic resistance.[2,3] We observed slower neutralization of pH in the cavity simulation studies compared to the well perfused infection studies. For the antibiotic to be effective, the right dose of the medication must be delivered to the site of infection to eradicate the biofilm.

7.2. FUTURE WORK

The results of the in vivo studies present opportunities for further evaluations in a number of directions. Future directions can be segregated into in vitro and in vivo evaluations. The in vitro component includes evaluation of the sensor to detect minute localized pH changes on the sensor gel and compare them to the pH changes within the microenvironment of the biofilm. This can be done by elucidating the effect of sensor film thickness on pH measurements by comparing the pH of the biofilm detected by our sensor films (thick and thin films) with the pH (measured by confocal scanning laser microscopy) of a biofilm incorporating a fluorescent pH indicator (C-SNARF 4) to see how the pH varies through different thicknesses of the biofilm and whether our pH sensor measures the surface pH of the biofilm (the pH at the biofilm – sensor interface) or the average pH of different thicknesses of the biofilm. For this, biofilms can be treated with seminaphthorhodafluor-4F 5-(and-6) carboxylic acid (C-SNARF-4), a fluorescent ratiometric pH indicator, excited at 488 nm and emission detected at two channels (580 nm and 640 nm), the ratio of emission intensity (pixel values) between the two emission channels determines the pH of the microenvironment. Images can be taken at different heights of the sample to determine the pH in the bulk fluid, at the biofilm-fluid interface and within the micro-colony.

Future in vivo studies include studying infections for bone cavity simulations involving intramedullary rods and to develop a model for pH changes during osteomyelitis, and repetition of the experiments with an antibiotic treatment provided in days 7-14 to study effect of the antibiotic and ability to observe eradication or recurrence.

We conducted a preliminary study (Phase D) to develop a model for osteomyelitis and to evaluate the pH changes occurring on the bone surface instead of the implant surface. A detail description of the study is given in Appendix A. Below we summarize the key conclusion, which is that the sensor can be adapted to look at pH near the bone, and that the pH near the bone surface does not fall much if the bone is intact.

To address the question of pH at the surface of the bone, sensors will need to be placed on that surface. We have performed a pilot study to show feasibility for (1) placing a porous scintillator film near the bone surface and being able to detect pH changes through that porous film in vitro; (2) detecting pH through tissue using the porous scintillator layer. Figure 7.1 shows the photographs of the implants before and during surgery and postmortem images with the respective XELCI ratiometric images. In the preliminary results, we observed that the sensor functioned and was read with both XELCI and plain radiography, but leg angle position needs to be improved (e.g. using a goniometer to hold the leg), and the top cover needs to be better sealed. Additionally, future studies could include inducing osteomyelitis (bone infection) by introducing bacteria into a fractured bone.

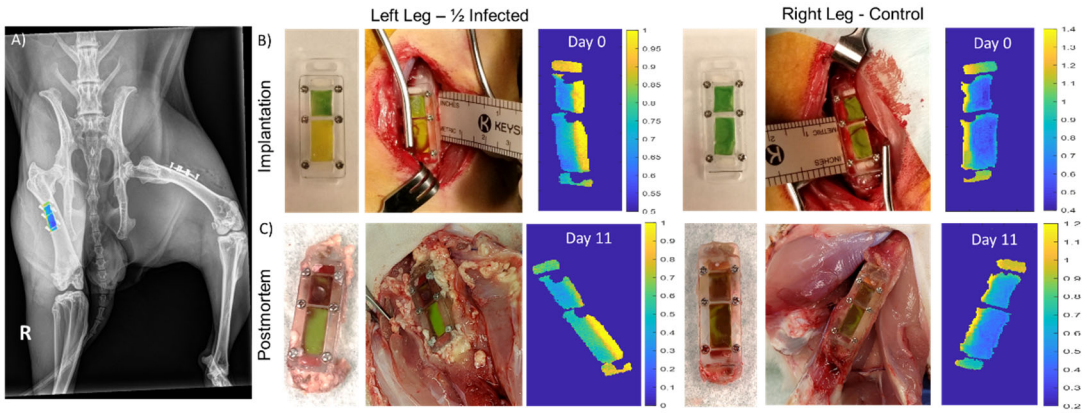

Figure 7.1: Study Summary (Phase D). A) Radiograph of the rabbit showing the two implanted sensors with the right implant overlaid with the respective XELCI image of the implant after postmortem. B) Implantation of the sensor modified plates in right and left legs. Photographs of the implants before and during surgery and XELCI images of the implants for Day 0 for each leg. C) Postmortem photographs of the retrieved implants from both legs and the respective XELCI images of the implants.

As far as the XELCI technique is concerned, improvements can be made in the signal collection efficiency (for example, the PMTs collect only 2-5% of the incident light), adding an X-ray chopper to measure luminescence lifetime and scanning scintillator nanoparticles in three dimensions for tomography. Additionally, XELCI can be extended to a wide variety of other analytes as it is able to detect local optical absorption. Some other analytes that will be interesting to study include: mechanical strain with the photoelastic effect and crack formation in reflective coatings, oxygen sensing with colorimetric and fluorescent dyes, and potentially more complex lateral flow assays.

In summary, XELCI is a novel imaging technique that can applied to measure surface specific chemical concentrations with high spatial resolution through deep tissue. We developed a pH sensor and applied XELCI to measure pH changes on the surface of

orthopedic implants ex vivo through chicken tissue and human cadaveric tissue, and in vivo in live rabbits during implant-associated infection.

7.3. REFERENCES

(1) Konttinen, Y. T.; Takagi, M.; Mandelin, J.; Lassus, J.; Salo, J.; Ainola, M.; Li, T.-F.; Virtanen, I.; Liljeström, M.; Sakai, H.; Kobayashi, Y.; Sorsa, T.; Lappalainen, R.; Demulder, A.; Santavirta, S. Acid Attack and Cathepsin K in Bone Resorption Around Total Hip Replacement Prosthesis. *J. Bone Miner. Res.* **2001**, *16* (10), 1780–1786. https://doi.org/10.1359/jbmr.2001.16.10.1780.

(2) Stewart, P. S.; Costerton, J. W. Antibiotic Resistance of Bacteria in Biofilms. *The Lancet* **2001**, *358* (9276), 135–138. https://doi.org/10.1016/S0140-6736(01)05321-1.

(3) Stewart, P. S.; Franklin, M. J. Physiological Heterogeneity in Biofilms. *Nat. Rev. Microbiol.* **2008**, *6* (3), 199–210. https://doi.org/10.1038/nrmicro1838.

APPENDICES

Appendix A:
Phase D: Studying Bone pH (Pilot Study, Rabbit 9)

In a review of U.S. war-trauma patients from 2003 to 2007 with femoral and tibial fractures treated by the damage control orthopedics (DCO), fracture site infection occurred in 40%, with suspected osteomyelitis in 17%.[1,2] Contamination of the soft tissue in severe open fractures associated with trauma results in a relatively high occurrence of chronic osteomyelitis.[3] Osteomyelitis is the infection of the bone either due to spread of the infection through the bloodstream to the bone or via exposure to an open bone fracture or surgery. Thus, there is a need to study infection of the bone in addition to the soft tissue infection and to develop a model for osteomyelitis.

In order to examine pH near the bone cortex compared to on the surface of the implant, we designed an implant with a closed lid on top and holes in the bottom to allow for monitoring of pH changes through the underside of the implant surface directly in contact with the bone as shown in figure A.1A. To allow the scintillator layer to be H+ permeable for the fluids to reach the pH sensitive gel to record the pH changes occurring next to the bone surface, the scintillator particles were enclosed in HydroMed (an ether-based hydrophilic urethanes used in medical devices) instead of the hydrophobic PDMS (Polydimethylsiloxane) layer. To synthesize the HydroMed-scintillator film, 0.35 g of HydroMed was dissolved in 7 g of Dichloromethane and 3 g of the scintillator particles added. The mixture was stirred well to get a homogenous suspension of particles and spread on a Teflon block. Evaporation of the DCM yielded a thin film of HydroMed with scintillator particles. This was placed on the porous bottom implant followed by the pH

sensitive films. A schematic of the contents of each chamber for both the control and infected implants accompanied by a photograph of the prepared implant is also given in figure A.1 B-C. The sensor gels in the small control chambers (green in color) in both implants were covered with 0.7% agarose dissolved in PBS. The infected chamber (yellow color) for the inoculated implant contained 1.5% TSA supplemented with 1% glucose and 5000 cfu of S. aureus. The big chamber in the control implant contained 1.5% TSA supplemented with 1% glucose but no bacteria. Reference chambers contained only the HydroMed-scintillator film.

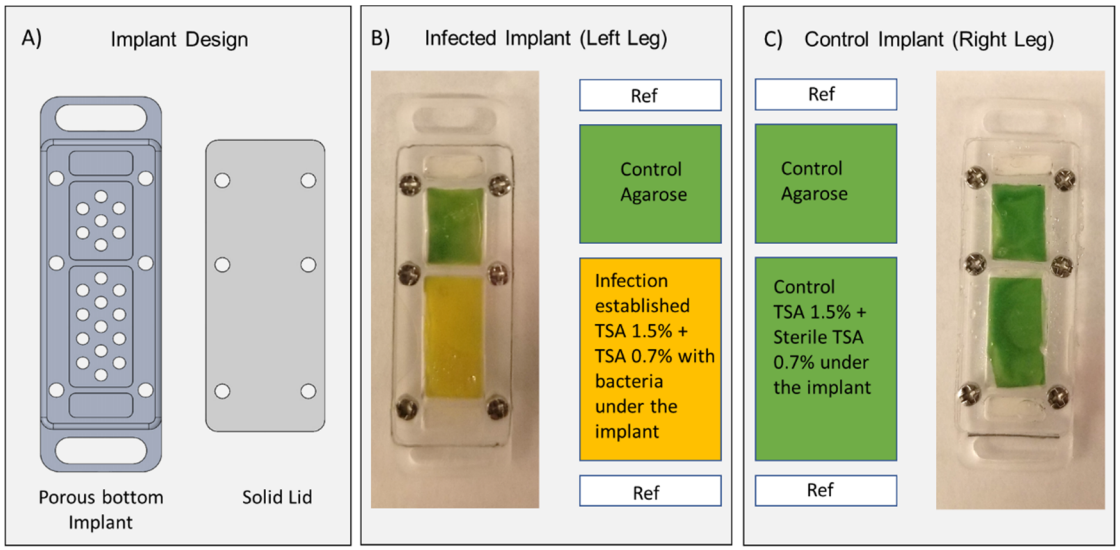

Figure A.1: Implant schematic. A) Solidworks model of the s with a porous bottom to allow for diffusion from the underside of the implant close to the bone and a solid lid to seal the top. B-C) Photographs and schematic of the contents of each chamber of the sensor modified plate to be implanted in the left and right legs.

The HydroMed-scintillator film was tested in vitro to make sure the film and the implant design allows for fluid exchange and rate of pH neutralization was studied. The infected implant was covered with 0.7% agarose dissolved in PBS in the same manner as

previous in vitro studies simulating body condition (Chapter 6). Initially we observed the spread of infection from the infected chamber to the control chamber through the underside of the implant indicated by the acidic pH in both chambers (yellow color) shown in figure A.2 for Day 1 and 2. The pH started to neutralize on Day 3 and neutralization was complete on Day 4.

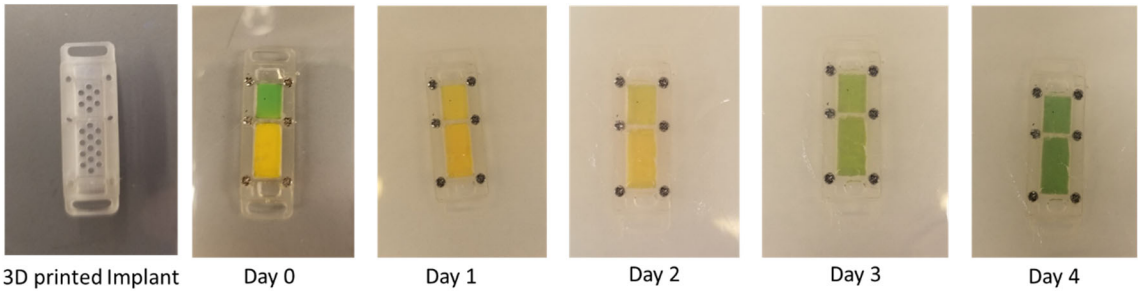

Figure A.2: In vitro neutralization of infected implant with holes in the bottom covered with a solid lid (no pin-hole). The implant was prepared with a control gel in small chamber and inoculated gel in big chamber, the top was sealed with the lid and the implant placed in a petri dish containing 0.7% agarose dissolved in PBS. Photos were taken every day to see the pH changes. Yellow = acidic pH, Green = neutral to physiological pH.

To simulate infection on surface of bone, we added extra inoculum on the underside of the left implant (0.7% TSA with bacteria) and a sterile layer of TSA was add3d on the underside of the control implant. The sensor was implanted by using surgical glue on the edges of the implant without disturbing the bottom TSA layer and imaged using XELCI (figure A.4). Photographs of the implants before and during surgery and postmortem images of the retrieved implants are shown in figure A.5. Infection was evident in the tissue surrounding the left implant but the bone showed no signs of infection or erosion as can be seen in the postmortem radiograph of the rabbit. Seepage of blood affected the visual observation of the gel colors in the chambers. XELCI images

had signal variations due to orientation of the implant in the rabbit and the tissue thickness across the implant. The XELCI images indicated a slight difference between the pH of the infected and control chambers in the left implant but the data needs to be normalized to the signal gradient of both references for a quantitative comparison.

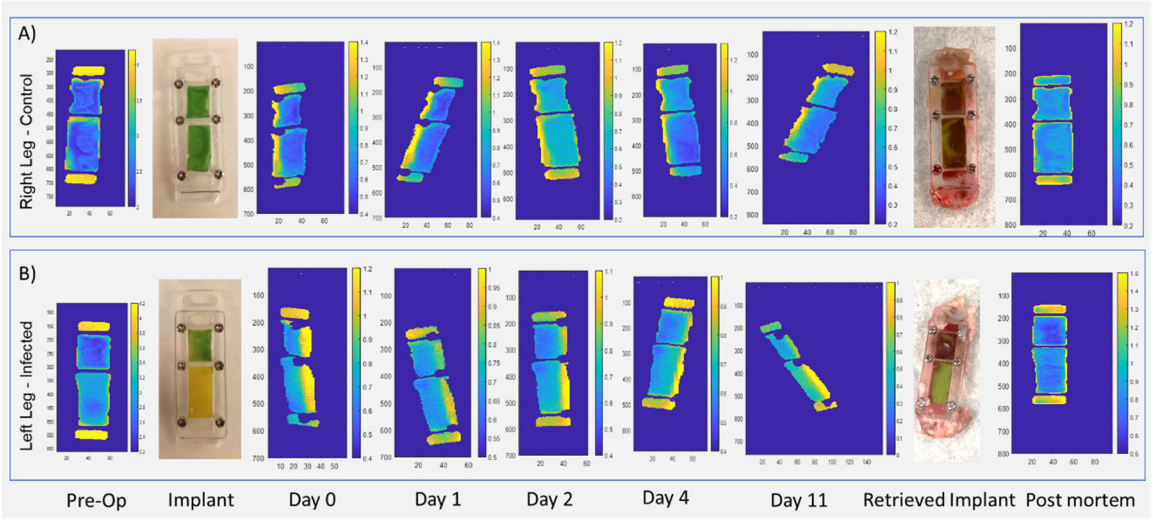

Figure A.3: Study Summary: Photographs and pre-op XELCI images of the sensor modified orthopedic plates implanted in the right femur (control leg) and the left femur (low pH leg) of the rabbit. The control implant has two reference (white) and two control (green) chambers. The low pH implant has two reference (white), one control (green) and one low pH (yellow) chamber. In-vivo XELCI images (ratio) of the sensor modified orthopedic plates through tissue in live rabbit imaged over a period of 11 days followed by postmortem implant retrieval and imaging.

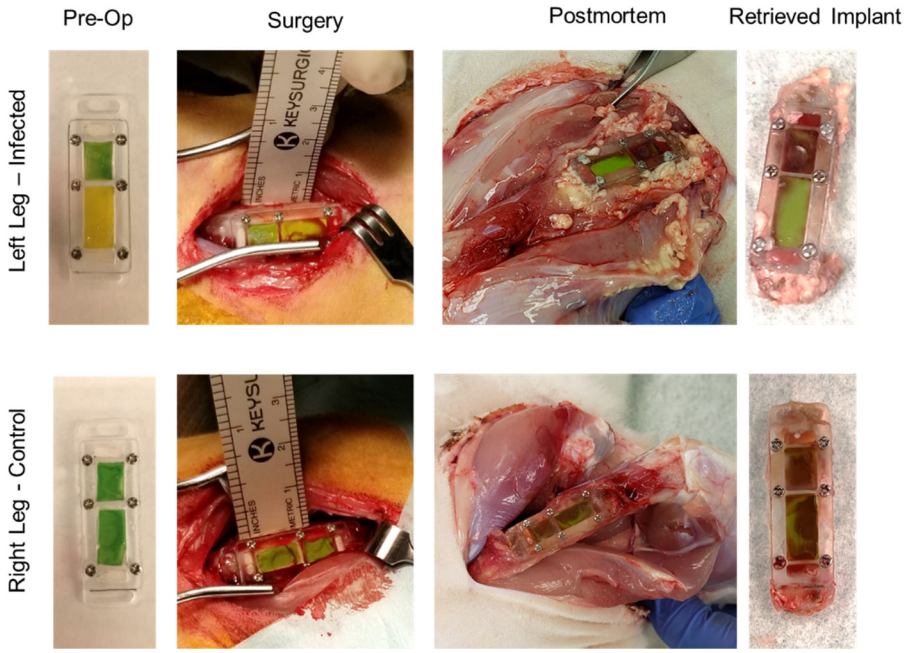

Figure A.4: Postmortem Summary (Phase D). Photographs of the sensor modified orthopedic plates before surgery (pre-op), during surgery and postmortem photographs of the same for both legs.

The sensor responded to the pH changes and the implant design was suitable but the lid edges need to be sealed better to prevent blood seepage. Presence of blood can cause false pH changes in the imaging as it makes the images appear blue (indicative of a basic pH) and make the interpretation more difficult. Given the water absorbing nature of the HydroMed-scintillator film, it needs to be cut a little smaller than the chamber size and hydrated before putting in the implant to avoid warps in the XELCI images. It is hard to distinguish between small changes of pH that might be (and appears to be) present between the infected and control implants (big chambers) based on the visual observation. In order to make visual observations easier and reliable for next time, it is

recommended to have fresh pH 7.4, pH 7 and pH 6.5 references in same picture with same lighting conditions as the retrieved implants.

The goal of this study was to serve a model to study the pH changes associated with osteomyelitis. However, the osteomyelitis did not occur. Therefore, we need to develop a new model for osteomyelitis to study pH changes, possibly, by waiting for a longer duration after inoculation and puncturing or scoring the bone to infect it. There is a possibility of association of osteomyelitis and bone erosion with fixation of plates using screws that necessitates the drilling of hole through the bone, thus making it accessible to the bacteria. Having a hole in the bone will also help to see localized pH changes as shown by sensor if occurring in the sensor region right on top of the exposed bone that can be verified by X-ray images.

REFERENCES

(1) Mody, R. M.; Zapor, M.; Hartzell, J. D.; Robben, P. M.; Waterman, P.; Wood-Morris, R.; Trotta, R.; Andersen, R. C.; Wortmann, G. Infectious Complications of Damage Control Orthopedics in War Trauma. J. Trauma 2009, 67 (4), 758–761. https://doi.org/10.1097/TA.0b013e3181af6aa6.

(2) Petersen, K.; Riddle, M. S.; Danko, J. R.; Blazes, D. L.; Hayden, R.; Tasker, S. A.; Dunne, J. R. Trauma-Related Infections in Battlefield Casualties from Iraq. Ann. Surg. 2007, 245 (5), 803–811. https://doi.org/10.1097/01.sla.0000251707.32332.c1.

(3) Forsberg, J. A.; Potter, B. K.; Cierny, G.; Webb, L. Diagnosis and Management of Chronic Infection. J. Am. Acad. Orthop. Surg. 2011, 19 Suppl 1, S8–S19. https://doi.org/10.5435/00124635-201102001-00003.

Appendix B:
MATLAB Script

MOTIMIT

For analyzing data acquired using the initial XELCI setup (with liquid light guide)

```
function [I6t,I7t,R,Pixeldwelltime, I6, I7] = motimit(allmotorpositions,rawI1, rawI2, stepsize,alltimings,bg6,bg7,thr6,thr7)

%This script plots the 620 nm and 700 nm intensities acquired separately as pseudo color intensity images

%and as a ratio image of I6/I7 intensities

%A check of whether the script is working properly is to compare

%sum(rawI1) to sum(I7) for each row, if the signal is allocated properly,

%the sums should be identical (except for signal collected after motor moves to end).

if nargin<4,

   stepsize=0.5;

end;

[Max, Ind]= max(allmotorpositions'); %Max(k) is the maximum value of row k; Ind(k) is the column this maximum value is found.

Cols=ceil(Max(1)/stepsize); %number of columns (pixels) in each row = max motor position/stepsize. Assuming min motorposition = 0.

Rows=size(Max,2); %number of rows (pixels) in the final image

I6=zeros([Rows Cols]); %Initialize image at 620nm

I7=zeros([Rows Cols]); %Initialize image at 700nm

Pixeldwelltime=zeros([Rows Cols]); %Initialize dwell time array
```

```
for k=1:Rows, %

   j=1;

   for i=1:Ind(k),

      if rawI1(k,i)>1000000 || rawI2(k,i)>1000000

         display('unexpectedly high signal rawintensity'); display(rawI1(k,i));
display(rawI2(k,i)); display([k i j]);

         rawI1(k,i)=0; rawI2(k,i)=0; alltimings(k,i)=0;

      end;



      if allmotorpositions(k,i)<=j*stepsize, %motor position still within pixel, alot signal
to that pixel

         I7(k,j)=I7(k,j)+rawI1(k,i);

         I6(k,j)=I6(k,j)+rawI2(k,i);

         Pixeldwelltime(k,j)=Pixeldwelltime(k,j)+alltimings(k,i);

      elseif allmotorpositions(k,i)>j*stepsize, %moved past the end of pixel

         if i==1,      %beginning of row

            j=ceil(allmotorpositions(k,i)/stepsize);

            I7(k,j)=rawI1(k,i);

            I6(k,j)=rawI2(k,i);

            Pixeldwelltime(k,j)=alltimings(k,i);



            %display(I6(k,j));

            %display([k j i]);
```

```
        else        %moved past end of pixel, not the beginning of row

            dtrav=allmotorpositions(k,i)-allmotorpositions(k,i-1);

            if allmotorpositions(k,i)<=(j+1)*stepsize,   %moved past the end of first pixel
but not past end of second: alot signal to the first and second pixel in proportion to
distance travelled

                I7(k,j)=I7(k,j)+rawI1(k,i)*(j*stepsize-allmotorpositions(k,i-1))/dtrav;

                I7(k,j+1)=rawI1(k,i)*(allmotorpositions(k,i)-j*stepsize)/dtrav;

                I6(k,j)=I6(k,j)+rawI2(k,i)*(j*stepsize-allmotorpositions(k,i-1))/dtrav;

                I6(k,j+1)=rawI2(k,i)*(allmotorpositions(k,i)-j*stepsize)/dtrav;

                Pixeldwelltime(k,j)=Pixeldwelltime(k,j) + alltimings(k,i)*(j*stepsize-
allmotorpositions(k,i-1))/dtrav;

                Pixeldwelltime(k,j+1)=alltimings(k,i)*(allmotorpositions(k,i)-
j*stepsize)/dtrav;



                j=j+1;



            else   %moved past the end of first and second pixel, i.e. alot signal to more than
two pixels

                display('large distance travelled compared to pixel size... interpolating');

                display([k i j]);



                I7(k,j)=I7(k,j)+rawI1(k,i)*(j*stepsize-allmotorpositions(k,i-1))/dtrav;  %alot
signal to end of first pixel in proportion to distance travelled
                I6(k,j)=I6(k,j)+rawI2(k,i)*(j*stepsize-allmotorpositions(k,i-1))/dtrav;
                Pixeldwelltime(k,j)=Pixeldwelltime(k,j)+alltimings(k,i)*(j*stepsize-
allmotorpositions(k,i-1))/dtrav;
                dtravrem=allmotorpositions(k,i)-j*stepsize;  %distance travelled past end of
pixel
```

```
                stepsleft=dtravrem/stepsize; %steps past end of first pixel
                I6rem=rawI2(k,i)*dtravrem/dtrav; %signal remaining to alot
                I7rem=rawI1(k,i)*dtravrem/dtrav;
                Pixeldwellrem=alltimings(k,i)*dtravrem/dtrav;
                   for l=1:floor(stepsleft),
                      I6(k,j+l)=I6rem/stepsleft;
                      I7(k,j+l)=I7rem/stepsleft;
                      Pixeldwelltime(k,j+l)=Pixeldwellrem/stepsleft;
                   end;
                j=j+l;
                I6remlastpx=I6rem*(stepsleft-floor(stepsleft))/stepsleft; %distance into the
last pixel
                I7remlastpx=I7rem*(stepsleft-floor(stepsleft))/stepsleft;
                Pdwelllastpx=Pixeldwellrem*(stepsleft-floor(stepsleft))/stepsleft;
                I6(k,j+1)=I6remlastpx;
                I7(k,j+1)=I7remlastpx;
                Pixeldwelltime(k,j+1)=Pdwelllastpx;
                j=j+1;
             end; %if allmotorpositions(k,i)>(j+1)*stepsize
          end; %i=1
       end; %if allmotorpositins <j*stepsize
    end; %for i=1:Ind(k)
 end; %for k=1:Rows
I6=flipud(fliplr(I6)); %Invert rows and columns to match photo. We could also reverse in
the save labview code, or rotate motors.
I7=flipud(fliplr(I7)); %Invert rows and columns to match photo.
Pixeldwelltime=flipud(fliplr(Pixeldwelltime));

I6t=I6./Pixeldwelltime*1000;  %counts/ms
I6t(isnan(I6t))=0;
I7t=I7./Pixeldwelltime*1000;    %counts/ms
I7t(isnan(I7t))=0;

figure; imagescp(I6t,0.01,0.99); colorbar; axis('equal', 'tight');
figure; imagescp(I7t,0.01,0.99); colorbar; axis('equal', 'tight');
if nargin<9, %Calculate threshold and background for ratio
    if nargin == 6, Cp=bg6;
    else
        Cp=0.5 %cutoff percentile assume that intensities above this percentile are data, and
below are background.
    end;
    s6=sort(I6t(:));
    s7=sort(I7t(:));
    bg6=s6(floor(size(s6,1)*Cp*.5))
```

```
    bg7=s7(floor(size(s7,1)*Cp*.5))
    thr6=s6(floor(size(s6,1)*Cp))
    thr7=s7(floor(size(s7,1)*Cp))
end;
R=Ratio(I6t,I7t, bg6, bg7, thr6, thr7); colorbar; axis('equal', 'tight');
```

Appendix C:
MATLAB Script

MOTIMIT2

For analyzing data acquired using the optimized XELCI setup (with acrylic light guide)

```
function [I6t,I7t,R,Pixeldwelltime, I6, I7] = motimit2(allmotorpositions,rawintensity1,
rawintensity2, stepsize,alltimings,bg6,bg7,thr6,thr7)

%This script calculates the 620 nm intensity by subtracting the 700 nm intensity from the
total intensity and plots the intensities as pseudo color intensity images and as a ratio
image of the I6/I7 intensities.



rawintensity2=rawintensity2-rawintensity1;  %I6 = Itotal–I7. Previous code had I6 and I7
acquired separately.



if nargin<4,

   stepsize=0.5;

end;

[Max, Ind]= max(allmotorpositions'); %Max(k) is the maximum value of row k; Ind(k) is
the column this maximum value is found.

Cols=ceil(Max(1)/stepsize); %number of columns (pixels) in each row = max motor
position/stepsize. Assuming min motorposition = 0.

Rows=size(Max,2); %number of rows (pixels) in the final image

I6=zeros([Rows Cols]); %Initialize image at 600nm

I7=zeros([Rows Cols]); %Initialize image at 700nm

Pixeldwelltime=zeros([Rows Cols]); %Initialize dwell time array
```

```
for k=1:Rows, %
   j=1;
   for i=1:Ind(k),
      if rawintensity1(k,i)>1000000 || rawintensity2(k,i)>1000000
         display('unexpectedly high signal rawintensity'); display(rawintensity1(k,i));
display(rawintensity2(k,i)); display([k i j]);
         rawintensity1(k,i)=0; rawintensity2(k,i)=0; alltimings(k,i)=0;
      end;

      if allmotorpositions(k,i)<=j*stepsize, %motor position still within pixel, alot signal
to that pixel
         I7(k,j)=I7(k,j)+rawintensity1(k,i);
         I6(k,j)=I6(k,j)+rawintensity2(k,i);
         Pixeldwelltime(k,j)=Pixeldwelltime(k,j)+alltimings(k,i);
      elseif allmotorpositions(k,i)>j*stepsize, %moved past the end of pixel
         if i==1,      %beginning of row
            j=ceil(allmotorpositions(k,i)/stepsize);
            I7(k,j)=rawintensity1(k,i);
            I6(k,j)=rawintensity2(k,i);
            Pixeldwelltime(k,j)=alltimings(k,i);

            %display(I6(k,j));
            %display([k j i]);
```

```
        else        %moved past end of pixel, not the beginning of row

            dtrav=allmotorpositions(k,i)-allmotorpositions(k,i-1);

            if allmotorpositions(k,i)<=(j+1)*stepsize,   %moved past the end of first pixel
but not past end of second: alot signal to the first and second pixel in proportion to
distance travelled

                I7(k,j)=I7(k,j)+rawintensity1(k,i)*(j*stepsize-allmotorpositions(k,i-1))/dtrav;

                I7(k,j+1)=rawintensity1(k,i)*(allmotorpositions(k,i)-j*stepsize)/dtrav;

                I6(k,j)=I6(k,j)+rawintensity2(k,i)*(j*stepsize-allmotorpositions(k,i-1))/dtrav;

                I6(k,j+1)=rawintensity2(k,i)*(allmotorpositions(k,i)-j*stepsize)/dtrav;

                Pixeldwelltime(k,j)=Pixeldwelltime(k,j) + alltimings(k,i)*(j*stepsize-
allmotorpositions(k,i-1))/dtrav;

                Pixeldwelltime(k,j+1)=alltimings(k,i)*(allmotorpositions(k,i)-
j*stepsize)/dtrav;



                j=j+1;



            else   %moved past the end of first and second pixel, i.e. alot signal to more than
two pixels

                display('large distance travelled compared to pixel size... interpolating');

                display([k i j]);



                I7(k,j)=I7(k,j)+rawintensity1(k,i)*(j*stepsize-allmotorpositions(k,i-1))/dtrav;
%alot signal to end of first pixel in proportion to distance travelled

                I6(k,j)=I6(k,j)+rawintensity2(k,i)*(j*stepsize-allmotorpositions(k,i-1))/dtrav;

                Pixeldwelltime(k,j)=Pixeldwelltime(k,j)+alltimings(k,i)*(j*stepsize-
allmotorpositions(k,i-1))/dtrav;
```

```
            dtravrem=allmotorpositions(k,i)-j*stepsize;  %distance travelled past end of
pixel

            stepsleft=dtravrem/stepsize; %steps past end of first pixel

            I6rem=rawintensity2(k,i)*dtravrem/dtrav; %signal remaining to alot

            I7rem=rawintensity1(k,i)*dtravrem/dtrav;

            Pixeldwellrem=alltimings(k,i)*dtravrem/dtrav;

              for l=1:floor(stepsleft),

                 I6(k,j+l)=I6rem/stepsleft;

                 I7(k,j+l)=I7rem/stepsleft;

                 Pixeldwelltime(k,j+l)=Pixeldwellrem/stepsleft;

              end;

            j=j+l;

            I6remlastpx=I6rem*(stepsleft-floor(stepsleft))/stepsleft; %distance into the
last pixel

            I7remlastpx=I7rem*(stepsleft-floor(stepsleft))/stepsleft;

            Pdwelllastpx=Pixeldwellrem*(stepsleft-floor(stepsleft))/stepsleft;

            I6(k,j+1)=I6remlastpx;

            I7(k,j+1)=I7remlastpx;

            Pixeldwelltime(k,j+1)=Pdwelllastpx;

            j=j+1;

          end; %if allmotorpositions(k,i)>(j+1)*stepsize

        end; %i=1

      end; %if allmotorpositins <j*stepsize
```

```
    end; %for i=1:Ind(k)

end; %for k=1:Rows

%I6=flipud(fliplr(I6)); %Invert rows and columns to match photo. We could also reverse in the save labview code, or rotate motors.

%I7=flipud(fliplr(I7)); %Invert rows and columns to match photo.

%Pixeldwelltime=flipud(fliplr(Pixeldwelltime));

I6=rot90(I6,3); %Rotate rows and columns 270 degrees (90 * 3) to match photo. We could also reverse in the save labview code, or rotate motors.

I7=rot90(I7,3); %Rotate rows and columns to match photo.

Pixeldwelltime=rot90(Pixeldwelltime,3);




I6t=I6./Pixeldwelltime*1000;  %counts/ms

I6t(isnan(I6t))=0;

I7t=I7./Pixeldwelltime*1000;    %counts/ms

I7t(isnan(I7t))=0;



figure; imagescp(I6t,0.01,0.99); colorbar; axis('equal', 'tight');

figure; imagescp(I7t,0.01,0.99); colorbar; axis('equal', 'tight');

if nargin<9,

    if nargin == 6, Cp=bg6;

    else

        Cp=0.5 %cutoff percentile assume that intensities above this percentile are data, and below are background.
```

```
    end;
    s6=sort(I6t(:));
    s7=sort(I7t(:));
    bg6=s6(floor(size(s6,1)*Cp*.5))
    bg7=s7(floor(size(s7,1)*Cp*.5))
    thr6=s6(floor(size(s6,1)*Cp))
    thr7=s7(floor(size(s7,1)*Cp))
end;
R=Ratio(I6t,I7t, bg6, bg7, thr6, thr7); colorbar; axis('equal', 'tight');
```

Appendix D:
ACS Copyright Permission

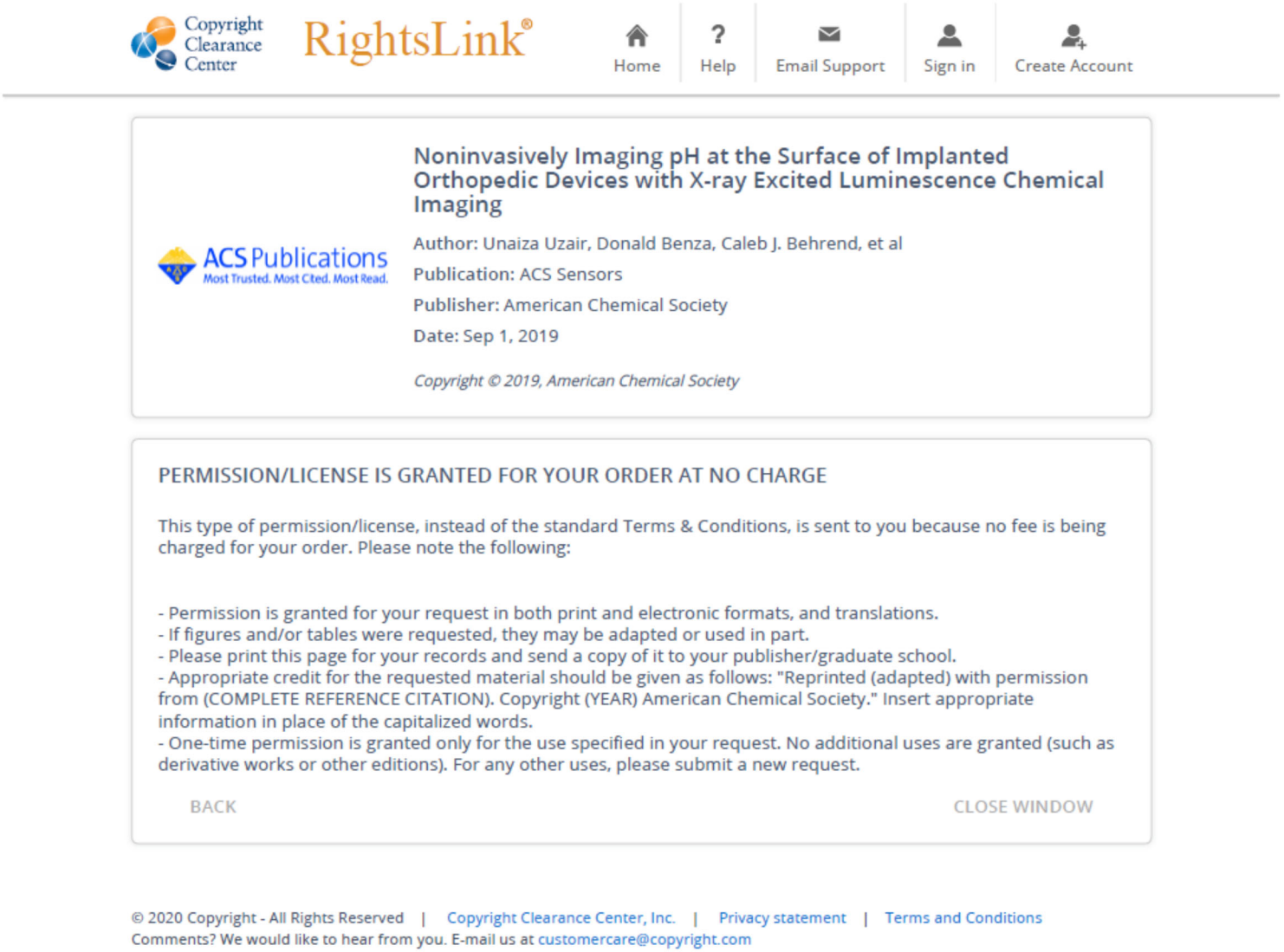

Copyright Clearance Center RightsLink®

Home | Help | Email Support | Sign in | Create Account

ACS Publications
Most Trusted. Most Cited. Most Read.

Noninvasively Imaging pH at the Surface of Implanted Orthopedic Devices with X-ray Excited Luminescence Chemical Imaging

Author: Unaiza Uzair, Donald Benza, Caleb J. Behrend, et al

Publication: ACS Sensors

Publisher: American Chemical Society

Date: Sep 1, 2019

Copyright © 2019, American Chemical Society

PERMISSION/LICENSE IS GRANTED FOR YOUR ORDER AT NO CHARGE

This type of permission/license, instead of the standard Terms & Conditions, is sent to you because no fee is being charged for your order. Please note the following:

- Permission is granted for your request in both print and electronic formats, and translations.
- If figures and/or tables were requested, they may be adapted or used in part.
- Please print this page for your records and send a copy of it to your publisher/graduate school.
- Appropriate credit for the requested material should be given as follows: "Reprinted (adapted) with permission from (COMPLETE REFERENCE CITATION). Copyright (YEAR) American Chemical Society." Insert appropriate information in place of the capitalized words.
- One-time permission is granted only for the use specified in your request. No additional uses are granted (such as derivative works or other editions). For any other uses, please submit a new request.

BACK CLOSE WINDOW

© 2020 Copyright - All Rights Reserved | Copyright Clearance Center, Inc. | Privacy statement | Terms and Conditions
Comments? We would like to hear from you. E-mail us at customercare@copyright.com